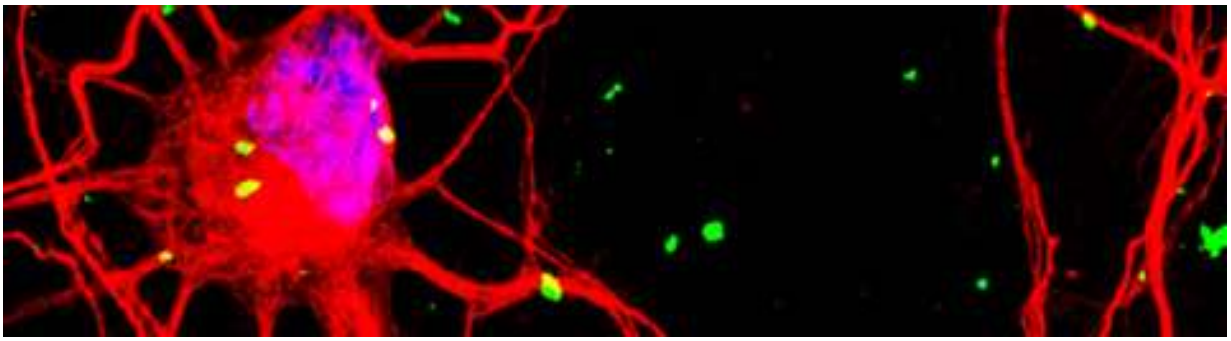

Corso di Dottorato in Neuroscienze
Curriculum Neuroscienze e Neurotecnologie
Ciclo XXXI

Discovery and Characterization of Novel Selective NKCC1 Inhibitors for Down Syndrome and Brain Disorders with Depolarizing GABAergic Transmission

Annalisa Savardi

Supervisor: Dr. Laura Cancedda
Dr. Marco De Vivo

ISTITUTO ITALIANO DI TECNOLOGIA

UNIVERSITÀ DEGLI STUDI DI GENOVA

Abbandona le grandi strade, prendi i sentieri.

Pitagora

Index

Abstract

Proper GABAergic transmission through Cl-permeable $GABA_A$ receptors is fundamental for physiological brain development and function. Indeed, defective GABAergic signaling -due to a high ratio of expression of the Cl importer NKCC1 and Cl exporter KCC2- has been implicated in several neurodevelopmental disorders (e.g., Down syndrome, DS). Interestingly, NKCC1 inhibition by the FDA-approved diuretic bumetanide reverts cognitive deficits in the TS65Dn mouse models of DS and core symptoms in a number of models of other brain disorders. However, the required chronic treatment with bumetanide is burdened by its diuretic side effects caused by the antagonism of the kidney Cl^- importer NKCC2, which leads to hypokalemia and jeopardizes drug compliance. Crucially, these issues would be solved by selective NKCC1 inhibitors, thus devoid of the diuretic effect. Starting from bumetanide's structure, we applied a computational ligand-based approach to design new molecular entities that we tested *in vitro* for their capacity to selectively block NKCC1. Among the 3 newly-identified and highly promising NKCC1 inhibitors, one showed excellent solubility and metabolic stability *in vitro.* Moreover, analysis of WT and Ts65Dn mice systemically treated with this NKCC1 inhibitor revealed no diuretic effect. Finally, chronic treatment with our novel, selective NKCC1 inhibitor was able to rescue cognitive deficits in Ts65Dn mice in four different memory tasks, with no major signs of toxicity. Thus, our selective NKCC1 inhibitor devoid of the diuretic effect could represent a suitable and solid therapeutic strategy for the treatment of Down syndrome and all the brain disorders with depolarizing GABAergic transmission.

Introduction

1. Brain Development and the role of GABA

Three distinct yet partially overlapping phases are involved in the establishment of neuronal circuits during development: an early, innate activity-independent phase, a later phase driven by spontaneous patterns of neuronal activity, and a final phase dependent on neuronal activity driven by sensory experience. During the first two phases, neuronal progenitors proliferate and differentiate, and newly born neurons mature morphologically and migrate to their final location in the brain, establishing a first set of neuronal connections (Ben-Ari, 2001; Spitzer, 2006). After the development of sensory organs, the final phase starts, and neuronal activity driven by sensory experience from the external environment refines the initial neuronal circuitry (Feller, 1999; Hadders-Algra, 2018; Leighton & Lohmann, 2016).

GABA (γ-aminobutyric acid) is the first neurotransmitter to be functional in developing neuronal networks and it plays major roles in all three phases of brain development. GABA is synthesized in the CNS from the L-glutamic acid by the enzyme L-glutamic acid decarboxylase (GAD), which is present in two isoforms, GAD65 and GAD67 (Buddhala et al., 2009). GABA exerts its action by binding two different types of receptors: the ionotropic $GABA_A$ receptor ($GABA_AR$) and the metabotropic $GABA_B$ receptor ($GABA_BR$). $GABA_A$Rs are ligand-gated ion channels formed by the assembly of 5 different subunits. There are nineteen subunits (α1-6, β1-3, γ1-3, δ, ε, θ, π, ρ1-3), and they can be present in different combinations of five, thereby conferring $GABA_A$Rs' diverse properties with respect to ionic current dynamics, cellular localization, and physiological functions (Has & Chebib, 2018; Koduvayur et al., 2014). $GABA_A$Rs are mostly permeable to chloride (Cl^-) and they mediate slow and tonic extra-synaptic currents or fast and phasic synaptic currents, depending on the presence of the different combination of the receptor subunits (Figure 1). Tonic currents are mediated by low concentrations of ambient GABA that escaped from the synaptic cleft and can activate subtypes of extrasynaptic $GABA_A$

receptors with high affinity (Brickley et al., 1999; Cellot & Cherubini, 2013; Farrant & Nusser, 2005). Conversely, the phasic GABAergic inhibition occurs at the post-synaptic site of the cleft, when GABA is released at a high concentration from the presynaptic vesicles. During early brain development, before the onset of GABAergic synaptic activity, extrasynaptic tonic currents play a major role (Brickley et al., 1999; Farrant & Nusser, 2005; Kilb et al., 2013).

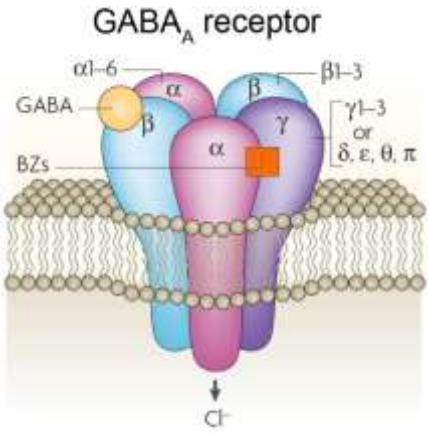

Figure 1 Representation of the subunit composition of the $GABA_AR$. Different combinations of the subunits create different pool of synaptic and exprasynaptic receptors Modified from Jacob et al. 2008

For both tonic and phasic GABAergic currents, Cl^- can flow through the $GABA_AR$ in both directions, depending on its concentration gradient across the cell membrane and the membrane resting potential of the neuron. In the adult CNS under physiological conditions, there is a low Cl^- concentration inside the cell. Thus, the direction of Cl^- flow is inward, and GABA exerts hyperpolarizing and inhibitory actions (Kahle et al., 2013). Conversely, during early neurodevelopment, there is a high Cl^- concentration inside the cell. Thus, opening of the $GABA_AR$ causes a Cl^- efflux from the cell and GABA depolarizes the membrane (Kahle et al., 2013). This depolarization leads to activation of voltage-gated calcium channels and removal of the Mg^{2+} block from NMDA receptors, causing further membrane depolarization and calcium influx into the cell. This is vital for the activation of second messengers that participate in neuronal migration, differentiation and synaptogenesis (Ben-Ari, 2002, 2014; Cellot & Cherubini, 2013; Leinekugel et al., 1997; Takayama & Inoue, 2010).

Later in development, when the first coarse connectivity among developing neurons is built, depolarizing GABA also controls spontaneous neuronal activity in the form of network action potential bursts of different shapes across brain areas and species. Interestingly, these bursts of spontaneous neuronal activity during development have been described in the rodent, chick, turtle, ferret and rabbit (Aguado et al., 2003; Ben-Ari, 2001; Wong, 1999). Moreover, evidence exists that in primate fetuses there is a complex hippocampal network capable of generating spontaneous and paroxysmal synchronized activities *in utero* (Khazipov et al., 2001). Interestingly, early patterns of neuronal synchronized activity have also been described in humans (preterm babies) by EEG and fMRI studies (Arichi et al., 2017; Khazipov & Luhmann, 2006; Tolonen et al., 2007). Nevertheless, the contribution of depolarizing GABA during these early patterns of neuronal activity in humans has not been investigated yet.

Notably, when GABA switches its action from depolarizing and mostly excitatory to hyperpolarizing and inhibitory later in life, the neuronal network activity oscillations disappear ((Leitch et al., 2005), but see (Makinen et al., 2018)) for *in vitro* evidence in human pluripotent stem cell-derived neural culture). Interestingly, for at least some brain structures, this phenomenon coincides with the development of complex behavior related to that specific brain structure. For example, the striatum completes its immature activity patterns precisely when pups begin coordinated locomotor behavior (Dehorter, Vinay, et al., 2012).

Finally, proper GABAergic transmission is fundamental during critical periods of enhanced neuronal connectivity and plasticity driven by sensory system experiences deriving from individuals' own life experiences (M. R. Begum & Sng, 2017; Berardi et al., 2000; Hensch, 2004; Hensch & Fagiolini, 2005; Hensch & Quinlan, 2018; Sommeijer et al., 2017; Takesian & Hensch, 2013; H. Zhang et al., 2018).

2. Chloride transporters in physiological brain development

The understanding of the mechanisms regulating intracellular Cl^- concentration during development has gained a lot of attention in recent years because of the fundamental role of Cl^- in modulating GABAergic

transmission and its consequent implication in neurodevelopmental processes. In neurons, the main regulators of Cl^- homeostasis are the cation-chloride co-transporters (CCCs) (Blaesse et al., 2009; H. Li et al., 2002), especially the sodium-potassium-chloride cotransporter isoform 1 (NKCC1) and the potassium-chloride symporter isoform 2 (KCC2). NKCC1 is highly expressed in immature neurons during development, as it transports Cl^- inside the cells, leading to a high intracellular Cl^- concentration (~30 mM), and depolarizing and mostly excitatory GABA actions (Achilles et al., 2007; Dzhala et al., 2005) (Figure 2, left). On the other hand, KCC2 is highly expressed in mature neurons, where it keeps the intracellular Cl^- level at low values (4-6 mM; (Delpire & Kahle, 2017), thereby determining the hyperpolarizing and inhibitory GABA action (Ben-Ari, 2002, 2014; Rivera et al., 1999; Stein et al., 2004) (Figure 2, right).

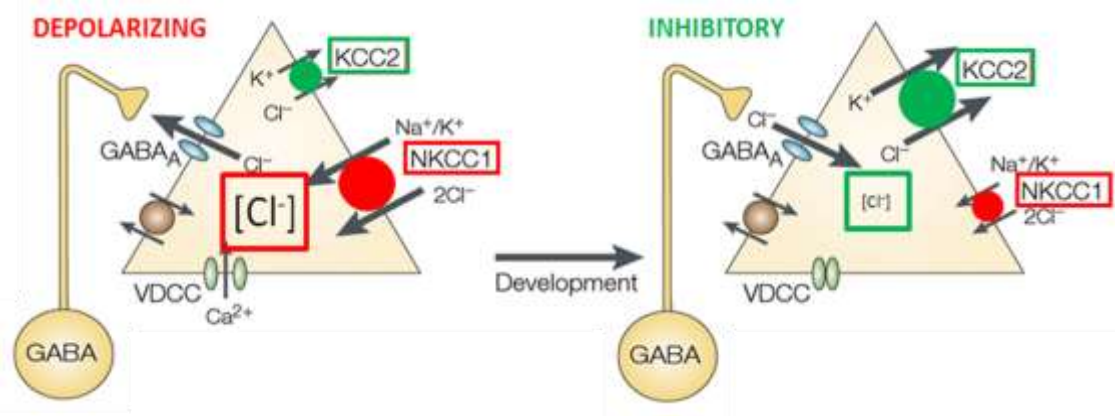

Figure 2. Representation of the different CCCs expression in embryonic (left) and adult (right) neurons. Left: The high NKCC1 expression during early development leads to a high Cl^- concentration inside the cells, thus determining a Cl^- efflux when $GABA_AR$ opens and the cell depolarization. Right: In the adulthood the high KCC2 expression determine a low Cl^- concentration inside the cell. When $GABA_AR$ opens, the Cl^- influx in the cell determine the neuron hyperpolarization.

Interestingly, this pattern of expression for NKCC1 and KCC2 develops earlier in the evolutionary older structures (e.g., spinal cord, brainstem, hypothalamus; (Watanabe & Fukuda, 2015) (Figure 3). Indeed, NKCC1 and KCC2 are highly expressed in the mouse spinal cord from E11.5-E13.5 (Delpy et al., 2008) and starting from E15.5, NKCC1 decreases its expression, while KCC2 remains highly expressed. This difference generates the depolarizing to hyperpolarizing GABA switch in motor neurons around E17.5 (Branchereau et al., 2002). Notably, recordings at E18.5 in mice showed that motorneurons exhibited

GABA and glycine (that also binds to Cl^--permeable ionic receptors) excitation in the absence of KCC2, thus highlighting its importance in inhibitory activity (Hubner et al., 2001).

In the hypothalamus, the presence of NKCC1 mRNA expression was not clear in rodent embryos, and its expression was weak postnatally. Conversely, at E14.5, KCC2 mRNA is strongly present and maintains its expression into adulthood in rodents (H. Li et al., 2002; C. Wang et al., 2002).

In the thalamus, NKCC1 mRNA is not present during the embryonic stages in rats (C. Wang et al., 2002). Conversely, KCC2 mRNA is already found at E12 in rodents, when the region begins forming, with the exception of the dorsomedial part, which expresses KCC2 later at E18 (H. Li et al., 2002; C. Wang et al., 2002; Watanabe & Fukuda, 2015). Notably, NKCC1 mRNA is stably expressed postnatally in rats (from soon after birth into adult life), suggesting a possible low hyperpolarizing or even depolarizing action of GABA in the adult thalamus (C. Wang et al., 2002; Watanabe & Fukuda, 2015).

In the rat cerebellum, NKCC1 mRNA was not detected in early developing Purkinje cells at any postnatal age. Conversely, KCC2 mRNA was found at E15.5 in mouse Purkinje cells and at P1 in rat Purkinje cells when the cells begin differentiation (Mikawa et al., 2002). Interestingly, NKCC1 mRNA was observed in rats in the external granule layer, where the immature granule cells (later developing in comparison to Purkinje cells) are located at P7 and P14, and in the internal granular layer in post-migratory granule cells after P7 (Mikawa et al., 2002). Moreover, KCC2 transcripts were detectable already at P3 in mouse and at P7 in rat granule cells (Mikawa et al., 2002; Stein et al., 2004).

In the rat hippocampus, NKCC1 mRNA is strongly present in the neuroepithelium at E18 (Watanabe & Fukuda, 2015), peaking in the first postnatal week and then decreasing by P14-P15 (Pfeffer et al., 2009; Plotkin et al., 1997; C. Wang et al., 2002). Instead, KCC2 mRNA signals can be detected first in the CA3 region at E15.5 and in the CA1 region at E18.5 in mice; it then reaches adult levels at P15 (Stein et al., 2004). In the same study, western blot analysis showed a time course of KCC2 protein expression closely parallel to the detection of the KCC2 transcript described above (Stein et al., 2004).

In the neocortex, NKCC1 transcripts have been detected as early as E12.5 in scattered cells of the mouse neuroepithelium and in the ventricular zone (VZ) of the ganglionic eminences (H. Li et al., 2002; Watanabe & Fukuda, 2015) where the neuronal progenitors are located. By E14.5, NKCC1 mRNA is upregulated in the proliferative zones of the lateral and medial ganglionic eminence in mice (Watanabe & Fukuda, 2015). Then, NKCC1 expression in the VZ decreases in late mouse embryonic development (E17-P0; (Caviness et al., 1995)). In the differentiated cells of the cortical plate both mRNA and protein of NKCC1 are strongly present in rats (Li et al., 2002; (Watanabe & Fukuda, 2015)). Interestingly, KCC2 mRNA signals are not detected in the mouse neocortex until P0 (H. Li et al., 2002; C. Wang et al., 2002). Although most of the work on the presence or absence of the CCCs is based on mRNA evidence, some data on the protein expression are available for the rat neocortex. In particular, NKCC1 is highly expressed postnatally between P3-P14, whereas KCC2 is expressed at low levels during the first two weeks after birth and is upregulated by P21 (Dzhala et al., 2005).

Finally, NKCC1 is highly expressed both in the developing and adult choroid plexus in mice and rats (Kanaka et al., 2001; H. Li et al., 2002). There, NKCC1 is located on the apical membrane of epithelial cells and it plays a key role in the formation of the cerebrospinal fluid (CSF). Conversely, KCC2 is not expressed in the choroid plexus epithelial cells in mice (Steffensen et al., 2018).

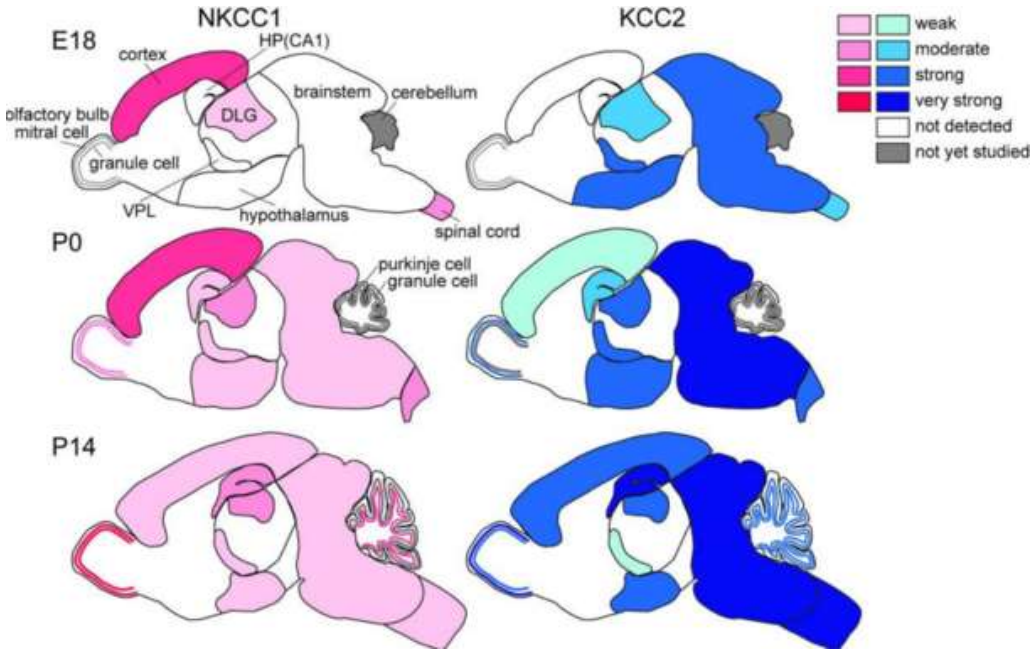

Figure 3. Representation of the different expression profiles of NKCC1 (left) and KCC2 (right) in the CNS. DLG: dorsal lateral geniculate nucleus; HP: hippocampus; VLP: ventral posterior thalamic nucleus. From Watanabe and Fukuda 2015.

The developmental expression profiles of NKCC1 and KCC2 have also been investigated in humans. At the mRNA level, both NKCC1 and KCC2 increased with gestational age across the second trimester and after birth in the prefrontal cortex, while only KCC2 increased in the hippocampus across the second trimester, but both NKCC1 and KCC2 increased after birth (Hyde et al., 2011). A more recent study instead found lower levels of NKCC1 mRNA during the prenatal period (10 post conception week (PCW)-birth) with an increase in the postnatal age (birth-90 years) in the 16 brain areas analyzed (Sedmak et al., 2016). At the protein level, the expression of NKCC1 in the time window between PCW 31-41 was high with a peak at PCW 35 and decreased from the first year of life (PCW 54-92) to adulthood in the parietal cortex. KCC2 expression was low during the entire fetal and neonatal period (PCW 20-41) and increased over the first year of life (Dzhala et al., 2005). Nevertheless, other studies found a robust presence of both KCC2 mRNA and protein during the second half of gestation in the neocortex, indicating that high KCC2 expression starts prenatally (Kaila et al., 2014). Notably, expression of KCC2 was observed as early as PCW16 in a subset of subplate neurons (Bayatti et al., 2008). Moreover, KCC2-immunoreactive neurons were described in the hippocampus and entorhinal cortex as

early as PCW 25 (which was the earliest age tested), and these neurons reach adult levels during the first six postnatal months (Dzhala et al., 2005; Sedmak et al., 2016). Interestingly, the overall ratio of NKCC1 to KCC2 is very high in pediatric human brains, and it decreases until approximately 2 years of life and then it remains at the adult levels (Jansen et al., 2010).

2.1. The role of NKCC1 and KCC2 in neuronal proliferation, migration and network integration.

The important roles of NKCC1 and KCC2 in driving and regulating fundamental processes of proper brain development has been widely demonstrated in rodents by diverse experimental approaches ranging from knock out (KO) animals to modulating the expression and/or the activity of the two CCCs by pharmacological inhibition (e.g., with the widely used FDA-approved drugs bumetanide and furosemide), RNA interference, overexpression (Schulte et al., 2018).

2.1.1 NKCC1 plays a key role in cell proliferation and apoptosis

The role of NKCC1 in brain cell proliferation has been demonstrated by a number of studies. In particular, *ex vivo* investigations have shown that NKCC1 is expressed in radial glial cells in rats (progenitors of excitatory cortical neurons; (H. Li et al., 2002; Noctor et al., 2001) in the cortex, although it is not in βIII-tubulin- (a marker of post-mitotic neurons) positive regions (H. Li et al., 2002). Interestingly, NKCC1 is highly expressed also in the ganglionic eminence, the brain region that gives birth to GABAergic interneurons (H. Li et al., 2002). In agreement with the abovementioned studies, NKCC1 knockdown mice have defects in the proliferation of neural precursor cells of the SVZ (Young et al., 2012) (Figure 4) and in the proliferation of the neural progenitors of the lateral ganglionic eminences (Magalhaes & Rivera, 2016). Moreover, pharmacological blocking of NKCC1 with bumetanide inhibits cell proliferation in neuronal precursors of the subventricular zone in mice (Sun et al., 2012). The role of NKCC1 in brain cell proliferation has been demonstrated also *in vitro* in mouse oligodendrocyte precursor cells, where NKCC1 inhibition is associated with attenuation in cell cycle progression (Fu et al., 2015).

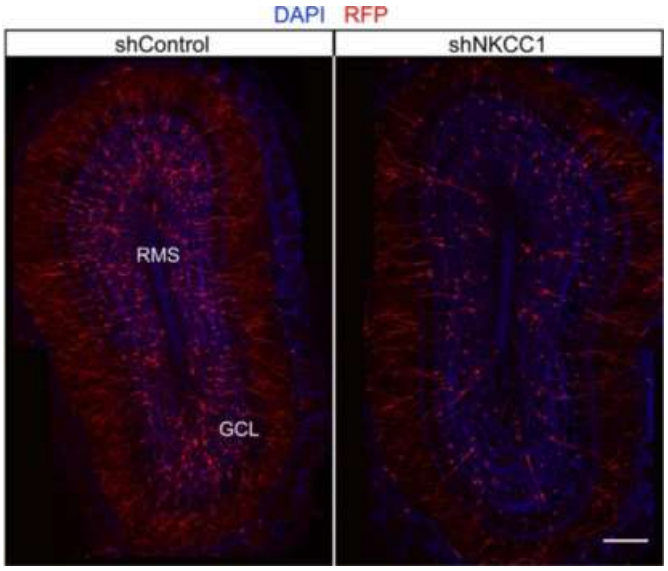

Figure 4. NKCC1 KO in NPCs of the olfactory bulb results in a reduction of neuron production. RFP indicate the electroporated neurons with respectively shRNA control (shControl) or the shRNA against NKCC1 (shNKCC1). RMS: rostral migratory stream; GCL: granule cell layer. Scale bar: 100µm. Adapted from Young et al. 2012.

Another fundamental stage where NKCC1 plays a role is programmed cell death during development. In particular, NKCC1 is implicated in the activity-regulated cell death in Cajal-Retzius neurons, a population that mostly disappears by apoptosis early in life in the mouse developing cortex (Blanquie et al., 2017). Pharmacological inhibition of NKCC1 by bumetanide *in vitro* or genetic deletion of the cotransporter *in vivo* (NKCC1−/− mice) rescued the population of Cajal-Retzius neurons from apoptosis (Blanquie et al., 2017).

2.1.2 NKCC1 and KCC2 regulate neuronal migration

The depolarizing GABA transmission by high expression of NKCC1 in the ventricular zone and cortical plate (Shimizu-Okabe et al., 2002) plays a role in the migration of newly generated rat cortical neurons (Behar et al., 1996; Behar et al., 1998; Heck et al., 2007). In particular, both knocking down of NKCC1 (shRNA) and pharmacological manipulations of NKCC1 by bumetanide in neuroblasts in mice from the rostral migratory stream in organotypic slice cultures reduced migratory speed without affecting the direction of the migration (Mejia-Gervacio et al., 2011). Although this piece of evidence points to a

possible role for NKCC1 in physiological interneuron migration, a direct demonstration of the involvement of NKCC1 in cortical excitatory-neuron migration is still missing. Indeed, the knockdown of NKCC1 *in vivo* in mice during neurodevelopment through *in utero* electroporation resulted in a disruption of cortical neuron morphology, but unfortunately, neuronal migration was not evaluated in that same study (D. D. Wang & Kriegstein, 2008). Nevertheless, several lines of evidence suggest that altered expression of NKCC1 underlies cortical malformations and neuronal ectopy in pathological conditions (Fukuda & Wang, 2013; Koyama et al., 2012; Shimizu-Okabe et al., 2007). In particular, high expression of NKCC1 and low expression of KCC2 were found in cortical plate neurons involved in micro-gyral cortical malformations in rodents *in vivo* (Fukuda & Wang, 2013; Shimizu-Okabe et al., 2007). Moreover, either knockdown of NKCC1 by RNA interference or its pharmacological inhibition by bumetanide both rescued the migration deficits of granule cells in the dentate gyrus in a rat model of febrile seizures *in vivo* (Koyama et al., 2012). Furthermore, some evidence indicates a role for NKCC1 in the migration of glioma cells both *in vitro* and *in vivo* in mice (Haas & Sontheimer, 2010). While these *in vivo* studies suggest that high NKCC1 expression could affect neural migration and pathological conditions, it is not clear whether physiological levels of NKCC1 regulate migration *in vivo* in non-pathological conditions.

Similar to the case of NKCC1, some evidence exists that KCC2 also mediates migration of interneurons, where its upregulation works as a stop signal both *in vitro* and *in vivo* in mice (Figure 5) and in organotipic cultures from a ferret model of cortical dysplasia (Abbah & Juliano, 2014; Bortone & Polleux, 2009; Inamura et al., 2012; Miyoshi & Fishell, 2011). On the other hand, KCC2 expression in excitatory neurons increases only after they have completed their migration across different cortical layers and other brain areas in rats (Cancedda et al., 2007). In agreement with these data, overexpression of KCC2 in newly born excitatory cortical neurons did not affect their migration in rats (Cancedda et al., 2007). Nevertheless, this may possibly be because high levels of taurine inhibit KCC2 function at embryonic stages, thus preserving the depolarizing GABA signaling (Inoue et al., 2012). Interestingly, a

structural role for KCC2 in neural crest cell migration and early radial glia migration in mice (at E9.5) was reported to occur through the interaction with the cytoskeleton-associated protein 4.1N and independently of the ion-transport action (Horn et al., 2010).

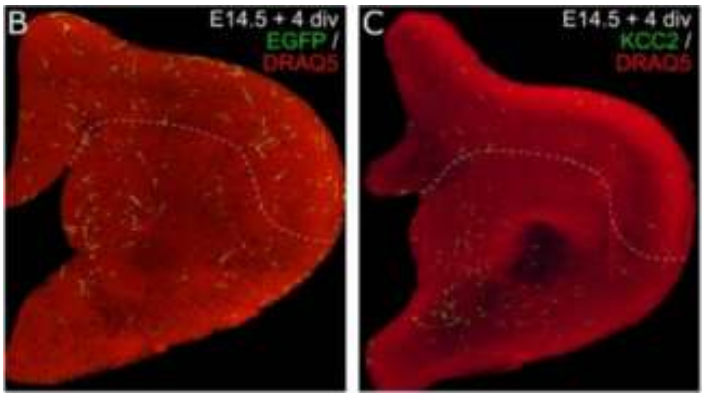

Figure 5. Precocious KCC2 expression reduced migration of interneuron. **B**: Interneurons electroporated with EGFP (control) showed a robust migration from medial ganglionic eminence (MGE) to the cortex. **C**: Interneurons expressing precocious KCC2 showed a marked reduced migration to the cortex. Adapted from Bortone and Polleux 2009.

2.1.3 NKCC1 and KCC2 regulate neuronal morphological maturation

Both NKCC1 and KCC2 play fundamental roles in neuronal branching and in the establishment, maintenance and plasticity of synapses (Kaila et al., 2014; Khalilov et al., 2011; Sedmak et al., 2016). In particular, a high Cl^- concentration maintained by the high expression of NKCC1 and the low expression of KCC2, is fundamental for neuronal morphological maturation.

For example, NKCC1 was observed in the tip of growing neurites (K. Nakajima et al., 2007), and both its knockdown by RNA interference (K. Nakajima et al., 2007; K. Nakajima et al., 2011a, 2011b) or its pharmacological inhibition by treatment with bumetanide (K. I. Nakajima & Marunaka, 2016) abolished neurite outgrowth *in vitro* in PC12 cells. Accordingly, knockdown of NKCC1 *in vivo* disrupted the dendritic maturation of mouse cortical neurons (D. D. Wang & Kriegstein, 2008; Young et al., 2012) (Figure 6A). Moreover, NKCC1 activation is also required for neurite growth in injured rodent adult neurons *in vivo* (Modol et al., 2015; Pieraut et al., 2007; Pieraut et al., 2011). Furthermore, NKCC1 has been involved in the maturation of both rodent excitatory and inhibitory synapses (Nakanishi et al., 2007;

Pfeffer et al., 2009; D. D. Wang & Kriegstein, 2008). Although NKCC1 -/- mice do not exhibit morphological alteration of hippocampal dendritic arborization, they presented delayed maturation of GABAergic and glutamatergic synapses (Pfeffer et al., 2009). Accordingly, *in utero* NKCC1 knockdown in mouse excitatory cortical neurons affected the physiological development of excitatory and inhibitory synapses (D. D. Wang & Kriegstein, 2008). Moreover, pharmacological NKCC1 inhibition by bumetanide during mouse cortical development disrupted AMPA synapse maturation, although it did not affect NMDA receptor signaling (D. D. Wang & Kriegstein, 2011).

In line with studies on NKCC1 downregulation/inhibition, premature expression of KCC2 by *in utero* electroporation in a subpopulation of rat cortical neuron progenitors severely impacted morphological maturation, with fewer and shorter neurites ((Cancedda et al., 2007) (Figure 6B); but see (Fiumelli et al., 2013)) together with an altered number of dendritic spines (Fiumelli et al., 2013). Moreover, overexpression of KCC2 *in utero* also increased the number of dendritic spines (Fiumelli et al., 2013). Interestingly, KCC2 is highly expressed in the head of rodent dendritic spines, where AMPA and NMDA receptors are located; there, it also plays a role in the maintenance of glutamatergic synapses (Blaesse & Schmidt, 2015; Chamma et al., 2012). Notably, KCC2 exerts this role independently of its Cl^- transporter activity and *via* interaction with the submembrane actin cytoskeleton by binding to 4.1 N protein in mice (H. Li et al., 2007). Further studies showed that KCC2 constrains lateral diffusion of AMPA receptors and regulates their content at the spine again through the regulation of actin dynamics (Chevy et al., 2015; Gauvain et al., 2011; Llano et al., 2015). In agreement with previous studies, KCC2 knockout mice exhibit large alterations in synaptic and neuronal network activity in the CA3 region of the hippocampus (Khalilov et al., 2011).

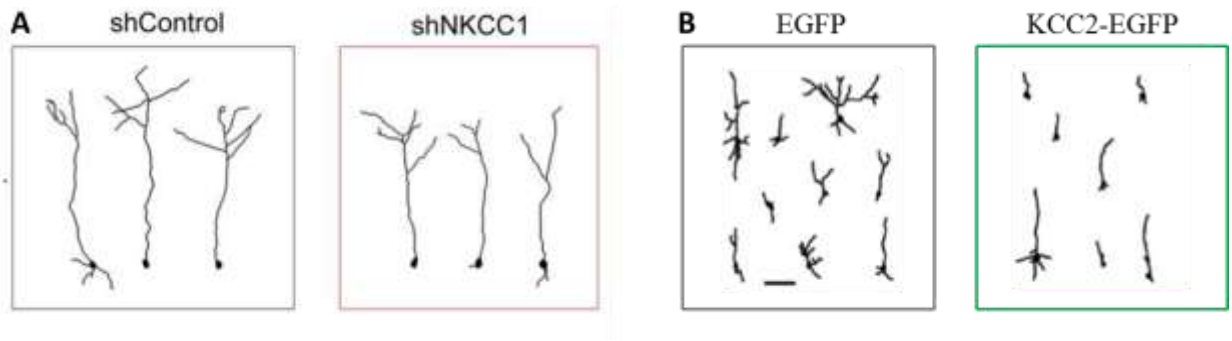

Figure 6: Both NKCC1 downregulation (A) and KCC2 premature upregulation (B) caused impaired dendrite branching. **A**: Representative reconstruction of neurons electroporated with shRNA control (shControl; left) and shRNA against NKCC1 (shNKCC1; right). Adapted from Young et al 2012. **B**: Representative reconstruction of neurons electroporated with EGFP (left) or KCC2-EGFP (right). Scale bar: 100µm. Modified from Cancedda et al. 2007.

Finally, premature KCC2 overexpression found in a rat model of atypical febrile seizures and in a variant of KCC2 found in an Australian family with febrile seizures cause a reduction in dendritic spine number (Awad et al., 2016; Puskarjov, Seja, et al., 2014) Interestingly, the reduction of the premature KCC2 expression rescued the alterations in spine density and morphology and the seizure susceptibility in the same rat model of febrile seizures (Awad et al., 2016).

2.2. The role of NKCC1 and KCC2 in the critical period of brain plasticity

The critical period for sensory system plasticity has been widely investigated in the visual system, starting from the pioneering studies of Hubel and Wiesel in the middle part of the 20th century [or, late 1950's]. Interestingly, proper development of GABAergic transmission is crucial for both the opening and the closure of the critical period plasticity in the visual cortex. Indeed, manipulation of inhibition, by prematurely enhancing or reducing GABAergic signaling during development interferes with the onset of the rodent critical period plasticity (Fagiolini et al., 2004; Fagiolini & Hensch, 2000; Huang et al., 1999; Iwai et al., 2003). Notably, reducing GABAergic activity in adult animals reopens the critical period in the visual cortex (Harauzov et al., 2010). More recently, Deidda and colleagues demonstrated that depolarizing GABA during early postnatal development plays a pivotal role in the critical period for visual cortical plasticity later in life. In particular, they observed that pharmacological inhibition of

NKCC1 with bumetanide from P3 to P8 in rats extended the duration of the critical period into adulthood, with a mechanism dependent on the neurotrophin BDNF (Deidda, Allegra, et al., 2015).

2.3. Expression and role of other NKCCs and KCCs in the developing brain.

In addition to NKCC1, the NKCC family also contains NKCC2. NKCC2 is highly expressed in the apical membrane of the epithelial cells of the thick ascending limb in the kidney and the macula densa cells (specialized sensor cells detecting changes in the fluid composition of the distal tubule), where it facilitates the reabsorption of sodium and Cl^- ions into the blood (Delpire & Gagnon, 2018; A. Edwards et al., 2014). Moreover, NKCC2 is strongly expressed in the epithelial layer of the endolymphatic sac in humans, a part of the vestibular system (Kakigi et al., 2009). Notably, NKCC2 immunoreactivity is also present in vasopressinergic and oxytocinergic neurons in the hypothalamo-neurohypophyseal system in the rat brain (Konopacka et al., 2015). Blockade of NKCC2 leads to pronounced natriuresis, kaliuresis and diuresis (Becker et al., 2003; Castrop & Schiessl, 2014; Gamba & Friedman, 2009; Hannemann et al., 2009; Schiessl & Castrop, 2015). Loss of function mutations of the gene coding for NKCC2 result in Bartter's syndrome, which is characterized by hypokalemic alkalosis, hyponatremia and hypotension (Simon et al., 1996).

The less studied members of the KCC family (KCC1, KCC3 and KCC4) are also expressed in the developing brain. KCC1 mRNA was exclusively detected in the choroid plexus during mouse brain development (H. Li et al., 2002), but mRNA levels have been found in neuronal and glial cells in diverse regions (olfactory bulb, hippocampus, choroid plexus, posterior hypothalamic nucleus) of the adult rat CNS *in vivo* (Kanaka et al., 2001). Interestingly, KCC1 negatively regulates NGF-induced neurite outgrowth *in vitro* in PC12 cells (Nagao et al., 2012). KCC3 mRNA is weakly represented in the embryonic rodent brain (H. Li et al., 2002), but both the mRNA and the protein are widely present in adult cortical, hippocampal, brainstem and cerebellar Purkinje neurons (Pearson et al., 2001; Shekarabi et al., 2011). Moreover, KCC3 protein is expressed in white matter-rich structures in the rodent brain, spinal cord and peripheral nerves, indicating a role of KCC3 in myelination (Pearson et al., 2001). Furthermore,

KCC3 regulates the cell volume in mouse peripheral nerve fibers (Flores et al., 2018). In agreement with the previous findings, KCC3 −/− mice exhibited axonal swelling, hypomyelination and demyelination in sciatic nerves (Byun & Delpire, 2007; Howard et al., 2002). Interestingly, these mice recapitulate most of the symptoms of human peripheral neuropathy associated with agenesis of the corpus callosum (ACCPN, also known as Andermann syndrome). This severe sensorimotor neuropathy is characterized by locomotor abnormalities and areflexia and has been associated with loss-of-function mutations in KCC3 gene (Bowerman et al., 2017; Howard et al., 2002; Uyanik et al., 2006).

KCC4 is highly expressed in the embryonic mouse brain, including choroid plexus, peripheral ganglia, ventricular zones and the nucleus of the trigeminal nerve (H. Li et al., 2002). Along with NKCC1, KCC4 plays a role in cochlear development, as KCC4 KO mice exhibit deafness. KCC4 loss possibly exerts that effect by causing the death of hair cells by osmotic perturbation or membrane depolarization (Boettger et al., 2002).

Spatiotemporal expression of the KCC transporters has been studied also in humans. In particular, KCC1 mRNA was first observed in the cortex of the cerebellum at embryonal stages (between PCW 10-13) and also found in other brain regions (hippocampus, striatum and thalamus between PCW 21 and birth; (Sedmak et al., 2016). KCC3 mRNA was described in the cortex, cerebellum, hippocampus, amygdala, striatum and thalamus in all the stages of development and adulthood (age range: 5 PCW–82 years; (Sedmak et al., 2016). KCC4 mRNA was detected at low levels in the cortex both at prenatal and postnatal ages (Kaila et al., 2014), but not detected in a subsequent study in any brain region (Sedmak et al., 2016). KCC2 mRNA was not detected in any brain region (Sedmak et al., 2016).

3. Chloride transporters in neurodevelopmental disorders

Neurodevelopmental disorders (NDs) are chronic psychiatric/neurological conditions that affect 4-5% of the population (Mitchell, 2011). In general, NDs result from an altered timing and asynchrony of developmental processes induced by both genetic and environmental factors, which cause defective growth of the central nervous system. Although they display very different etiologies, most of the NDs share a number of features (e.g., impairments in learning, memory, emotional regulation, sociality, and self-control) and some comorbidity (e.g., increased seizure susceptibility and sleep disorders). Interestingly, many of these common features have been associated with common alterations in GABAergic transmission. In particular, several studies demonstrated a high intracellular Cl^- concentration and a depolarizing GABA action attributable to an altered NKCC1/KCC2 ratio in a wide range of NDs (Figure 7), including epilepsy, autism spectrum disorders, Asperger syndrome, Rett syndrome, Fragile X syndrome, schizophrenia, tuberous sclerosis complex, traumatic brain injury, glioma and Down syndrome (Ben-Ari, 2017; Jaggi et al., 2015; Medina et al., 2014; Schulte et al., 2018; Wu, Che, et al., 2016).

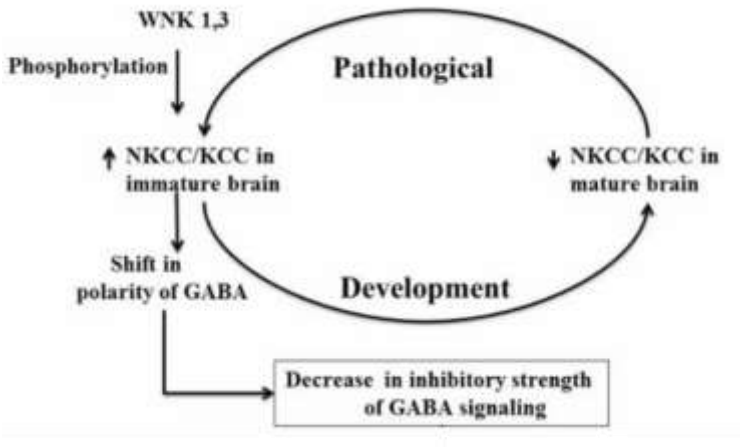

Figure 7: Representative cartoon of the NKCC1/KCC2 ratio expression in physiological and pathological development. High expression ratio of NKCC/KCC2 leads to a shift in the GABA polarity trough more depolarized values determining less inhibitory and depolarizing GABA action, implicated in several neurological disorder. Adapted from Jaggi et al. 2015.

Interestingly, restoration of physiological Cl^- concentration by pharmacological intervention aimed at inhibiting NKCC1 or enhancing KCC2 activity has led to positive outcomes in rodent models and patients

with these conditions (Ben-Ari, 2017; Jaggi et al., 2015; Medina et al., 2014; Schulte et al., 2018). Currently, the most used approach to restore intracellular Cl^- concentration in mouse models of brain pathologies as well as in clinical studies in patients has been the inhibition of NKCC1 with bumetanide. Another recently investigated option to restore intracellular Cl^- concentration has been the enhancement of KCC2 activity by the compound CLP257. This has been explored in cultured cell lines and in spinal cord slices obtained from rats with peripheral nerve injury, a condition characterized by KCC2 hypofunction (Gagnon et al., 2013). Interestingly, CLP257, by modulating KCC2 activity, was also able to exert an antinociceptive action in rats with peripheral nerve injury (Gagnon et al., 2013). Nevertheless, a recent study showed that CLP257 was not able to modulate KCC2 activity *in vitro* in the same cultured cell line used previously, opening the possibility that the behavioral effects of CLP257 observed by Gagnon and colleagues may be independent of KCC2 modulation (Cardarelli et al., 2017). Again, this study was challenged by Gagnon and colleagues, who replied to the Cardarelli and co-workers objection confirming their previous findings (Gagnon et al., 2017), thus indicating the need for further investigation.

Finally, recent studies evaluated other components involved in NKCC1 and KCC2 regulation that could be considered in the future as possible therapeutic targets. For example, the insulin-like growth factor-1 was able to decrease the NKCC1/KCC2 ratio in developing rat neurons *in vivo*, promoting the GABA switch from depolarizing to hyperpolarizing (Baroncelli et al., 2017). Moreover, the kinase WNK-SPAK, which can activate NKCC1 and deactivate KCC2 through its phosphorylation state (Kahle et al., 2010), could also be an interesting target to modulate the NKCC1/KCC2 ratio (de Los Heros et al., 2014; Kahle et al., 2015).

Here, we give a brief description of the involvement of altered NKCC1 and KCC2 expression/function in the pathogenesis of some neurodevelopmental disorders, considering some examples of therapeutic approaches. We describe more in detail the case of Down syndrome at the end of this section.

3.1. Epilepsy

Epilepsy is a neurological disorder characterized by epileptic seizures. These are caused by altered, excessive or hypersynchronous neuronal activity in the brain (Chang & Lowenstein, 2003). Several pieces of evidence suggest that neuronal hyperexcitability and hypersynchronization is the result of an alteration of the delicate balance between excitatory and inhibitory synaptic activity. Interestingly, an imbalance in NKCC1 and KCC2 activity together with depolarizing GABAergic action have been observed in several animal models of epilepsy (Ben-Ari, 2017; Di Cristo et al., 2018). The first lines of evidence about the involvement of CCCs in epileptogenic activity came from the late 90s, when four independent studies found that the antagonism of NKCC1 with furosemide or bumetanide caused a block of epileptic activity both *in vitro* and *in vivo* in rats (Hochman et al., 1995; Hochman et al., 1999; Hochman & Schwartzkroin, 2000; Schwartzkroin et al., 1998). In 2002, four other works demonstrated the direct relationship between NKCC1, KCC2 and epileptic pathogenesis. In particular, high NKCC1 expression was indicated as a factor influencing the increased susceptibility to seizures in the developing brain. In this study, bumetanide administration was able to rescue epileptiform activity both *in vitro* and *in vivo* during development in rodents (Dzhala et al., 2005). Moreover, increased expression of NKCC1 was found in the amygdala-kindling model of seizures in rats (Okabe et al., 2002). Furthermore, a decrease in KCC2 expression was found in the mouse hippocampus after kindling-induced seizures (Rivera et al., 2002). Finally, mice deficient in KCC2 showed frequent seizures (Woo et al., 2002). This may be possibly due to a shift in the reversal potential for $GABA_AR$-driven Cl^- currents (E_{Cl}), which leads to smaller $GABA_AR$ hyperpolarization and/or to less reuptake of potassium and chloride during high-frequency spikes (Woo et al., 2002). Stemming from these first works, several other studies in rodent models confirmed the involvement of an altered NKCC1/KCC2 ratio in the pathogenesis of epilepsy. A number of these studies also confirmed positive outcomes upon bumetanide treatment (Almeida et al., 2011; Amadeo et al., 2018; Baek et al., 2016; Cleary et al., 2013; Dzhala et al., 2008; Dzhala et al., 2010; D. A. Edwards et al., 2010; Eftekhari, Mehrabi, et al., 2014; Hu et al., 2017; Kelley et al., 2018; Koyama et al., 2012; X. Li et al., 2008; Loscher et al., 2013; MacKenzie & Maguire, 2015; MacKenzie et al.,

2016; Marguet et al., 2015; Mazarati et al., 2009; Nardou et al., 2009; Reid et al., 2013; Robel et al., 2015; Santos et al., 2017; Sivakumaran & Maguire, 2016; Tao et al., 2016; Tollner, Brandt, Erker, et al., 2015; F. Wang et al., 2017; J. Zhang et al., 2016).

Interestingly, an imbalance in the NKCC1/KCC2 ratio is also present in human patients. First, upregulation of NKCC1 and/or downregulation of KCC2 was found in the hippocampal subiculum and hippocampi obtained from patients affected by temporal lobe epilepsy (Huberfeld et al., 2015; Huberfeld et al., 2007; Munoz et al., 2007; Palma et al., 2006; Sen et al., 2007). Then, other studies found altered expression of NKCC1 and/or KCC2 in the cortical malformation of patients affected by medically intractable epilepsy (Aronica et al., 2007; Sen et al., 2007; Shimizu-Okabe et al., 2011) in hypothalamic hamartoma, a rare epileptogenic lesion associated with gelastic seizures (D. Y. Kim et al., 2008), in cortical samples from epileptic children (Jansen et al., 2010), and in peritumoral tissues with high seizure susceptibility (Conti et al., 2011; Pallud et al., 2014). Notably, an increased expression of NKCC1 and a decreased expression of KCC2 were observed also in brain samples obtained from patient affected by Dravet syndrome, an infantile encephalopathy characterized by severe epilepsy and cognitive impairment (Ruffolo et al., 2018). Interestingly, bumetanide treatment ameliorated seizure frequency in temporal lobe epilepsy (Eftekhari, Mehrabi, et al., 2014). Moreover, bumetanide was able to reduce seizure duration and frequency in a child affected by intractable multifocal seizures (Kahle, Barnett, et al., 2009). Nevertheless, the NEMO trial, assessing the efficacy and safety of the use of bumetanide for the treatment of acute neonatal encephalopathy seizures (Pressler et al., 2015), was recently interrupted due to poor bumetanide antiepileptic action and ototoxicity (Ben-Ari et al., 2016). Moreover, the involvement of KCC2 in the pathogenesis of epilepsy has been recently questioned based on conflicting results showing increased KCC2 expression in epileptic brain tissue from both human (Jansen et al., 2010; Karlocai et al., 2016) and rodent models (Awad et al., 2016; Galanopoulou, 2008; Khirug et al., 2010). Nevertheless, the conflicting results showed both decreased and increased KCC2 expression in epilepsy; this discrepancy could depend on brain region, stage of disease, gender, or the influence of seizures themselves (Di Cristo

et al., 2018). Thus, although the involvement of alterations of NKCC1 and KCC2 expression/activation in epilepsy is clearly demonstrated, deeper studies to better investigate their delicate modulation and assess the possibility of targeting them with pharmacological approaches are still required.

3.2. Autism Spectrum Disorders

Autism spectrum disorders (ASD) are a group of syndromes characterized by different etiologies, but common core symptoms (e.g., repetitive behaviors, deficits in social interaction and language impairment; (Pizzarelli & Cherubini, 2011), suggesting that possibly there are common mechanisms underlying ASD pathology. Moreover, ASD can be comorbid with other neurodevelopmental syndromes such as epilepsy (M. L. Lewis et al., 2018), Rett syndrome (Percy, 2011), Fragile X syndrome (Kaufmann et al., 2017), or Down syndrome (J. Moss et al., 2013). Several pieces of evidence, both from rodent models and humans, indicate that commonly altered GABAergic transmission could underlie ASD pathology (Cellot & Cherubini, 2014). In particular, the pioneering observation of a paradoxical effect upon the administration of $GABA_A$-signaling-enhancing benzodiazepine diazepam in autistic children (e.g., anxiety and aggression (Marrosu et al., 1987), suggested the possibility of depolarizing GABA action in ASD. This idea prompted researchers to test whether the inhibition of NKCC1 by bumetanide could be a valid therapeutic strategy in five autistic children (Lemonnier & Ben-Ari, 2010). The amelioration of some behavioral aspect related to ASD upon bumetanide treatment opened the way for a larger clinical trial designed for 54 autistic patients (Lemonnier et al., 2012) and consequently a phase II clinical study (Lemonnier et al., 2017). These studies confirmed that bumetanide is able to ameliorate the core symptoms of ASD. Moreover, bumetanide resulted efficient in the treatment of a young girl with Asperger syndrome, a neurodevelopmental disorder belonging to ASD (Grandgeorge et al., 2014). In parallel to the clinical studies, KCC2 expression was altered in the VPA rat model of ASD. Interestingly, bumetanide administration in VPA-treated pregnant rats resulted in the rescue of core behaviors related to ASD in their offspring (Eftekhari, Shahrokhi, et al., 2014; Tyzio et al., 2014). Nevertheless, the lack of studies addressing bumetanide treatment at developmental stages that can be compared to those of

patients in clinical trials and the paucity of mouse models of autism tested among the many that exist, highlights the need for further investigation.

3.3. Rett Syndrome

Rett syndrome (RTT) is a neurodevelopmental disorder caused by mutations in the X-linked Methyl-CpG-binding protein (MECP2) gene. Mecp2 is a regulator of the transcription of a number of genes by promoter methylation. Individuals affected by RTT grow normally until the age of 6-18 months but then develop various symptoms (e.g., cognitive impairment, seizures, altered motor function and stereotypic behaviors; (Ehinger et al., 2018). As for autism, several pieces of evidence indicate a possible alteration in the GABAergic signaling in RTT rodent models and humans (Cellot & Cherubini, 2014). The first evidence regarding alterations in the NKCC1/KCC2 balance came from a study of CSF obtained from RTT patients, where a decreased level of KCC2 expression was found (Duarte et al., 2013). More recently, deficits in KCC2 expression have been found in human progenitor cells from RTT patients (Tang et al., 2016) and in a mouse model of RTT (Banerjee et al., 2016). Interestingly, IGF1 treatment ameliorated the severity of the syndrome both in RTT mouse models (Castro et al., 2014; Tropea et al., 2009) and in RTT patients (Khwaja et al., 2014; Pini et al., 2016), thus suggesting its implementation in the treatment of NDs (Bou Khalil, 2017). Nevertheless, further investigation of the NKCC1/KCC2 ratio and its consequence on GABA signaling are needed to better clarify the role of the two CCCs in the pathogenesis of RTT and their possible involvement as therapeutic targets.

3.4. Fragile X syndrome

Fragile X syndrome (FXS) is a genetic disorder caused by mutations in the X-linked FMR1 gene encoding for Fragile X mental retardation protein (FRMP). FRMP is a regulator of the translation of several mRNAs. FXS individuals show cognitive deficits, autistic behavior, hypersensitivity to sensory stimuli and comorbidity with epilepsy (Morel et al., 2018). These symptoms led researchers to hypothesize an excitatory/inhibitory imbalance, as previously observed in ASD and epilepsy. In

particular, driven by the positive outcome of the earlier pilot study on autistic patients (Lemonnier et al., 2012), the same authors treated a FXS child with bumetanide (Lemonnier et al., 2013). Interestingly, bumetanide administration resulted in the amelioration of the score of each of the 5 clinical tests performed to probe autistic core symptoms (Lemonnier et al., 2013), opening the route to larger clinical trials. In agreement with the clinical study, FXS mice showed a delay in the developmental switch of GABA polarity from depolarizing to hyperpolarizing, due to increased expression of NKCC1 (He et al., 2014). The same year, Tyzio and colleagues found increased Cl^- concentrations in hippocampal slices from FXS mice at P15 and P30 due to a decreased level of KCC2. Fetal treatment with bumetanide right before birth was able to recover the intracellular Cl^- concentration, GABAergic transmission and the behavioral features related to autism later in life (Eftekhari, Shahrokhi, et al., 2014; Tyzio et al., 2014). Recently, treatment of FXS mice with bumetanide during the critical period of somatosensory cortex plasticity rectified GABA polarity and synaptic plasticity and allowed long-lasting restoration of proper somatosensory-circuit formation (He et al., 2018). Moreover, a recent study found that bumetanide treatment by itself was insufficient to completely rescue social impairment in the automated tube test in FXS mice, suggesting the need for a combination therapy (Zeidler et al., 2017). Nevertheless, in the same study, the combination of the genetic reduction of mGluR5 expression together with bumetanide treatment worsened social impairment, indicating that the combination therapy needs to be better investigated in terms of drug type, targeting pathway and time window of administration (Zeidler et al., 2017). Although there are only a few studies in animal models and in humans, the abovementioned evidence supports the involvement of the NKCC1/KCC2 imbalance in the pathogenesis of FXS syndrome and their modulation as a possible therapeutic strategy.

3.5. Schizophrenia

Schizophrenia is a neurodevelopmental disorder characterized by psychosis and cognitive impairments, leading to disability and premature mortality (D. A. Lewis, 2012). In particular, the clinical manifestations can be divided into three categories: positive symptoms (e.g., hallucinations), negative

symptoms (e.g., depression and apathy) and cognitive symptoms (D. A. Lewis, 2012). The etiology of schizophrenia is still under investigation, but a large body of literature agrees on the contribution of both genetic and environmental factors. GABAergic transmission seems again to play an important role in the pathogenesis of this ND (Balu & Coyle, 2011). In particular, the first pieces of evidence of impaired Cl^- homeostasis in schizophrenia came from a study on the prefrontal cortex (and later the hippocampus) of schizophrenic patients, where NKCC1 expression was increased (Dean et al., 2007; Hyde et al., 2011). A few years later, alterations in SLC12A2 and SLC12A5 genes, encoding for NKCC1 and KCC2, respectively, were indicated as susceptibility genes for schizophrenia development in patients (J. Y. Kim et al., 2012; Merner et al., 2015; Merner et al., 2016; Potkin et al., 2009). Furthermore, increased expression of two kinases regulating NKCC1 and KCC2 activity, OXSR1 and WNK3, was found in the prefrontal cortex of schizophrenic subjects, indicating a possible increase in NKCC1 activity and a decrease in KCC2 function in schizophrenic patients (Arion & Lewis, 2011). In addition, an altered NKCC1/KCC2 ratio was described in two different mouse models of schizophrenia (Larimore et al., 2017; Yang et al., 2015). Finally, an interplay between NKCC1 and the protein Disrupted in schizophrenia 1 (DISC1, an intrinsic regulator of neurogenesis implicated in schizophrenia) has been demonstrated to be fundamental for the regulation of the dendritic development of newborn neurons during adult neurogenesis in the mouse hippocampus (J. Y. Kim et al., 2012), suggesting possible involvement of NKCC1 in the pathogenic mechanisms underlying schizophrenia.

Of note, *in vitro* evidence from Amin and coworkers revealed an imbalance in NKCC1 and KCC2 expression also in DiGeorge Syndrome (a condition conferring high risk of schizophrenia), which caused hyperexcitability of the network recovered by bumetanide application to the neuronal culture (Amin et al., 2017).

Bumetanide treatment in schizophrenic patients reduced the severity of the symptoms and hallucinations (Lemonnier et al., 2016; Rahmanzadeh, Eftekhari, et al., 2017), without ameliorating the total score of the general positive and negative syndrome scale (PANSS) and the brief psychiatric rating scale (BPRS)

(Rahmanzadeh, Shahbazi, et al., 2017). Interestingly, intranasal administration of oxytocin reduced the severity of symptoms in schizophrenic patients in several studies (Brambilla et al., 2016; Davis et al., 2014; Davis et al., 2013; Feifel et al., 2012; Feifel et al., 2010; Fischer-Shofty et al., 2013; Gibson et al., 2014; Goldman et al., 2011; Lee et al., 2013; Modabbernia et al., 2013; Ota et al., 2018; Pedersen et al., 2011; Shin et al., 2015; Woolley et al., 2017; Woolley et al., 2014), but see (Cacciotti-Saija et al., 2015; Caravaggio et al., 2017; Dagani et al., 2016; Horta de Macedo et al., 2014; Jarskog et al., 2017). In light of the ability of oxytocin to regulate GABA signaling in fetal and newborn rodents (Ben-Ari, 2018; Eftekhari, Shahrokhi, et al., 2014; Khazipov et al., 2008; Leonzino et al., 2016; Tyzio et al., 2006; Tyzio et al., 2014), it is tempting to hypothesize that oxytocin exerts its therapeutic effect on schizophrenic patients also by regulating CCCs. A deeper investigation of the molecular mechanisms underlying the possible relation between the oxytocin system and CCCs could open new avenues for the treatment of schizophrenia and other NDs.

3.6. Tuberous Sclerosis Complex

Tuberous sclerosis complex (TSC) is a multiorgan genetic disorder caused by loss of function mutations of the TSC1 or TSC2 genes (van Slegtenhorst et al., 1997). This pathology is characterized by the presence of cortical tubers (i.e., dysplastic lesions), source of focal epilepsy, autistic behaviors and intellectual disability. Given the imbalance of the NKCC1/KCC2 ratio in epilepsy (Schulte et al., 2018), the investigation of CCCs in tuberous sclerosis has gained interest. TSC patients present an increased NKCC1/KCC2 ratio in extracts from cortical tubers (Ruffolo et al., 2016; Talos et al., 2012). An altered GABA reversal potential was also described in the cortical tissues (Ruffolo et al., 2016). Altogether, these studies suggest a possible involvement of NKCC1/KCC2 imbalance in the pathogenesis of TSC in patients. Nevertheless, a better investigation of both the pathogenic mechanisms and possible therapies needs to be performed in rodent models.

3.7. Traumatic brain injury

Traumatic brain injury (TBI) is caused by an injury to the brain due to external objects or forces. When TBI occurs in early childhood, the cortical and subcortical lesions lead to altered neurodevelopmental processes and consequent cognitive defects persisting for the lifetime of the individual (Bonnier et al., 2007; Jonsson et al., 2013; Keenan et al., 2007). The neurodevelopmental damages occurring after a TBI are the result of a cascade of events, called secondary brain injury, including damage of the blood-brain barrier, inflammation, excitotoxicity, edema, ischemia and neuronal damage (e.g., excitotoxicity, aberrant ionic homeostasis, axonal disconnection and death; (Ghajar, 2000; Park et al., 2008). One of the mechanisms underlying this cascade of events is possibly an imbalance of NKCC1 and KCC2 expression. Indeed, three independent studies found that NKCC1 was upregulated in the hippocampus and choroid plexus of traumatic brain injury rat models and that bumetanide administration decreased the inflammatory response and neuronal damage (Lu et al., 2008; Lu et al., 2006; Lu et al., 2007). Then, other studies confirmed the fundamental role of NKCC1 in TBI-induced rodent hippocampal aberrant neurogenesis (Lu et al., 2015), neuronal and astrocytic apoptosis (Hui et al., 2016; M. Zhang et al., 2017), cerebral edema (Lu et al., 2017; M. Zhang et al., 2016), seizures (Liang & Huang, 2017; F. Wang et al., 2017) BBB disruption (J. Zhang et al., 2017) and microvascular failure (Simard et al., 2010). Finally, a recent work described decreased KCC2 expression in the rat parietal cortex after TBI, which was rescued by melatonin administration leading to amelioration of neural apoptosis and brain edema (Wu, Shao, et al., 2016). The deep understanding of the involvement of both NKCC1 and KCC2 in the secondary brain injury upon TBI suggests timely pharmacological interventions to prevent the consequent neurodevelopmental alterations observed in TBI children.

3.8. Glioma

Gliomas are brain tumors derived from glial cells and are the most frequent pediatric brain tumors. Given their unique properties in comparison to those affect the adults, pediatric gliomas can be considered to be neurodevelopmental disorders (Baker et al., 2016). They will thus be discussed in this section. Among

pediatric gliomas, there is wide heterogeneity from histopathological and therapeutic standpoints. There are treatable low-grade tumors and incurable or fatal high-grade tumors. The severity level of glioma and the transition from low-grade to high-grade tumors is generally linked with the ability to migrate and invade other areas. The invasion phenomena have been widely studied in recent years to unravel their underlying mechanisms and find possible pharmacological targets. Among the mechanisms involved, NKCC1 and other transporters and channels play a role in tumor metastasis (Sontheimer, 2008). Accordingly, bumetanide administration reduced glioma invasion in mice (Haas & Sontheimer, 2010). Further studies both in primary patient-derived glioblastoma cells *in vitro*, and in mice *in vivo*, found that the involvement of NKCC1 in glioma cell migration was mediated by modulation of the cytoskeleton and regulation of cell volume (Garzon-Muvdi et al., 2012; Schiapparelli et al., 2017), opening the possibility of NKCC1 as a specific therapeutic target to decrease cell invasion in pediatric glioma patients.

4. Chloride transporters in Down syndrome

Down syndrome (DS) is caused by the triplication of human chromosome 21 (Hsa21) and it is one of the most common genetic causes of intellectual disability and congenital birth defects. Many health issues characterize persons with DS (Antonarakis & Epstein, 2006; Desai, 1997; Nadel, 2003; Parker et al., 2010), with almost all individuals presenting with cognitive deficits (Dierssen, 2012; Edgin et al., 2012; Pennington et al., 2003; Vicari et al., 2013).

Several studies investigated possible mechanisms involved in cognitive impairment, taking advantage of diverse murine genetic models of DS (Dierssen, 2012). The Ts65Dn mouse (Reeves et al., 1995) is the most characterized and widely used. These mice are characterized by the presence of an extra chromosome derived from mouse chromosome 16, representing the long arm of human chromosome 21, fused to the centromere of the murine chromosome 17 (Antonarakis et al., 2004). Interestingly, Ts65Dn mice recapitulate many features of DS. In particular, these mice show impairment in neuronal

development (Belichenko et al., 2004; Chakrabarti et al., 2010; Chakrabarti et al., 2007; Contestabile et al., 2010; Contestabile et al., 2007), defects of synaptic plasticity (Contestabile et al., 2013; Costa & Grybko, 2005; Kleschevnikov et al., 2004; Siarey et al., 1999; Siarey et al., 1997), impaired hippocampus-dependent memory functions (Contestabile et al., 2013; Costa et al., 2008; Fernandez et al., 2007; Reeves et al., 1995), hyperactivity (Escorihuela et al., 1995; Reeves et al., 1995; Sago et al., 2000) and sleep disorders (Colas et al., 2008; Das et al., 2015; Stewart et al., 2007).

4.1. Down Syndrome and GABAergic Transmission

The first lines of evidence regarding the involvement of defective GABAergic transmission in DS found an increased number of GABAergic interneurons in the cortex and hippocampus of adult and adolescent Ts65Dn mice, respectively (Chakrabarti et al., 2010; Perez-Cremades et al., 2010). These alterations were accompanied by an increase in spontaneous GABAergic postsynaptic events in CA1 pyramidal neurons of adult Ts65Dn mice (Chakrabarti et al., 2010). Interestingly, subsequent studies by electrophysiological recordings of spontaneous, miniature and evoked GABAergic postsynaptic currents, and release probability as well as immunohistochemical and electron microscopy studies on the number/density of the GABAergic synapses and their locations provided seemingly contrasting and often inconsistent results, depending on the parameters analyzed, hippocampal subregion and age of the animals (P. V. Belichenko et al., 2009; Belichenko et al., 2004; Best et al., 2012; Chakrabarti et al., 2010; Garcia-Cerro et al., 2014; Hanson et al., 2007; Hernandez-Gonzalez et al., 2015; Hernandez et al., 2012; A. M. Kleschevnikov, P. V. Belichenko, J. Gall, et al., 2012; Kurt et al., 2000; Kurt et al., 2004; Martinez-Cue et al., 2013; Mitra et al., 2012; Mojabi et al., 2016; Stagni et al., 2013). Moreover, studies of DS autoptic brain samples and analysis of cortical neuronal progenitors obtained from DS individuals have shown a general reduction in the GABAergic system at various levels (Bhattacharyya et al., 2009; Kobayashi et al., 1990; Ross et al., 1984), in seemingly inconsistence with the first evidence describing increased GABAergic transmission in Ts65Dn mice.

Thus, the evidence in Ts65Dn mice and brain samples taken altogether suggests that, besides an increased number of GABAergic interneurons, hippocampal subregion and age-dependent differences, compensatory mechanisms and a general increase in the excitability of the interneurons may be present in DS (Contestabile et al., 2017).

Interestingly, further studies demonstrated that the altered GABAergic transmission affected synaptic plasticity in DS mice, experimentally measured with long-term potentiation (LTP) protocols in acute brain slices of adult Ts65Dn mice (N. P. Belichenko et al., 2009; Belichenko et al., 2015; Belichenko et al., 2007; Costa & Grybko, 2005; Fernandez et al., 2007; A. M. Kleschevnikov, P. V. Belichenko, M. Faizi, et al., 2012; Kleschevnikov et al., 2004).

Given that several pieces of evidence suggested that the cognitive deficits and abnormalities in synaptic plasticity observed in Ts65Dn mice derive, at least in part, from an excess of $GABA_A$-mediated neurotransmission in the hippocampal circuitry, diverse studies evaluated $GABA_A$ receptors as a possible therapeutic target to rescue cognitive impairment in DS. For 10 years, numerous independent groups tested $GABA_A$ receptor inhibitors targeting diverse subunits and consistently found a rescue in LTP and hippocampal cognitive abilities in Ts65Dn mice (Braudeau, Dauphinot, et al., 2011; Braudeau, Delatour, et al., 2011; Fernandez et al., 2007; Martinez-Cue et al., 2014; Martinez-Cue et al., 2013; Mohler, 2012; Potier et al., 2014; Rueda et al., 2008). Similar results were obtained by treating Ts65Dn animals with fluoxetine, an inhibitor of serotonin reuptake ((Begenisic et al., 2014; Bianchi et al., 2010; Guidi et al., 2014; Stagni et al., 2015), but see (Heinen et al., 2012)) or exposing the Ts65Dn animals to an enriched environment (Begenisic et al., 2015; Begenisic et al., 2011; Martinez-Cue et al., 2002; Martinez-Cue et al., 2005). Since both fluoxetine and exposure to an enriched environment reduced GABAergic signaling (Baroncelli et al., 2010; Begenisic et al., 2014; Begenisic et al., 2015; Begenisic et al., 2011; Caiati & Cherubini, 2013; Maya Vetencourt et al., 2008; Mendez et al., 2012; Sale et al., 2007), it is possible that the effects on Ts65Dn mice may be due, at least in part, to modulation of GABAergic transmission, as in all the studies reported above for $GABA_A$ receptor inhibitors.

These lines of evidence reinforce the hypothesis of a causal link between the increased GABAergic transmission, synaptic plasticity abnormalities and cognitive deficits of DS mice (Chakrabarti et al., 2010; Kleschevnikov et al., 2004) and highlight GABAergic transmission as a possible therapeutic target in DS. On the other hand, both individuals with DS and DS mouse models show an increased susceptibility to seizures (Arya et al., 2011; Gholipour et al., 2017; Goldberg-Stern et al., 2001; Lott, 2012; Lott & Dierssen, 2010; Rissman & Mobley, 2011; Robertson et al., 2015; Smigielska-Kuzia et al., 2009; Stafstrom et al., 1991; Westmark et al., 2010) and hyperactivity (Deidda, Parrini, et al., 2015; Escorihuela et al., 1995; J. F. Moss, 2017; Pueschel et al., 1991; Reeves et al., 1995; Sago et al., 2000), and individuals with DS often show anxiety traits (Dekker et al., 2018; Haddad et al., 2018; Vicari et al., 2013), pointing to excess excitation rather than inhibition in DS.

4.2. NKCC1 is Implicated in Depolarizing $GABA_AR$ Signaling in Down Syndrome

In 2015, Deidda and colleagues proposed a new perspective about $GABA_AR$ transmission in DS (Deidda, Parrini, et al., 2015). In their work, the efficacy and polarity of $GABA_AR$ signaling were investigated in adult Ts65Dn mice. Surprisingly, they found that GABAergic transmission was depolarizing and mostly excitatory rather than hyperpolarizing and inhibitory in adult DS mice. In particular, they described an increase in spike frequency in Ts65Dn hippocampal and neocortex acute slices in comparison to wild type (WT), both in baseline conditions and upon application of GABA. Accordingly, blockade of endogenous $GABA_A$ signaling by the application of the $GABA_AR$ antagonist bicuculline resulted in a reduction in the spike frequency in neurons from Ts65Dn brain slices.

The excitatory action of GABA in Ts65Dn brain slices was accompanied by a shift E_{Cl} to more positive potentials. Indeed, taking advantage of the gramicidin-perforated patch clamp, a technique that allows maintenance of the endogenous intracellular Cl^- concentration, they observed that Ts65Dn neurons

exhibited a less negative E_{Cl} (-58 mV) in comparison to WT neurons (-66 mV). The use of gramicidin-perforated patch-clamp was key, considering that another study conducted to investigate E_{Cl} in Ts65Dn mice by whole-cell patch-clamp did not detect these differences (A. M. Kleschevnikov, P. V. Belichenko, J. Gall, et al., 2012). Of note, an E_{Cl} value above the membrane resting potential suggests an outward Cl^- current. This was indeed described by Deidda and colleagues by Cl^- imaging in CA1 neurons from Ts65Dn acute brain slice.

Interestingly, the same study found that the defective GABAergic signaling was due to an increased expression of NKCC1 protein (Figure 8), which they found in the entire hippocampus, the CA3-CA1 subregion and cortices of adult Ts65Dn mice compared to WT littermates. Interestingly, Deidda and coworkers found increased NKCC1 expression also in hippocampi from DS individuals, providing a parallel between the animal model and humans. Conversely, no changes in KCC2 protein expression both in Ts65Dn mice and DS individuals were detected. Notably, the authors did not find a significant increase in NKCC1 mRNA in adult Ts65Dn mice.

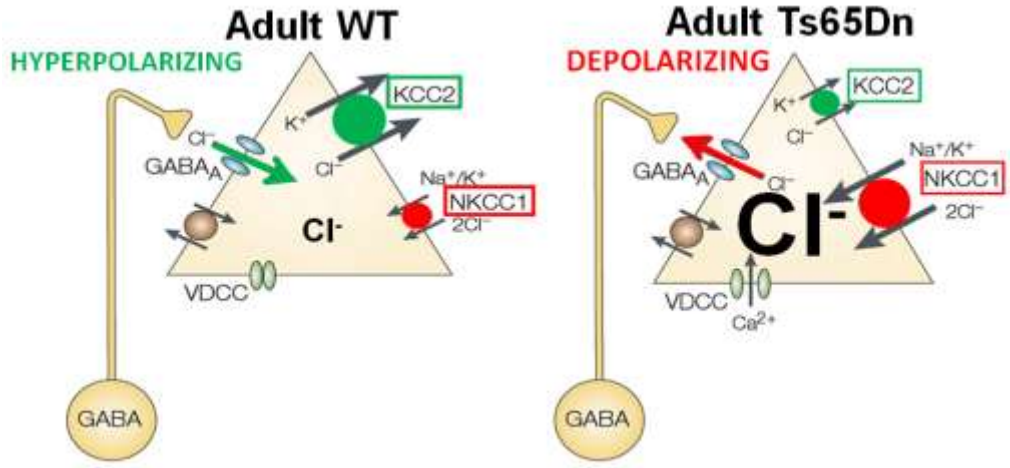

Figure 8. Representation of the different CCCs expression in WT adult (left) and in Ts65Dn adult (right) neurons. Left: In the adulthood the high KCC2 expression determine a low Cl^- concentration inside the cell. When $GABA_AR$ opens, the Cl^- influx in the cell determine the neuron hyperpolarization. Right: The upregulation of NKCC1 in Ts65Dn neurons leads to an high Cl^- concentration inside the cells, thus determining a Cl^- efflux when $GABA_AR$ opens and the cell depolarization.

4.3. Bumetanide treatment rescues the altered GABAergic transmission, synaptic plasticity and cognitive deficits in Ts65Dn Mice

Considering that the increased expression of NKCC1 is the possible cause of the aberrant GABAergic transmission in Ts65Dn mice, Deidda and colleagues evaluated NKCC1 inhibition by bumetanide as a potential therapeutic strategy. Bath application of bumetanide was able to rescue E_{Cl}, with a reduction of spontaneous spiking activity and a decrease in the GABA-induced spike frequency in hippocampal acute slices of adult Ts65Dn mice. Conversely, there was no significant effect of bumetanide application in WT mice, confirming that the shift of E_{Cl} was responsible for depolarizing $GABA_AR$ signaling in adult Ts65Dn mice (Figure 9, left).

Moreover, bumetanide bath application to acute brain slices was able to recover the hippocampal CA1-CA3 LTP to WT levels, with no effect on the LTP in WT mice. Finally, Deidda and colleagues tested Ts65Dn mice and their WT littermates in three independent behavioral tasks to assess hippocampus-dependent long-term explicit memory after either an acute (1 time only), subchronic (1 week) or a chronic (4 weeks) systemic (intraperitoneal) treatment with bumetanide. Interestingly, they showed that all three treatments with bumetanide were able to fully recover the poor associative memory of Ts65Dn mice in the contextual fear conditioning test. Moreover, bumetanide was able to rescue the performance of Ts65Dn mice to the level of WT mice in the object-location test, showing a full recovery of spatial-memory performance. Finally, bumetanide administration was also able to rescue the novel-discrimination memory of Ts65Dn mice in the novel object recognition test (Deidda, Parrini, et al., 2015) (Figure 9, right).

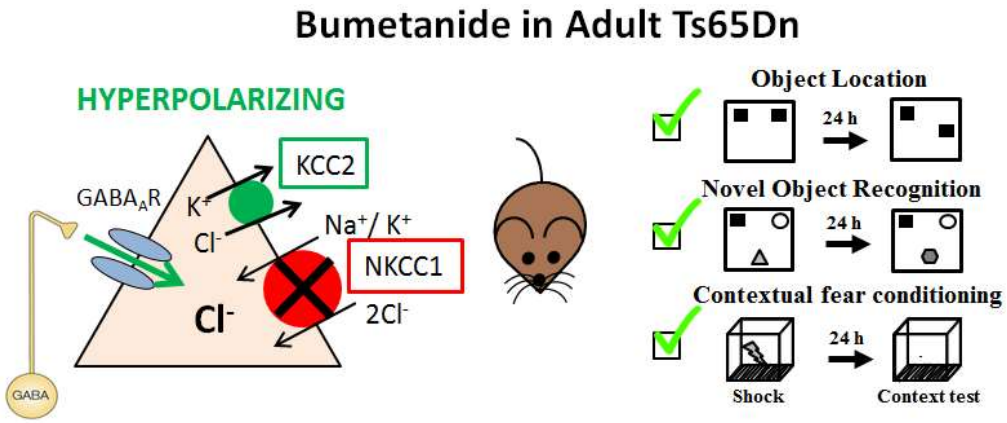

Figure 9. NKCC1 inhibition by bumetanide rescued Cl^- homeostasis, hyperpolarizing GABAergic transmission (left) and cognitive and memory deficits in Ts65Dn adult mice in three different tasks (right).

Notably, bumetanide exerted acute activity on NKCC1 and it did not provide long-lasting effects. Indeed, a drug withdrawal experimental protocol (i.e., a week of bumetanide washout after a four-week treatment) completely abolished the rescue observed in both LTP and behavioral tasks, indicating the requirement for chronic treatment (Deidda, Parrini, et al., 2015).

5. Chloride transporters in other neurological disorders

Recent lines of evidence suggest that an imbalance in NKCC1/KCC2 ratio is involved also in a number of neurological disorders other than NDs including Parkinson disease, Huntington disease, stroke and cerebral edema, peripheral nerve injury and neuropathic pain. As for the aforementioned NDs, restoration of physiological intracellular Cl^- concentration by pharmacological intervention aimed at inhibiting NKCC1 or enhancing KCC2 activity has led to positive outcomes in rodent models and patients with these conditions. Below is a brief description of recent findings showing how an altered NKCC1/KCC2 expression ratio is involved in the pathogenesis of these neurological disorders.

5.1. Parkinson Disease

Parkinson Disease (PD) is a neurodegenerative disorder characterized by severe motor deficits associated with loss of dopaminergic neurons in *substantia nigra pars compacta*, alterations in neurotransmission, , and inflammation (Kaur et al., 2018). Although the pathological mechanism underlying PD are still not completely clarified, alterations in GABAergic transmission seem to play a pivotal role (Blaszczyk, 2016). For instance, aberrant, giant GABAergic currents have been found in two rodent models of PD (Dehorter et al., 2009; Dehorter, Lozovaya, et al., 2012) and they are blocked by procedures which attenuate the PD symptoms in humans (e.g. l-DOPA). This suggest that a blocking of the giant GABAergic currents could provide a new therapeutic strategy (Damier et al., 2016). Thus, in light of the previous results on the use of bumetanide in seizures and autism which is able to restore the hyperpolarizing GABA, Damier and colleagues in 2016 tested bumetanide in four PD patients (Damier et al., 2016). Interestingly, they found that the drug was able to ameliorate the motor symptoms in all four patients and the gait and freezing in two of them (Damier et al., 2016). Accordingly, a recent study showed that bumetanide was able to recover the altered GABAergic transmission and to attenuate the motor deficits in a PD mouse model (Lozovaya et al., 2018). Although bumetanide showed positive results in both the studies, further investigation is required to assess the direct involvement of the CCCs in this disorder.

5.2. Huntington disease

Huntington disease (HD) is an autosomal dominant neurodegenerative disease caused by the expansion of the trinucleotide CAG beyond 35 repeats in the *huntingtin* gene. The disease is characterized by involuntary movements, cognitive impairment and behavioral changes associated with degeneration of neurons in the striatum and in the cortex (Caron et al., 2018). Recent evidence indicates that an altered GABA signaling may underlie HD pathogenesis. In particular, HD mice showed altered expression of $GABA_AR$ and a reduced level of both KCC2 transcript and protein (Hsu et al., 2017), resulted in

depolarized E_{Cl} in HD mice. Interestingly, bumetanide administration rescued physiological GABAergic transmission and hippocampal-dependent learning and memory deficits (Dargaei et al., 2018) in the HD mice. A deeper investigation of the molecular mechanisms underlying the alteration of CCCs both in rodent models and in human could open avenue for the treatment of HD by rescue of intracellular Cl^- concentration.

5.3. Stroke and cerebral edema

Stroke is a condition characterized by poor blood flow into the brain, causing cell death. Strokes are classified in two main groups: hemorrhagic and ischemic. The latter group accounts for approximately 80% of the strokes (Donnan et al., 2008). In particular, ischemic strokes are caused by a reduction of the blood flow usually due to arterial occlusions. Given that brain metabolism is based almost exclusively on the glucose delivered by the blood, a reduction of blood flow rapidly causes metabolism failure and consequent tissue damage (Kahle, Simard, et al., 2009). Specifically, the lack of energy to maintain proper cell volume leads to cell swelling. This, causes ion imbalance, generating disruption of the BBB and trans-endothelial passage of fluid in the extracellular space. This fluid accumulation in the intracellular and extracellular spaces, even worsened when the cerebral flow is reestablished, causes the formation of cerebral edema which is the major cause of mortality following stroke (Kahle, Simard, et al., 2009). The first evidence of the involvement of NKCC1 in cerebral edema came from two studies in the early 2000s, where NKCC1 protein was found upregulated and phosphorylated in the brain of a rat model of focal cerebral ischemia/reperfusion, indicating high activation of this transporter (Yan et al., 2003; Yan et al., 2001). Interestingly, inhibition of NKCC1 by brain perfusion of bumetanide through microdialysis attenuated edema and neuronal death (Yan et al., 2003; Yan et al., 2001). Accordingly, NKCC1 KO mice showed less white and gray matter damage after focal brain ischemia (Chen et al., 2005). Moreover, bumetanide administration before middle cerebral artery occlusion in a rat model of stroke, attenuated edema formation by inhibiting the NKCC1 located in luminal part of the BBB (Foroutan et al., 2005;

O'Donnell et al., 2006; O'Donnell et al., 2004). There, NKCC1 is over-expressed and over-active possibly due to the activation of the MAP kinases p38 JNK, ERK1/2 and AMPK (Wallace et al., 2011; Wallace et al., 2012; Yuen et al., 2014). In addition, the combination therapy of bumetanide and glibenclamide (i.e. an inhibitor of the channel SUR1/TRPM4 critical mediator of cerebral edema), was suggested to obtain a synergic action by trying to optimize the tissue preservation and the vascular circuit (Simard et al., 2010; Walcott et al., 2012). Furthermore, a recent study demonstrated that bumetanide treatment increased neurogenesis and behavioral recovery in rats after experimentally induced stroke (Xu et al., 2017). Interestingly, also the inhibition of WNK3 kinase signaling in WNK3 KO mice, by reducing NKCC1 phosphorylation and expression, decreases cerebral edema and improves neurological recovery after ischemic stroke (G. Begum et al., 2015). Finally, also in diabetes-induced-stroke associated with hyperglycemia and in diabetic ketoacidosis, NKCC1 has been demonstrated to be involved in edema formation in rat models and again bumetanide administration was able to reduce the edema (Glaser et al., 2010; Lam et al., 2005; Yuen et al., 2008; Yuen et al., 2014).

5.4. Neuropathic pain and peripheral nerve injury

Neuropathic pain is a condition caused by damage to the central or peripheral nervous system and it is characterized by exaggerated pain sensation called hyperalgesia, pain in response to non-noxious stimuli called allodynia and abnormal sensations called dysesthesia. The first evidence of the involvement of the CCCs in neuropathic pain, came from early 2000s when an increased expression of NKCC1 and KCC2 was observed in dorsal root ganglia and spinal sensory neurons in an acute arthritis model of neuropathic pain, while in chronic arthritis only NKCC1 was found increased (Morales-Aza et al., 2004). Accordingly, bumetanide and furosemide showed an anti-nociceptive action in formalin-induce nociception in rats (Granados-Soto et al., 2005). Then, other studies further investigated the involvement of the two CCCs, finding seemingly contrasting results in diverse rodent models. For instance, it is transiently phosphorylated, but not up-regulated in mouse models of mechanical hyperalgesia induced by

capsaicin (Galan & Cervero, 2005). Accordingly, bumetanide administration reduced allodynia and hyperalgesia in capsaicin-treated rats (Valencia-de Ita et al., 2006). Conversely, Nomura and colleagues found a decreased KCC2 expression in formalin-induced acute nociception in rats indicating that KCC2 -rather than NKCC1- is involved in the first phases of hyperalgesia (Nomura et al., 2006). Accordingly, spinal cord injection of KCC2 antisense oligonucleotide in WT rats causes behavioral hypersensitivity comparable to hyperalgesia by decreasing KCC2 expression (W. Zhang et al., 2008).

Interestingly, different studies found increased expression of NKCC1 and a decreased expression of KCC2 in rodent models of neuropathic pain following spinal cord and peripheral nerve injury. Notably, bumetanide administration showed an anti-hyperalgesic action in most of the above studies (Cramer et al., 2008; Hasbargen et al., 2010; Lopez-Alvarez et al., 2015; Modol et al., 2014; Wei et al., 2013). Nevertheless, NKCC1 activation is required for the regeneration of the injured peripheral nerves (Modol et al., 2015; Pieraut et al., 2007), thus complicating the scenario of a possible therapeutic intervention. Moreover, in a recent work, Castro and colleagues found a transient and small change in E_{Cl} in mice with chronic injury of the trigeminal nerve, -a model of neuropathic pain- suggesting that the Cl^- imbalance may not be significantly involved in the mechanism underlying chronic pain. Hence, although a number of studies indicated an altered NKCC1/KCC2 ratio as a possible cause of the decrease in inhibitory tone implicated in neuropathic pain, further investigations are required to better elucidate the mechanism underlying the CCCs expression both in neuropathic pain and in nerve regeneration and their targeting as a possible therapeutic strategy.

6. Further considerations on Bumetanide

Bumetanide (chemically 3-(butylamino)-4-phenoxy-5-sulfamoylbenzoic acid; Figure 10), is a loop diuretic and it exerts this action by blocking NKCC2 in the ascending loop of Henle in the kidney. Bumetanide was developed in the ‘60s (Asbury et al., 1972; Ostergaard et al., 1972) and nowadays is

indicated for the treatment of edemas caused by congestive heart failure, acute pulmonary congestion, hepatic disease and renal disease (Flamenbaum & Friedman, 1982; Ward & Heel, 1984).

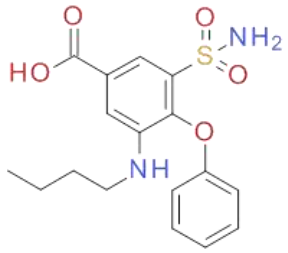

Figure 10: Structure of Bumetanide.

As discussed above, a fast-increasing number of recent studies have showed that bumetanide is able to recover several pathological phenotypes both in rodent models of brain disorders and in patients. This highlights the tremendous potential for repurposing (Strittmatter, 2014) of bumetanide in the treatment of a number of neurodevelopmental/neurological disorders. Nevertheless, there are still some open issues, which prevent bumetanide to become a solid therapeutic strategy for brain disorders.

First, being a potent diuretic, bumetanide causes hypokalemia, hypochloremia, metabolic alkalosis, hyperuricemia, and prerenal azotemia (Flamenbaum & Friedman, 1982) and indeed for instance in Italy it is currently only used in hospitals. Thus, the use of a strong diuretic to treat patients with severe behavioral impairments as in NDs or other neurological conditions may seriously jeopardize drug compliance during chronic, daily treatment, as for example required in a DS mouse model (Deidda, Parrini, et al., 2015). Moreover, NKCC2 is also expressed in vasopressinergic and oxytocinergic neurons in the hypothalamo-neurohypophyseal system and in the vestibular system, increasing the potential side effects of a chronic bumetanide treatment. In particular, bumetanide's negative effects on the auditory system have proved critical for the treatment of infants. Indeed, one clinical trial for the repurposing of bumetanide for the treatment of acute neonatal encephalopathy seizures was suspended due to induced deafness in some treated subjects (Ben-Ari et al., 2016). Second, a number of studies highlighted bumetanide's poor blood-brain barrier penetration (Brandt et al., 2010; Cleary et al., 2013; Puskarjov, Kahle, et al., 2014; Tollner, Brandt, Romermann, et al., 2015; Topfer et al., 2014) and recent

investigations considered bumetanide's low levels in the brain after systemic administration as incompatible with NKCC1 inhibition, thus questioning the brain expressed-NKCC1 as the target of bumetanide in ND (Romermann et al., 2017; S. Wang et al., 2015).

Thus, although bumetanide has shown positive outcomes in the treatment of core symptoms of a number of neurological disorders, the effectiveness of NKCC1 as a molecular target for these conditions, and the mechanism of bumetanide action need to be further investigated and confirmed. This would be a pre-requisite for any drug discovery effort aimed at finding new NKCC1 inhibitors devoid of all of the bumetanide's shortcomings.

7. NKCC1 is a valuable target to rescue cognitive impairment in DS

Although preclinical studies on animal models and clinical trials as well as case studies indicate positive outcomes of bumetanide treatments on several brain disorders, so far its putative mechanism/target has not yet been clarified. Other members of the Cancedda laboratory have tried to address this issue at least for DS. In particular, to support previous finding on the positive effect of chronic bumetanide on cognitive impairment in a mouse model of DS (Deidda, Parrini, et al., 2015) and to demonstrate NKCC1 as a potential molecular target for new therapeutic approaches members of the Cancedda laboratory (unpublished data) has recently investigated the effectiveness of a RNA interference-based NKCC1 downregulation in rescuing cognitive impairment in DS mice. In particular, they used artificial microRNAs, cloned into a lentiviral vector (AAV9), to knockdown (KD) NKCC1 in Ts65Dn mice. After confirming that NKCC1 downregulation by viral infection was able to restore the physiological Cl^- concentration and the inhibitory GABA transmission in cultured trisomic neurons, they have tested whether the specific KD of NKCC1 by a single viral injection in the hippocampus was able to rescue learning and memory deficits in adult Ts65Dn mice. Four weeks post injection, they found a complete rescue of cognitive performance of Ts65Dn mice in comparison to WT mice in four independent tests. Thus, although the mechanism of action of bumetanide has still not been clarified yet, these results have altogether clearly identified NKCC1 as potential molecular target for Down syndrome. Hence, a

compound which can selectively inhibit NKCC1, and thus devoid of the side effects of bumetanide, could represent a valuable therapeutic strategy for DS and possibly the other neurological disorders characterized by impaired Cl^- homeostasis and depolarizing GABAergic transmission.

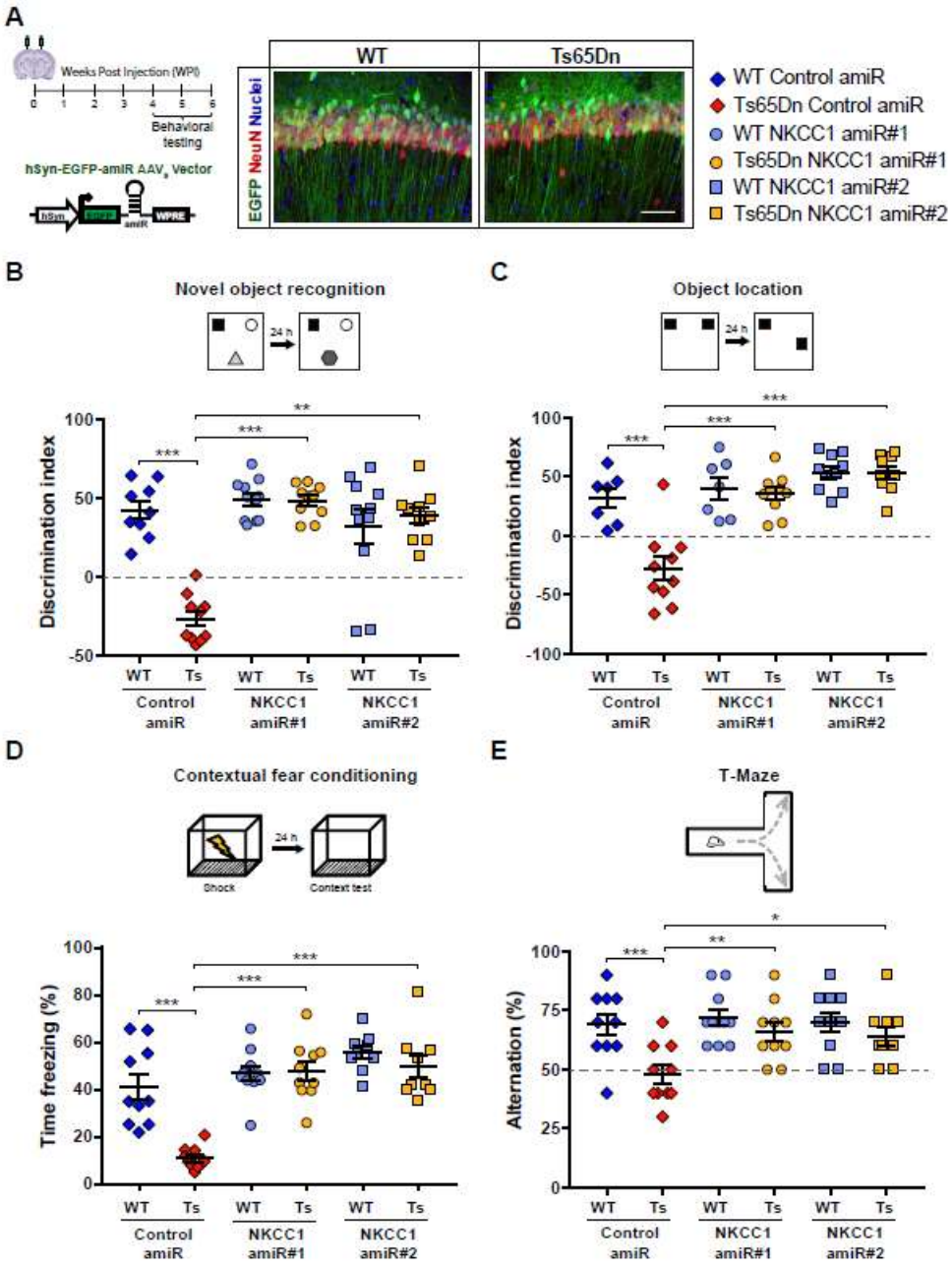

Figure 11. A) Left: schematic cartoon of the experimental protocol for viral injection to knock down NKCC1 in WT and Ts65Dn mice and the consequent behavioral analysis**. Right:** examples images of WT and Ts65Dn hippocampi injected with lentiviral vector (in green) encoding for two different miRNA knocking down NKCC1 expression. **B-E)** Effect of knock down of NKCC1 in novel object recognition (B), object location (C), contextual fear conditioning (D) and T- maze (E) tasks. Unpublished data of other members of the Cancedda laboratory.

Aim of the project

Several lines of evidence indicate impaired Cl^- homeostasis by dysregulation of NKCC1/KCC2 expression ratio or function as a potential causal mechanism underlying the phenotypic manifestation of a number of neurological disorders. Interestingly, many preclinical studies, clinical case studies and clinical trials point to a valuable therapeutic approach to restore physiological Cl^- homeostasis to treat neurologic patients with a known diuretic drug (bumetanide), which can be readily repurposed in humans. Although bumetanide provides an invaluable pharmacological tool for a quick assessment -directly in patients- of the positive effects of blocking NKCC1 activity, its extensive usage may be hampered by its diuretic and other side effects due to inhibition of the kidney transporter NKCC2. In particular, excessive diuresis may jeopardize the compliance with chronic treatment by patients with serious conditions, often characterized by cognitive issues as in DS and ASD. Moreover, its poor BBB penetration questioned brain-expressed NKCC1 as an effective target and opened debates about the real mechanism of action of bumetanide in neurological disorders. Nevertheless, recent findings from our lab demonstrated that specific knockdown of NKCC1 was able to restore physiological Cl^- concentration and GABAergic transmission in trisomic neurons *in vitro*, and learning and memory in the Ts65Dn mouse model of DS. These results identified NKCC1 as a targetable molecule for treating Down syndrome and possibly other neurological disorders characterized by aberrant Cl^- homeostasis.

This project aims at discovering novel compounds able to modulate GABAergic activity through the *selective* inhibition of the Cl^- importer NKCC1, thus being devoid of unwanted diuretic and related side effects associated to the unfavorable inhibition of the cognate, kidney-specific, NKCC2 transporter.

Results

1. Setup of a functional NKCC-transporter assay: the chloride assay

To screen *in vitro* the new compound efficiency in blocking NKCC1 and NKCC2, we setup a functional NKCC transporter assay. This is based on the detection of the variation of Cl^- ion concentration in the cell through a Cl^- sensitive membrane-tagged yellow fluorescent protein (mbYFPQS, Addgene). mbYFPQS fluorescence is inversely dependent on the concentration of Cl^- inside the cell. In particular, the assay consists of monitoring the variation of fluorescence intensity in HEK293 cells transfected with NKCC1, NKCC2 or the empty plasmid (as control-mock), loaded with mbYFPQS and maintained in a Cl^- free-hypotonic solution. Upon application of NaCl in the bath, Cl^- ions enter into cells by NKCC1 and NKCC2 transport and bind mbYFPQS, thus determining a fluorescence decrease. Therefore, in this assay, one can indirectly estimate Cl^- transporter activity by mbYFPQS fluorescence variations.

First, we evaluated transfection efficiency in our experiments by assessing the expression of NKCC1 or NKCC2 in HEK293-transfected cells in comparison to the control-mock by western blot analysis (Figure 12).

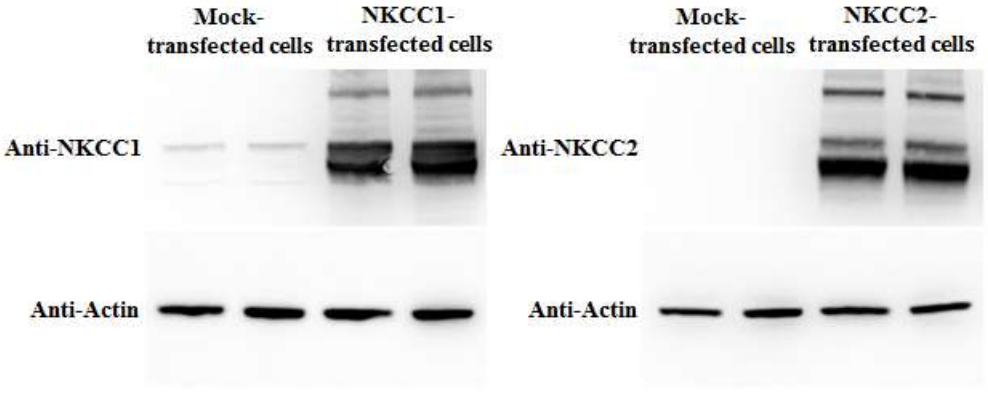

Figure 12: Western blot analysis of the expression of NKCC1 (Left) and NKCC2 (right) in untransfected (mock) and NKCC1- or NKCC2-transfected HEK293 cells. Transfection of NKCC1 or NKCC2 plasmids results in a high expression of the related protein in comparison to the mock-cells transfected with the empty plasmid.

As a first step of the assay validation, we evaluated whether the transfected transporters were functionally active. We collected 80 secs of fluorescence baseline in cells transfected with control plasmid, NKCC1 or NKCC2. Upon application of 444 mM of NaCl, we assessed fluorescence intensity for another 60 secs. During this period, we observed a fluorescence decrease in the transfected cells in comparison to the non-transfected ones, which is indicative of NKCC1 and NKCC2 activities (Figure 13). For the representation of the fluorescent traces in time (Figure 13, left), we normalized the fluorescence value for each time point to the average of the fluorescence value of the first 20 sec of baseline. For quantification of average effects as we represented by the bar plots (Figure 13, right), we expressed the decrease in fluorescence upon NaCl application as the average of the last 10 secs of fluorescence again normalized to the baseline before NaCl application.

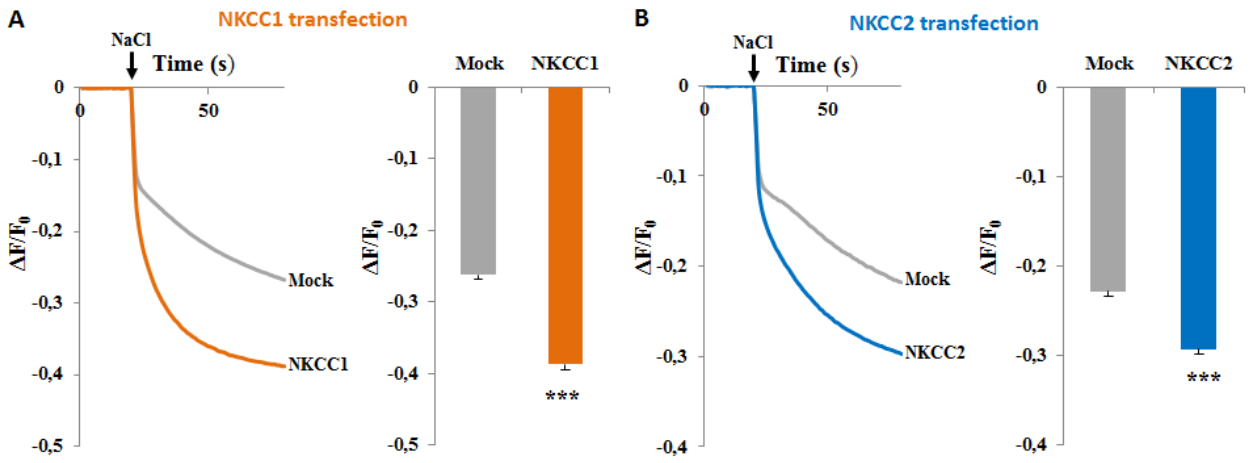

Figure 13 A) Left: example traces obtained in the chloride assay on untransfected (mock) or NKCC1- transfected HEK293 cells. The arrow indicates the addition of NaCl (final concentration 74 mM) used to initiate the flux of chloride. **Right**: quantification of the fluorescence decrease upon the NaCl application in the untrasfected (mock) or NKCC1-transfected HEK293 cells. **B) Left**: example traces obtained in the chloride assay on untransfected (mock) or NKCC2- transfected HEK293 cells. The arrow indicates the addition of NaCl (final concentration 74 mM) used to initiate the flux of chloride. **Right**: quantification of the fluorescence decrease upon the NaCl application in the untransfected (mock) or NKCC2-transfected HEK293 cells. Data represents mean ± sem from 15 independent experiments. *** $p<0.001$ Mann-Whitney Rank Sum Test

To further validate the Cl assay in HEK293 cells, we next monitored the fluorescence in mock, NKCC1 and NKCC2-transfected cell treated with DMSO (0.1%-1%) as control or with the known inhibitors of NKCC1 and NKCC2 (bumetanide and furosemide). As shown in figure 14, pre-incubation at two different concentrations (10 µM, 100 µM) with bumetanide or furosemide significantly reduced the decrease in fluorescence in mock, NKCC1- and NKCC2 -transfected cells, indicative of a reduced ion flux and thus transporter inhibition. Notably, the decreased fluorescence observed also in the mock-transfected cells treated with bumetanide and furosemide indicates that HEK293 cells express endogenous Cl^- transporters (including NKCC1 observed in western blot analysis), which are bumetanide/furosemide sensitive. Thus, we setup a normalization of the fluorescence values that could exclude the contribution of Cl^- changes dependent on transporters/receptors other than NKCC1 or NKCC2. In particular, we subtracted the $\Delta F/F_0$ value obtained from mock-transfected cells (either control or treated) to the respective $\Delta F/F_0$ value obtained from the cells transfected with NKCC1 or NKCC2. We then presented in the figures all the data as a percentage of the fluorescence decrease *vs* the value of the control DMSO.

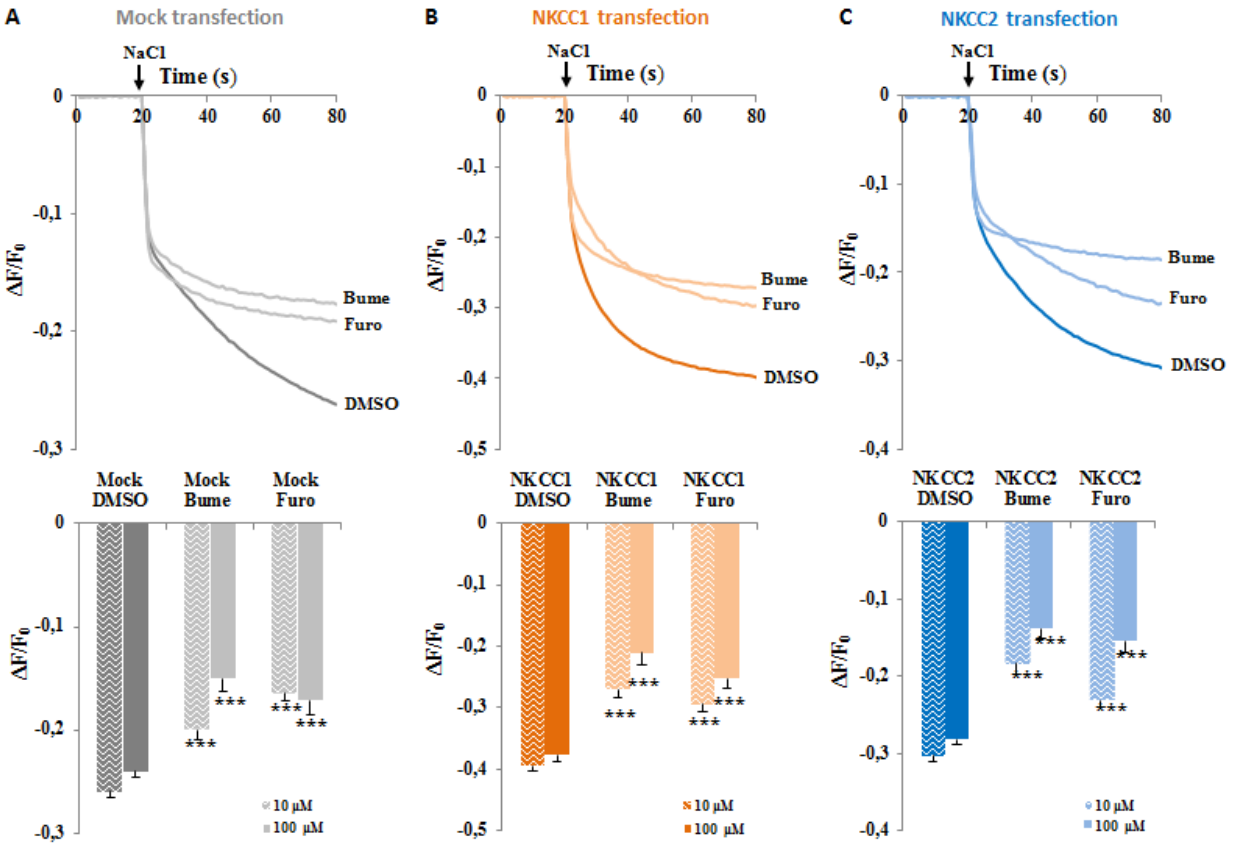

Figure 14. A) Top: example traces obtained in the chloride assay on untransfected (mock) HEK293 cells treated with DMSO as negative control, bumetanide (Bume) and furosemide (Furo) as positive controls. **Bottom**: quantification of the fluorescence decrease upon the NaCl application in mock-transfected HEK293 cells treated with DMSO, bumetanide and furosemide. **B) Top**: example traces obtained in the chloride assay on NKCC1-transfected HEK293 cells treated with DMSO as negative control, bumetanide (Bume) and furosemide (Furo) as positive controls. **Bottom:** quantification of the fluorescence decrease upon the NaCl application in NKCC1-transfected HEK293 cells treated with DMSO, bumetanide and furosemide. **C) Top**: example traces obtained in the chloride assay on NKCC2-transfected HEK293 cells treated with DMSO as negative control, bumetanide (Bume) and furosemide (Furo) as positive controls**. Bottom**: quantification of the fluorescence decrease upon the NaCl application in NKCC2-transfected HEK293 cells treated with DMSO, bumetanide and furosemide. Data represents mean ± sem from 5 independent experiments. *** p<0.001 Kruskal-Wallis One Way Analysis of Variance on Ranks, Dunn's *post hoc* test

2. Design, synthesis and testing of novel bumetanide analogues

To decipher among the structural and chemicophysical properties of bumetanide what the responsible for the inhibition of NKCC1 *vs* NKCC2 are, we designed and synthesized novel bumetanide analogues. This strategy provided information that allowed building an informative structure-activity relationship. This in turn, provided highlights into what is indeed essential for selective NKCC1 inhibition.

We developed a synthetic strategy to obtain a number of novel bumetanide analogs, which bear modifications at different anchor points of bumetanide's core scaffold (Figure 15). Based on the 3-amino-4-phenoxy-5-sulfamoil-benzoic acid core of bumetanide, we explored the implication of the substituents in positions R1, R3 and R5, by medicinal chemical efforts coupled with a systematic analysis of the newly synthesized compounds' ability to inhibit NKCC1 or NKCC2. We synthesized 19 new compounds analog to bumetanide.

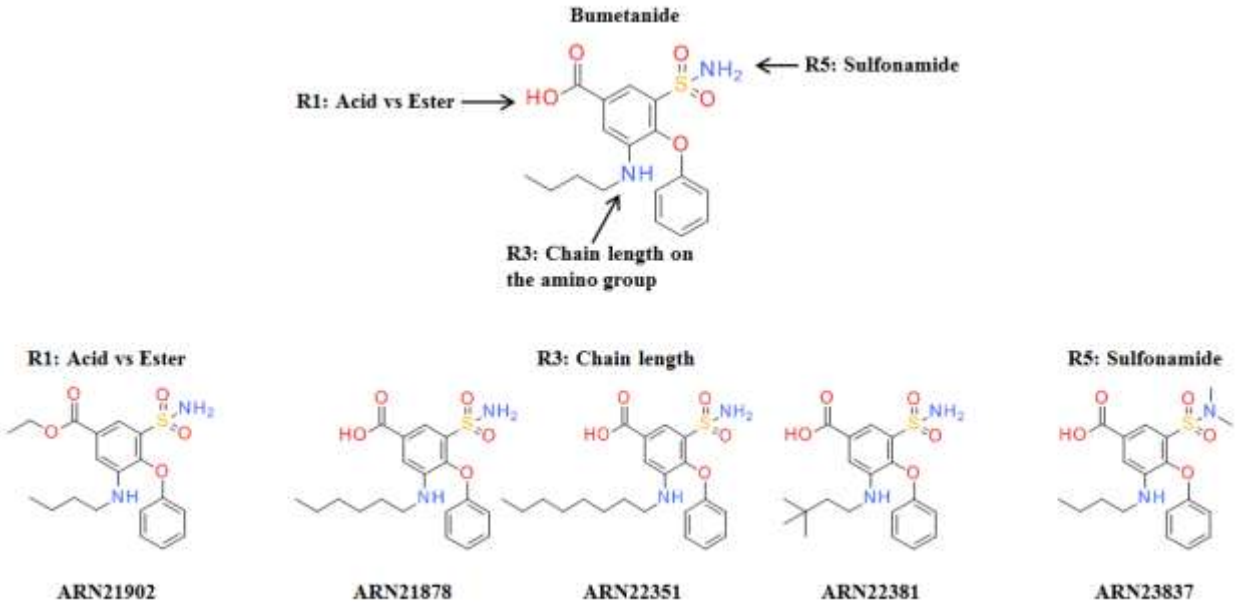

Figure 15. Structures of bumetanide and close analogues. **Top**: Schematic representation of the point of intervention in the bumetanide structures to synthesize 5 novel bumetanide analogues. **Bottom**: Structures of the five bumetanide analogues. ARN21902 was synthesized by substituting the acid with the ester; ARN21878, ARN22351 and ARN22381 show modification in the carbon chain on the amino group: ARN21878 and ARN22351 have a longer chain, ARN 22381 show a bulker chain. ARN22837 show dimethylation in the sulfonamide.

Then, we tested (by the chloride assay in HEK293 cells) the inhibitory activity of the new analogues and compared it to that of bumetanide and furosemide (as positive controls). We normalized the data as described above, and expressed them as % of inhibition *vs* DMSO-treated cells. As shown in figure 16, bumetanide inhibited NKCC1 at a 58.8 ± 5.6 % and NKCC2 at 82.7 ± 20.4 % at 10 μM, and NKCC1 at 71.7 ± 7 % and NKCC2 at 80.5 ± 9 % at 100 μM. Consistent with the literature indicating effective NKCC

inhibition only at high concentration (Ramsay et al., 1978), furosemide did not show a significant inhibition of NKCC1 or NKCC2 at 10 μM, but inhibited NKCC1 at 56.3 ± 6 % and NKCC2 at 57.2 ± 10.2 % at 100 μM. Then, we tested the newly synthesized compounds for NKCC1 and NKCC2 inhibitory activity. ARN21902, which bears an ester moiety in R1, displayed a complete loss in activity against both NKCC1 and NKCC2, indicating that the acidic group in R1 is fundamental to maintain activity against the two CCCs. Interestingly, the elongation of the carbon chain on the amino group in R3 determined a gain in selectivity toward NKCC1 compared to bumetanide. Indeed, both ARN21878 (*n*-hexyl chain) and ARN22351 (*n*-octyl chain) did not inhibit NKCC2 at 10 μM and inhibit NKCC2 at 61.9 ± 9,1 % (ARN21878) and 32.9 ± 11.55 % (ARN22351) at 100 μM, which was smaller than the 80.5 ± 9 % inhibition of bumetanide. Nevertheless, these compounds also showed a loss in potency against NKCC1 at 10 μM when compared to the 58.8 ± 5.6 % of inhibition of bumetanide, but maintained a good inhibition of NKCC1 at 100 μM of 90 ± 9.7 % (ARN21878) and ~ 22.4 ± 4.8 % (ARN22351), when compared to the 82.7 ± 20.4 % of inhibition of bumetanide. Conversely, preserving the C4 butyl chain length, with the insertion of terminal bulky 3,3-dimethylbutyl element in R3 (ARN22381) determined a loss of activity against NKCC1 at 10 μM, but maintained a 126 ± 6.9 % inhibition at 100 μM . When tested against NKCC2, ARN22381 exhibited a good inhibition both at 10 μM (48.4 ± 8.3 %) and at 100 μM (81.7 ± 7.1%), when compared to bumetanide's activity (82.7 ± 20.4 % at 10 μM; 80.5 ± 9 % at 100 μM). To investigate the role of the sulfonamide in R5, we synthesized a dimethylamino derivative (ARN23837). Strikingly, the switch from H-bond donor (HBD) / H-bond acceptor (HBA) of bumetanide to HBA of the sulfonamide of ARN23837 determined a complete loss of activity against NKCC2, still maintaining inhibition of NKCC1 at 100 μM (22.4 ± 6.7 %). Nevertheless, also in this case, the new compound lost efficacy of inhibition when compared to bumetanide (80.5 ± 9 %).

Thus, the synthesis and testing of the close derivatives of bumetanide allowed us to decipher some structural motifs which could decrease the activity against NKCC2 (i.e., elongation of the carbon chain in R3 and the dimethylation of the sulfonamide in R5. Nevertheless, none of the compounds exerted a

markedly higher NKCC2/NKCC1 selectivity, confirming data from the literature on other bumetanide analogues (Lykke et al., 2016). Altogether, these data suggest a large difficulty, to develop bumetanide derivatives with higher selectivity for NKCC1 *vs* NKCC2 than bumetanide (Lykke et al., 2016). Thus, we decided to seek new molecular entities, structurally unrelated to bumetanide, to find novel selective NKCC1 inhibitors without the unwanted effect on NKCC2. In directing our search, we nevertheless took advantage of the knowledge acquired from the experiments on bumetanide's analogues.

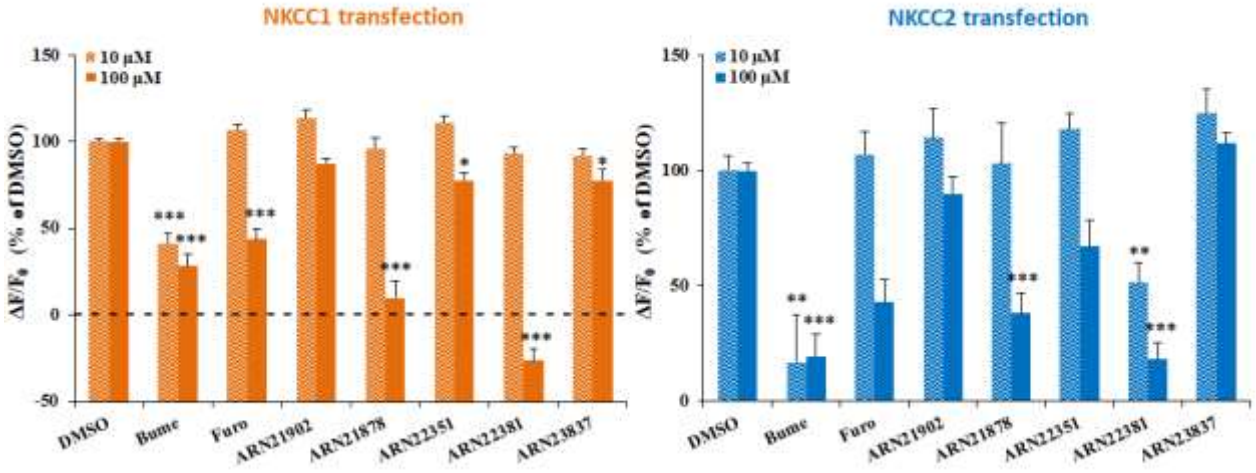

Figure 16. **Left**: quantification of the inhibitory activity of bumetanide (Bume 10, 100 µM) and furosemide (Furo 10, 100 µM) as positive controls and bumetanide analogues ARN21902, 21878, 22351, 22381 and 23837 (10, 100 µM). in NKCC1-transfected HEK293 cells. Data are presented as a percentage of the respective control DMSO. Data represents mean ± sem from 4 independent experiments. * P<0.05, *** P<0.001 Kruskal-Wallis One Way Analysis of Variance on Ranks , Dunn's *post hoc* test. **Right**: quantification of the inhibitory activity of bumetanide (Bume 10, 100 µM) and furosemide (Furo 10, 100 µM) as positive controls and bumetanide analogues ARN21902, 21878, 22351, 22381 and 22837 (10, 100 µM). in NKCC2-transfected HEK293 cells. Data are presented as a percentage of the respective control DMSO. Data represents mean ± sem from 3 independent experiments. * P<0.05, ** P<0.01, *** P<0.001 Kruskal-Wallis One Way Analysis of Variance on Ranks , Dunn's *post hoc* test.

3. Identification of *novel* hits that selectively block NKCC1

3.1 Screening from libraries

Through the application of a ligand-based computational strategy, applied to bumetanide and other known analog compounds (i.e. furosemide, asozemide, piretanide, chlorithiazide) with activity against the target

protein NKCC1, we identified a few key structural and chemicophysical properties that are shared among bumetanide and the other compounds. In particular, we built a preliminary pharmacophore model and we used it as a filter for the virtual screening of the proprietary chemical collection available at the D3 Department at IIT (Figure 17). This library contains a diverse and non-redundant set of ~15,000 molecules readily available for experimental testing. In a first set of experiments, we used the ligand-based to select 165 new compounds from the IIT library, which we tested for their ability to inhibit NKCC1 in the chloride assay in HEK293 cells. Among these compounds, 20% showed an NKCC1 inhibition ranging between 5%-10% at 10 µM, while the other 80% did not show any activity. Then, starting from the chemical structure of the active compounds, we refined the initial pharmacophore model and we performed a second and more specific screening of the D3's chemical collection, and chemical libraries from commercial vendors (Life chemicals and ZINC). In this second set of experiments, we selected 90 compounds (Figure 17, maroon).

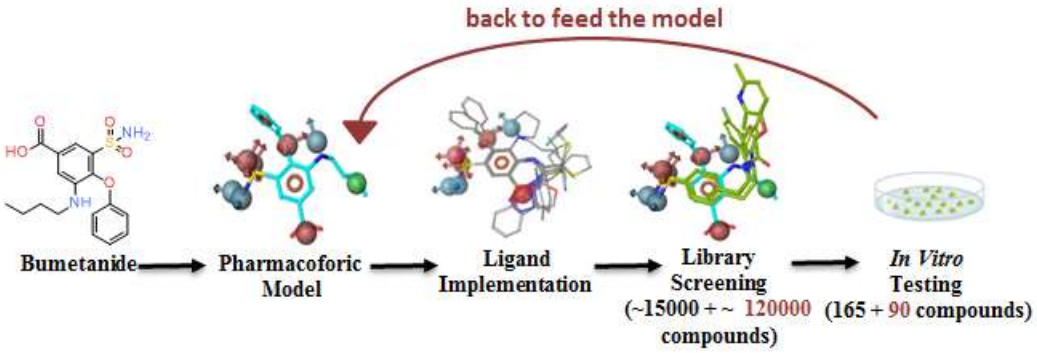

Figure 17. Using the structure of bumetanide and several close analogues, we designed a pharmacophore model with the key geometric and physicochemical features needed for activity. This model was used for the preliminary screening of the D3 internal library of small molecules. After the first screening of 167 compounds, we refined the pharmacophoric model to screen chemical libraries from commercial vendors, from which we selected 86 compounds to be tested *in vitro*.

Among these 90 compounds, only two showed a significant (although moderate) inhibitory activity against NKCC1 when tested in the Cl assay on HEK293 cells. In particular, two structurally related 2-amino-5-nitro-benzenesulfonamide (Figure 18) derivatives diversified for the substituent on the amino group, emerged as promising hit compounds. ARN22393, with a *n*-hexyl chain on amino group and a methylated

sulfonamide, showed a significant inhibition of NKCC1 of 29.4 ± 2.8 % at 100 µM. ARN22394, with a 3,3-dimethylbutyl chain on the amino group and a methylated sulfonamide, showed a significant inhibition of NKCC1 of 17.7 ± 3.9 % at 10 µM and of 28.6 ± 4.3 % at 100 µM. Although promising, the two compounds still showed low potency in NKCC1 inhibition compared to bumetanide. Thus, ARN22393 and ARN22394 were utilized as a starting point for the design and synthesis of new and more potent derivatives.

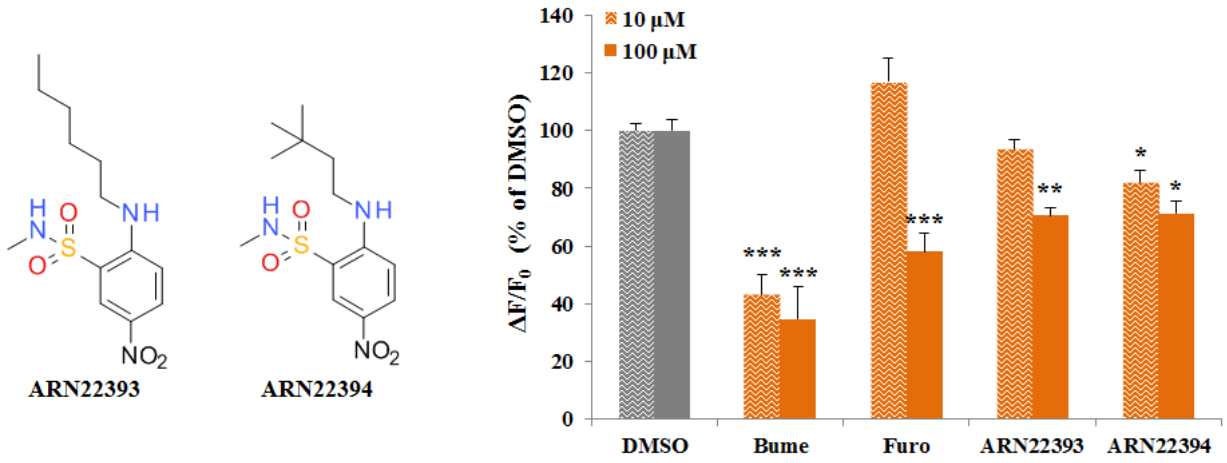

Figure 18. Left : Chemical structure of the compounds ARN22393 and ARN22394 obtained from the screening of pre-existing compound libraries. **Right:** Quantification of the inhibitory activity of bumetanide (Bume 10, 100 µM) and furosemide (Furo 10, 100 µM) as positive controls and ARN22393(10, 100 µM) and ARN22394 (10, 100 µM) obtained from the libraries screening in NKCC1-transfected HEK293 cells. Data are presented as a percentage of the respective control DMSO. Data represents mean ± sem from 3 independent experiments. * P<0.05, ** P<0.01, *** P<0.001 Kruskal-Wallis One Way Analysis of Variance on Ranks , Dunn's post hoc test.

3.2 Synthesis of new molecular entities

Based on the chemical core of ARN22393 and 22394, we synthesized 43 new compounds, which we tested in the chloride assay on HEK293 cells. Two main scaffolds were generated based on the substituents in position 1 of the aromatic ring: (**a**) a 2-amino-5-nitro-benzene-sulfonamide and (**b**) a 4-amino-3-sulfamoyl-benzoic acid (Figure 18). In particular, we compared the nitro group with the more drug-like carboxylic acid, which we demonstrated to be fundamental for the inhibition of the CCCs, and is predicted to confer to the new compounds higher balance between potency and solubility (Figure 19).

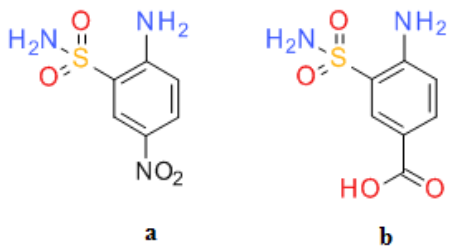

Figure 19. Chemical structure of the two scaffolds based on the substituents in position 1 of the aromatic ring: (**a**) 2-amino-5-nitro-benzenesulfonamide and (**b**) 4-amino-3-sulfamoyl-benzoic acid. From the manipulation of these two scaffolds, we generated 43 new compounds.

Although we synthesized and tested in the Cl- assay 12 new 2-amino-5-nitro-benzenesulfonamides (a), none of them exhibited enhanced potency in NKCC1 inhibition in comparison to the hit compounds (ARN22393 and ARN22394). In addition, low solubility issues burdened the 2-amino-5-nitro-benzenesulfonamide scaffold, and we halted the further synthetic efforts towards its investigation. Conversely, benzoic acid derivatives emerged as the best class in terms of potency when compared to nitrobenzenes. In particular, we performed numerous manipulations on this class by adding the structural motifs emerged from the screening of the bumetanide analogues (i.e.,the dimethylated sulfonamide and the *n*-octyl carbon chain on the amino group). Benzoic acid derivatives bearing the *n*-octyl substituent showed enhanced potency when compared to the shorter chain derivatives. In particular, ARN22642, characterized by a methyl sulfonamide and an *n*-octyl chain on the amino group significantly inhibited NKCC1 of 35.4 ± 17.3 % at 100 μM, although it did not show significant activity at 10 μM (Figure 20). Interestingly, when this modification was combined with dimethylation of the sulfonamide, the resulting derivative (ARN22430) exerted high inhibition, significantly increasing the activity to 70.6 ± 9.1 % at 100 μM, but still did not significantly inhibit NKCC1 at 10 μM (Figure 20).

Next, we tested ARN22642 and ARN22430 for their solubility and their preliminary absorption-distribution-metabolism-excretion (ADME) properties (Figure 20B), by assessing their half-life in mouse plasma and mouse liver homogenates (microsomes). We found that both compounds showed low solubility. Moreover, although they showed protracted half-life in mouse plasma (>60 mins), they

displayed very short half-life in mouse microsomes (12 mins ARN22642 and 13 mins ARN22430). To overcome this issue, we tried to protect the terminal methyl of the *n*-octyl carbon chain (the most eligible point of metabolism) by adding different substituents. In particular, we tested the bioisostheric trifluoromethyl group, which is widely used in medicinal chemistry to ameliorate properties of promising compounds (Studer, 2012). The resulting terminal trifluoromethylated analogue (ARN23746) showed a substantial improvement in solubility (> 250 μM) and a longer half-life both in mouse plasma (> 120 mins) and in mouse microsomes (> 60 mins). Moreover, ARN23746 showed an increased potency displaying an NKCC1 inhibition of 37.1 ± 5 % at 10 μM, which is comparable to bumetanide's activity of 51 ± 4.2 % (Figure 20 D). Moreover, ARN23746 inhibited NKCC1 of 88.5 ± 11.7 % at 100 μM in comparison to 71 ± 6 % inhibitory activity of bumetanide (Figure 19 C-D). Thus, by applying the information collected from data derived from bumetanide's derivatives, we found three new compounds (ARN22642, ARN22430, and ARN23746) able to efficiently inhibit NKCC1. We thus characterized these three compounds extensively for their *in vitro* activity and specificity.

A

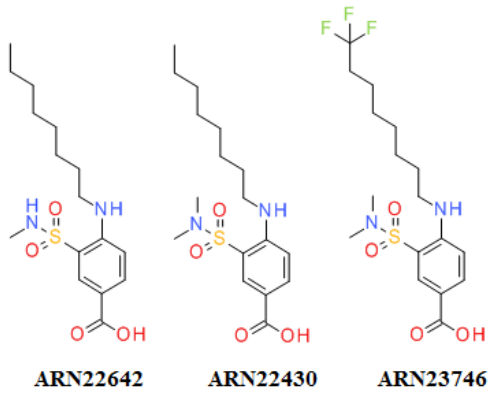

B

ARN	Kinetic solubility PBS pH 7.4	$t_{1/2}$ plasma (mouse)	$t_{1/2}$ liver microsomes (mouse)
ARN22642	53 µM	> 60 mins	12 mins
ARN22430	52 µM	> 120 mins	13 mins
ARN23746	> 250 µM	> 120 mins	> 60 mins

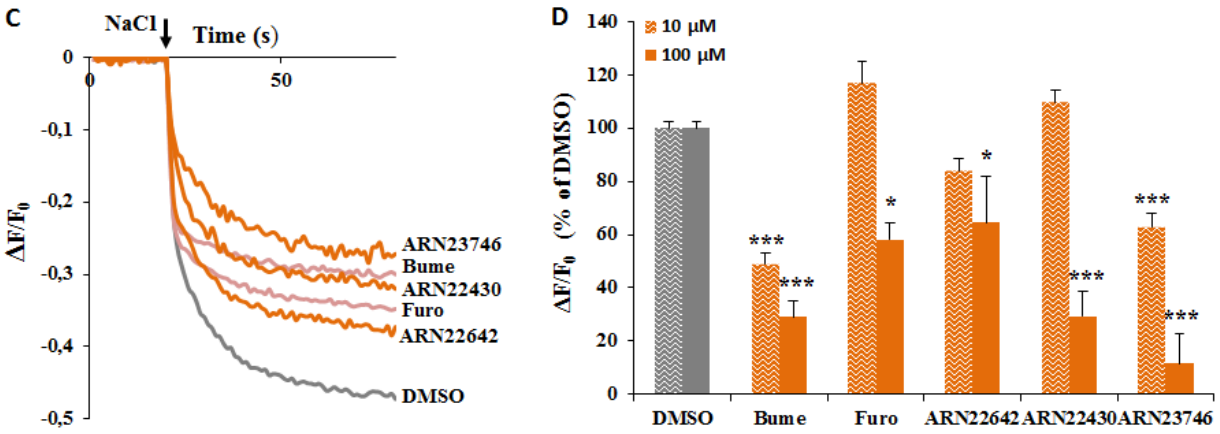

Figure 20. A) Chemical structures of the compounds ARN22642, ARN22430 and ARN23746 obtained from the manipulation of the scaffold in Figure 18. **B)** Table showing the ADME properties of ARN22642, ARN22430 and 23746. **C)** Examples traces obtained in the chloride assay on NKCC1-transfected HEK293 cells treated with DMSO as negative control, bumetanide (Bume) and furosemide (Furo) as positive controls, and ARN22642, ARN22430 and ARN23746 (100 µM of each compound in these examples). **D)** Quantification of the inhibitory activity of bumetanide (Bume 10, 100 µM) and furosemide (Furo 10, 100 µM) as positive controls and ARN22642 (10, 100 µM), ARN22430 (10, 100 µM) and ARN23746 (10, 100 µM) in NKCC1-transfected HEK293 cells. Data are presented as a percentage of the respective control DMSO. Data represents mean ± sem from 3 independent experiments. *P<0.05, ** P<0.01, *** P<0.001 Kruskal-Wallis One Way Analysis of Variance on Ranks , Dunn's *post hoc* test.

4. Set up of Calcium kinetic assay and testing of the three most promising compounds

To further confirm the activity on NKCC1 of the 3 novel molecular entities (ARN22642, ARN22430, ARN2376), we tested their ability to revert the depolarizing GABA signaling in young neurons, indirectly measured as calcium influx into the cells with an *in vitro* calcium kinetic assay in primary neuronal cultures. This assay takes advantage of the physiological, endogenous, high-expression of NKCC1 in immature neurons, which causes depolarizing actions of GABA, able to activate voltage-gated Ca^{2+}

channels. Thus, in immature neurons, a compound that blocks NKCC1 is predicted to inhibit Ca^{2+} responses upon GABA application (Figure 21).

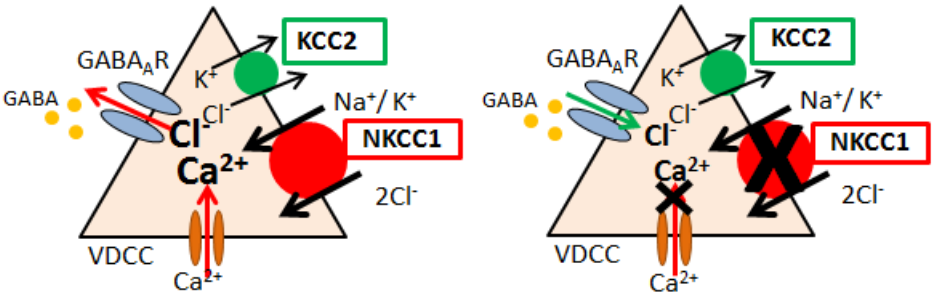

Figure 21. Schematic representation of the calcium kinetic assay performed in primary neuronal cultures. Left: physiological high-expression of NKCC1 in immature neurons causes depolarizing GABA transmission, which activates voltage-gated Ca^{2+} channels determining a calcium influx. Right: in immature neurons, a compound that blocks NKCC1 is predicted to reduce the GABA depolarizing action, thus inhibiting Ca^{2+} responses upon GABA application.

We cultured hippocampal immature neurons for 3 days *in vitro* (3DIV) and loaded them for 15 min with a calcium-sensitive dye (Fluo4, Invitrogen) in extracellular solution. Then, we treated the neurons with bumetanide and furosemide (as a positive control) or each of our 3 best compounds diluted in extracellular solution for 15 min. As a functional readout, we monitored the level of fluorescence in the neuronal cultures pretreated with bumetanide, furosemide or our new compounds (ARN22642, ARN22430, ARN2376) upon application of GABA (100 µM, for 20 sec). To test for neuronal viability, we applied KCl (90 mM, for 40 sec) after GABA treatment. Indeed, KCl strongly depolarizes neurons causing high activation of voltage-gated Ca^{2+} channels in live cells, which can be taken as an indication of cell viability. To quantify the effect of bumetanide and our new compounds on NKCC1 inhibition, we thus normalized the fluorescence values upon GABA application to the fluorescence levels after KCl application in treated neurons. As shown in figure 22, all tested compounds significantly reduced the increase in fluorescence upon GABA application in comparison to DMSO-treated controls, without affecting the fluorescence level upon KCl application. In agreement with the chloride assay, bumetanide displayed an inhibition of calcium entry of 51.9 ± 2.3 % at 10 µM and 54.7 ± 2.5 % at 100 µM, and ARN23746 displayed an inhibition of 45.7 ± 4.3 % at 10 µM and 92.8 ± 1.9 % at 100 µM. Surprisingly,

in this assay, furosemide, ARN22642 and ARN22430 showed a significant activity also at 10 µM. In particular, furosemide showed an inhibition of calcium entry of 36.3 ± 3 % at 10 µM and 62.4 ± 2.8 % at 100 µM, ARN22642 inhibited calcium entry of 18.6 ± 5.3% at 10 µM and 46.3 ± 3.7% at 100 µM, and ARN22430 inhibited calcium entry of 44.8 ± 4.1 % at 10 µM and 76 ± 8.8 % at 100 µM.

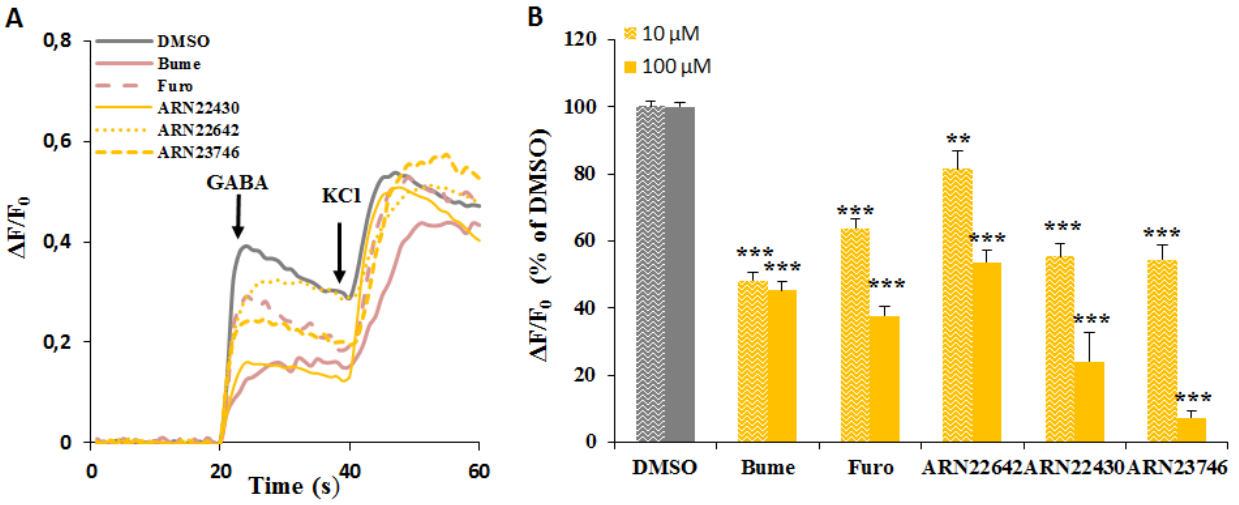

Figure 22. A) Example traces obtained in the calcium kinetic assay on 3DIV neurons. The arrow indicates the addition of GABA (final concentration 100 µM) and KCl (90 mM) used to evaluate the cell viability (100 µM of each compound in these examples) **B)** Quantification of effect of Bumetanide (Bume 10, 100 µM), Furosemide (Furo 10, 100 µM),ARN22642, ARN22430 and ARN23746 (10, 100 µM) in the calcium kinetic assay on 3 DIV neurons. Data are resented as a percentage of the control DMSO. Data represents mean ± sem from 3 independent experiments. ** P<0.01, *** P<0.001 Kruskal Wallis one-way ANOVA, Dunn's *post hoc* test.

Thus, although the new molecular entities were able to significantly reduce the GABA depolarizing signaling in young neurons, the seeming inconsistency of the activity of furosemide, ARN22642 and ARN22430 between the chloride assay and the calcium assay, required further investigation.

5. Electrophysiological recordings of GABA currents

To better clarify the high efficiency of furosemide, ARN22642 and 22430 to inhibit Ca^{2+} responses upon GABA application, in comparison to the moderate inhibition of NKCC1 in the chloride assay, we measured the ability of these compounds to inhibit $GABA_AR$. Indeed, the inhibition in Ca^{2+} responses measured in the calcium assay, could be explained by a strong NKCC1 inhibition, but also by a possible

direct antagonism of $GABA_A$ receptors. Interestingly, it is known that furosemide, antagonizes the $GABA_A$ receptor in cerebral cortex and cerebellum (Korpi et al., 1995; Korpi & Luddens, 1997; Minier & Sigel, 2004). Thus, we measured the amplitude of evoked $GABA_A$ currents after application of bumetanide (as a negative control), furosemide (as a positive control), ARN22642, ARN22430 and ARN23746. As concentration we chose 10 µM to detect even small inhibitory efficacy of the drugs. As shown in Figure 23, bumetanide and ARN23746 did not alter $GABA_A$-current amplitude. Conversely, furosemide showed 19.4 ± 5 % reduction in the $GABA_A$-current amplitude, in agreement with the literature. Notably, ARN22430 showed a significant inhibition of GABA current of a 20.6 ± 2.6 % and ARN22642 showed a moderate, but not significant reduction of GABA current of 8.6 ± 5 %.

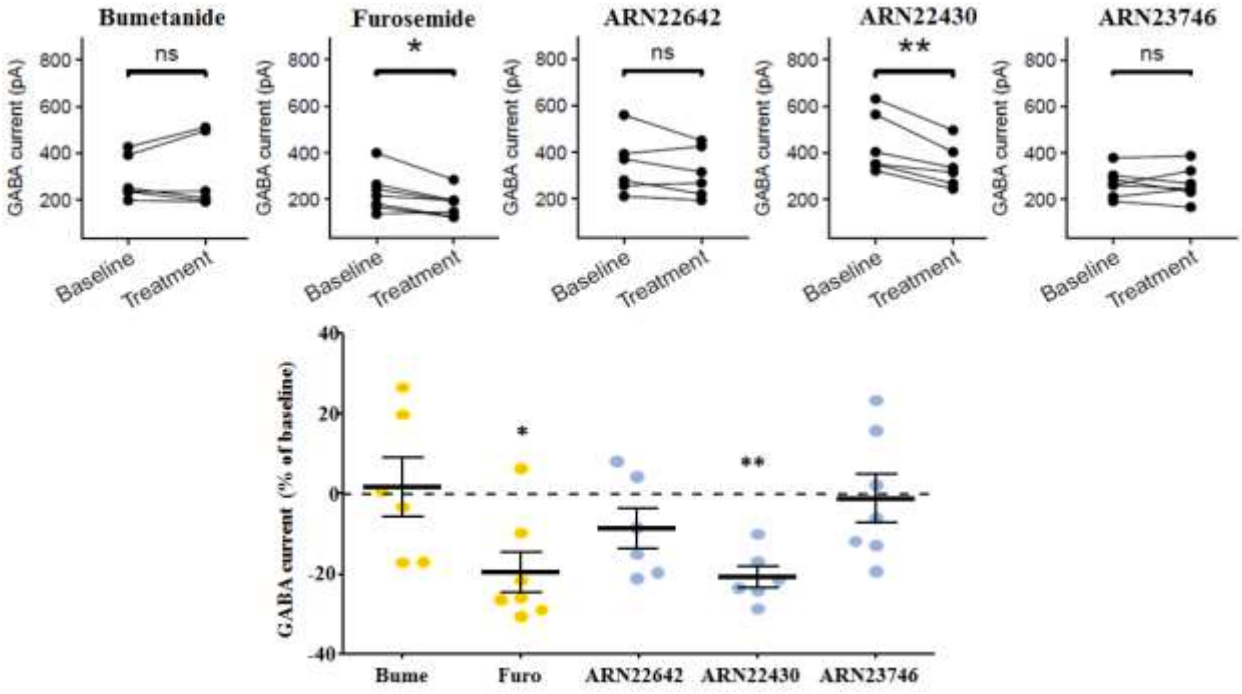

Figure 23: Top: Amplitude of evoked $GABA_A$ currents before (Baseline) and after 5 minutes of 10µM drug application (Treatment); circles connected by lines represent individual cells, Paired t-test. **Bottom**: Mean ± SEM of amplitude change of GABA-evoked currents showed in the top graphs. Drug responses were normalized to the amplitude of the GABA current before drug application. Reported significances were obtained in the top graphs (*P<0.05, ** P<0.01).

Taken together, these results indicate that among the ~300 compound tested, ARN23746 was the one showing the higher inhibition of NKCC1 in the chloride assay, which was confirmed in the calcium assay, and it did not show any significant inhibition of the $GABA_AR$. Hence, we further proceeded with the *in vitro* characterization of this "lead compound".

6. *In vitro* characterization of ARN23746

6.1 ARN23746 restores the physiological chloride concentration in Ts65Dn neurons

As previously demonstrated by Deidda and colleagues, hippocampal Ts65Dn neurons show an increased intracellular Cl^- concentration in comparison to WT littermates, which is due to an increased expression of NKCC1 (Deidda, Parrini, et al., 2015). Thus, we further tested ARN23746 efficacy to block NKCC1 in hippocampal cultured Ts65Dn neurons where we predicted that it would restore physiological intracellular Cl^- concentration. We prepared hippocampal neuron cultures from Ts65Dn and WT embryo littermates and performed the experiments at 15 DIV, when the GABA switch from depolarizing to hyperpolarizing has already occurred in cultures (Ganguly et al., 2001). We measured the intracellular Cl^- concentration upon treatment with DMSO (as negative control), bumetanide and furosemide (as positive controls), and ARN23746. To measure intracellular Cl^- concentration, we took advantage of the chloride-sensitive dye MQAE, which fluorescence is inversely correlated with the concentration of chloride. As shown in figure 24, we confirmed that Ts65Dn neurons are characterized by an increased intracellular Cl^- level (corresponding to lower MQAE fluorescence intensity) in comparison to WT neurons. As expected, bumetanide and furosemide at 10 μM were able to significantly restore the intracellular Cl^- concentration to WT levels. Interestingly, also ARN23746 at 10 μM significantly restored Cl^- to physiological levels, without significantly affecting the Cl^- concentration in WT neurons.

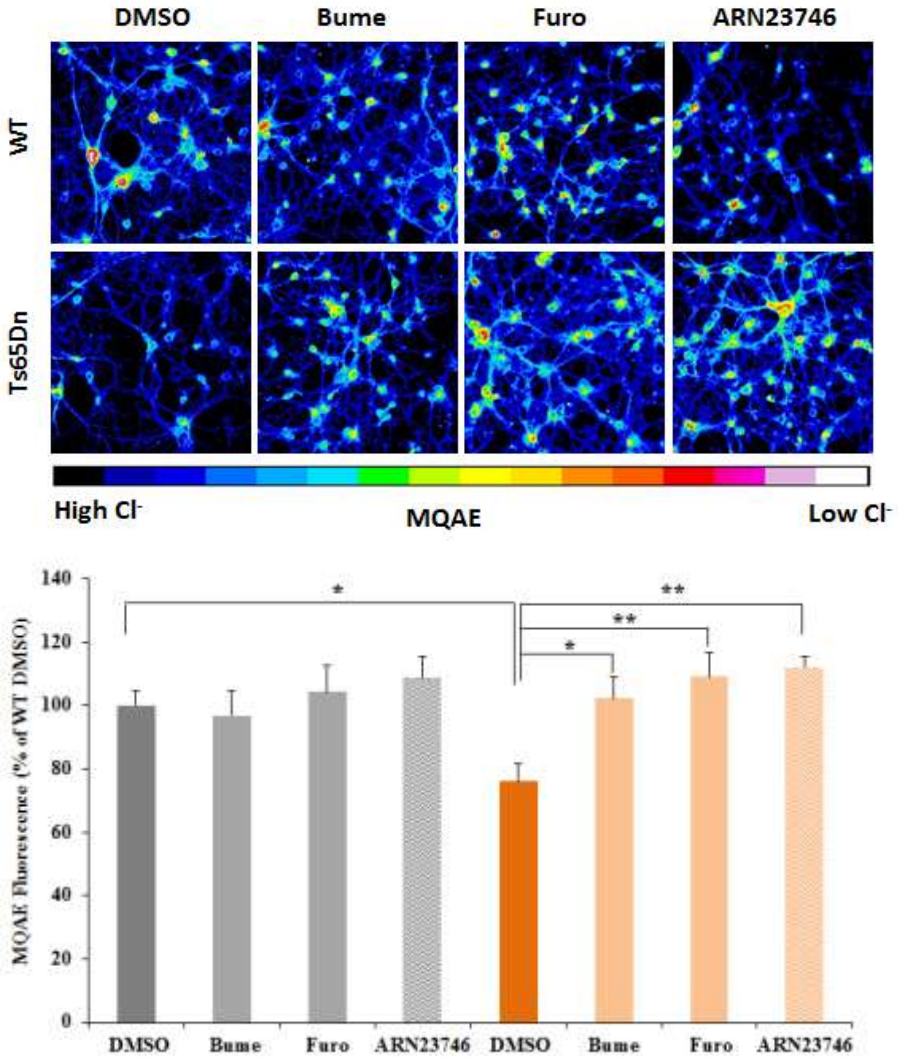

Figure 24: Top: representative pseudo-color images (colored scale below) of the intracellular Cl^- concentration measured with the MQAE chloride dye, in WT and Ts65Dn hippocampal neurons after treatment with DMSO (as negative control), Bumetanide and Furosemide (as positive controls) and ARN23746. **Bottom:** quantification of effect of Bumetanide (Bume 10 µM), Furosemide (Furo 10 µM) and ARN23746 (10 µM) in modulating intracellular chloride concentration in 15DIV cultured neurons from hippocampus of WT and Ts65Dn mice. Data represents mean ± sem from 3 independent experiments * P<0.05, ** P<0.01; Two Way Analysis of Variance, Tukey's *post hoc* test.

6.2 ARN23746 does not show a significant inhibition of NKCC2

Once we validated the efficiency of ARN23746 in inhibiting NKCC1 in three independent assays, we investigated its activity against NKCC2. To this aim, we took advantage of the previously described chloride assay on HEK293 cells transfected with NKCC2. As shown in figure 25, bumetanide at 10 µM

significantly inhibited NKCC2to 82.7 ± 20.4 %. Conversely, ARN23746 did not show a significant inhibitory activity on NKCC2.

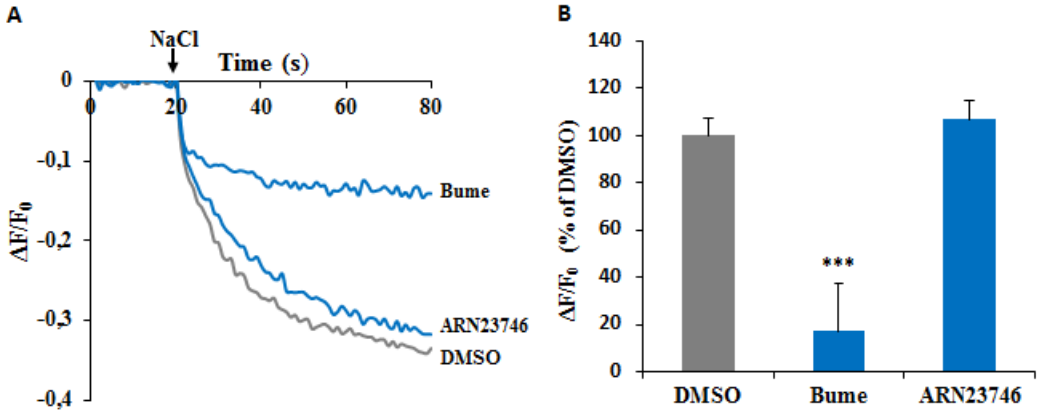

Figure 25. A) Example traces obtained in the chloride assay on NKCC2-transfected HEK293 cells treated with DMSO as negative control, bumetanide (Bume) as positive control and ARN23746. **B)** Quantification of the inhibitory activity of bumetanide (Bume 10µM) as positive control and ARN23746 (10 µM) in NKCC2-transfected HEK293 cells. Data are resented as a percentage of the respective control DMSO. Data represents mean ± sem from 5 independent experiments*** P<0.001; Kruskal-Wallis One Way Analysis of Variance on Ranks , Dunn's *post hoc* test.

6.3 ARN23746 show an excellent solubility and metabolic stability *in vitro*

In view of *in vivo* studies with systemic administration of compound ARN23746, we first evaluated some chemical and physical proprieties. In particular, we measured the solubility of ARN2346 in PBS at pH 7.4. As reported in Table 1, ARN23746 showed an excellent kinetic solubility, reaching the target concentration of 250 µM, and its thermodynamic solubility reached a maximum concentration of 181 µM in PBS. Next, we tested the plasmatic stability of ARN23746 in mouse plasma. The compound demonstrated a long plasmatic stability with a half-life of over 120 minutes. Furthermore, to evaluate the metabolization of ARN23746, we assessed its stability in microsomes obtained from mouse and rat. ARN23746 showed excellent half-life in both species (Table 1). Moreover, ARN23746 displayed also protracted half-life in microsomes obtained from human liver (Table 1). Then, we explored metabolism in rat and human more deeply by identifying possible metabolites. Two main metabolites were detected by liquid chromatography–mass spectrometry (LC-MS). In particular, one showed ARN23746 mass + 176

Dalton (Da) assignable to the glucuronic acid conjugation product, and the other one showed ARN23746 mass – 14 Da assignable to the N-desmethyl derivative (Figure 26).

Interestingly, when the rate of formation of these metabolites was compared in rat *vs* human liver homogenates, rat metabolism resulted more prone to dealkylation (Figure 26), giving rise to the N-desmethyl derivative. Conversely, in human microsomes the main metabolic path was the conjugation with glucuronic acid. Notably, ARN23746 displayed low intrinsic clearance in both species (Table 1).

Analysis	**Species**	**ARN23746**
Kinetic solubility PBS pH 7.4	-	> 250 µM
Thermodynamic solubility PBS pH 7.4	-	181 µM
$t_{1/2}$ plasma	mouse	> 120 min
$t_{1/2}$ liver microsomes	mouse	> 60 min
Residual liver compound	mouse	65%
$t_{1/2}$ liver microsomes	rat	189 min
$t_{1/2}$ liver microsomes	human	395 min
Intrinsic clearance	rat	0,00366 ml*min^{-1}*million cells^{-1}
Intrinsic clearance	human	0,00220 ml*min^{-1}*million cells^{-1}

Table 1 Preliminary absorption-distribution-metabolism-excretion properties of ARN23746

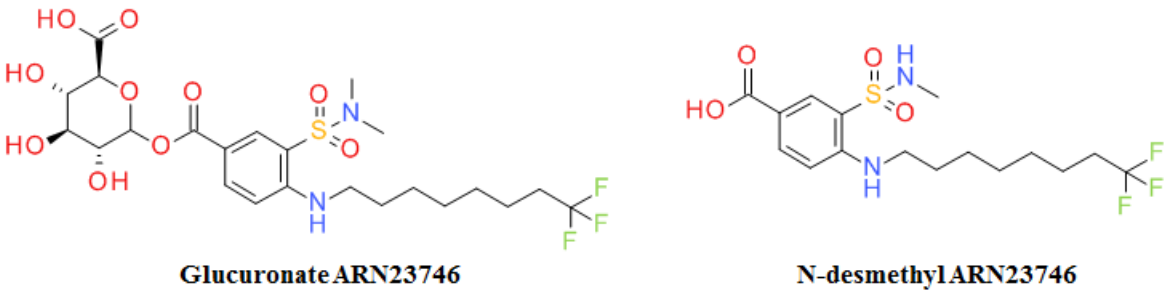

Figure 26. Structure of the two main metabolites of ARN23746 identified in rat and human.

Altogether, these studies indicate that ARN23746 shows a satisfying preliminary ADME profile. Thus, we selected ARN23746 for further evaluation *in vivo*.

7. ARN23746 does not exert significant diuretic effect *in vivo*

Next, we assessed ARN23746 diuretic effect in WT and TS65Dn mice. To this aim, we treated 2-4 month mice with an intra peritoneal (ip) injection of ARN23746 dissolved in PBS at 0.2 mg kg^{-1}, which are the same route of administration and dosage used for bumetanide in the previous study from our lab (Deidda, Parrini, et al., 2015). As a positive control, we used indeed bumetanide at the dose of 0.2 mg kg^{-1}. As a negative control, we used the same amount of DMSO dissolved in PBS (vehicle). The day of the experiment, we treated WT and Ts65Dn mice with DMSO, bumetanide or ARN23746, and we placed them into a metabolic cage (Tecniplast) for 2 hrs, where they found free food and water. After 2 hrs, we collected and measured the urine volume (Figure 27A). As expected, bumetanide administration significantly increased the urine volume both in WT and Ts65Dn mice when compared with vehicle-treated mice (Figure 27B). Conversely, ARN23746 treatment had no significant diuretic effect both in WT and Ts65Dn mice, when compared with vehicle-treated mice (Figure 27B).

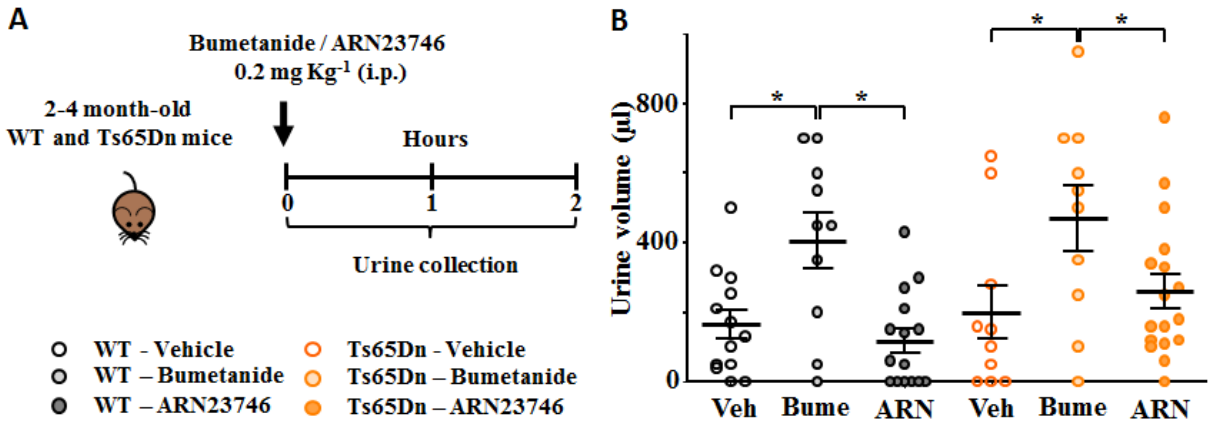

Figure 27. A) Schematic cartoon of the experimental protocol for the treatment of WT and Ts65Dn mice with bumetanide (control) and with the compound ARN23746 for the assessment of their diuretic effect. **B)** Quantification of the urine volume in mice treated with vehicle (WT, *n* = 13, Ts65Dn, *n* = 9), bumetanide (WT, *n* = 10, Ts65Dn, *n* = 10) or ARN23746 (WT, *n* = 12, Ts65Dn, *n* = 13). * P<0.05, two-way ANOVA Tukey's *post hoc* test.

8. ARN23746 is able to rescue memory deficits in Down syndrome mice

Next, we investigated ARN23746 efficacy in rescuing cognitive impairment in Ts65Dn mice, as previously tested with bumetanide (Deidda, Parrini, et al., 2015). In particular, we evaluated both the short-term working memory and the long-term hippocampus-dependent explicit memory after a subchronic, systemic treatment with ARN23746 (0.2 mg kg^{-1}, IP, daily; Figure 28).

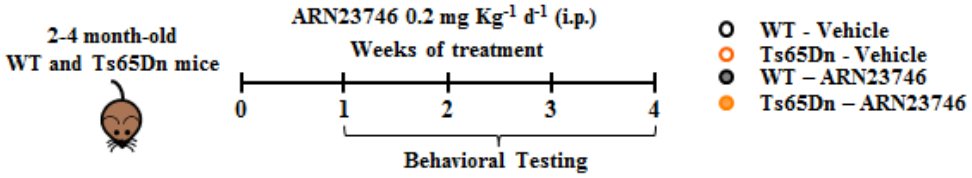

Figure 28. Schematic cartoon of the experimental protocol for the treatment of WT (black circle in graphs) and Ts65Dn (orange circles in graphs) mice with the compound ARN23746 for its efficacy assessment.

First, we assessed the efficacy of ARN23746 in restoring short-term memory, by testing mice in the T-maze task (spontaneous alteration protocol, 11 trial). The test was conducted similarly to what had previously described for Ts65Dn mice (A. M. Kleschevnikov, P. V. Belichenko, M. Faizi, et al., 2012). In this test, mice are started from the base of a T-shaped maze (Figure 29, left) and they are allowed to choose one of the two arms (first choice). If they remember the previous choice, mice will choose the arm not visited in the trial before, after the first trial. The alternate choice of each arm is considered as correct, whereas the choice of the same arm as in the previous trial (reflective of a poor short-term memory) is considered as negative. The final score for each animal is calculated by the number of the correct choices over the total of 10 trials. Confirming data from literature (A. M. Kleschevnikov, P. V. Belichenko, M. Faizi, et al., 2012), Ts65Dn showed poor short-term memory in comparison to WT littermates. ARN23746 treatment completely rescued the number of correct choices of Ts65 mice in comparison to WT animals (Figure 29, right).

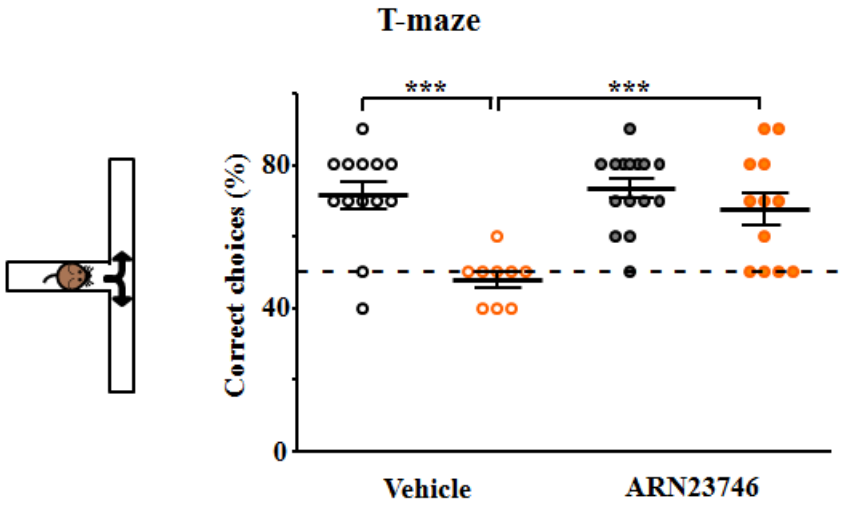

Figure 29. **Left**: schematic representation of the T-maze task. **Right:** quantification of the correct choices in mice treated with vehicle (WT, *n* = 12, Ts65Dn, *n* = 9) or ARN23746 (WT, *n* = 14, Ts65Dn, *n* = 12). ****P* < 0.001, two-way ANOVA Tukey's *post hoc* test.

Then, we assessed the long-term memory in three independent tasks (i.e., object location, novel object recognition and contextual fear conditioning). We assessed spatial memory in the object location task (OL). The test measures the ability of mice to recognize the new location of a familiar object with respect spatial external cues (Figure 30, top). As previously described (Deidda, Parrini, et al., 2015), vehicle-treated Ts65Dn mice showed impaired spatial memory, as demonstrated by a poor discrimination index reflective of poor discernment of the new object position. ARN23746 treatment restored the performance of Ts65Dn mice to the level of WT (Figure 30A). The effect of ARN23746 in the OL test was not due to alterations in the object preference or in the total object exploration during the acquisition phase (Figure 30B and 30C). Interestingly, during the trial phase, Ts65Dn mice treated with ARN23746 showed a significant increase in exploration time (Figure 30D), possibly indicative of a more explorative interest forthe objects. Nevertheless, given that the exploration of the single object was normalized on the total exploration time for each group, the increased exploration in Ts65Dn mice treated with ARN23746 did not affect the results on the discrimination index in the test.

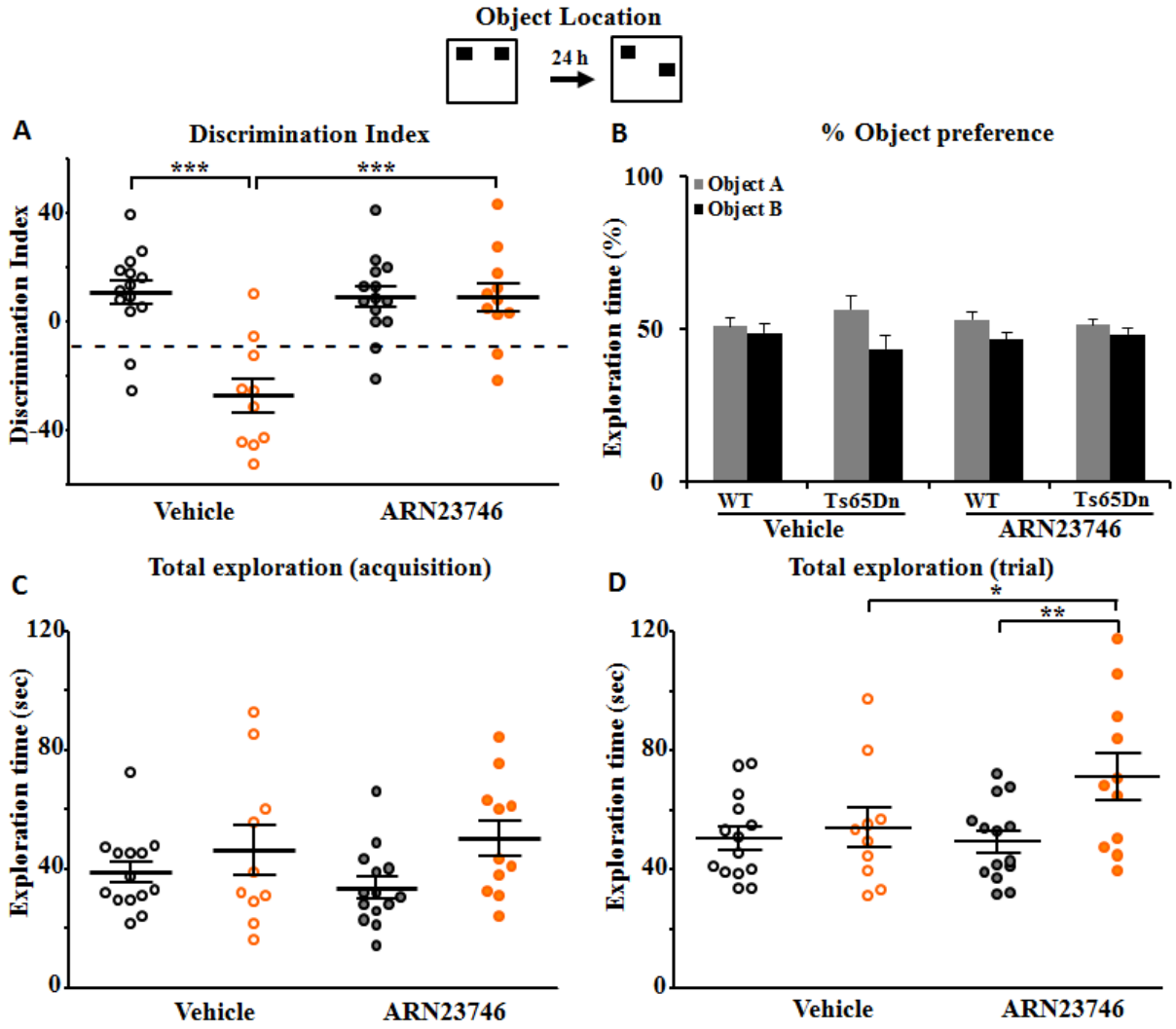

Figure 30 Top, schematic representation of the object-location test. **A)** Quantification of the discrimination index in mice treated with vehicle (WT, *n* = 14, Ts65Dn, *n* = 10) or ARN23746 (WT, *n* = 14, Ts65Dn, *n* = 12). ***$P < 0.001$, two-way ANOVA Tukey's post hoc test. **B)** Quantification of the percentage of time spent exploring the two objects during the acquisition phase. **C)** Quantification of the percentage of the total time spent exploring the objects during the acquisition phase. **D)** Quantification of the percentage of the total time spent exploring the objects during the trial phase. *$P < 0.05$,**$P < 0.01$, two-way ANOVA Tukey's *post hoc* test.

We next assessed the recognition memory in the novel-object recognition (NOR) test. This task measures the preference of mice for a novel object *versus* previously encountered familiar objects. As previously demonstrated (Deidda, Parrini, et al., 2015), Ts65Dn mice showed poor recognition memory in comparison to WT littermates. Interestingly, ARN23746 administration was able to completely rescue the poor novel-discrimination ability of Ts65Dn mice (Figure 31A). The effect of ARN23746 in NOR test

was not due to alterations in the object preference or in total object exploration (Figure 31B,C,D). Although there was a preference of ~10% of the object B within the same group in all four groups, the preference was not significantly different among the four groups (Figure 31B).

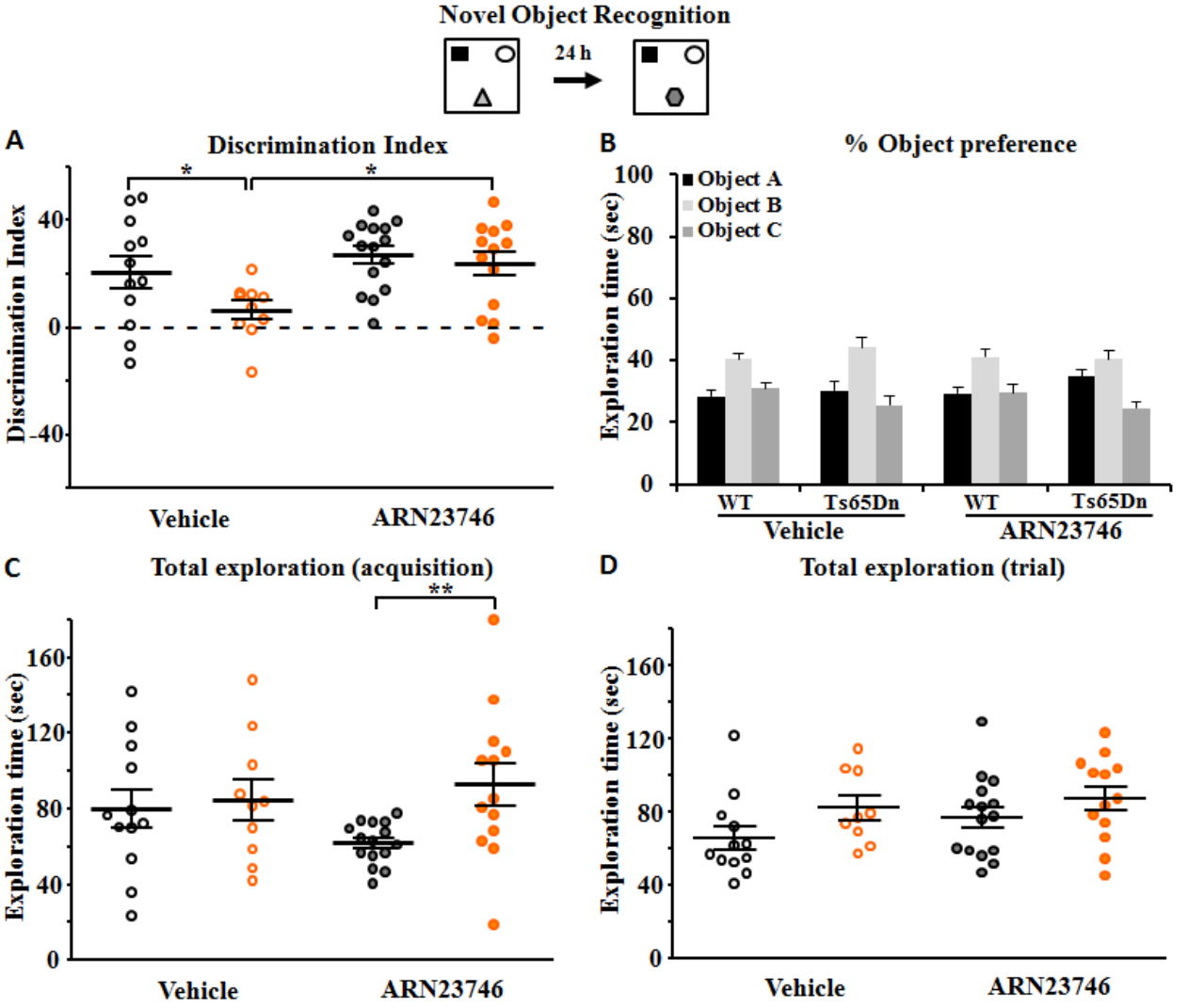

Figure 31. Top: schematic representation of the novel-object recognition test. **A)** Quantification of the discrimination index in mice treated with vehicle (WT, *n* = 13, Ts65Dn, *n* = 11) or ARN23746 (WT, *n* = 15, Ts65Dn, *n* = 12). * P<0.05, two-way ANOVA Tukey's *post hoc* test. **B)** Quantification of the percentage of time spent exploring the three objects during the acquisition phase. **C)** Quantification of the percentage of the total time spent exploring the objects during the acquisition phase. **P < 0.01, two-way ANOVA Tukey's *post hoc* test. **D)** Quantification of the percentage of the total time spent exploring the objects during the trial phase.

Finally, we evaluated associative memory in the contextual fear conditioning test (CFC). This task measures the freezing response that takes place after pairing of a foot shock (conditioning) with a

particular context represented by the grid releasing the shock (Figure 32, Top). As previously demonstrated (Deidda, Parrini, et al., 2015), Ts65Dn mice showed poor freezing response after the re-exposure to the grid context 24h after conditioning. Notably, ARN23746 treatment fully restored the associative memory in Ts65Dn by rescuing the poor freezing response (Figure 32A), without inducing changes in non-associative freezing (freezing response measured in a new context; Figure 32B).

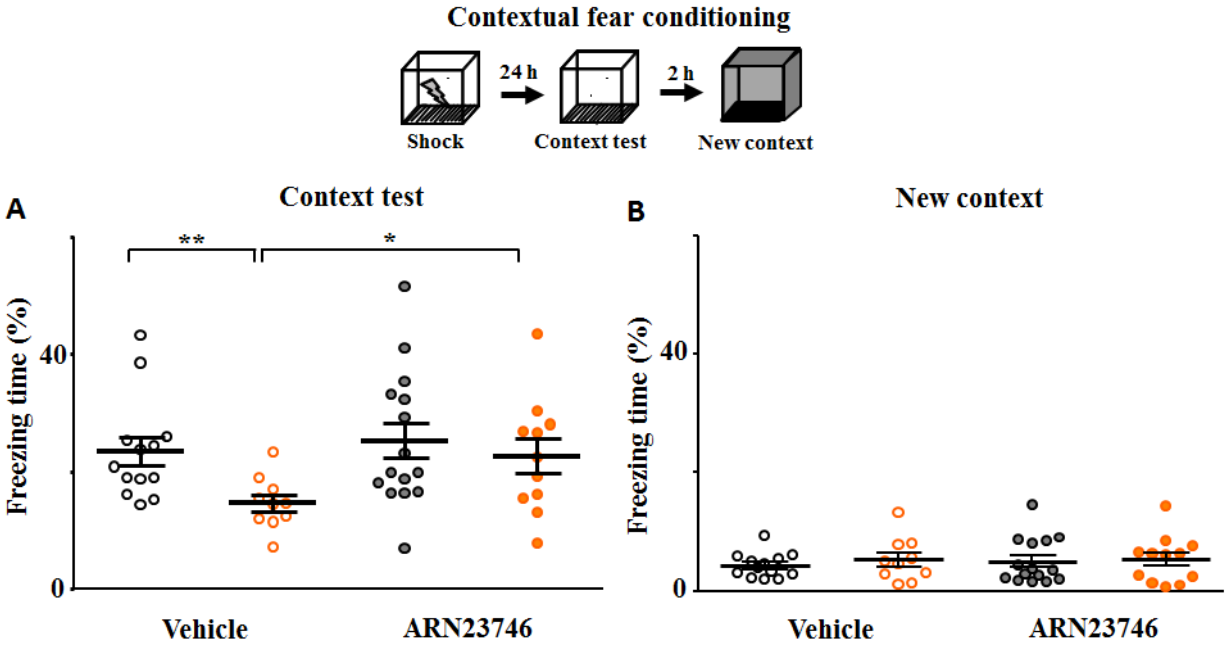

Figure 32. Top, schematic representation of the contextual fear-conditioning test**. A)** Quantification of the freezing response in mice treated with vehicle (WT, *n* = 13, Ts65Dn, *n* = 11;) or ARN23746 (WT, *n* = 15, Ts65Dn, *n* = 12). * P<0.05, ** P<0.01, two-way ANOVA Tukey's post hoc test. **B)** Quantification of the freezing response in mice treated with vehicle (WT, *n* = 13, Ts65Dn, *n* = 11;) or ARN23746 (WT, *n* = 15, Ts65Dn, *n* = 12) during the exposition to the new context.

9. Evaluation of toxicity of ARN23746 after *in vivo* chronic treatment

To assess any toxicity following ARN23746 systemic administration, we first monitored the weight of treated animals during the four weeks of chronic treatment. As reported in figure 33A, a four week-daily treatment with ARN23746 did not affect body weight, nor the general health state of the mice, as evaluated by daily eye assessment. Moreover, on the same animals we measured the viscera index

(viscera weight/body weight) for the kidneys, liver, spleen, lungs, and brain. As shown in the Figure 33B, chronic treatment with ARN23746 did not alter the weight of internal organs.

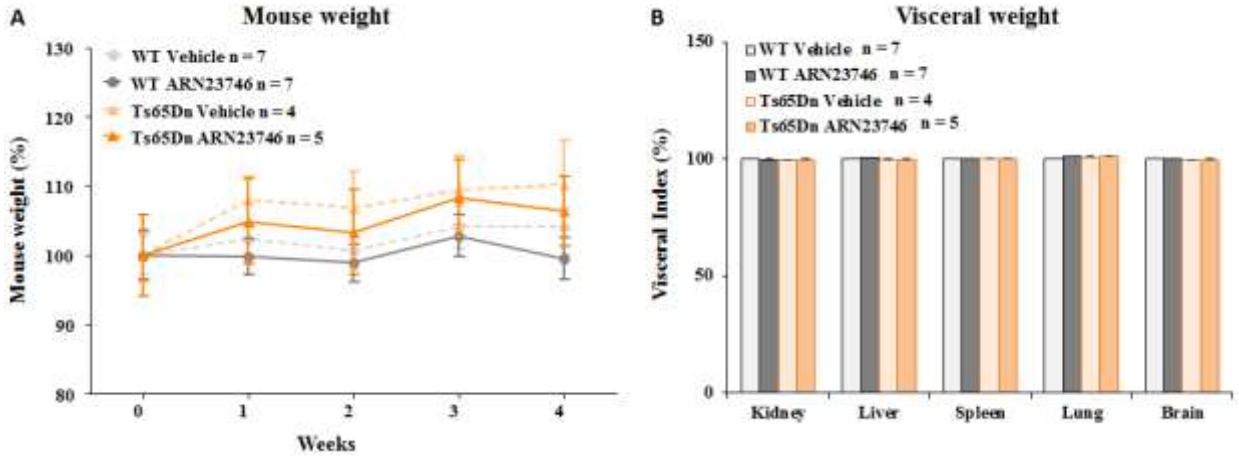

Figure 33. A) Quantification of the body weight of WT and TS65Dn mice across the four weeks of treatment with vehicle (control) and ARN23746. **B)** Visceral index expressed as viscera weight/body weight of 5 different organs collected from WT and TS65Dn mice after chronic treatment with vehicle (control) and ARN23746**.**

Moreover, we assessed the histopathological profile of liver, kidney and spleen. In particular, from each organ, we analyzed five sections stained with hematoxylin-eosin, marker of nucleus and cytoplasm respectively and gold standard of medical diagnosis. As shown in Table 2 and in figure 34, we did not found major abnormalities following ARN23746 chronic treatment. Indeed, across the 14 WT mice (7 treated with vehicle and 7 treated with ARN23746) and the 9 Ts65Dn mice (4 treated with vehicle and 5 treated with ARN23746) we found some morphological alterations in the liver of only two WT vehicle-treated mice and one Ts65Dn vehicle-treated mouse, in one kidney of one WT vehicle-treated mouse, one WT ARN23746-treated mouse and one Ts65Dn vehicle-treated mouse, and in the spleen of one WT vehicle-treated mouse and of one Ts65Dn vehicle-treated mouse. These results are compatible with the individual variability already described in mice and cannot be ascribed at any toxic effect of ARN23746. In particular, the focal angiectasis observed in the liver could occur spontaneously and occasionally. Angiectasis consists of dilated sinusoidal spaces that are lined by endothelial cells. Hepatocytes adjacent

to angiectatis appeared normal in dimension and morphology. Moreover, these alterations were observed only in vehicle-treated mice. With respect to kidneys, they generally undergo rapid autolysis, which could determine some alteration similar to degeneration and necrosis. In our case, no significant change in glomerular and tubular morphology were found. Only in one mouse was observed a cyst that may be congenital and should be noted as an isolated finding in the absence of other renal pathology. Finally, no evidence of alterations associated with chronic treatment with ARN23746 were detected in spleen except of two focal autolysis, however localized, observed in red pulp of two mice.

Tissue	Group	Physiological morphology (n. of animals)	Pathological morphology (n. of animals)
Liver	WT Vehicle	5	2
	WT ARN23746	7	0
	Ts65Dn Vehicle	3	1
	Ts65Dn ARN23746	5	0
Kidney	WT Vehicle	6	1
	WT ARN23746	6	1
	Ts65Dn Vehicle	3	1
	Ts65Dn ARN23746	5	0
Spleen	WT Vehicle	6	1
	WT ARN23746	6	1
	Ts65Dn Vehicle	4	0
	Ts65Dn ARN23746	5	0

Table 2. Number of WT and Ts65Dn mice showing a physiological or pathological morphology of liver, kidney and spleen after four weeks of treatment with vehicle (control) or with ARN23746.

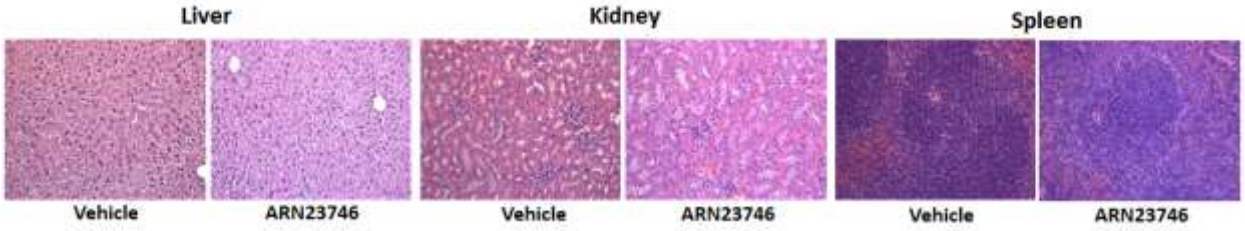

Figure 34. Examples hematoxylin-eosin images of liver, kidney and spleen sections from mice treated with vehicle (control) or ARN23746.

Discussion

A large and fast-growing body of literature indicates that an aberrant Cl^- homeostasis, due to an imbalance in NKCC1 *vs* KCC2 activity and/or expression, is implicated in several neurological disorders. Accordingly, several studies indicated NKCC1 inhibition by bumetanide as a valuable therapeutic strategy to ameliorate core symptoms in a number of animal models of these neurological disorders (Ben-Ari, 2017; Schulte et al., 2018). Moreover, several clinical trials and case studies indicate positive outcomes of bumetanide treatment also in patients (Ben-Ari, 2017).

1. Current issues with a NKCC1-inhibition therapy by bumetanide.

Although NKCC1 inhibition is a promising target for the treatment of diverse neurodevelopmental disorders, a chronic treatment seems to be required. Indeed, in a clinical study demonstrating a positive therapeutic effect of bumetanide on ASD children, Lemonnier and colleagues found a clear trend in CARS test score to return to pretreatment values at the end of a 1 month wash-out period (Lemonnier et al., 2012). Moreover, a week of drug withdrawal after a monthly treatment with bumetanide resulted in cognitive deficits in DS mice that were comparable to untreated DS mice (Deidda, Parrini, et al., 2015). Considering the strong diuretic effect of bumetanide (Flamenbaum & Friedman, 1982), which leads to hypokalemia and ionic imbalance (Lemonnier et al., 2012; Lemonnier et al., 2017), bumetanide repurposing is thus not a sustainable therapeutic approach that is compatible with a lifelong treatment of several years. In the last decades, the life expectancy of DS individuals has indeed increased dramatically, from just 9 years in 1930 to more than 60 years to date (Bittles et al., 2007). This is mainly attributable to the remarkable amelioration in medical care for the general population and in particular for people with DS. In particular, improvements in antibiotic treatments and vaccinations has contributed to a decrease of death for pneumonia and other infections (Alsubie & Rosen, 2018). Moreover, the improved outcomes of cardiac surgery and the better understanding of the heart defects frequent in DS has led to increased survival and to better quality of life of DS subjects (Versacci et al., 2018).

Beside strong diuresis, potential ototoxicity represents another severe side effect of bumetanide. In particular, the effects on the auditory system have proved critical for the treatment of infants. Indeed, one clinical trial for the repurposing of bumetanide for the treatment of acute neonatal encephalopathy seizures was suspended due to induced deafness in some treated subjects (Ben-Ari et al., 2016). So far, diverse studies identified changes in cochlear potentials and damage in cochlear *stria vascularis* as the main ototoxic effect following loop-diuretic administration. Although the clear mechanisms underlying ototoxicity are still under investigation, inhibition of sodium-potassium ATPase pump, adenylate cyclase and NKCC transporters are among the most accredited mechanisms (Ding et al., 2016). In particular, inhibition of NKCC1 in the cochlea, (Delpire et al., 1999) and inhibition of NKCC2 expressed in endolymphatic sac at the membranous labyrinth (Akiyama et al., 2010; Kakigi et al., 2009) possibly contribute to the inner ear damage and ototoxic effect by loop diuretics which inhibit both NKCC1 and NKCC2.

Finally, bumetanide could further aggravate the osmotic fluid balance (Konopacka et al., 2015) and could possibly affect social behavior, sexual motivation, pair bonding and maternal responses to stress, by acting on vasopressinergic and oxytocinergic neurons in the hypothalamo-neurohypophyseal system. Indeed, NKCC2 is also expressed in these neurons, where it regulates fluid balance following dehydration (Konopacka et al., 2015), but possibly also all the behaviors and biological processes controlled by the two hormones in the CNS and in periphery.

Thus, although clinical trials and case studies indicate positive outcomes of bumetanide treatment also in patients, its strong diuretic effect and consequent ionic imbalance, as well as its ototoxicity and potential effect on vasopressinergic and oxytocinergic neurons strongly hamper the possibility of bumetanide to become a reliable clinical option. In this scenario, a new compound ARN23746 able to selectively inhibit NKCC1 thus devoid of diuretic effects and with possibly reduced ototoxicity, osmotic imbalance and as behavioral side effects, may be a more sustainable therapeutic treatment in the future. ARN23746 as a potent and more selective NKCC1 inhibitor

Our *in vitro* studies demonstrated that ARN23746 is able to inhibit NKCC1 with a higher efficiency than bumetanide. For this assessment, we set up two different cellular assays: the chloride assay in HEK293 cells and the calcium assay in primary neurons in culture. With the chloride assay in HEK293 cells, we assessed NKCC1 inhibition through indirect estimate of the Cl flux *via* the transporter by measuring the variation in intracellular Cl concentration. With the calcium assay, we assessed NKCC1 inhibition through evaluating the ability of our compound to revert the depolarizing GABA signaling in young neurons, indirectly measured as calcium influx into the cells. Interestingly, both in the case of bumetanide and ARN23746 the two assays produced comparable results. Conversely, furosemide, ARN22642 and ARN22430 showed seemingly increased potency in the calcium assay, which we demonstrated was attributable to the inhibition of $GABA_A$ receptor, as already known for furosemide (Korpi et al., 1995; Korpi & Luddens, 1997; Minier & Sigel, 2004). Notably, ARN23746 showed a NKCC1 inhibitory activity comparable with the activity of bumetanide at 10 µm, but displayed a higher potency than bumetanide at 100 µm. This sharp increase in activity in comparison to bumetanide, could suggest that our compound is acting by binding NKCC1 in a cooperative manner. In this type of binding, the occupation of the binding sites by the ligand is indeed not a linear function of the ligand's concentration, and the affinity for the ligand depends on the amount of the bound ligand (Stefan & Le Novere, 2013). Binding *in vitro* assays and dose-response curves will be necessary to further investigate the type of binding between ARN23746 and NKCC1. Moreover, the resolution of NKCC1structure, coupled with binding assays and mutagenesis studies, will elucidate how NKCC1 modulates ion permeation and how bumetanide and ARN23746 affect NKCC1.

In our *in vitro* assays ARN23746 showed no significant inhibitory activity of NKCC2, in comparison to the significant inhibitory activity of bumetanide at 10 µM. Conversely, at the same concentration ARN23746 was able to significantly inhibit NKCC1 at levels comparable to bumetanide. Thus, the inhibition ratio of NKCC1/NKCC2 is markedly in favor of ARN23746 when compared to bumetanide. Consistently, at the *in vivo* dosage at which bumetanide rescued cognitive impairments but it is diuretic in

DS mice (0.2 mg/Kg), ARN23746 still recued cognitive deficits but it did not show any significant diuretic effect. Possibly, at the same dosage ARN23746 does not inhibit NKCC2 expressed in endolymphatic sac and/or in vasopressinergic and oxytocinergic neurons, thus reducing, at least in part, the ototoxic effect of bumetanide and other osmotic and behavioral side effects. These findings indicated ARN23746 as a promising candidate for further drug development of selective and potent NKCC1 inhibitors.

2. Challenges of drug development.

Drug development is a long, arduous risky and costly process. It is characterized by numerous steps which range from the identification and synthesis of new chemical compounds with possible biological activity, to the direct screening in *in vitro* assays and *in vivo* preclinical studies in animal models to identify a lead compound. Then, chemical modifications of the lead compound are designed to maximize its therapeutic effect and minimize its side effects. In recent years, computational drug design based on target-structure approaches has aided to lessen the risks, costs and duration of classical drug development (Chaudhari et al., 2017). Nevertheless, NKCC1 structure is still unknown. Thus, to screen for new NKCC1 inhibitors in libraries of pre-existing novel compounds, we applied here a ligand-based strategy, which took advantage of the structure of the known NKCC1-inhibitor (bumetanide, furosemide and asozemide). Moreover, the initial synthesis of close analogues of bumetanide guided us in the understanding of bumetanide's structural motifs able to decrease the activity against NKCC2, which we applied to the hit compounds selected from the library screenings.

Although these computational and other several strategies have been adopted to accelerate the process of drug discovery and increase the positive outcomes, pharmaceutical companies face remarkable challenges in improving the efficiency of the drug development process (i.e. the number of new drugs approved by the FDA per billion US$ spent). Actually, the cost of developing new compounds has increased from US$ 800 million in 2001 to the currently estimated US$ 3 billion (Mak & Pichika, 2018). The decline in efficiency of the drug development process is possibly due to several factors, including: (a) the presence

of more stringent regulations to avoid risks of severe drug side-effects that occurred in the past (Notably, 62% of new compounds in Phase IIb and Phase III clinical trials do not reach the clinic, mainly for failure in clinical safety and efficacy; (Mak & Pichika, 2018)); (b) the bias in target identification, which is often screwed toward targets that are known already; (c) the fact that the drugs addressing the easily tractable targets have been already developed, and often only more difficult targets are left.

The drug development process is even more costly and risky for compounds targeting the CNS, which is clearly reflected by a marked lack of new classes of compounds for the very vast majority of neurological disorders. This is firstly due to the many challenges in the identification of possible drug targets for complex CNS disorders, whose underlying pathological mechanisms are often still poorly understood. Moreover, lack of appropriate animal models, difficulty in brain penetration due to the presence of the BBB, absence of reliable biomarkers for assessment of treatment efficacy in the case of behavioral deficits characteristic of brain disorders, and incomplete knowledge of the natural history of CNS diseases have further decreased the success in developing new compounds (Gribkoff & Kaczmarek, 2017). Hence, many pharmaceutical companies dismissed or significantly reduced their CNS programs (Gribkoff & Kaczmarek, 2017). In this scenario, the identification of clear and safe targets, possibly validated in humans through *ad hoc* clinical protocols could be the first step to partially overcome the lack of new compounds targeting the CNS. Below, we will discuss these issues specially referring to our new compound ARN23746.

3. NKCC1 as a molecular target for the rescue of diagnostic behaviors in brain disorders

The finding that systemic treatment (i.e., i.p. or per os) by the NKCC1 inhibitor bumetanide can rescue diagnostic impaired behaviors in animal models and patients has suggested NKCC1 as a possible molecular target in a number of brain disorders. Nevertheless, this notion has been challenged by the fact that bumetanide's suboptimal BBB penetration has been considered in recent years incompatible with NKCC1 inhibition *in vivo* (Puskarjov, Kahle, et al., 2014; Romermann et al., 2017; Tollner, Brandt, Romermann, et al., 2015; S. Wang et al., 2015) For example, after 1 hour from i.p. injection of 0.3 mg/kg

in neonatal rats, only ~1 ng/g of bumetanide *per* brain tissue was detected. This corresponds approximately to a concentration of ~3 nM, which is orders of magnitude lower than the ~200–300 nM half-maximal inhibitory concentration of bumetanide required for NKCC1 inhibition *in vitro* (Puskarjov, Kahle, et al., 2014). Although this incompatibility between the *in vivo* concentration reached by bumetanide after systemic injection and the half-maximal inhibitory concentration *in vitro* is of great concern, one should be careful to directly translate *in vitro* results to the *in vivo* situation, as the bumetanide *in vivo* concentration required for biological effects on intracellular Cl^- concentration is still not known. Moreover, it is not known to what extent intracellular concertation should be restored to lead to positive behavioral outcomes, and finally this extent could vary from behavior to behavior and across the diverse brain disorders.

Besides regulation of intraneuronal Cl^- concentration by inhibition of brain NKCC1, bumetanide could act by being a diuretic, thus through its well-known osmotic regulation and/or by altering ionic balance (Hochman, 2012). Moreover, being a small molecule, bumetanide could have unpredictable other targets both in the brain and out of the brain that may in fact be relevant to the rescue of the diverse behaviors in the specific brain disorders (Brandt et al., 2018). Interestingly, few studies tested the effectiveness of bumetanide following direct brain infusion. For example, bumetanide infusion in the brain lateral ventricle rescued the spatial memory deficit in the R6/2 mouse model of Huntington's disease (HD) comparably to systemic administration (Dargaei et al., 2018). Moreover, intra-amygdala infusion of bumetanide inhibited the acquisition of the fear-potentiated startle response, as previously observed following systemic administration (Ko et al., 2018). Although these studies suggest the brain as the possible site of action for pro-cognitive and anxiolytic activity of bumetanide in HD and anxiety disorders respectively, the causal link between NKCC1 inhibition and rescue of behavioral deficits in diverse brain disorders remains elusive. The recent evidence from members of the Cancedda laboratory (and reported here) showing that NKCC1 downregulation by RNA interference through a single viral injection in the

hippocampus was able to rescue learning and memory deficits in adult Ts65Dn mice clearly identified NKCC1 as molecular target for cognitive impairment in DS.

Here, we demonstrated that also our newly synthesized NKCC1 inhibitor, is able to rescue cognitive deficits in adult Ts65Dn mice, further strengthening the notion that brain NKCC1 inhibition is causally linked to rescue of behavioral deficits in DS mice. Interestingly, given that most of the brain defects occurring in DS as well as in the other ND described above originate during development, an early therapeutic strategy in pups could be even more beneficial than in the treatment in adults. Indeed, acting when neuronal networks are still plastic during development could ameliorate symptoms that treatments in adulthood were not able to reverse, possibly due to present miswiring in the neuronal circuit. For example, bumetanide treatment in adult Ts65Dn mice failed to rescue hyperactivity and seizure susceptibility, whereas an earlier treatment could be beneficial (Deidda, Parrini, et al., 2015). Moreover, early pharmacological treatments in NDs could also lead to beneficial behavioral effects that persist into adulthood. This could eliminate or most likely reduce the need for chronic pharmacological treatments in adulthood.

Notably, the new selective NKCC1 inhibitor is devoid of the diuretic effect, thus indicating that the osmotic regulation and/or the alteration of ionic balance are, at least, not the only mechanism by which bumetanide restores cognition in DS.

One intriguing hypothesis is that bumetanide and ARN23746, besides binding to NKCC1 expressed in the brain, could also act by binding to NKCC1 expressed at the BBB and/or at the choroid plexus. Interestingly, high NKCC1 expression in the choroid plexus has proved fundamental for the formation of the CSF. Accordingly, NKCC1 inhibition by bumetanide or furosemide reduces CSF production (Steffensen et al., 2018). Thus, bumetanide and ARN23746 by acting at the NKCC1 expressed at the BBB and at the choroid plexus could decrease the potassium (K^+) concentration in the CSF, leading to a decrease of extracellular K^+ concentration in the brain. We hypothesize that this could hamper the

cotransport of Cl by reducing the activity of NKCC1 expressed at the plasma membrane of the neurons, resulting in a net decrease of intracellular Cl concentration.

In the last few weeks, we have started investigating this hypothesis by assessing NKCC1 function at decreasing extracellular K^+ concentrations, taking advantage of the chloride assay previously described. Interestingly, we found that lowering the K^+ concentration in the extracellular solution determined a decrease in Cl^- influx in HEK393 cells (estimated as a lower decrease in mbYFPQS fluorescence), thus preliminarily confirming our hypothesis (Figure 35). Notably, the actions of NKCC1 inhibitors in the brain parenchyma or at the BBB/choroid plexus could occur simultaneously, thus leading to a synergic effect on lowering the intracellular Cl concentration in neurons.

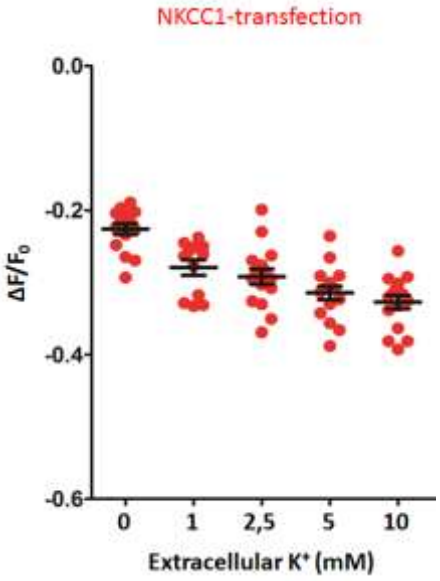

Figure 35. Quantification of the Cl^- influx *via* NKCC1, following variation in extracellular K^+ with the chloride assay. Less decrease in fluorescence (upon NaCl application) was observed lowering the extracellular K^+, indicating that less chloride is entering in to the cells *via* NKCC1.

4. Clinical trials with bumetanide to validate NKCC1 as a molecular target in humans.

Currently, a total of 15 clinical studies (case , pilot, phase I and phase II studies) have been performed to assess the therapeutic effect of bumetanide in ASD (Du et al., 2015; Hadjikhani et al., 2018; Hadjikhani et

al., 2015; Lemonnier & Ben-Ari, 2010; Lemonnier et al., 2012; Lemonnier et al., 2013; Lemonnier et al., 2017), Fragile X (Lemonnier et al., 2013), Asperger syndrome (Grandgeorge et al., 2014), 15q11.2 duplication syndrome (Bruining et al., 2015), neonatal seizures and temporal lobe epilepsy (Eftekhari et al., 2013; Kahle, Barnett, et al., 2009; Pressler et al., 2015), schizophrenia (Lemonnier et al., 2016; Rahmanzadeh, Eftekhari, et al., 2017) and Parkinson disease (Damier et al., 2016). Interestingly, in all these studies (beside the Nemo trial failed because of the bumetanide's ototoxic effect (Ben-Ari et al., 2016)) bumetanide administration resulted in amelioration of the core diagnostic symptoms of these pathologies.

Besides being a first (although not ideal) therapeutic option for many unmet medical needs, these results are of great importance in the attempt to pursue a full-fledged drug discovery program for potent and selective novel NKCC1 inhibitors because:

1) They validate NKCC1 as a valuable molecular target also in patients. Interestingly, upregulation of NKCC1 was reported in samples from DS (Deidda, Parrini, et al., 2015) and schizophrenic subjects (Dean et al., 2007; Hyde et al., 2011). The investigation of NKCC1/KCC2 expression also in all the other neurological disorders that benefit from a treatment with bumetanide could further widen the knowledge of the molecular mechanism underling these diseases. Interestingly, studies performed in animal models indicate that most of these conditions are characterized by KCC2 (rather than NKCC1) dysregulation (Di Cristo et al., 2018; Eftekhari, Shahrokhi, et al., 2014; Tyzio et al., 2014; Wu, Che, et al., 2016; Wu, Shao, et al., 2016). This indicates that, no matter which one of the two transporters is dysregulated, it is the NKCC1/KCC2 ratio imbalance that needs to be targeted to restore the physiological Cl^- homeostasis. In this respect, the possible combinational therapy with the newly discovered KCC2 activator CLP257 (Gagnon et al., 2013; Gagnon et al., 2017), could increase the beneficial effect of bumetanide (and possibly ARN23746) in ameliorating the core symptoms of pathologies characterized by impaired Cl homeostasis.

2) They provide specific indications regarding the planning of the clinical trial protocols for each of the disorder where bumetanide has been tested. The same protocols could be easily applied also to ARN23746, when ready to be tested in clinic.

5. Concluding remarks.

Altogether, our studies identified a new potent and selective NKCC1 inhibitor, ARN23746. The usage of this compound to rescue cognitive impairment in DS mice independent of the diuretic effect (or other NKCC2-dependent effects) typical of bumetanide has shed light into the mechanism of NKCC1-dependent regulation of learning and memory. Moreover, being devoid of diuretic effect *in vivo*, displaying excellent solubility and metabolic stability *in vitro* and showing no toxicity following *in vivo* chronic treatment, ARN23746 could represent in the future a solid and sustainable therapeutic strategy for DS and possibly for all other neurological conditions characterized by impaired Cl homeostasis.

Methods

HEK cell culture and transfection

HEK 293 cells were cultured in Dulbecco's MEM (DMEM) (Life Technologies) supplemented with 10% fetal bovine serum (Life Technologies), 1% L-glutamine, 100 U/ml penicillin, and 100 µg/ml streptomycin (Life Technologies) and maintained at 37°C in a 5% CO_2 humidified atmosphere. The cells were transfected with Lipofectamin 2000 (Life Technologies). In particular 3 million HEK cells were plated in a 10 cm cell culture dish and were loaded with a transfection solution constituted by 5 ml of DMEM (Dulbecco's Modified Eagle Medium, (Life Technologies)), 4 ml Opti-MEM (Life Technologies), 8 ug of DNA plasmid coding for NKCC1, or NKCC2 together with the Cl-sensitive YFP and 32 ul of Lipofectamin for each condition. After 4 hour the cells were collected and plated in a 96-well black-walled, clear-bottomed plate at a density of $2.5x10^4$.

Neurons culture

Primary cultures of dissociated hippocampal neurons were prepared from E18 C57Bl6/J plated in the 96-well plate at density of 30,000 cells per well. Neurons were maintained in Neurobasal medium (Invitrogen) supplemented with 2% B-27 supplement (Invitrogen) , 0.5 mM glutamine (Invitrogen), 50 U/mL of penicillin (Invitrogen) and 50 µg/mL of streptomycin (Invitrogen). The cells were incubated at 37°C and 5% CO_2 until DIV 3 and then used for the calcium kinetic assay.

Drug Preparation for *in vitro* and *in vivo* assays

All the tested compound *in vitro* were dissolved in DMSO in a stock solution of 10mM. Then, depending on the final concentration used in the assays (10µM or 100 µM), the compound stock solution was dissolved 1:1000 or 1:100 in assay buffer. As control we used assay buffer supplemented with 0.1% DMSO or 1% DMSO respectively. For the *in vivo* experiments, bumetanide and ARN23746 were dissolved in DMSO in a stock solution of 1 mg/ml. The day of the injection the stock solution was

dissolved in PBS at the concentration of 0.02 mg/kg and injected in a volume of 10ul/g to have a final concentration of 0.2 mg/kg.

Western Blot

Cell culture samples were homogenized in RIPA buffer (1% NP40, 0.5% Deoxycholic acid, 0.1% SDS, 150 mM NaCl 1 mM EDTA, 50 mM Tris, pH 7.4) containing 1% (v/v) protease and phosphatase inhibitor cocktails (Sigma). Then, after 30' incubation in ice, the samples were clarified through centrifugation at 20,000 x g. The protein concentration of samples was determined with BCA kit (Pierce). Equivalent amounts of protein (20 µg) were loaded on the 4-12% Bis-Tris NuPAGE precast gels (Invitrogen) and the electrophoresis were performed in NuPage apparatus. Next, gels were transferred onto nitrocellulose membranes (Whatman). The equal amount of protein loaded was verified by staining with 0.1% Ponceau. Thus, membranes were blocked for 1 h in 5% milk in Tris-buffered saline (10 mM Tris, 150 mM NaCl, pH 8.0) plus 0.1% Tween- 20 and incubated overnight at 4 °C with primary antibodies for: rabbit anti-actin (1:10000, Sigma), mouse anti-NKCC1 (clone T4; 1:4000, Developmental Studies Hybridoma Bank), rabbit anti-KCC2 (1:4000, Millipore) and sheep anti-NKCC2 (1:2000, MRC-PPU). Next, membranes were washed and incubated for 2 hr at room temperature with HRP-conjugated goat secondary antibodies (Thermo; 1:5000). Thus, membranes were developed with SuperSignal West Pico chemiluminescent substrate and the chemiluminescent signals were acquired on the LAS 4000 Mini imaging system (GE Healthcare). Bands were later quantified by measuring the mean intensity of the band signal using ImageJ.

Chloride kinetic assay in HEK cells

We performed the chloride kinetic assay on the cells plated in the 96-well after 48 hrs from the transfection. This assay was based on the use of a Cl sensor (Cl-sensitive membrane-targeted YFP, mbYFPQS, Addgene)(Watts et al., 2012) to measure the NKCC-driven changes in intracellular Cl.

Briefly, we transfected HEK293 cells with NKCC1 or NKCC2 or mock construct (control) together with the Cl-sensitive YFP. After 2DIV, we treated the cells with bumetanide and furosemide (as positive controls) or with each of our best compounds in 100 µl/well of Cl-free hypotonic solution (67.5 mM Na^+ Gluconate, 2.5mM K^+ Gluconate, 15mM HEPES pH 7.4, 50 mM Glucose, 1mM Na_2HPO_4, 1 mM NaH_2PO_4, 1 mM $MgSO_4$, 1 mM $CaSo_4$ * $2H_2O$). The different tested compounds and drugs were loaded at a concentration of 10 and 100 µM. After 30 min of incubation, we loaded the plate onto the Victor 3V (Perkin Elmer) where we monitored the fluorescence decrease upon the application of 74 mM NaCl. In detail, the chloride sensitive YFP was excited at 490 nm and detected at 520 nm and the time course fluorescent data were recorded over a period of 80 s. For each well we performed a continuously recording fluorescence for 20 s of baseline and for 60s after 74 mM NaCl injection (20 µl of a 6X NaCl).

Calcium kinetic assay

Calcium kinetic assay was performed on hippocampal neurons prepared from mouse C57Bl/6J embryos on E18, and plated in a 96 well plate. At 3 DIV the neurons were loaded with a calcium-sensitive day (Fluo4, Invitrogen) in extracellular solution (145 mM NaCl, 5 mM KCl, 10 mM HEPES, 5.55 mM Glucose, 1 mM MgCl2, 2 mM CaCl2). After 15 min neurons were treated with bumetanide (as a positive control) or each of our best compounds (10, 100 µM) in extracellular solution for 15 min. Thus we loaded the plate onto the Victor 3V (Perkin Elmer) and we monitored the level of fluorescence upon application of GABA (100 µM, for 20 sec). To test for neuronal viability, we also applied KCl (90 mM, for 40 sec) after GABA treatment. To quantify the effect of bumetanide and our new compounds on NKCC1 inhibition, we thus normalized the fluorescence values upon GABA application to the fluorescence levels upon KCl (90 mM) application in treated neurons.

Electrophysiological recordings

Neurons from hippocampal cell cultures (DIV12-20) were recorded at room temperature (22-24°C) in an extracellular solution containing in mM: 145 NaCl, 5 KCl, 10 HEPES, 5.55 Glucose, 1 MgCl2, 2 CaCl2. Cells were visualized with an upright microscope (Olympus BX51WI) with infrared differential interference contrast optics. Patch pipettes (3-5 MΩ) were filled with an intracellular solution containing in mM: 100 K-Gluconate, 45 KCl, 10 HEPES, 3 MgCl2, 2 MgATP, 0.6 EGTA and 0.3 NaGTP; GABA currents were evoked by keeping the cell's membrane potential at -65 mV and puffing 20 µM GABA (10 psi, 20-50 ms) using a Picospritzer III (Parker Instrumentation). Access resistance (Ra) was monitored during voltage-clamp recordings and traces with more than 25 MΩ Ra or a variation bigger than 20% between different sweeps were discarded. Evoked GABA-currents were obtained by averaging 5 sweeps for each experimental condition. Signals were sampled at 20 kHz and low pass filtered at 10 kHz with an Axon Multiclamp 700B (Molecular Devices).

MQAE intracellular chloride imaging

Imaging of intracellular Cl^- in hippocampal neurons was performed with the fluorescent chloride-sensitive indicator MQAE [N-(Ethoxycarbonylmethyl)-6-Methoxyquinolinium-Bromide] as previously described (Deidda, Parrini, et al., 2015). MQAE dye detects Cl^- ions *via* diffusion-limited collisional quenching, resulting in a concentration-dependent decrease of fluorescence emission upon an increase in Cl^- concentration (Verkman et al., 1989). Hippocampal neurons at 15 DIV were loaded with 5 mM MQAE (Molecular Probes) and with the different treatment, DMSO (0.1 %, negative control), furosemide (10 µM, positive control), bumetanide (10 µM, positive control), ARN23746 (10 µM) for 30 minutes at 37°C. Coverslips were then transferred to a holding chamber and perfused (2 mL/min) with extracellular solution (NaCl 124 mM, KCl 5 mM, $CaCl_2$ 2 mM, $MgCl_2$ 1 mM, Hepes 10 mM, D-glucose 5.5 mM, pH 7.4) with addition of the drug/compound tested at 25°C for 5 minutes before imaging. Images were taken with a Nikon A1 scanning confocal microscope equipped with a 20X air-objective (NA 0.75). MQAE was excited with a 405 nm diode laser and fluorescence collected with a 525/50 nm band-pass emission

filter. All excitation and acquisition parameters (laser intensity, PMT offset and gain) were keep constant throughout experiments. Image analysis was performed with NIS-Elements software (Nikon) by measuring the mean fluorescent intensity of regions of interest (ROIs) centered on the cell body of individual neurons expressing from 6 randomly-selected fields for each coverslip. For each experiment, the average fluorescent intensity of all ROIs from a coverslip was normalized to the average fluorescent intensity of control samples (WT neurons treated with DMSO) in the same experiment. Pseudo-color images were generated by ImageJ software (http://rsbweb.nih.gov/ij/).

Animals and treatment

Ts65Dn and WT mice were generated by repeated backcross of Ts65Dn female to C57BL/6JEi x C3SnHeSnJ (B6EiC3) F1 males (obtained from the Jackson Laboratories). Animals were genotyped by PCR as previously described by Duchon, A., *et al.*2011. Animals aged between 8 and 16 weeks were used for experiments. Both males and females were used for the analysis of diuresis; only males were used for behavioral experiments. Ts65Dn and WT littermates were randomly assigned to vehicle groups (2% DMSO in saline), bumetanide (Sigma, 0.2 mg/Kg body weight) or ARN23746 (0.2 mg/Kg body weight) or, and treated daily by intraperitoneal injection (i.p.). On the day of behavioral testing, injection was performed at least 1 hour before the beginning of the task.

Behavioral testing

Mice were tested after 1 week of treatment with four different tasks. During the behavioral experiment, animals were continuously daily treated. The tasks were video recorded and then analyzed manually in blind. Briefly:

***Object Location test* (*OL*)**. The test evaluates the spatial memory by measuring the ability of mice to recognize the new location of a familiar object. The test was performed in a grey acrylic arena (44x44

cm). Mice were first habituated to the chamber for 15 min on the day 1. The next day, during the acquisition phase mice were exposed to 2 identical objects for 15 min. After 24 hours, during the test session, one of the two objects was moved to a novel location and the mice were tested for their ability to recognize the new location of the object for 15 min. After each trial the objects and the arena were cleaned with 70% ethanol. The time spent exploring each object was calculated by measuring the second when mice show investigative behavior (*i.e.*, head orientation, sniffing occurring within < 1.0 cm) or clear contact the object with the nose. A discrimination index was calculated as the percent time spent investigating the object in the new location minus the percent time spent investigating the object in the old location [Discrimination Index = (New Object Location Exploration Time/Total Exploration Time X 100) – (Old Object Location Exploration Time/Total Exploration Time X 100].

Novel Object recognition test (NOR). The test evaluates the long-term object recognition memory by measuring the ability of mice to recognize a new object respect to the familiar ones. The test was performed in a grey acrylic arena (44*44 cm). In the first day, mice were habituated to the arena by freely exploring the chamber for 15 minutes. The second day during the acquisition phase mice were free to explore 3 different objects for 15 min. After 24 hours, one of the object used during the acquisition phase, was replaced with a novel object and the mice were tested for their ability to recognize the new object for 15 min. The object used during the test were different in shape, color, size and material. After each trial the objects and the arena were cleaned with 70% ethanol. The time spent exploring each object was calculated by measuring the second when mice show investigative behavior (*i.e.*, head orientation, sniffing occurring within < 1.0 cm) or clear contact the object with the nose. The time spent exploring each object, expressed as a percentage of the total exploration time, was measured for each trial. The discrimination index was calculated as the difference between the percentages of time spent investigating the novel object and the time spent investigating the familiar objects: discrimination index = (novel object

exploration time/total exploration time*100) - (familiar object exploration time/total exploration time *100).

C*ontextual fear conditioning test (CFC)*. The test evaluates the long-term associative memory by measuring the freezing time of the animals placed in a place where 24hrs before received an adverse stimulus (electric shock).The experiments were performed in a fear conditioning system (TSE) consisting of a transparent acrylic conditioning chamber (23x23 cm) equipped with a stainless-steel grid floor. Mice were held outside the experimental room in their home cages prior to testing and individually transported to the conditioning apparatus in standard cages. The chamber was cleaned with 70% ethanol after each trial. Mice were placed in the conditioning chamber and they received one electric shock (2s, 0.75mA constant electric current) through the floor grid 3 minutes later. Mice were removed 15s upon the shock. 24 hours later, mice were placed in the same chamber for 3 minutes and they were moved to a new context (black chamber with plastic gray floor and vanilla odor) after 2 hours. The freezing behavior was scored by a trained operator blinded to the experimental groups.

T-Maze. The T-maze test (spontaneous alteration protocol, 11 trials)evaluate the short term memory by analyzing the correct choice of the unexplored arm. The test was conducted similarly to what previously described for Ts65Dn mice (A.M. Kleschevnikov et al., 2012). The T-maze apparatus was made of black, opaque, acrylic plastic and consisted of a start arm and two perpendicular goal arms each equipped with a sliding door. For each trial, a mouse was first confined in the start chamber and after 20 seconds the sliding door was removed. After the mouse had entered (with all four limbs) in one of the two goal arms, the opposite goal arm was closed with the corresponding sliding door. The mouse was left to explore the remaining part of the apparatus and, when the animal spontaneously returned to the start chamber, the previously closed goal arm was opened. The mouse was then given the possibility to choose again one of the two goal arms. The procedure was repeated 11 times (for a total of 10 possible alternations). Entry

into a goal arm opposite to the one previously chosen was defined as a correct alternation, whereas entry into the previously visited arm was defined as non-correct alternation. Alternation score was defined as the percentage of correct alternations (*i.e.*, left–right or right–left) over the total number of possible alternations.

For behavioral experiments, we adopted the following exclusion criteria independently of genotype or treatment (before blind code break). In the CFC test, we excluded mice showing very high non-associative freezing in the new context: more than 30 seconds freezing during the 3 minutes test. In the OL and NOR test, we excluded animals showing very low explorative behavior: less than 10 seconds of direct objects exploration during the 15 minutes test. In the T-maze test we excluded mice not concluding the 10 trials within 10 minutes of test.

Diuresis Analysis

Diuresis analysis were performed tacking advantage of metabolic cages (Tecniplast) which are equipped with a funnel and a plastic cone able to separate urine and feces. After ip treatment with vehicle, bumetanide or ARN23746 animals were placed inside the metabolic cages (one animal for each cage) where free food and water are available. After two hours mice are returned in their home cages and urine, collected in a vial, are measured and stored at -80°C.

Statistical analysis

The results are presented as the means ± SEM. The statistical analysis was performed using SigmaPlot (Systat) software. Where appropriate, the statistical significance was assessed using the following parametric test: Student's t test one-way ANOVA followed by Dunnet *post hoc* test, two-way ANOVA followed by all pairwise Tukey or Holm-Sidak *post hoc* test. In case of normal distribution or equal

variance assumptions were not valid, statistical significance was evaluated using Mann-Whitney Rank Sum Test, Kruskal-Wallis One Way ANOVA with Dunn's *post hoc* test or ANOVA on ranks followed by all pairwise Dunn's *post hoc* test. P values < 0.05 were considered significant.

Ethical approval declaration

A veterinarian was employed to maintain health and comfort of the animals. Mice were housed in filtered cages in a temperature-controlled room with a 12:12 hour dark/light cycle with *ad libitum* access to water and food. All animal experiments were performed in accordance with the guidelines established by the European Community Council Directive 2010/63/EU of September 22nd, 2010 and were approved by the Italian Ministry of Health.

Table A

ARN Number	Chemical structure	Class
ARN16655_Z_02	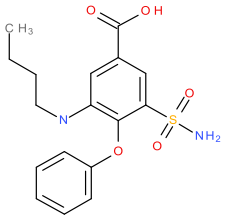	Bumetanide analogue
ARN21845_Z_01	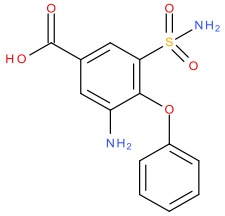	Bumetanide analogue
ARN21895_Z_01	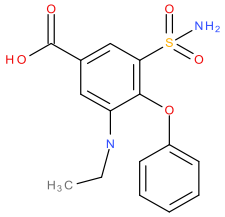	Bumetanide analogue
ARN21878_Z_01	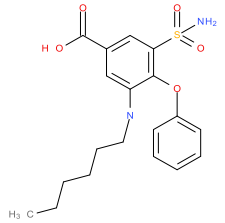	Bumetanide analogue
ARN22351_Z_01	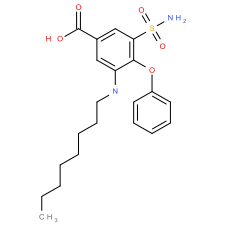	Bumetanide analogue
ARN22381_Z_01	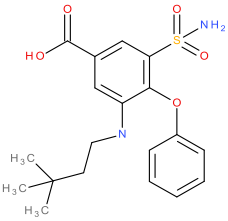	Bumetanide analogue

ARN21876_Z_01	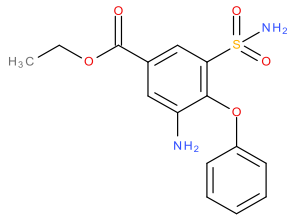	Bumetanide analogue
ARN21889_Z_01	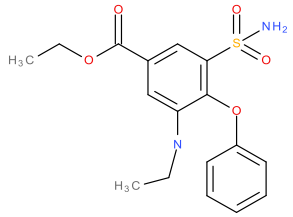	Bumetanide analogue
ARN21902_Z_01	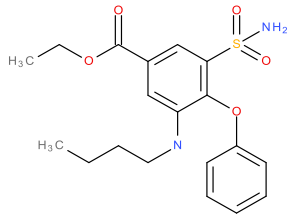	Bumetanide analogue
ARN21858_Z_01	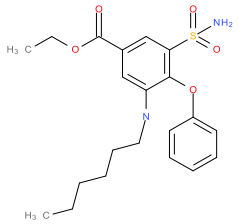	Bumetanide analogue
ARN22013_Z_01	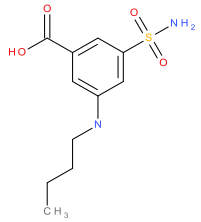	Bumetanide analogue
ARN22133_Z_01	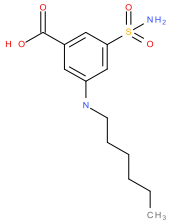	Bumetanide analogue
ARN22353_Z_01	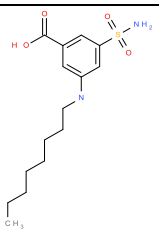	Bumetanide analogue

ARN22349_Z_01	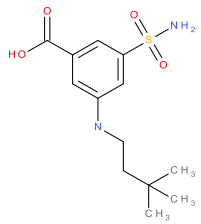	Bumetanide analogue
ARN23837_Z_01	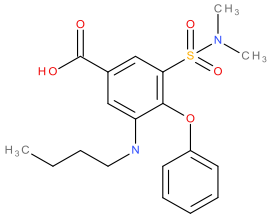	Bumetanide analogue
ARN23860_Z_01	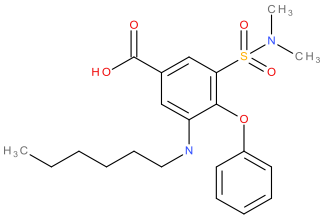	Bumetanide analogue
ARN23861_Z_01	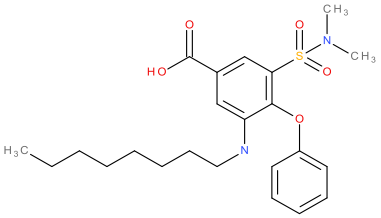	Bumetanide analogue
ARN23862_Z_01	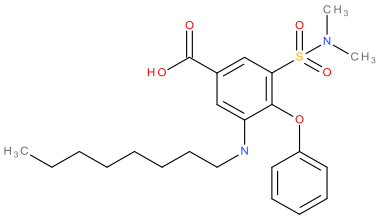	Bumetanide analogue
ARN4393_Z_01	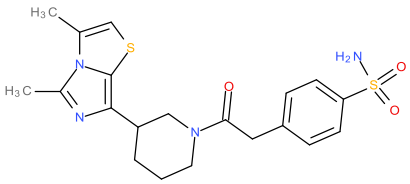	IIT library
ARN5106_Z_01	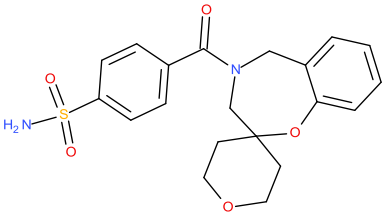	IIT library

ARN9768_Z_01	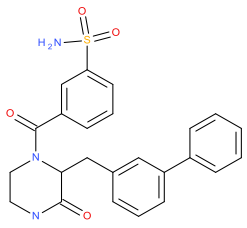	IIT library
ARN10751_Z_01	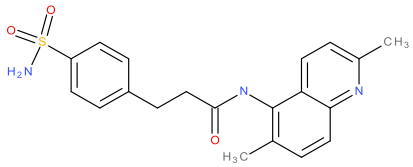	IIT library
ARN10975_Z_01	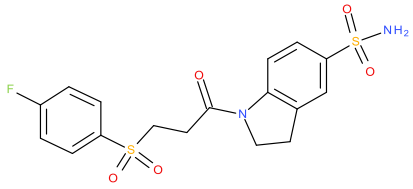	IIT library
ARN12092_Z_01	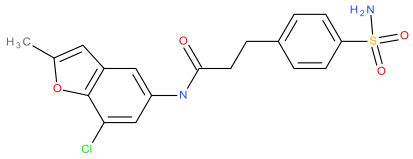	IIT library
ARN10286_Z_01	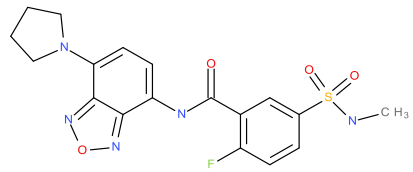	IIT library
ARN12377_Z_01	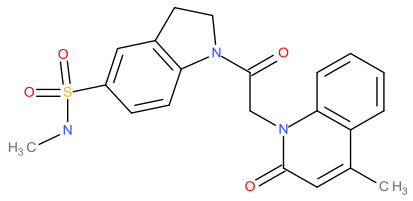	IIT library
ARN12404_Z_01	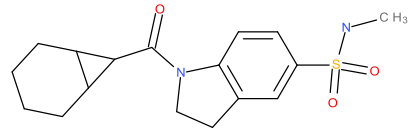	IIT library

ARN12746_Z_01	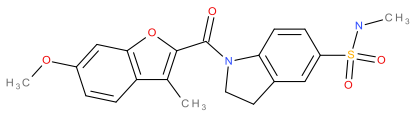	IIT library
ARN3894_Z_01	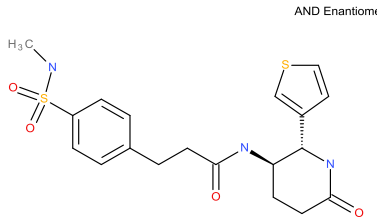	IIT library
ARN4673_Z_01	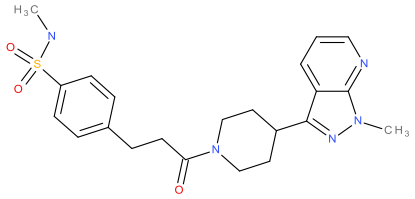	IIT library
ARN4837_Z_01	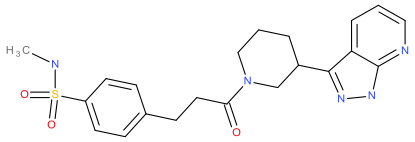	IIT library
ARN5264_Z_01	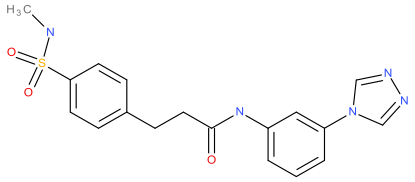	IIT library
ARN5265_Z_01	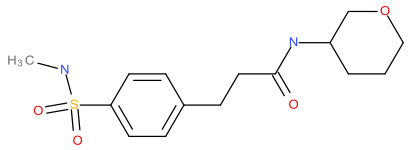	IIT library
ARN5277_Z_01	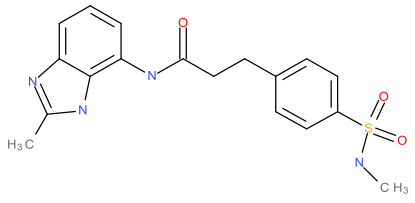	IIT library

ARN5954_Z_01	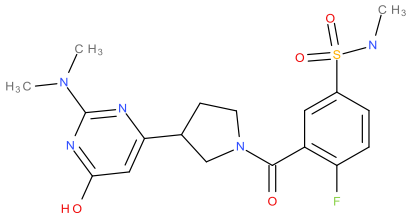	IIT library
ARN9425_Z_01	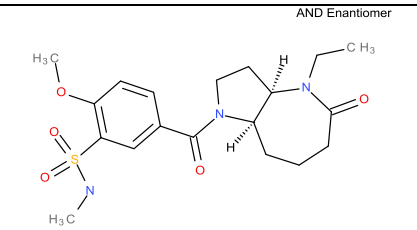	IIT library
ARN2876_Z_01	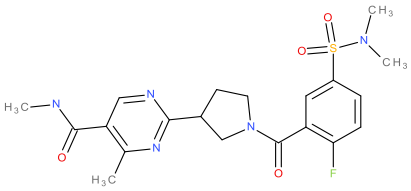	IIT library
ARN3163_Z_01	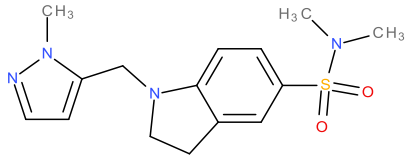	IIT library
ARN3554_Z_01	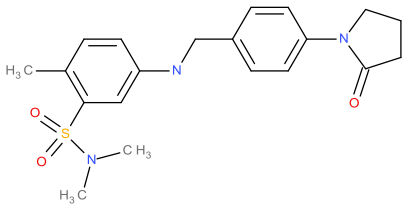	IIT library
ARN4077_Z_01	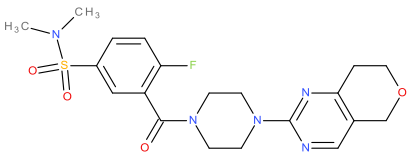	IIT library
ARN5698_Z_01	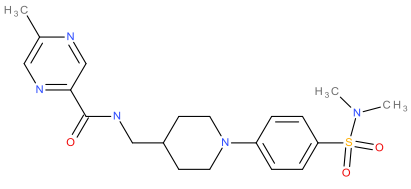	IIT library

ARN5858_Z_01	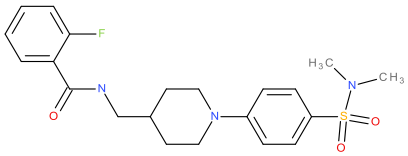	IIT library
ARN6498_A_01	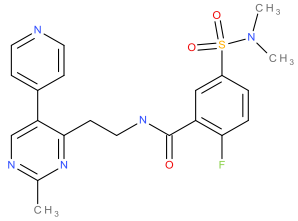	IIT library
ARN7620_Z_01	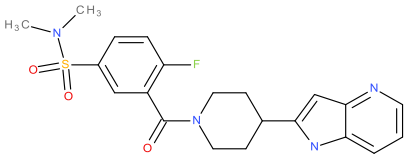	IIT library
ARN10223_Z_01	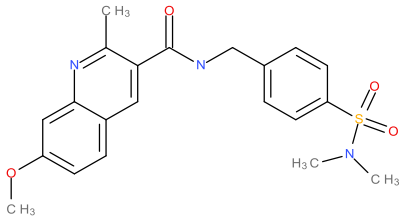	IIT library
ARN10516_Z_01	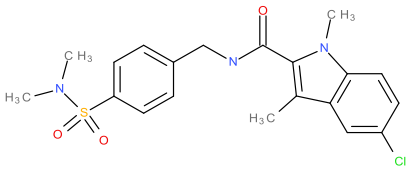	IIT library
ARN10630_Z_01	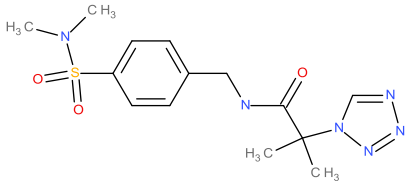	IIT library
ARN10641_Z_01	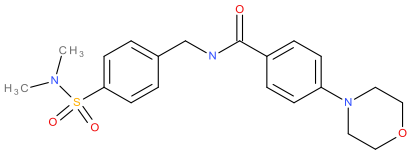	IIT library

ARN11080_Z_01	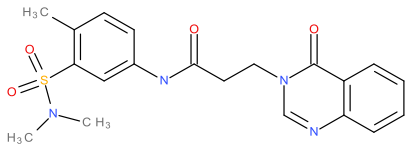	IIT library
ARN11153_Z_01	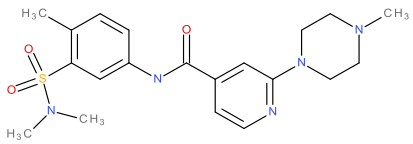	IIT library
ARN11542_Z_01	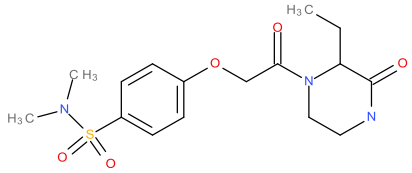	IIT library
ARN11564_Z_01	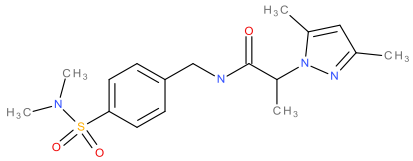	IIT library
ARN11830_Z_01	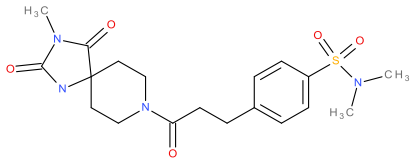	IIT library
ARN11867_Z_01	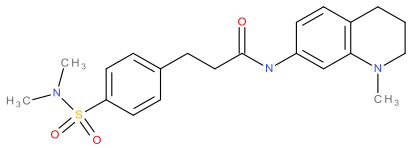	IIT library
ARN11895_Z_01	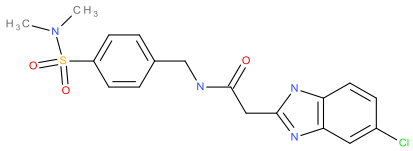	IIT library

ARN11901_Z_01	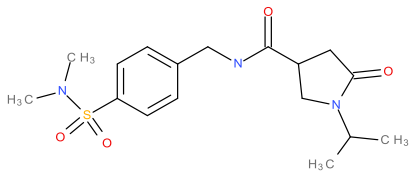	IIT library
ARN12013_Z_01	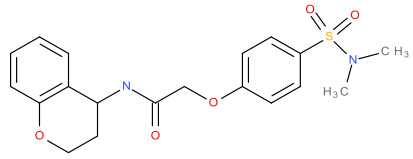	IIT library
ARN12043_Z_01	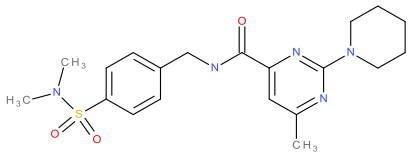	IIT library
ARN12277_Z_01	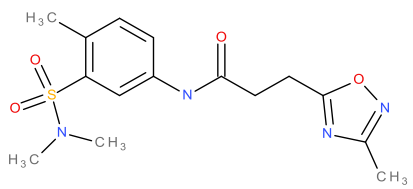	IIT library
ARN12278_Z_01	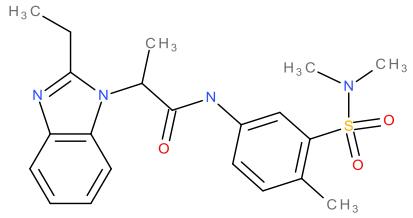	IIT library
ARN12348_Z_01	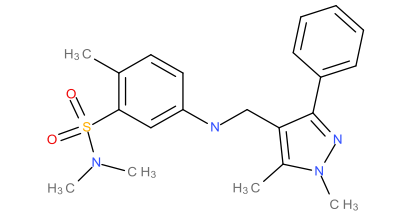	IIT library
ARN12482_Z_01	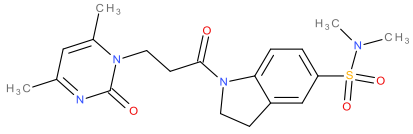	IIT library

ARN12849_Z_01	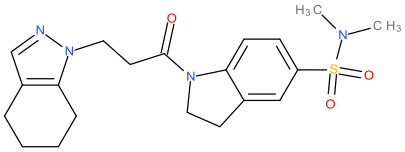	IIT library
ARN12944_Z_01	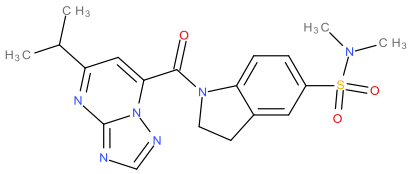	IIT library
ARN13410_Z_01	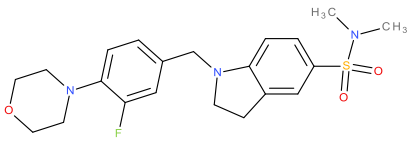	IIT library
ARN13412_Z_01	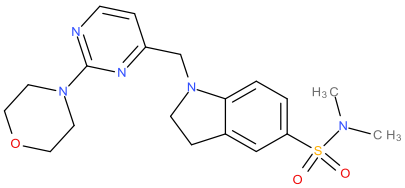	IIT library
ARN13611_Z_01	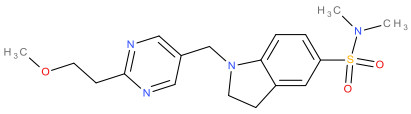	IIT library
ARN13710_Z_01	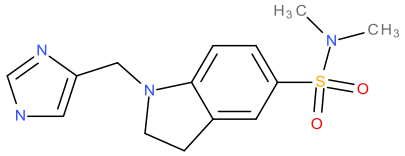	IIT library
ARN13889_Z_01	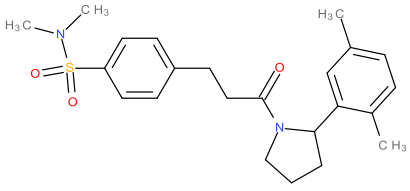	IIT library

ARN13985_Z_01	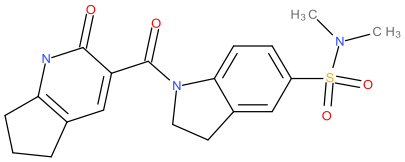	IIT library
ARN1247_Z_01	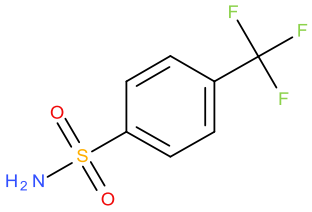	IIT library
ARN21761_Z_01	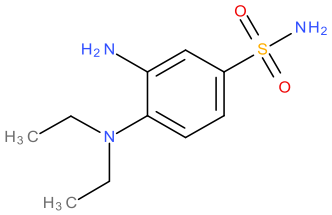	IIT library
ARN21762_Z_01	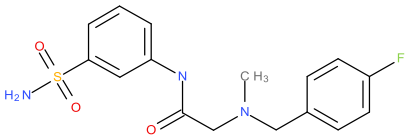	IIT library
ARN21763_Z_01	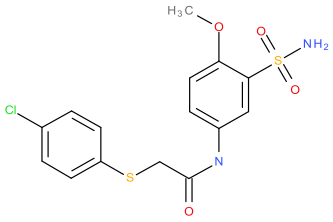	IIT library
ARN21764_Z_01	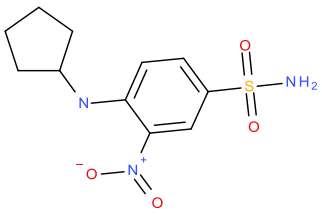	IIT library
ARN21765_Z_01	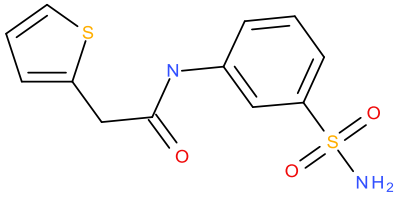	IIT library

ARN21766_Z_01	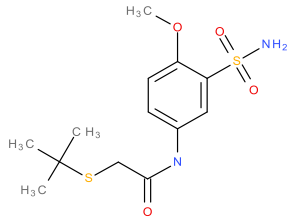	IIT library
ARN21767_Z_01	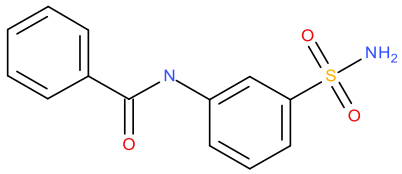	IIT library
ARN21768_Z_01	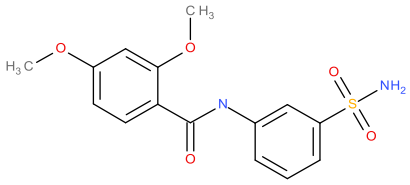	IIT library
ARN21769_Z_01	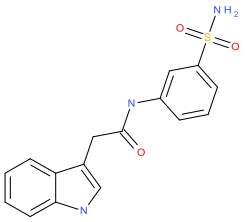	IIT library
ARN21770_Z_01	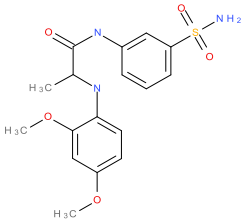	IIT library
ARN21771_Z_01	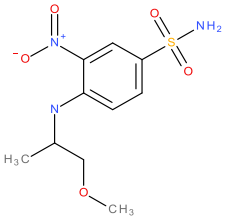	IIT library
ARN21772_Z_01	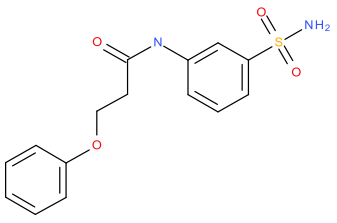	IIT library

ARN21773_Z_01	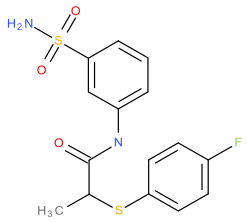	IIT library
ARN21774_Z_01	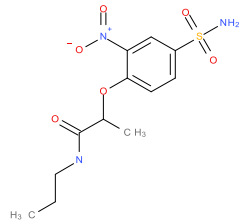	IIT library
ARN21775_Z_01	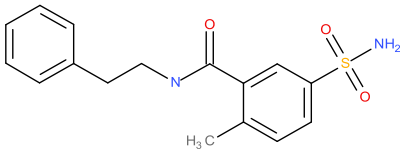	IIT library
ARN21776_Z_01	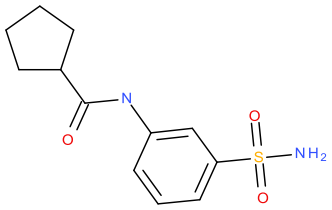	IIT library
ARN21777_Z_01	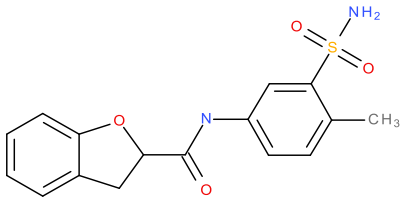	IIT library
ARN21778_Z_01	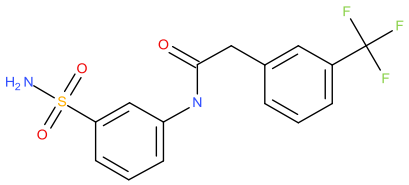	IIT library
ARN21779_Z_01	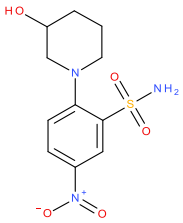	IIT library

ARN21780_Z_01	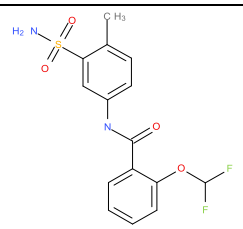	IIT library
ARN21781_Z_01	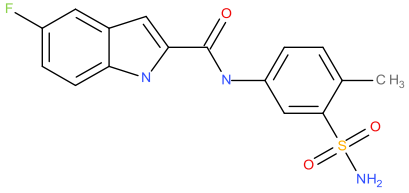	IIT library
ARN21782_Z_01	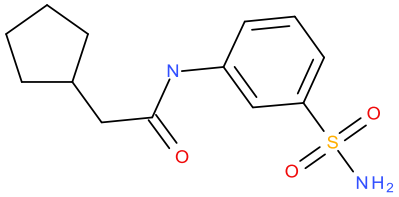	IIT library
ARN21783_Z_01	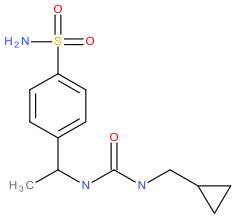	IIT library
ARN21784_Z_01	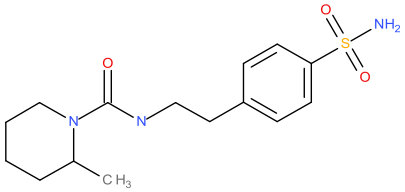	IIT library
ARN21785_Z_01	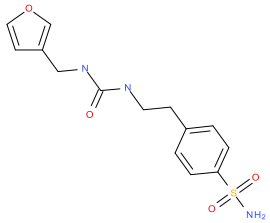	IIT library
ARN21786_Z_01	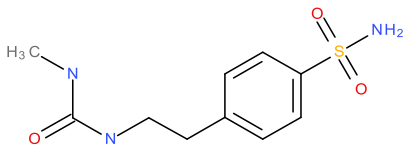	IIT library

ARN21787_Z_01	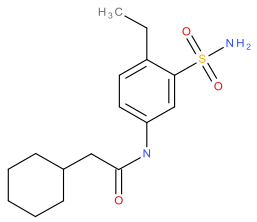	IIT library
ARN21788_Z_01	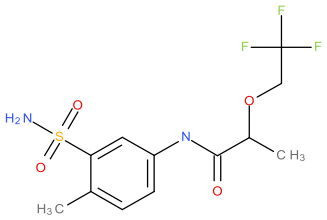	IIT library
ARN21789_Z_01	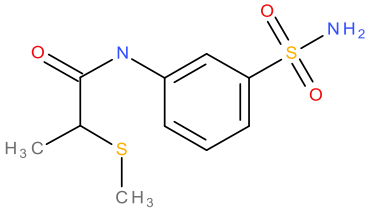	IIT library
ARN21790_Z_01	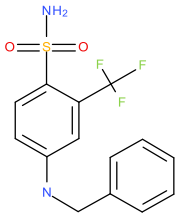	IIT library
ARN21791_Z_01	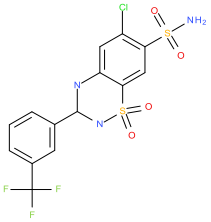	IIT library
ARN21792_Z_01	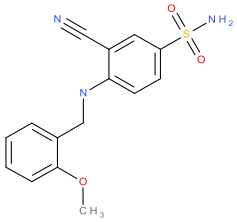	IIT library
ARN21793_Z_01	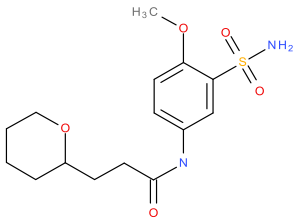	IIT library

ARN21794_Z_01	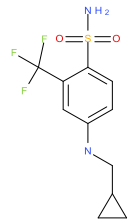	IIT library
ARN21795_Z_01	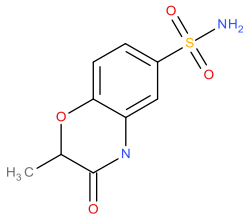	IIT library
ARN21796_Z_01	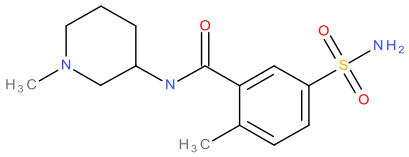	IIT library
ARN21797_Z_01	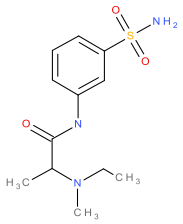	IIT library
ARN21798_Z_01	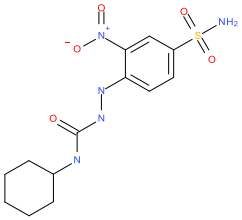	IIT library
ARN21799_Z_01	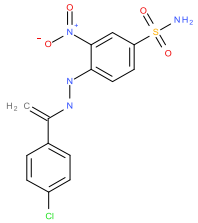	IIT library
ARN21800_Z_01	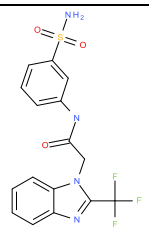	IIT library

ARN21801_Z_01	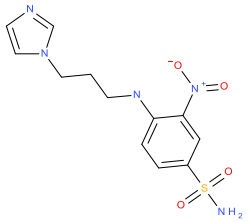	IIT library
ARN21802_Z_01	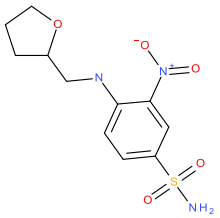	IIT library
ARN21803_Z_01	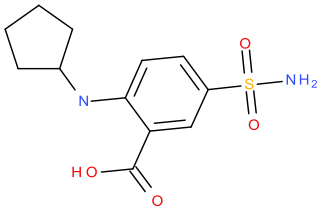	IIT library
ARN21804_Z_01	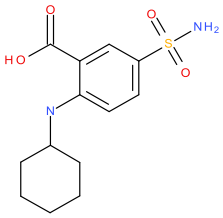	IIT library
ARN21805_Z_01	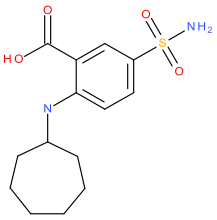	IIT library
ARN21806_Z_01	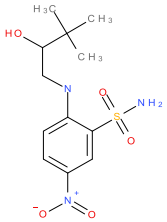	IIT library
ARN21807_Z_01	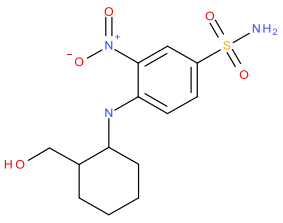	IIT library

ARN21808_Z_01	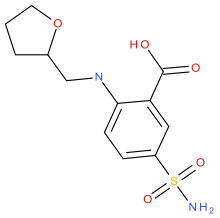	IIT library
ARN21809_Z_01	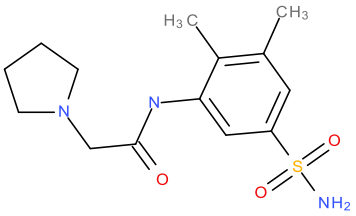	IIT library
ARN21810_Z_01	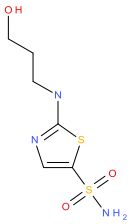	IIT library
ARN21811_Z_01	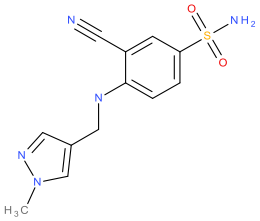	IIT library
ARN21812_Z_01	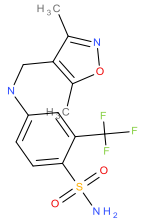	IIT library
ARN21813_Z_01	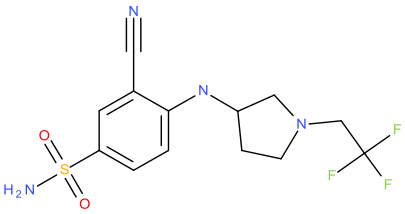	IIT library
ARN21814_Z_01	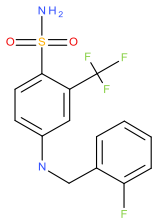	IIT library

ARN21815_Z_01	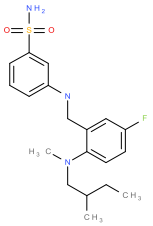	IIT library
ARN21816_Z_01	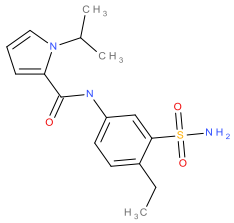	IIT library
ARN21817_Z_01	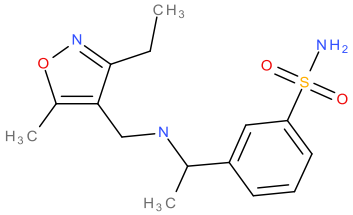	IIT library
ARN21818_Z_01	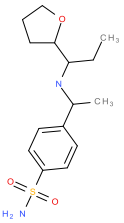	IIT library
ARN21819_Z_01	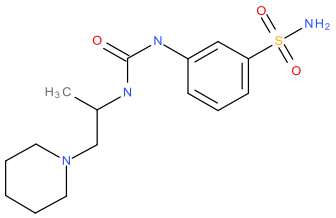	IIT library
ARN21820_Z_01	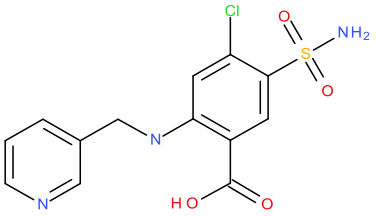	IIT library
ARN21821_Z_01	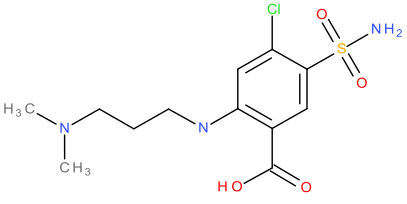	IIT library

ARN21822_Z_01	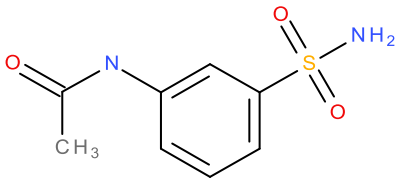	IIT library
ARN21823_Z_01	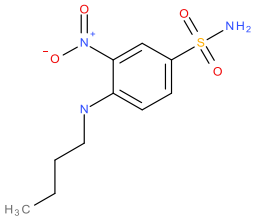	IIT library
ARN21824_Z_01	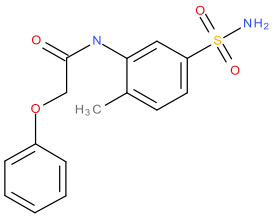	IIT library
ARN21825_Z_01	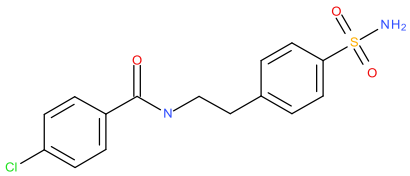	IIT library
ARN21826_Z_01	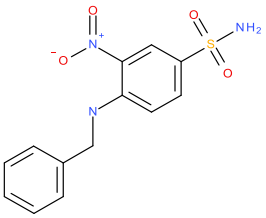	IIT library
ARN21827_Z_01	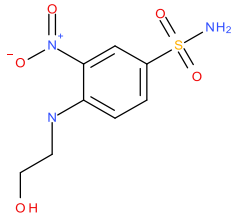	IIT library
ARN21828_Z_01	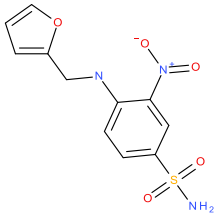	IIT library

ARN21829_Z_01	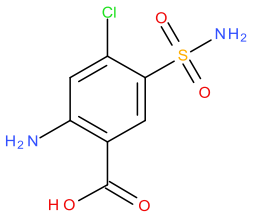	IIT library
ARN21830_Z_01	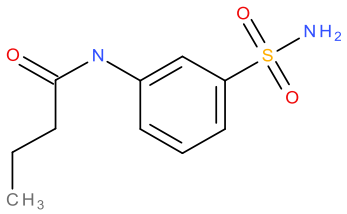	IIT library
ARN21831_Z_01	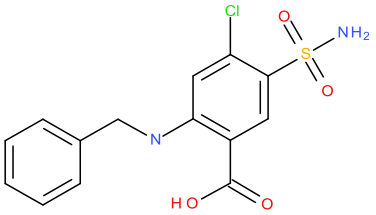	IIT library
ARN17439_Z_01	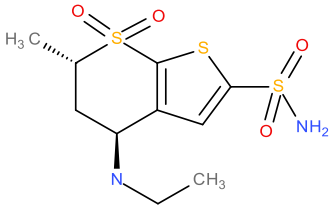	IIT library
ARN21832_Z_01	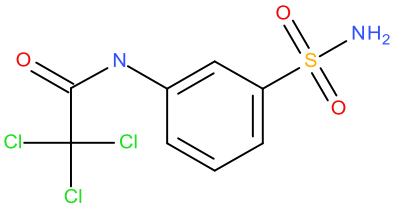	IIT library
ARN21833_Z_01	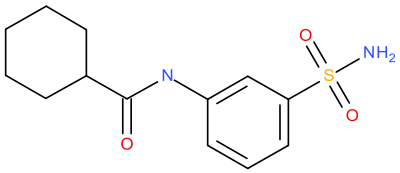	IIT library
ARN21834_Z_01	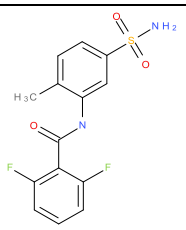	IIT library

ARN21835_Z_01	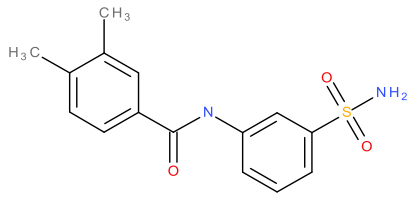	IIT library
ARN21836_Z_01	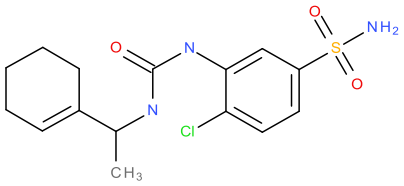	IIT library
ARN21837_Z_01	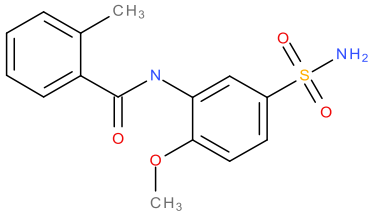	IIT library
ARN21838_Z_01	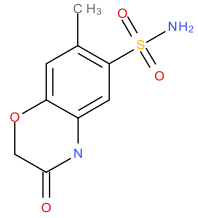	IIT library
ARN21839_Z_01	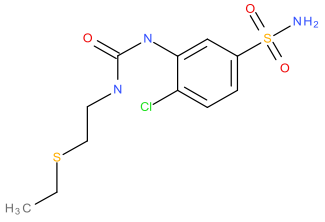	IIT library
ARN21840_Z_01	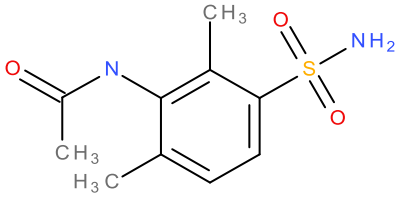	IIT library
ARN21841_Z_01	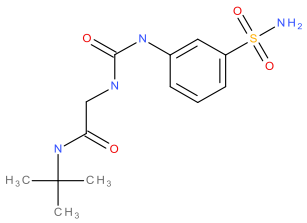	IIT library

ARN21842_Z_01	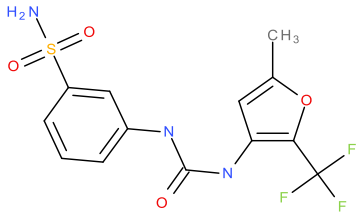	IIT library
ARN21843_Z_01	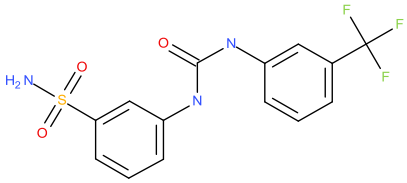	IIT library
ARN21844_Z_01	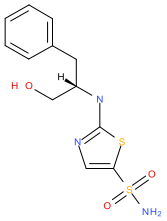	IIT library
ARN21855_Z_01	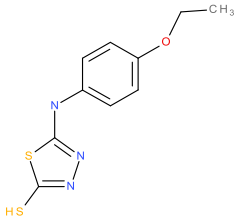	IIT library
ARN0106_Z_01	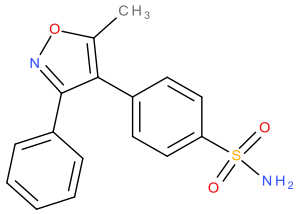	IIT library
ARN0107_Z_01	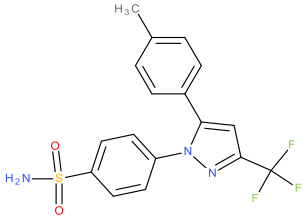	IIT library
ARN2982_Z_01	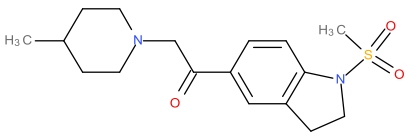	IIT library

ARN4445_Z_01	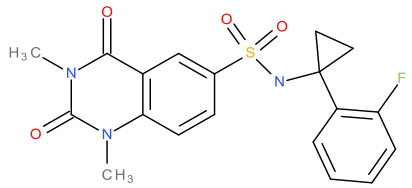	IIT library
ARN4563_Z_01	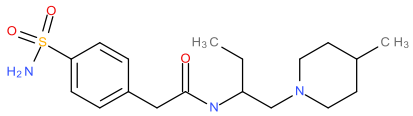	IIT library
ARN4706_Z_01	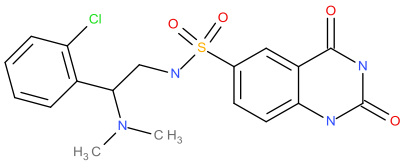	IIT library
ARN5796_A_01	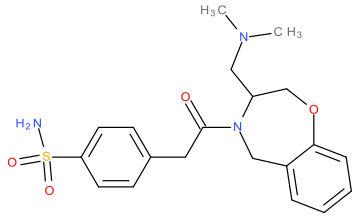	IIT library
ARN7397_Z_01	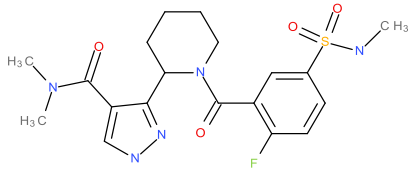	IIT library
ARN9288_Z_01	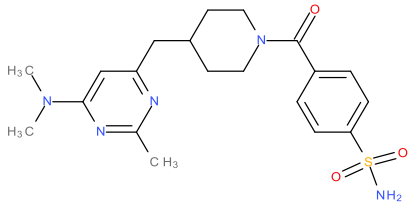	IIT library
ARN9687_Z_01	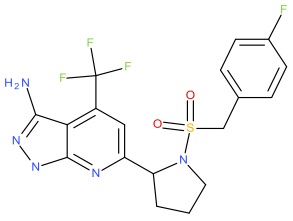	IIT library

ARN10239_Z_01	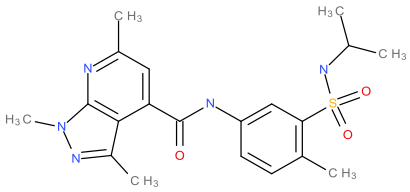	IIT library
ARN10251_Z_01	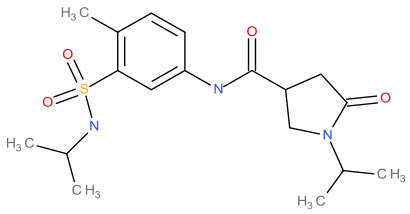	IIT library
ARN10326_Z_01	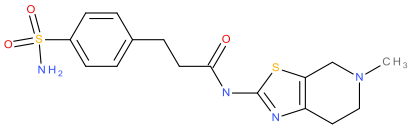	IIT library
ARN10449_Z_01	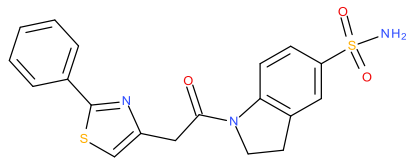	IIT library
ARN10694_Z_01	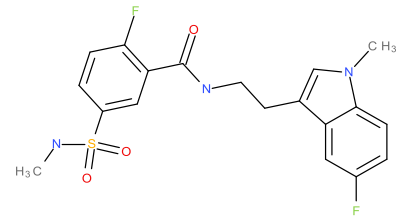	IIT library
ARN10966_Z_01	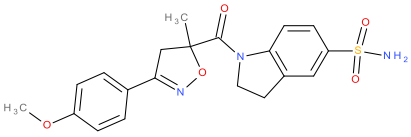	IIT library
ARN10974_Z_01	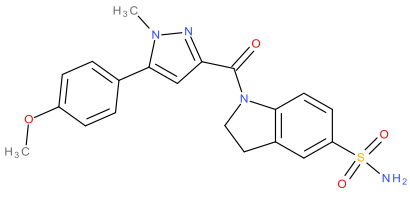	IIT library

ARN11552_Z_01	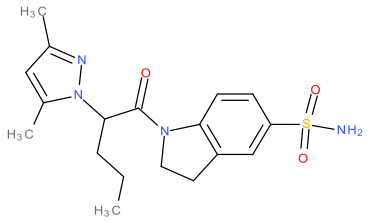	IIT library
ARN11800_Z_01	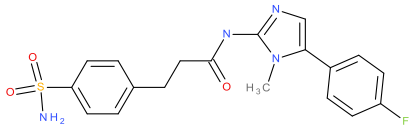	IIT library
ARN11951_Z_01	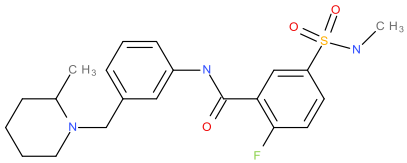	IIT library
ARN12069_Z_01	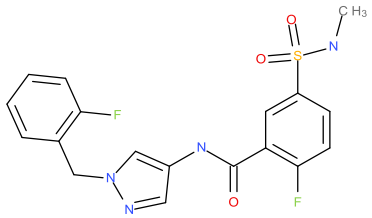	IIT library
ARN12785_Z_01	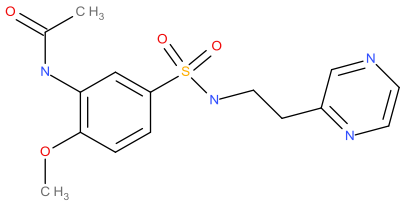	IIT library
ARN13436_Z_01	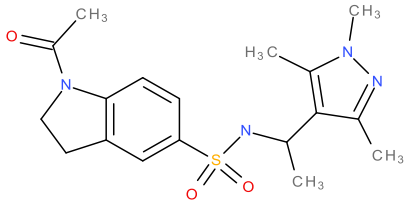	IIT library
ARN14604_Z_01	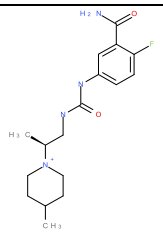	IIT library

ARN14619_Z_01	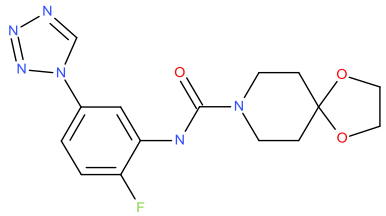	IIT library
ARN19905_Z_01	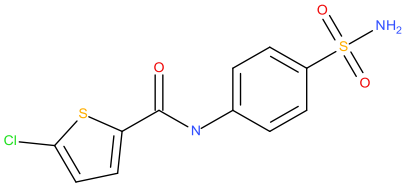	Commercial vendors
ARN19906_Z_01	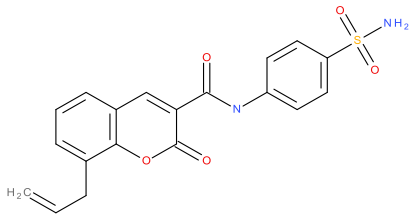	Commercial vendors
ARN19990_Z_01	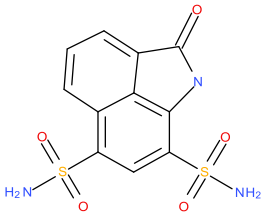	Commercial vendors
ARN19907_Z_01	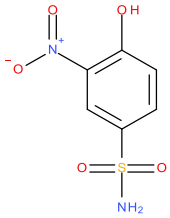	Commercial vendors
ARN19908_Z_01	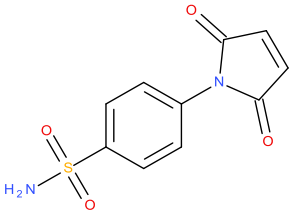	Commercial vendors
ARN19909_Z_01	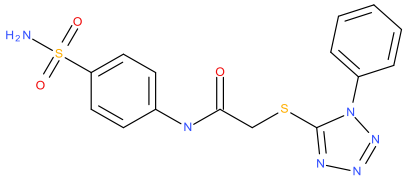	Commercial vendors

ARN19910_Z_01	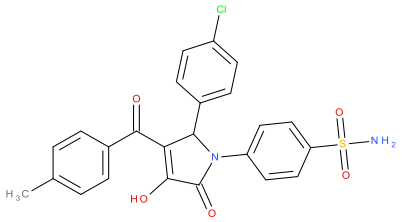	Commercial vendors
ARN19911_Z_01	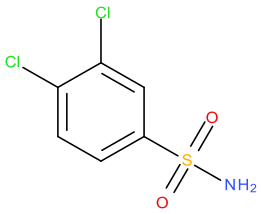	Commercial vendors
ARN19991_Z_01	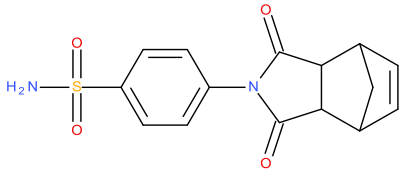	Commercial vendors
ARN19912_Z_01	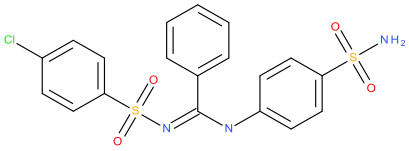	Commercial vendors
ARN19913_Z_01	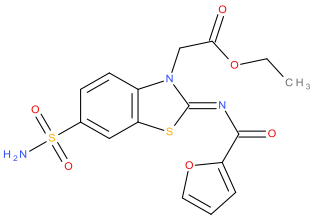	Commercial vendors
ARN19914_Z_01	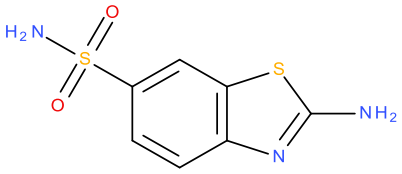	Commercial vendors
ARN19915_Z_01	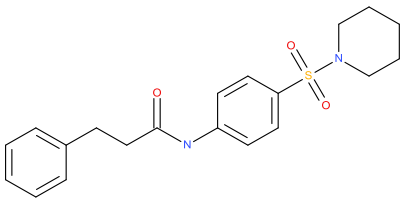	Commercial vendors

ARN19916_Z_01	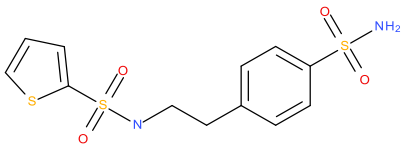	Commercial vendors
ARN19917_Z_01	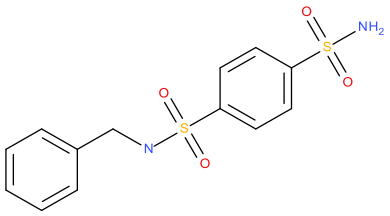	Commercial vendors
ARN19918_Z_01	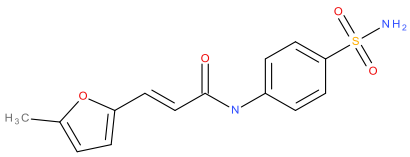	Commercial vendors
ARN19919_Z_01	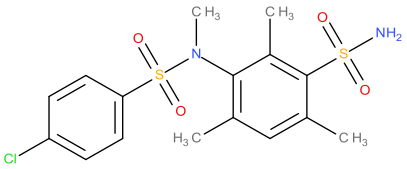	Commercial vendors
ARN19920_Z_01	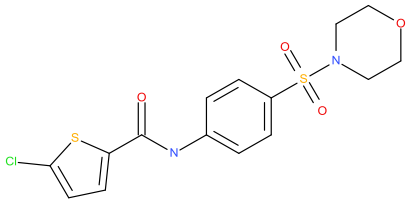	Commercial vendors
ARN19921_Z_01	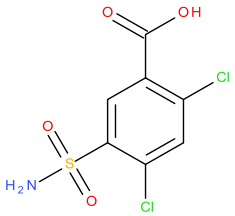	Commercial vendors
ARN19922_Z_01	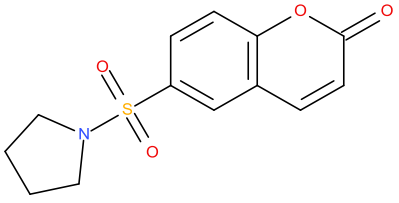	Commercial vendors

ARN19923_Z_01	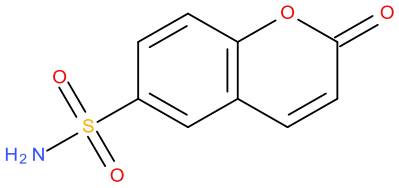	Commercial vendors
ARN19924_Z_01	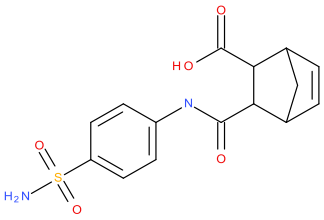	Commercial vendors
ARN19925_Z_01	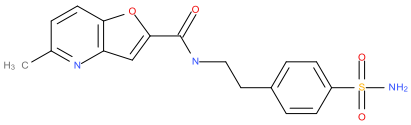	Commercial vendors
ARN19926_Z_01	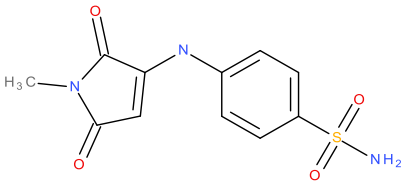	Commercial vendors
ARN19927_Z_01	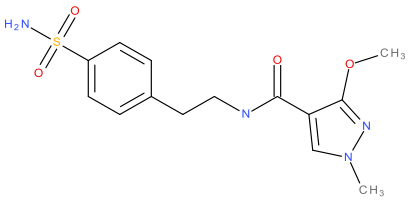	Commercial vendors
ARN19928_Z_01	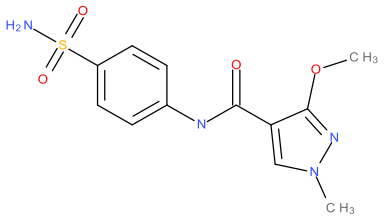	Commercial vendors
ARN19929_Z_01	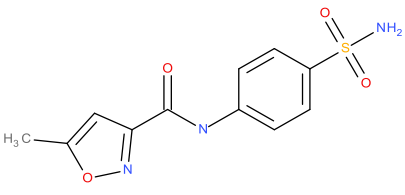	Commercial vendors

ARN19930_Z_01	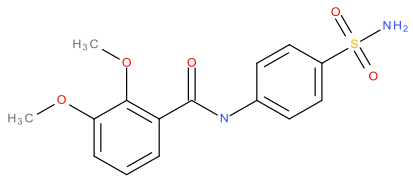	Commercial vendors
ARN19931_Z_01	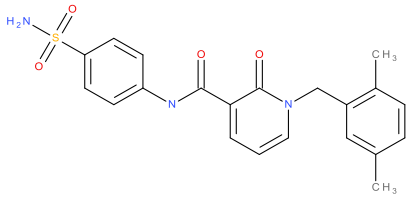	Commercial vendors
ARN19932_Z_01	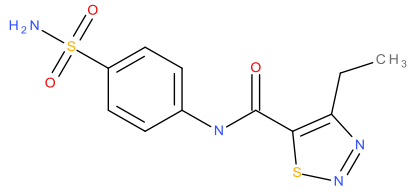	Commercial vendors
ARN19933_Z_01	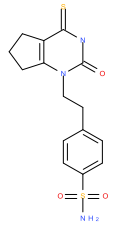	Commercial vendors
ARN19934_Z_01	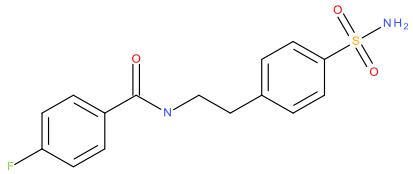	Commercial vendors
ARN19935_Z_01	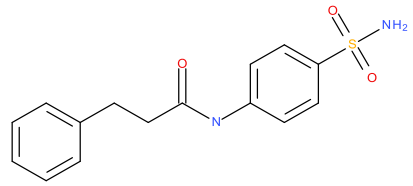	Commercial vendors
ARN19936_Z_01	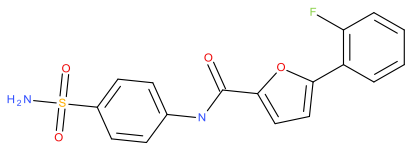	Commercial vendors

ARN19937_Z_01	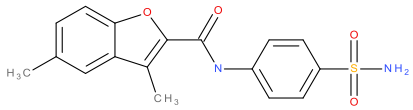	Commercial vendors
ARN19938_Z_01	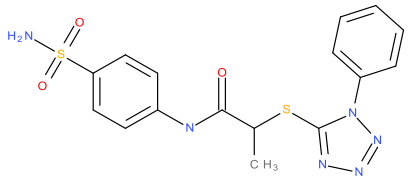	Commercial vendors
ARN19992_Z_01	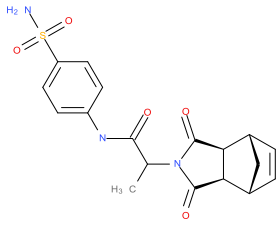	Commercial vendors
ARN19939_Z_01	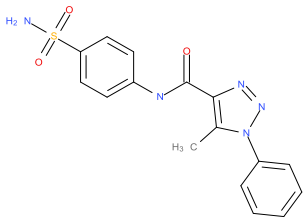	Commercial vendors
ARN19940_Z_01	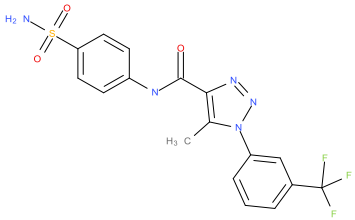	Commercial vendors
ARN19941_Z_01	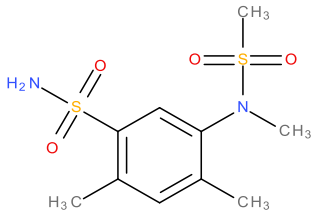	Commercial vendors
ARN19942_Z_01	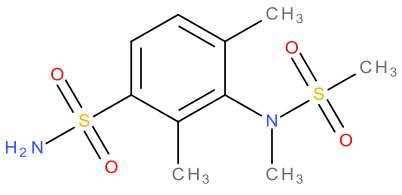	Commercial vendors

ARN19943_Z_01	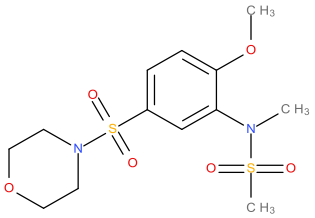	Commercial vendors
ARN19944_Z_01	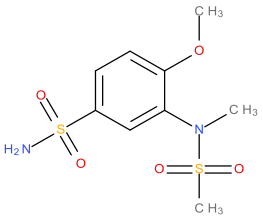	Commercial vendors
ARN19945_Z_01	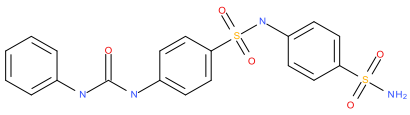	Commercial vendors
ARN19946_Z_01	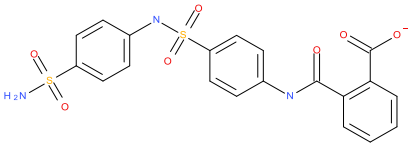	Commercial vendors
ARN19947_Z_01	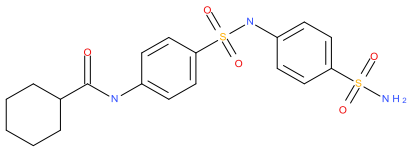	Commercial vendors
ARN19948_Z_01	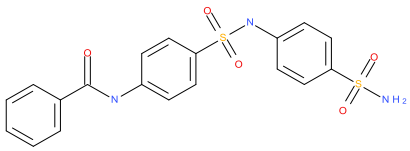	Commercial vendors
ARN19949_Z_01	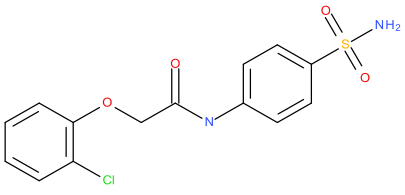	Commercial vendors

ARN19950_Z_01	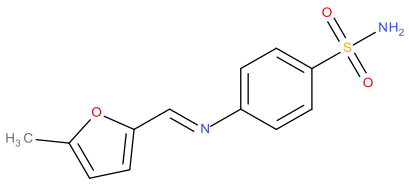	Commercial vendors
ARN19951_Z_01	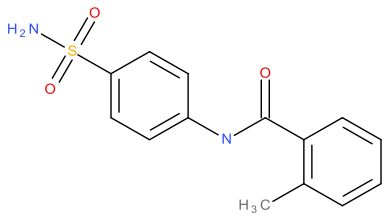	Commercial vendors
ARN19952_Z_01	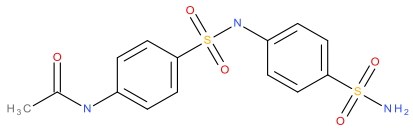	Commercial vendors
ARN19953_Z_01	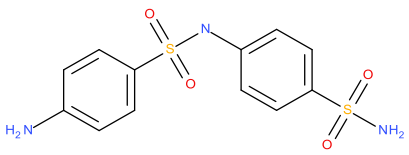	Commercial vendors
ARN19954_Z_01	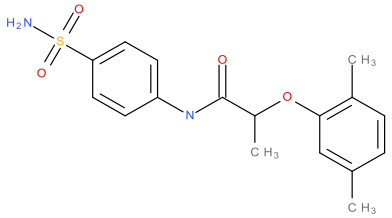	Commercial vendors
ARN19955_Z_01	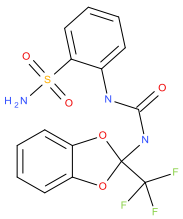	Commercial vendors
ARN19956_Z_01	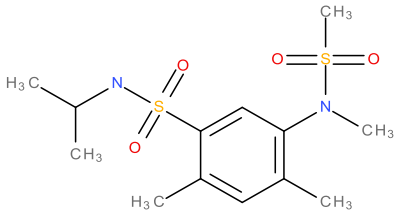	Commercial vendors

ARN19957_Z_01	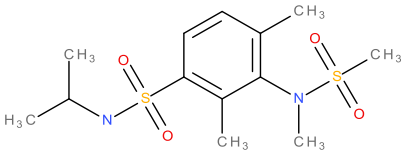	Commercial vendors
ARN19958_Z_01	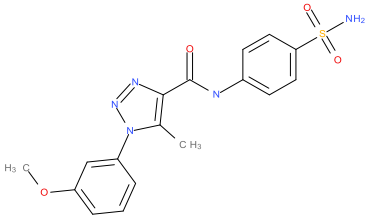	Commercial vendors
ARN19959_Z_01	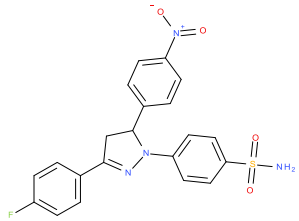	Commercial vendors
ARN19960_Z_01	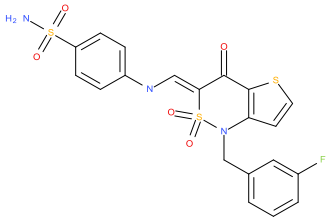	Commercial vendors
ARN19961_Z_01	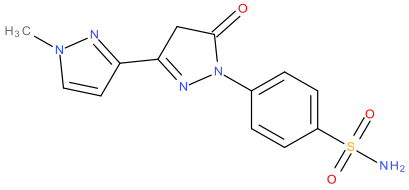	Commercial vendors
ARN19962_Z_01	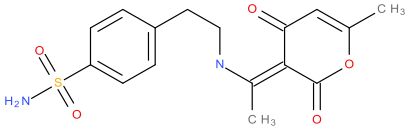	Commercial vendors
ARN19963_Z_01	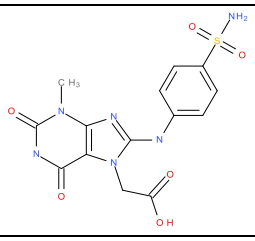	Commercial vendors

ARN19964_Z_01	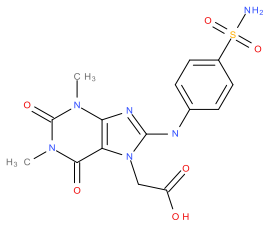	Commercial vendors
ARN19965_Z_01	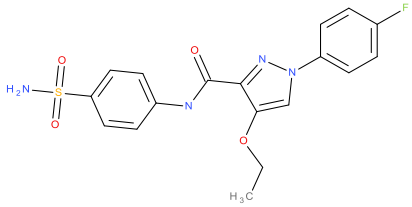	Commercial vendors
ARN19966_Z_01	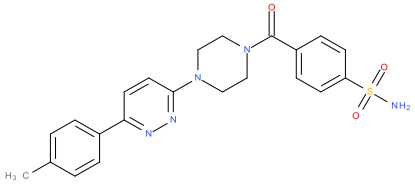	Commercial vendors
ARN19967_Z_01	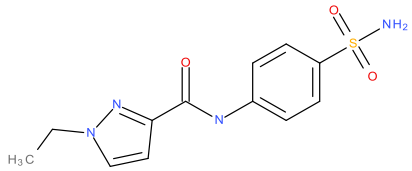	Commercial vendors
ARN19968_Z_01	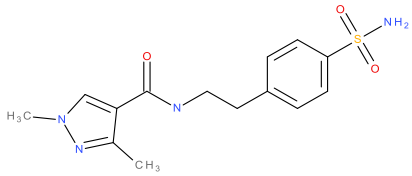	Commercial vendors
ARN19969_Z_01	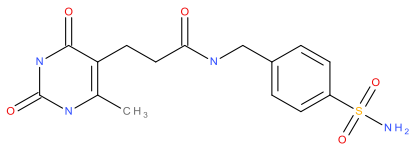	Commercial vendors
ARN19970_Z_01	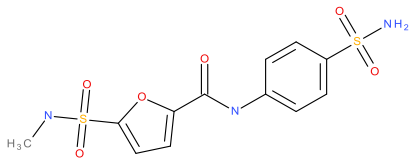	Commercial vendors

ARN19971_Z_01	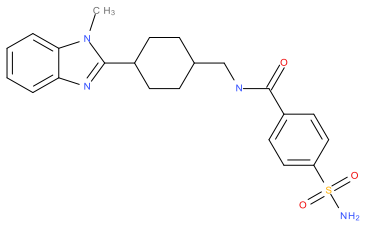	Commercial vendors
ARN19972_Z_01	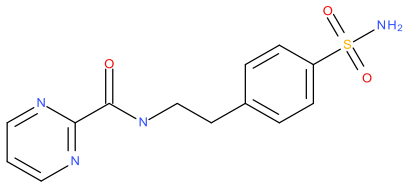	Commercial vendors
ARN19973_Z_01	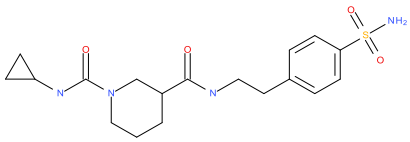	Commercial vendors
ARN19974_Z_01	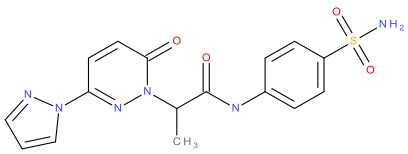	Commercial vendors
ARN19975_Z_01	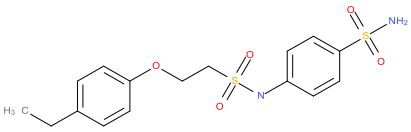	Commercial vendors
ARN19976_Z_01	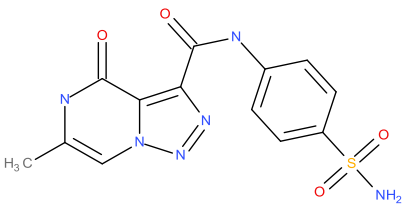	Commercial vendors
ARN19977_Z_01	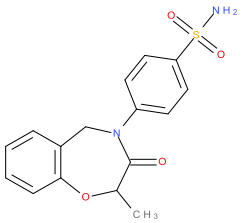	Commercial vendors

ARN19978_Z_01	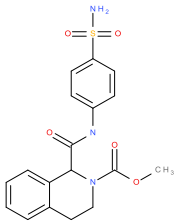	Commercial vendors
ARN19979_Z_01	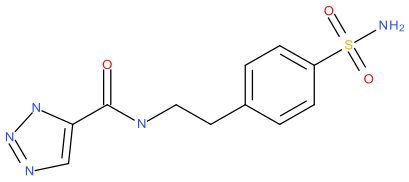	Commercial vendors
ARN19980_Z_01	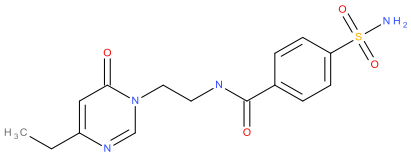	Commercial vendors
ARN19981_Z_01	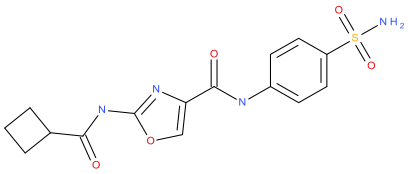	Commercial vendors
ARN19982_Z_01	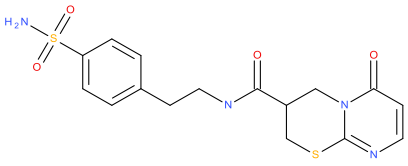	Commercial vendors
ARN19983_Z_01	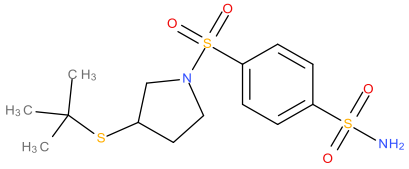	Commercial vendors
ARN19984_Z_01	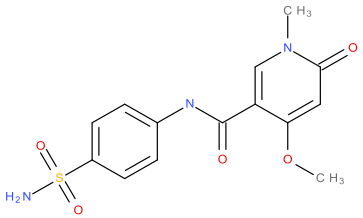	Commercial vendors

ARN19985_Z_01	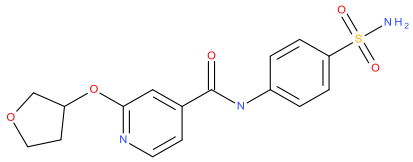	Commercial vendors
ARN19986_Z_01	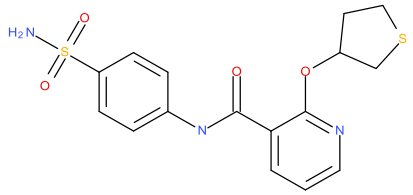	Commercial vendors
ARN19987_Z_01	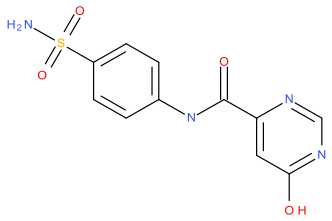	Commercial vendors
ARN19988_Z_01	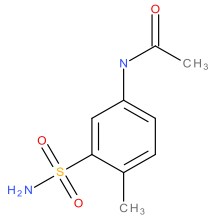	Commercial vendors
ARN19989_Z_01	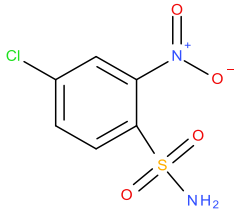	Commercial vendors
ARN22393_Z_01	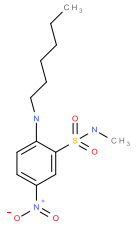	IIT library
ARN22394_Z_01	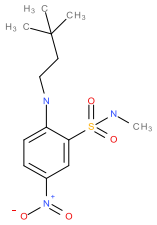	IIT library

ARN22132_Z_01	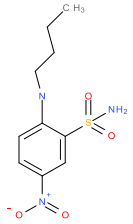	Nitro-benzene-sulfonamide
ARN22131_Z_01	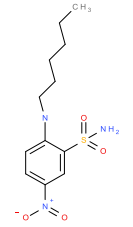	Nitro-benzene-sulfonamide
ARN22134_Z_01	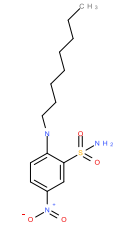	Nitro-benzene-sulfonamide
ARN22311_Z_01	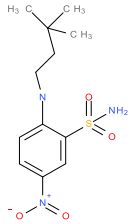	Nitro-benzene-sulfonamide
ARN22392_Z_01	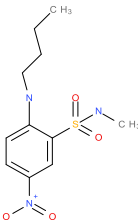	Nitro-benzene-sulfonamide
ARN22393_Z_01	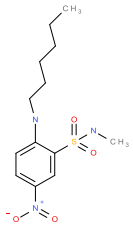	Nitro-benzene-sulfonamide
ARN22395_Z_01	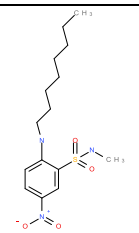	Nitro-benzene-sulfonamide

ARN22394_Z_01	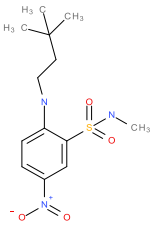	Nitro-benzene-sulfonamide
ARN22377_Z_01	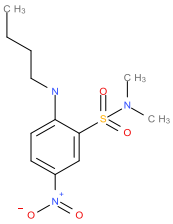	Nitro-benzene-sulfonamide
ARN22312_Z_01	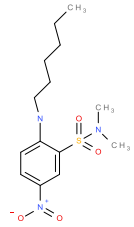	Nitro-benzene-sulfonamide
ARN22378_Z_01	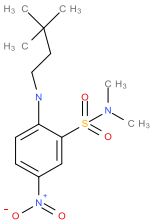	Nitro-benzene-sulfonamide
ARN22379_Z_01	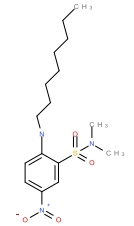	Nitro-benzene-sulfonamide
ARN22375_Z_01	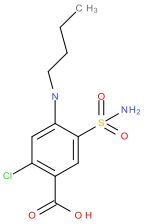	Sulfamoyl-benzoic acid
ARN22348_Z_01	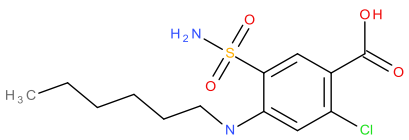	Sulfamoyl-benzoic acid

ARN22357_Z_01	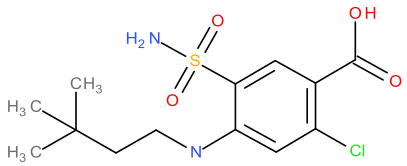	Sulfamoyl-benzoic acid
ARN22358_Z_01	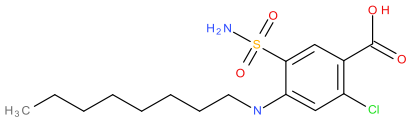	Sulfamoyl-benzoic acid
ARN22380_Z_01	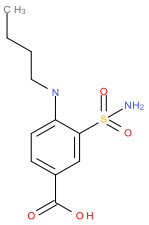	Sulfamoyl-benzoic acid
ARN22356_Z_01	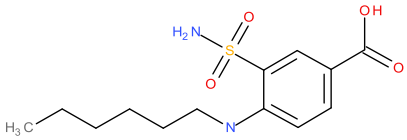	Sulfamoyl-benzoic acid
ARN22374_Z_01	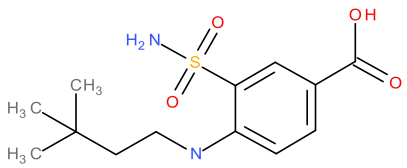	Sulfamoyl-benzoic acid
ARN22376_Z_01	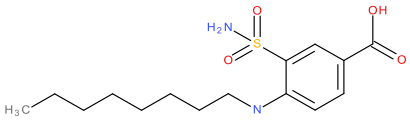	Sulfamoyl-benzoic acid
ARN22635_Z_01	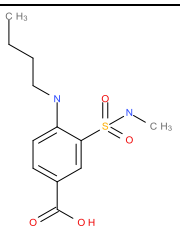	Sulfamoyl-benzoic acid

ARN22636_Z_01	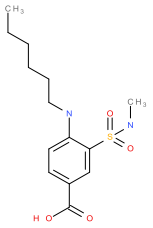	Sulfamoyl-benzoic acid
ARN22642_Z_01	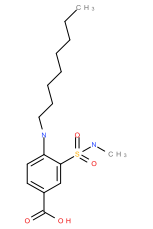	Sulfamoyl-benzoic acid
ARN22640_Z_01	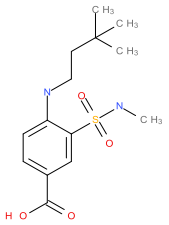	Sulfamoyl-benzoic acid
ARN22402_Z_01	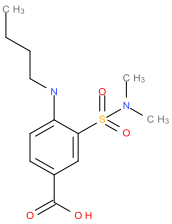	Sulfamoyl-benzoic acid
ARN22396_Z_01	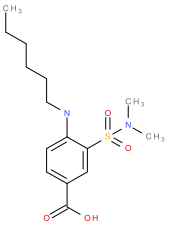	Sulfamoyl-benzoic acid
ARN22430_Z_01	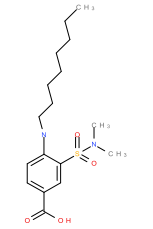	Sulfamoyl-benzoic acid
ARN22429_Z_01	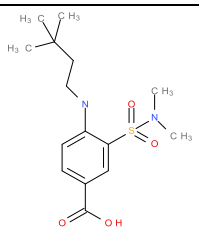	Sulfamoyl-benzoic acid

ARN22655_Z_01	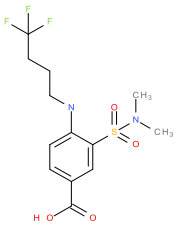	Sulfamoyl-benzoic acid
ARN23726_Z_01	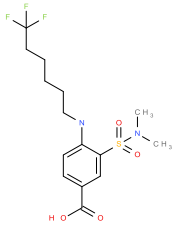	Sulfamoyl-benzoic acid
ARN23746_Z_01	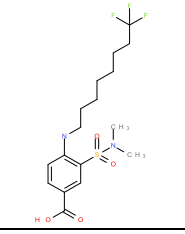	Sulfamoyl-benzoic acid
ARN22657_Z_01	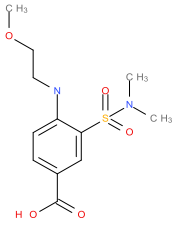	Sulfamoyl-benzoic acid
ARN23741_Z_01	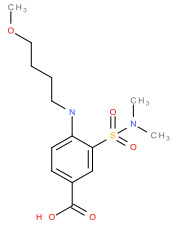	Sulfamoyl-benzoic acid
ARN23758_Z_01	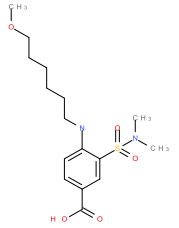	Sulfamoyl-benzoic acid
ARN24231_Z_01	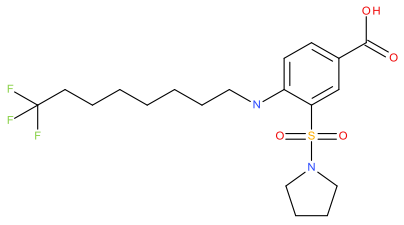	Sulfamoyl-benzoic acid

ARN24232_Z_01	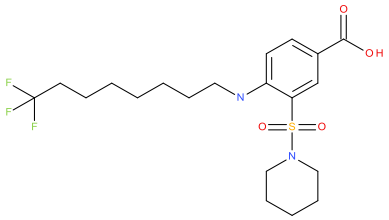	Sulfamoyl-benzoic acid
ARN24233_Z_01	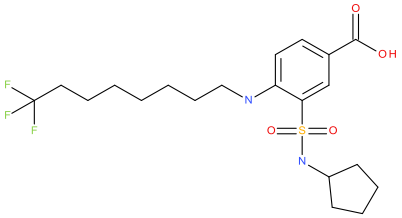	Sulfamoyl-benzoic acid
ARN24234_Z_01	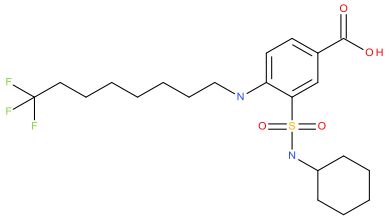	Sulfamoyl-benzoic acid
ARN24255_Z_01	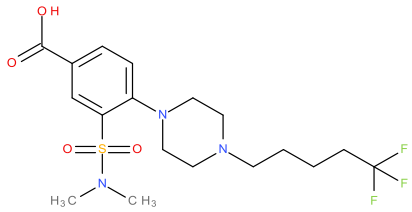	Sulfamoyl-benzoic acid
ARN24256_Z_01	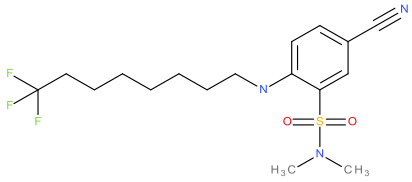	Sulfamoyl-benzoic acid
ARN24290_Z_01	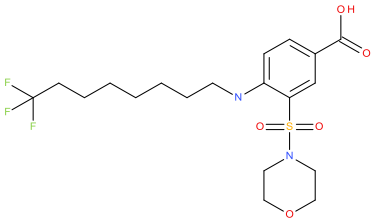	Sulfamoyl-benzoic acid
ARN24367_Z_01	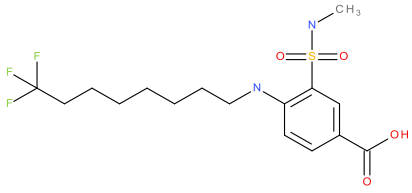	Sulfamoyl-benzoic acid

ARN24092_Z_01	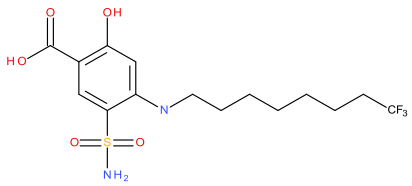	Sulfamoyl-benzoic acid

References

Abbah, J., Juliano, S. L. (2014). Altered migratory behavior of interneurons in a model of cortical dysplasia: the influence of elevated GABAA activity. *Cereb Cortex, 24*(9), 2297-2308.

Achilles, K., Okabe, A., Ikeda, M., Shimizu-Okabe, C., Yamada, J., Fukuda, A., Luhmann, H. J., Kilb, W. (2007). Kinetic properties of Cl uptake mediated by Na+-dependent K+-2Cl cotransport in immature rat neocortical neurons. *J Neurosci, 27*(32), 8616-8627.

Aguado, F., Carmona, M. A., Pozas, E., Aguilo, A., Martinez-Guijarro, F. J., Alcantara, S., Borrell, V., Yuste, R., Ibanez, C. F., Soriano, E. (2003). BDNF regulates spontaneous correlated activity at early developmental stages by increasing synaptogenesis and expression of the K+/Cl- co-transporter KCC2. *Development, 130*(7), 1267-1280.

Akiyama, K., Miyashita, T., Matsubara, A., Mori, N. (2010). The detailed localization pattern of Na+/K+/2Cl- cotransporter type 2 and its related ion transport system in the rat endolymphatic sac. *J Histochem Cytochem, 58*(8), 759-763.

Almeida, A. C., Scorza, F. A., Rodrigues, A. M., Arida, R. M., Carlesso, F. N., Batista, A. G., Duarte, M. A., DaCosta, J. C. (2011). Combined effect of bumetanide, bromide, and GABAergic agonists: an alternative treatment for intractable seizures. *Epilepsy Behav, 20*(1), 147-149.

Alsubie, H. S., Rosen, D. (2018). The evaluation and management of respiratory disease in children with Down syndrome (DS). *Paediatr Respir Rev, 26*, 49-54.

Amadeo, A., Coatti, A., Aracri, P., Ascagni, M., Iannantuoni, D., Modena, D., Carraresi, L., Brusco, S., Meneghini, S., Arcangeli, A., Pasini, M. E., Becchetti, A. (2018). Postnatal Changes in K(+)/Cl(-) Cotransporter-2 Expression in the Forebrain of Mice Bearing a Mutant Nicotinic Subunit Linked to Sleep-Related Epilepsy. *Neuroscience, 386*, 91-107.

Amin, H., Marinaro, F., De Pietri Tonelli, D., Berdondini, L. (2017). Developmental excitatory-to-inhibitory GABA-polarity switch is disrupted in 22q11.2 deletion syndrome: a potential target for clinical therapeutics. *Sci Rep, 7*(1), 15752.

Antonarakis, S. E., Epstein, C. J. (2006). The challenge of Down syndrome. *Trends Mol Med, 12*(10), 473-479.

Antonarakis, S. E., Lyle, R., Dermitzakis, E. T., Reymond, A., Deutsch, S. (2004). Chromosome 21 and down syndrome: from genomics to pathophysiology. *Nat Rev Genet, 5*(10), 725-738.

Arichi, T., Whitehead, K., Barone, G., Pressler, R., Padormo, F., Edwards, A. D., Fabrizi, L. (2017). Localization of spontaneous bursting neuronal activity in the preterm human brain with simultaneous EEG-fMRI. *Elife, 6*.

Arion, D., Lewis, D. A. (2011). Altered expression of regulators of the cortical chloride transporters NKCC1 and KCC2 in schizophrenia. *Arch Gen Psychiatry, 68*(1), 21-31.

Aronica, E., Boer, K., Redeker, S., Spliet, W. G., van Rijen, P. C., Troost, D., Gorter, J. A. (2007). Differential expression patterns of chloride transporters, Na+-K+-2Cl--cotransporter and K+-Cl--cotransporter, in epilepsy-associated malformations of cortical development. *Neuroscience, 145*(1), 185-196.

Arya, R., Kabra, M., Gulati, S. (2011). Epilepsy in children with Down syndrome. *Epileptic Disord, 13*(1), 1-7.

Asbury, M. J., Gatenby, P. B., O'Sullivan, S., Bourke, E. (1972). Bumetanide: potent new "loop" diuretic. *Br Med J, 1*(5794), 211-213.

Awad, P. N., Sanon, N. T., Chattopadhyaya, B., Carrico, J. N., Ouardouz, M., Gagne, J., Duss, S., Wolf, D., Desgent, S., Cancedda, L., Carmant, L., Di Cristo, G. (2016). Reducing premature KCC2 expression rescues seizure susceptibility and spine morphology in atypical febrile seizures. *Neurobiol Dis, 91*, 10-20.

Baek, H., Yi, M. H., Pandit, S., Park, J. B., Kwon, H. H., Zhang, E., Kim, S., Shin, N., Kim, E., Lee, Y. H., Kim, Y., Kim, D. W., Kang, J. W. (2016). Altered expression of KCC2 in GABAergic interneuron contributes prenatal stress-induced epileptic spasms in infant rat. *Neurochem Int, 97*, 57-64.

Baker, S. J., Ellison, D. W., Gutmann, D. H. (2016). Pediatric gliomas as neurodevelopmental disorders. *Glia, 64*(6), 879-895.

Balu, D. T., Coyle, J. T. (2011). Neuroplasticity signaling pathways linked to the pathophysiology of schizophrenia. *Neurosci Biobehav Rev, 35*(3), 848-870.

Banerjee, A., Rikhye, R. V., Breton-Provencher, V., Tang, X., Li, C., Li, K., Runyan, C. A., Fu, Z., Jaenisch, R., Sur, M. (2016). Jointly reduced inhibition and excitation underlies circuit-wide changes in cortical processing in Rett syndrome. *Proc Natl Acad Sci U S A, 113*(46), E7287-E7296.

Baroncelli, L., Cenni, M. C., Melani, R., Deidda, G., Landi, S., Narducci, R., Cancedda, L., Maffei, L., Berardi, N. (2017). Early IGF-1 primes visual cortex maturation and accelerates developmental switch between NKCC1 and KCC2 chloride transporters in enriched animals. *Neuropharmacology, 113*(Pt A), 167-177.

Baroncelli, L., Sale, A., Viegi, A., Maya Vetencourt, J. F., De Pasquale, R., Baldini, S., Maffei, L. (2010). Experience-dependent reactivation of ocular dominance plasticity in the adult visual cortex. *Exp Neurol, 226*(1), 100-109.

Bayatti, N., Moss, J. A., Sun, L., Ambrose, P., Ward, J. F., Lindsay, S., Clowry, G. J. (2008). A molecular neuroanatomical study of the developing human neocortex from 8 to 17 postconceptional weeks revealing the early differentiation of the subplate and subventricular zone. *Cereb Cortex, 18*(7), 1536-1548.

Becker, M., Nothwang, H. G., Friauf, E. (2003). Differential expression pattern of chloride transporters NCC, NKCC2, KCC1, KCC3, KCC4, and AE3 in the developing rat auditory brainstem. *Cell Tissue Res, 312*(2), 155-165.

Begenisic, T., Baroncelli, L., Sansevero, G., Milanese, M., Bonifacino, T., Bonanno, G., Cioni, G., Maffei, L., Sale, A. (2014). Fluoxetine in adulthood normalizes GABA release and rescues hippocampal synaptic plasticity and spatial memory in a mouse model of Down syndrome. *Neurobiol Dis, 63*, 12-19.

Begenisic, T., Sansevero, G., Baroncelli, L., Cioni, G., Sale, A. (2015). Early environmental therapy rescues brain development in a mouse model of Down syndrome. *Neurobiol Dis, 82*, 409-419.

Begenisic, T., Spolidoro, M., Braschi, C., Baroncelli, L., Milanese, M., Pietra, G., Fabbri, M. E., Bonanno, G., Cioni, G., Maffei, L., Sale, A. (2011). Environmental enrichment decreases GABAergic inhibition and improves cognitive abilities, synaptic plasticity, and visual functions in a mouse model of Down syndrome. *Front Cell Neurosci, 5*, 29.

Begum, G., Yuan, H., Kahle, K. T., Li, L., Wang, S., Shi, Y., Shmukler, B. E., Yang, S. S., Lin, S. H., Alper, S. L., Sun, D. (2015). Inhibition of WNK3 Kinase Signaling Reduces Brain Damage and Accelerates Neurological Recovery After Stroke. *Stroke, 46*(7), 1956-1965.

Begum, M. R., Sng, J. C. G. (2017). Molecular mechanisms of experience-dependent maturation in cortical GABAergic inhibition. *J Neurochem, 142*(5), 649-661.
Behar, T. N., Li, Y. X., Tran, H. T., Ma, W., Dunlap, V., Scott, C., Barker, J. L. (1996). GABA stimulates chemotaxis and chemokinesis of embryonic cortical neurons via calcium-dependent mechanisms. *J Neurosci, 16*(5), 1808-1818.
Behar, T. N., Schaffner, A. E., Scott, C. A., O'Connell, C., Barker, J. L. (1998). Differential response of cortical plate and ventricular zone cells to GABA as a migration stimulus. *J Neurosci, 18*(16), 6378-6387.
Belichenko, N. P., Belichenko, P. V., Kleschevnikov, A. M., Salehi, A., Reeves, R. H., Mobley, W. C. (2009). The "Down syndrome critical region" is sufficient in the mouse model to confer behavioral, neurophysiological, and synaptic phenotypes characteristic of Down syndrome. *J Neurosci, 29*(18), 5938-5948.
Belichenko, P. V., Kleschevnikov, A. M., Becker, A., Wagner, G. E., Lysenko, L. V., Yu, Y. E., Mobley, W. C. (2015). Down Syndrome Cognitive Phenotypes Modeled in Mice Trisomic for All HSA 21 Homologues. *PLoS One, 10*(7), e0134861.
Belichenko, P. V., Kleschevnikov, A. M., Masliah, E., Wu, C., Takimoto-Kimura, R., Salehi, A., Mobley, W. C. (2009). Excitatory-inhibitory relationship in the fascia dentata in the Ts65Dn mouse model of Down syndrome. *J Comp Neurol, 512*(4), 453-466.
Belichenko, P. V., Kleschevnikov, A. M., Salehi, A., Epstein, C. J., Mobley, W. C. (2007). Synaptic and cognitive abnormalities in mouse models of Down syndrome: exploring genotype-phenotype relationships. *J Comp Neurol, 504*(4), 329-345.
Belichenko, P. V., Masliah, E., Kleschevnikov, A. M., Villar, A. J., Epstein, C. J., Salehi, A., Mobley, W. C. (2004). Synaptic structural abnormalities in the Ts65Dn mouse model of Down Syndrome. *J Comp Neurol, 480*(3), 281-298.
Ben-Ari, Y. (2001). Developing networks play a similar melody. *Trends Neurosci, 24*(6), 353-360.
Ben-Ari, Y. (2002). Excitatory actions of gaba during development: the nature of the nurture. *Nat Rev Neurosci, 3*(9), 728-739.
Ben-Ari, Y. (2014). The GABA excitatory/inhibitory developmental sequence: a personal journey. *Neuroscience, 279*, 187-219.
Ben-Ari, Y. (2017). NKCC1 Chloride Importer Antagonists Attenuate Many Neurological and Psychiatric Disorders. *Trends Neurosci, 40*(9), 536-554.
Ben-Ari, Y. (2018). Oxytocin and Vasopressin, and the GABA Developmental Shift During Labor and Birth: Friends or Foes? *Front. Cell. Neurosci*.
Ben-Ari, Y., Damier, P., Lemonnier, E. (2016). Failure of the Nemo Trial: Bumetanide Is a Promising Agent to Treat Many Brain Disorders but Not Newborn Seizures. *Front Cell Neurosci, 10*, 90.
Berardi, N., Pizzorusso, T., Maffei, L. (2000). Critical periods during sensory development. *Curr Opin Neurobiol, 10*(1), 138-145.
Best, T. K., Cramer, N. P., Chakrabarti, L., Haydar, T. F., Galdzicki, Z. (2012). Dysfunctional hippocampal inhibition in the Ts65Dn mouse model of Down syndrome. *Exp Neurol, 233*(2), 749-757.
Bhattacharyya, A., McMillan, E., Chen, S. I., Wallace, K., Svendsen, C. N. (2009). A critical period in cortical interneuron neurogenesis in down syndrome revealed by human neural progenitor cells. *Dev Neurosci, 31*(6), 497-510.
Bianchi, P., Ciani, E., Guidi, S., Trazzi, S., Felice, D., Grossi, G., Fernandez, M., Giuliani, A., Calza, L., Bartesaghi, R. (2010). Early pharmacotherapy restores neurogenesis and cognitive performance in the Ts65Dn mouse model for Down syndrome. *J Neurosci, 30*(26), 8769-8779.
Bittles, A. H., Bower, C., Hussain, R., Glasson, E. J. (2007). The four ages of Down syndrome. *Eur J Public Health, 17*(2), 221-225.
Blaesse, P., Airaksinen, M. S., Rivera, C., Kaila, K. (2009). Cation-chloride cotransporters and neuronal function. *Neuron, 61*(6), 820-838.
Blaesse, P., Schmidt, T. (2015). K-Cl cotransporter KCC2--a moonlighting protein in excitatory and inhibitory synapse development and function. *Pflugers Arch, 467*(4), 615-624.
Blanquie, O., Liebmann, L., Hubner, C. A., Luhmann, H. J., Sinning, A. (2017). NKCC1-Mediated GABAergic Signaling Promotes Postnatal Cell Death in Neocortical Cajal-Retzius Cells. *Cereb Cortex, 27*(2), 1644-1659.
Blaszczyk, J. W. (2016). Parkinson's Disease and Neurodegeneration: GABA-Collapse Hypothesis. *Front Neurosci, 10*, 269.
Boettger, T., Hubner, C. A., Maier, H., Rust, M. B., Beck, F. X., Jentsch, T. J. (2002). Deafness and renal tubular acidosis in mice lacking the K-Cl co-transporter Kcc4. *Nature, 416*(6883), 874-878.
Bonnier, C., Marique, P., Van Hout, A., Potelle, D. (2007). Neurodevelopmental outcome after severe traumatic brain injury in very young children: role for subcortical lesions. *J Child Neurol, 22*(5), 519-529.
Bortone, D., Polleux, F. (2009). KCC2 expression promotes the termination of cortical interneuron migration in a voltage-sensitive calcium-dependent manner. *Neuron, 62*(1), 53-71.
Bou Khalil, R. (2017). Is insulin growth factor-1 the future for treating autism spectrum disorder and/or schizophrenia? *Med Hypotheses, 99*, 23-25.
Bowerman, M., Salsac, C., Bernard, V., Soulard, C., Dionne, A., Coque, E., Benlefki, S., Hince, P., Dion, P. A., Butler-Browne, G., Camu, W., Bouchard, J. P., Delpire, E., Rouleau, G. A., Raoul, C., Scamps, F. (2017). KCC3 loss-of-function contributes to Andermann syndrome by inducing activity-dependent neuromuscular junction defects. *Neurobiol Dis, 106*, 35-48.
Brambilla, M., Cotelli, M., Manenti, R., Dagani, J., Sisti, D., Rocchi, M., Balestrieri, M., Pini, S., Raimondi, S., Saviotti, F. M., Scocco, P., de Girolamo, G. (2016). Oxytocin to modulate emotional processing in schizophrenia: A randomized, double-blind, cross-over clinical trial. *Eur Neuropsychopharmacol, 26*(10), 1619-1628.
Branchereau, P., Chapron, J., Meyrand, P. (2002). Descending 5-hydroxytryptamine raphe inputs repress the expression of serotonergic neurons and slow the maturation of inhibitory systems in mouse embryonic spinal cord. *J Neurosci, 22*(7), 2598-2606.
Brandt, C., Nozadze, M., Heuchert, N., Rattka, M., Loscher, W. (2010). Disease-modifying effects of phenobarbital and the NKCC1 inhibitor bumetanide in the pilocarpine model of temporal lobe epilepsy. *J Neurosci, 30*(25), 8602-8612.
Brandt, C., Seja, P., Tollner, K., Romermann, K., Hampel, P., Kalesse, M., Kipper, A., Feit, P. W., Lykke, K., Toft-Bertelsen, T. L., Paavilainen, P., Spoljaric, I., Puskarjov, M., MacAulay, N., Kaila, K., Loscher, W. (2018). Bumepamine, a brain-permeant benzylamine derivative of bumetanide, does not inhibit NKCC1 but is more potent to enhance phenobarbital's anti-seizure efficacy. *Neuropharmacology, 143*, 186-204.
Braudeau, J., Dauphinot, L., Duchon, A., Loistron, A., Dodd, R. H., Herault, Y., Delatour, B., Potier, M. C. (2011). Chronic Treatment with a Promnesiant GABA-A alpha5-Selective Inverse Agonist Increases Immediate Early Genes Expression during Memory Processing in Mice and Rectifies Their Expression Levels in a Down Syndrome Mouse Model. *Adv Pharmacol Sci, 2011*, 153218.

Braudeau, J., Delatour, B., Duchon, A., Pereira, P. L., Dauphinot, L., de Chaumont, F., Olivo-Marin, J. C., Dodd, R. H., Herault, Y., Potier, M. C. (2011). Specific targeting of the GABA-A receptor alpha5 subtype by a selective inverse agonist restores cognitive deficits in Down syndrome mice. *J Psychopharmacol, 25*(8), 1030-1042.
Brickley, S. G., Cull-Candy, S. G., Farrant, M. (1999). Single-channel properties of synaptic and extrasynaptic GABAA receptors suggest differential targeting of receptor subtypes. *J Neurosci, 19*(8), 2960-2973.
Bruining, H., Passtoors, L., Goriounova, N., Jansen, F., Hakvoort, B., de Jonge, M., Poil, S. S. (2015). Paradoxical Benzodiazepine Response: A Rationale for Bumetanide in Neurodevelopmental Disorders? *Pediatrics, 136*(2), e539-543.
Buddhala, C., Hsu, C. C., Wu, J. Y. (2009). A novel mechanism for GABA synthesis and packaging into synaptic vesicles. *Neurochem Int, 55*(1-3), 9-12.
Byun, N., Delpire, E. (2007). Axonal and periaxonal swelling precede peripheral neurodegeneration in KCC3 knockout mice. *Neurobiol Dis, 28*(1), 39-51.
Cacciotti-Saija, C., Langdon, R., Ward, P. B., Hickie, I. B., Scott, E. M., Naismith, S. L., Moore, L., Alvares, G. A., Redoblado Hodge, M. A., Guastella, A. J. (2015). A double-blind randomized controlled trial of oxytocin nasal spray and social cognition training for young people with early psychosis. *Schizophr Bull, 41*(2), 483-493.
Caiati, M. D., Cherubini, E. (2013). Fluoxetine impairs GABAergic signaling in hippocampal slices from neonatal rats. *Front Cell Neurosci, 7*, 63.
Cancedda, L., Fiumelli, H., Chen, K., Poo, M. M. (2007). Excitatory GABA action is essential for morphological maturation of cortical neurons in vivo. *J Neurosci, 27*(19), 5224-5235.
Caravaggio, F., Gerretsen, P., Mar, W., Chung, J. K., Plitman, E., Nakajima, S., Kim, J., Iwata, Y., Patel, R., Chakravarty, M. M., Remington, G., Graff-Guerrero, A., Menon, M. (2017). Intranasal oxytocin does not modulate jumping to conclusions in schizophrenia: Potential interactions with caudate volume and baseline social functioning. *Psychoneuroendocrinology, 81*, 80-87.
Cardarelli, R. A., Jones, K., Pisella, L. I., Wobst, H. J., McWilliams, L. J., Sharpe, P. M., Burnham, M. P., Baker, D. J., Chudotvorova, I., Guyot, J., Silayeva, L., Morrow, D. H., Dekker, N., Zicha, S., Davies, P. A., Holenz, J., Duggan, M. E., Dunlop, J., Mather, R. J., Wang, Q., Medina, I., Brandon, N. J., Deeb, T. Z., Moss, S. J. (2017). The small molecule CLP257 does not modify activity of the K(+)-Cl(-) co-transporter KCC2 but does potentiate GABAA receptor activity. *Nat Med, 23*(12), 1394-1396.
Caron, N. S., Dorsey, E. R., Hayden, M. R. (2018). Therapeutic approaches to Huntington disease: from the bench to the clinic. *Nat Rev Drug Discov, 17*(10), 729-750.
Castro, J., Garcia, R. I., Kwok, S., Banerjee, A., Petravicz, J., Woodson, J., Mellios, N., Tropea, D., Sur, M. (2014). Functional recovery with recombinant human IGF1 treatment in a mouse model of Rett Syndrome. *Proc Natl Acad Sci U S A, 111*(27), 9941-9946.
Castrop, H., Schiessl, I. M. (2014). Physiology and pathophysiology of the renal Na-K-2Cl cotransporter (NKCC2). *Am J Physiol Renal Physiol, 307*(9), F991-F1002.
Caviness, V. S., Jr., Takahashi, T., Nowakowski, R. S. (1995). Numbers, time and neocortical neuronogenesis: a general developmental and evolutionary model. *Trends Neurosci, 18*(9), 379-383.
Cellot, G., Cherubini, E. (2013). Functional role of ambient GABA in refining neuronal circuits early in postnatal development. *Front Neural Circuits, 7*, 136.
Cellot, G., Cherubini, E. (2014). GABAergic signaling as therapeutic target for autism spectrum disorders. *Front Pediatr, 2*, 70.
Chakrabarti, L., Best, T. K., Cramer, N. P., Carney, R. S., Isaac, J. T., Galdzicki, Z., Haydar, T. F. (2010). Olig1 and Olig2 triplication causes developmental brain defects in Down syndrome. *Nat Neurosci, 13*(8), 927-934.
Chakrabarti, L., Galdzicki, Z., Haydar, T. F. (2007). Defects in embryonic neurogenesis and initial synapse formation in the forebrain of the Ts65Dn mouse model of Down syndrome. *J. Neuroscience, 27*(43), 11483-11495.
Chamma, I., Chevy, Q., Poncer, J. C., Levi, S. (2012). Role of the neuronal K-Cl co-transporter KCC2 in inhibitory and excitatory neurotransmission. *Front Cell Neurosci, 6*, 5.
Chang, B. S., Lowenstein, D. H. (2003). Epilepsy. *N Engl J Med, 349*(13), 1257-1266.
Chaudhari, R., Tan, Z., Huang, B., Zhang, S. (2017). Computational polypharmacology: a new paradigm for drug discovery. *Expert Opin Drug Discov, 12*(3), 279-291.
Chen, H., Luo, J., Kintner, D. B., Shull, G. E., Sun, D. (2005). Na(+)-dependent chloride transporter (NKCC1)-null mice exhibit less gray and white matter damage after focal cerebral ischemia. *J Cereb Blood Flow Metab, 25*(1), 54-66.
Chevy, Q., Heubl, M., Goutierre, M., Backer, S., Moutkine, I., Eugene, E., Bloch-Gallego, E., Levi, S., Poncer, J. C. (2015). KCC2 Gates Activity-Driven AMPA Receptor Traffic through Cofilin Phosphorylation. *J Neurosci, 35*(48), 15772-15786.
Cleary, R. T., Sun, H., Huynh, T., Manning, S. M., Li, Y., Rotenberg, A., Talos, D. M., Kahle, K. T., Jackson, M., Rakhade, S. N., Berry, G., Jensen, F. E. (2013). Bumetanide enhances phenobarbital efficacy in a rat model of hypoxic neonatal seizures. *PLoS One, 8*(3), e57148.
Colas, D., Valletta, J. S., Takimoto-Kimura, R., Nishino, S., Fujiki, N., Mobley, W. C., Mignot, E. (2008). Sleep and EEG features in genetic models of Down syndrome. *Neurobiol Dis, 30*(1), 1-7.
Contestabile, A., Benfenati, F., Gasparini, L. (2010). Communication breaks-Down: from neurodevelopment defects to cognitive disabilities in Down syndrome. *Prog Neurobiol, 91*(1), 1-22.
Contestabile, A., Fila, T., Ceccarelli, C., Bonasoni, P., Bonapace, L., Santini, D., Bartesaghi, R., Ciani, E. (2007). Cell cycle alteration and decreased cell proliferation in the hippocampal dentate gyrus and in the neocortical germinal matrix of fetuses with Down syndrome and in Ts65Dn mice. *Hippocampus, 17*(8), 665-678.
Contestabile, A., Greco, B., Ghezzi, D., Tucci, V., Benfenati, F., Gasparini, L. (2013). Lithium rescues synaptic plasticity and memory in Down syndrome mice. *J Clin Invest, 123*, 348-361.
Contestabile, A., Magara, S., Cancedda, L. (2017). The GABAergic Hypothesis for Cognitive Disabilities in Down Syndrome. *Front Cell Neurosci, 11*, 54.
Conti, L., Palma, E., Roseti, C., Lauro, C., Cipriani, R., de Groot, M., Aronica, E., Limatola, C. (2011). Anomalous levels of Cl- transporters cause a decrease of GABAergic inhibition in human peritumoral epileptic cortex. *Epilepsia, 52*(9), 1635-1644.
Costa, A. C., Grybko, M. J. (2005). Deficits in hippocampal CA1 LTP induced by TBS but not HFS in the Ts65Dn mouse: a model of Down syndrome. *Neurosci Lett, 382*(3), 317-322.

Costa, A. C., Scott-McKean, J. J., Stasko, M. R. (2008). Acute injections of the NMDA receptor antagonist memantine rescue performance deficits of the Ts65Dn mouse model of Down syndrome on a fear conditioning test. *Neuropsychopharmacology, 33*(7), 1624-1632.
Cramer, S. W., Baggott, C., Cain, J., Tilghman, J., Allcock, B., Miranpuri, G., Rajpal, S., Sun, D., Resnick, D. (2008). The role of cation-dependent chloride transporters in neuropathic pain following spinal cord injury. *Mol Pain, 4*, 36.
Dagani, J., Sisti, D., Abelli, M., Di Paolo, L., Pini, S., Raimondi, S., Rocchi, M. B., Saviotti, F. M., Scocco, P., Totaro, S., Balestrieri, M., de Girolamo, G. (2016). Do we need oxytocin to treat schizophrenia? A randomized clinical trial. *Schizophr Res, 172*(1-3), 158-164.
Damier, P., Hammond, C., Ben-Ari, Y. (2016). Bumetanide to Treat Parkinson Disease: A Report of 4 Cases. *Clin Neuropharmacol, 39*(1), 57-59.
Dargaei, Z., Bang, J. Y., Mahadevan, V., Khademullah, C. S., Bedard, S., Parfitt, G. M., Kim, J. C., Woodin, M. A. (2018). Restoring GABAergic inhibition rescues memory deficits in a Huntington's disease mouse model. *Proc Natl Acad Sci U S A, 115*(7), E1618-E1626.
Das, D., Medina, B., Baktir, M. A., Mojabi, F. S., Fahimi, A., Ponnusamy, R., Salehi, A. (2015). Increased incidence of intermittent hypoxemia in the Ts65Dn mouse model of Down syndrome. *Neurosci Lett, 604*, 91-96.
Davis, M. C., Green, M. F., Lee, J., Horan, W. P., Senturk, D., Clarke, A. D., Marder, S. R. (2014). Oxytocin-augmented social cognitive skills training in schizophrenia. *Neuropsychopharmacology, 39*(9), 2070-2077.
Davis, M. C., Lee, J., Horan, W. P., Clarke, A. D., McGee, M. R., Green, M. F., Marder, S. R. (2013). Effects of single dose intranasal oxytocin on social cognition in schizophrenia. *Schizophr Res, 147*(2-3), 393-397.
de Los Heros, P., Alessi, D. R., Gourlay, R., Campbell, D. G., Deak, M., Macartney, T. J., Kahle, K. T., Zhang, J. (2014). The WNK-regulated SPAK/OSR1 kinases directly phosphorylate and inhibit the K+-Cl- co-transporters. *Biochem J, 458*(3), 559-573.
Dean, B., Keriakous, D., Scarr, E., Thomas, E. A. (2007). Gene expression profiling in Brodmann's area 46 from subjects with schizophrenia. *Aust N Z J Psychiatry, 41*(4), 308-320.
Dehorter, N., Guigoni, C., Lopez, C., Hirsch, J., Eusebio, A., Ben-Ari, Y., Hammond, C. (2009). Dopamine-deprived striatal GABAergic interneurons burst and generate repetitive gigantic IPSCs in medium spiny neurons. *J Neurosci, 29*(24), 7776-7787.
Dehorter, N., Lozovaya, N., Mdzomba, B. J., Michel, F. J., Lopez, C., Tsintsadze, V., Tsintsadze, T., Klinkenberg, M., Gispert, S., Auburger, G., Hammond, C. (2012). Subthalamic lesion or levodopa treatment rescues giant GABAergic currents of PINK1-deficient striatum. *J Neurosci, 32*(50), 18047-18053.
Dehorter, N., Vinay, L., Hammond, C., Ben-Ari, Y. (2012). Timing of developmental sequences in different brain structures: physiological and pathological implications. *Eur J Neurosci, 35*(12), 1846-1856.
Deidda, G., Allegra, M., Cerri, C., Naskar, S., Bony, G., Zunino, G., Bozzi, Y., Caleo, M., Cancedda, L. (2015). Early depolarizing GABA controls critical-period plasticity in the rat visual cortex. *Nat Neurosci, 18*(1), 87-96.
Deidda, G., Parrini, M., Naskar, S., Bozarth, I. F., Contestabile, A., Cancedda, L. (2015). Reversing excitatory GABAAR signaling restores synaptic plasticity and memory in a mouse model of Down syndrome. *Nat Med, 21*(4), 318-326.
Dekker, A. D., Sacco, S., Carfi, A., Benejam, B., Vermeiren, Y., Beugelsdijk, G., Schippers, M., Hassefras, L., Eleveld, J., Grefelman, S., Fopma, R., Bomer-Veenboer, M., Boti, M., Oosterling, G. D. E., Scholten, E., Tollenaere, M., Checkley, L., Strydom, A., Van Goethem, G., Onder, G., Blesa, R., Zu Eulenburg, C., Coppus, A. M. W., Rebillat, A. S., Fortea, J., De Deyn, P. P. (2018). The Behavioral and Psychological Symptoms of Dementia in Down Syndrome (BPSD-DS) Scale: Comprehensive Assessment of Psychopathology in Down Syndrome. *J Alzheimers Dis, 63*(2), 797-819.
Delpire, E., Gagnon, K. B. (2018). Na(+) -K(+) -2Cl(-) Cotransporter (NKCC) Physiological Function in Nonpolarized Cells and Transporting Epithelia. *Compr Physiol, 8*(2), 871-901.
Delpire, E., Kahle, K. T. (2017). The KCC3 cotransporter as a therapeutic target for peripheral neuropathy. *Expert Opin Ther Targets, 21*(2), 113-116.
Delpire, E., Lu, J., England, R., Dull, C., Thorne, T. (1999). Deafness and imbalance associated with inactivation of the secretory Na-K-2Cl co-transporter. *Nat Genet, 22*(2), 192-195.
Delpy, A., Allain, A. E., Meyrand, P., Branchereau, P. (2008). NKCC1 cotransporter inactivation underlies embryonic development of chloride-mediated inhibition in mouse spinal motoneuron. *J Physiol, 586*(4), 1059-1075.
Desai, S. S. (1997). Down syndrome: a review of the literature. *Oral Surg Oral Med Oral Pathol Oral Radiol Endod, 84*(3), 279-285.
Di Cristo, G., Awad, P. N., Hamidi, S., Avoli, M. (2018). KCC2, epileptiform synchronization, and epileptic disorders. *Prog Neurobiol, 162*, 1-16.
Dierssen, M. (2012). Down syndrome: the brain in trisomic mode. *Nat Rev Neurosci, 13*(12), 844-858.
Ding, D., Liu, H., Qi, W., Jiang, H., Li, Y., Wu, X., Sun, H., Gross, K., Salvi, R. (2016). Ototoxic effects and mechanisms of loop diuretics. *J Otol, 11*(4), 145-156.
Donnan, G. A., Fisher, M., Macleod, M., Davis, S. M. (2008). Stroke. *Lancet, 371*(9624), 1612-1623.
Du, L., Shan, L., Wang, B., Li, H., Xu, Z., Staal, W. G., Jia, F. (2015). A Pilot Study on the Combination of Applied Behavior Analysis and Bumetanide Treatment for Children with Autism. *J Child Adolesc Psychopharmacol, 25*(7), 585-588.
Duarte, S. T., Armstrong, J., Roche, A., Ortez, C., Perez, A., O'Callaghan Mdel, M., Pereira, A., Sanmarti, F., Ormazabal, A., Artuch, R., Pineda, M., Garcia-Cazorla, A. (2013). Abnormal expression of cerebrospinal fluid cation chloride cotransporters in patients with Rett syndrome. *PLoS One, 8*(7), e68851.
Dzhala, V. I., Brumback, A. C., Staley, K. J. (2008). Bumetanide enhances phenobarbital efficacy in a neonatal seizure model. *Ann Neurol, 63*(2), 222-235.
Dzhala, V. I., Kuchibhotla, K. V., Glykys, J. C., Kahle, K. T., Swiercz, W. B., Feng, G., Kuner, T., Augustine, G. J., Bacskai, B. J., Staley, K. J. (2010). Progressive NKCC1-dependent neuronal chloride accumulation during neonatal seizures. *J Neurosci, 30*(35), 11745-11761.
Dzhala, V. I., Talos, D. M., Sdrulla, D. A., Brumback, A. C., Mathews, G. C., Benke, T. A., Delpire, E., Jensen, F. E., Staley, K. J. (2005). NKCC1 transporter facilitates seizures in the developing brain. *Nat Med, 11*(11), 1205-1213.
Edgin, J. O., Mason, G. M., Spano, G., Fernandez, A., Nadel, L. (2012). Human and mouse model cognitive phenotypes in Down syndrome: implications for assessment. *Prog Brain Res, 197*, 123-151.

Edwards, A., Castrop, H., Laghmani, K., Vallon, V., Layton, A. T. (2014). Effects of NKCC2 isoform regulation on NaCl transport in thick ascending limb and macula densa: a modeling study. *Am J Physiol Renal Physiol, 307*(2), F137-146.
Edwards, D. A., Shah, H. P., Cao, W., Gravenstein, N., Seubert, C. N., Martynyuk, A. E. (2010). Bumetanide alleviates epileptogenic and neurotoxic effects of sevoflurane in neonatal rat brain. *Anesthesiology, 112*(3), 567-575.
Eftekhari, S., Mehrabi, S., Soleimani, M., Hassanzadeh, G., Shahrokhi, A., Mostafavi, H., Hayat, P., Barati, M., Mehdizadeh, H., Rahmanzadeh, R., Hadjighassem, M. R., Joghataei, M. T. (2014). BDNF modifies hippocampal KCC2 and NKCC1 expression in a temporal lobe epilepsy model. *Acta Neurobiol Exp (Wars), 74*(3), 276-287.
Eftekhari, S., Mehvari Habibabadi, J., Najafi Ziarani, M., Hashemi Fesharaki, S. S., Gharakhani, M., Mostafavi, H., Joghataei, M. T., Beladimoghadam, N., Rahimian, E., Hadjighassem, M. R. (2013). Bumetanide reduces seizure frequency in patients with temporal lobe epilepsy. *Epilepsia, 54*(1), e9-12.
Eftekhari, S., Shahrokhi, A., Tsintsadze, V., Nardou, R., Brouchoud, C., Conesa, M., Burnashev, N., Ferrari, D. C., Ben-Ari, Y. (2014). Response to Comment on "Oxytocin-mediated GABA inhibition during delivery attenuates autism pathogenesis in rodent offspring". *Science, 346*(6206), 176.
Ehinger, Y., Matagne, V., Villard, L., Roux, J. C. (2018). Rett syndrome from bench to bedside: recent advances. *F1000Res, 7*, 398.
Escorihuela, R. M., Fernandez-Teruel, A., Vallina, I. F., Baamonde, C., Lumbreras, M. A., Dierssen, M., Tobena, A., Florez, J. (1995). A behavioral assessment of Ts65Dn mice: a putative Down syndrome model. *Neurosci Lett, 199*(2), 143-146.
Fagiolini, M., Fritschy, J. M., Low, K., Mohler, H., Rudolph, U., Hensch, T. K. (2004). Specific GABAA circuits for visual cortical plasticity. *Science, 303*(5664), 1681-1683.
Fagiolini, M., Hensch, T. K. (2000). Inhibitory threshold for critical-period activation in primary visual cortex. *Nature, 404*(6774), 183-186.
Farrant, M., Nusser, Z. (2005). Variations on an inhibitory theme: phasic and tonic activation of GABA(A) receptors. *Nat Rev Neurosci, 6*(3), 215-229.
Feifel, D., Macdonald, K., Cobb, P., Minassian, A. (2012). Adjunctive intranasal oxytocin improves verbal memory in people with schizophrenia. *Schizophr Res, 139*(1-3), 207-210.
Feifel, D., Macdonald, K., Nguyen, A., Cobb, P., Warlan, H., Galangue, B., Minassian, A., Becker, O., Cooper, J., Perry, W., Lefebvre, M., Gonzales, J., Hadley, A. (2010). Adjunctive intranasal oxytocin reduces symptoms in schizophrenia patients. *Biol Psychiatry, 68*(7), 678-680.
Feller, M. B. (1999). Spontaneous correlated activity in developing neural circuits. *Neuron, 22*(4), 653-656.
Fernandez, F., Morishita, W., Zuniga, E., Nguyen, J., Blank, M., Malenka, R. C., Garner, C. C. (2007). Pharmacotherapy for cognitive impairment in a mouse model of Down syndrome. *Nat Neurosci, 10*(4), 411-413.
Fischer-Shofty, M., Brune, M., Ebert, A., Shefet, D., Levkovitz, Y., Shamay-Tsoory, S. G. (2013). Improving social perception in schizophrenia: the role of oxytocin. *Schizophr Res, 146*(1-3), 357-362.
Fiumelli, H., Briner, A., Puskarjov, M., Blaesse, P., Belem, B. J., Dayer, A. G., Kaila, K., Martin, J. L., Vutskits, L. (2013). An ion transport-independent role for the cation-chloride cotransporter KCC2 in dendritic spinogenesis in vivo. *Cereb Cortex, 23*(2), 378-388.
Flamenbaum, W., Friedman, R. (1982). Pharmacology, therapeutic efficacy, and adverse effects of bumetanide, a new "loop" diuretic. *Pharmacotherapy, 2*(4), 213-222.
Flores, B., Schornak, C. C., Delpire, E. (2018). A role for KCC3 in maintaining cell volume of peripheral nerve fibers. *Neurochem Int*.
Foroutan, S., Brillault, J., Forbush, B., O'Donnell, M. E. (2005). Moderate-to-severe ischemic conditions increase activity and phosphorylation of the cerebral microvascular endothelial cell Na+-K+-Cl- cotransporter. *Am J Physiol Cell Physiol, 289*(6), C1492-1501.
Fu, P., Tang, R., Yu, Z., Huang, S., Xie, M., Luo, X., Wang, W. (2015). Bumetanide-induced NKCC1 inhibition attenuates oxygen-glucose deprivation-induced decrease in proliferative activity and cell cycle progression arrest in cultured OPCs via p-38 MAPKs. *Brain Res, 1613*, 110-119.
Fukuda, A., Wang, T. (2013). A perturbation of multimodal GABA functions underlying the formation of focal cortical malformations: assessments by using animal models. *Neuropathology, 33*(4), 480-486.
Gagnon, M., Bergeron, M. J., Lavertu, G., Castonguay, A., Tripathy, S., Bonin, R. P., Perez-Sanchez, J., Boudreau, D., Wang, B., Dumas, L., Valade, I., Bachand, K., Jacob-Wagner, M., Tardif, C., Kianicka, I., Isenring, P., Attardo, G., Coull, J. A., De Koninck, Y. (2013). Chloride extrusion enhancers as novel therapeutics for neurological diseases. *Nat Med, 19*(11), 1524-1528.
Gagnon, M., Bergeron, M. J., Perez-Sanchez, J., Plasencia-Fernandez, I., Lorenzo, L. E., Godin, A. G., Castonguay, A., Bonin, R. P., De Koninck, Y. (2017). Reply to The small molecule CLP257 does not modify activity of the K(+)-Cl(-) co-transporter KCC2 but does potentiate GABAA receptor activity. *Nat Med, 23*(12), 1396-1398.
Galan, A., Cervero, F. (2005). Painful stimuli induce in vivo phosphorylation and membrane mobilization of mouse spinal cord NKCC1 co-transporter. *Neuroscience, 133*(1), 245-252.
Galanopoulou, A. S. (2008). Sexually dimorphic expression of KCC2 and GABA function. *Epilepsy Res, 80*(2-3), 99-113.
Gamba, G., Friedman, P. A. (2009). Thick ascending limb: the Na(+):K (+):2Cl (-) co-transporter, NKCC2, and the calcium-sensing receptor, CaSR. *Pflugers Arch, 458*(1), 61-76.
Ganguly, K., Schinder, A. F., Wong, S. T., Poo, M. (2001). GABA itself promotes the developmental switch of neuronal GABAergic responses from excitation to inhibition. *Cell, 105*(4), 521-532.
Garcia-Cerro, S., Martinez, P., Vidal, V., Corrales, A., Florez, J., Vidal, R., Rueda, N., Arbones, M. L., Martinez-Cue, C. (2014). Overexpression of Dyrk1A is implicated in several cognitive, electrophysiological and neuromorphological alterations found in a mouse model of Down syndrome. *PLoS One, 9*(9), e106572.
Garzon-Muvdi, T., Schiapparelli, P., ap Rhys, C., Guerrero-Cazares, H., Smith, C., Kim, D. H., Kone, L., Farber, H., Lee, D. Y., An, S. S., Levchenko, A., Quinones-Hinojosa, A. (2012). Regulation of brain tumor dispersal by NKCC1 through a novel role in focal adhesion regulation. *PLoS Biol, 10*(5), e1001320.
Gauvain, G., Chamma, I., Chevy, Q., Cabezas, C., Irinopoulou, T., Bodrug, N., Carnaud, M., Levi, S., Poncer, J. C. (2011). The neuronal K-Cl cotransporter KCC2 influences postsynaptic AMPA receptor content and lateral diffusion in dendritic spines. *Proc Natl Acad Sci U S A, 108*(37), 15474-15479.
Ghajar, J. (2000). Traumatic brain injury. *Lancet, 356*(9233), 923-929.

Gholipour, T., Mitchell, S., Sarkis, R. A., Chemali, Z. (2017). The clinical and neurobehavioral course of Down syndrome and dementia with or without new-onset epilepsy. *Epilepsy Behav, 68*, 11-16.
Gibson, C. M., Penn, D. L., Smedley, K. L., Leserman, J., Elliott, T., Pedersen, C. A. (2014). A pilot six-week randomized controlled trial of oxytocin on social cognition and social skills in schizophrenia. *Schizophr Res, 156*(2-3), 261-265.
Glaser, N., Yuen, N., Anderson, S. E., Tancredi, D. J., O'Donnell, M. E. (2010). Cerebral metabolic alterations in rats with diabetic ketoacidosis: effects of treatment with insulin and intravenous fluids and effects of bumetanide. *Diabetes, 59*(3), 702-709.
Goldberg-Stern, H., Strawsburg, R. H., Patterson, B., Hickey, F., Bare, M., Gadoth, N., Degrauw, T. J. (2001). Seizure frequency and characteristics in children with Down syndrome. *Brain Dev, 23*(6), 375-378.
Goldman, M. B., Gomes, A. M., Carter, C. S., Lee, R. (2011). Divergent effects of two different doses of intranasal oxytocin on facial affect discrimination in schizophrenic patients with and without polydipsia. *Psychopharmacology (Berl), 216*(1), 101-110.
Granados-Soto, V., Arguelles, C. F., Alvarez-Leefmans, F. J. (2005). Peripheral and central antinociceptive action of Na+-K+-2Cl-cotransporter blockers on formalin-induced nociception in rats. *Pain, 114*(1-2), 231-238.
Grandgeorge, M., Lemonnier, E., Degrez, C., Jallot, N. (2014). The effect of bumetanide treatment on the sensory behaviours of a young girl with Asperger syndrome. *BMJ Case Rep, 2014*.
Gribkoff, V. K., Kaczmarek, L. K. (2017). The need for new approaches in CNS drug discovery: Why drugs have failed, and what can be done to improve outcomes. *Neuropharmacology, 120*, 11-19.
Guidi, S., Stagni, F., Bianchi, P., Ciani, E., Giacomini, A., De Franceschi, M., Moldrich, R., Kurniawan, N., Mardon, K., Giuliani, A., Calza, L., Bartesaghi, R. (2014). Prenatal pharmacotherapy rescues brain development in a Down's syndrome mouse model. *Brain, 137*(Pt 2), 380-401.
Haas, B. R., Sontheimer, H. (2010). Inhibition of the Sodium-Potassium-Chloride Cotransporter Isoform-1 reduces glioma invasion. *Cancer Res, 70*(13), 5597-5606.
Haddad, F., Bourke, J., Wong, K., Leonard, H. (2018). An investigation of the determinants of quality of life in adolescents and young adults with Down syndrome. *PLoS One, 13*(6), e0197394.
Hadders-Algra, M. (2018). Early human brain development: Starring the subplate. *Neurosci Biobehav Rev, 92*, 276-290.
Hadjikhani, N., Asberg Johnels, J., Lassalle, A., Zurcher, N. R., Hippolyte, L., Gillberg, C., Lemonnier, E., Ben-Ari, Y. (2018). Bumetanide for autism: more eye contact, less amygdala activation. *Sci Rep, 8*(1), 3602.
Hadjikhani, N., Zurcher, N. R., Rogier, O., Ruest, T., Hippolyte, L., Ben-Ari, Y., Lemonnier, E. (2015). Improving emotional face perception in autism with diuretic bumetanide: a proof-of-concept behavioral and functional brain imaging pilot study. *Autism, 19*(2), 149-157.
Hannemann, A., Christie, J. K., Flatman, P. W. (2009). Functional expression of the Na-K-2Cl cotransporter NKCC2 in mammalian cells fails to confirm the dominant-negative effect of the AF splice variant. *J Biol Chem, 284*(51), 35348-35358.
Hanson, J. E., Blank, M., Valenzuela, R. A., Garner, C. C., Madison, D. V. (2007). The functional nature of synaptic circuitry is altered in area CA3 of the hippocampus in a mouse model of Down's syndrome. *J Physiol, 579*(Pt 1), 53-67.
Harauzov, A., Spolidoro, M., DiCristo, G., De Pasquale, R., Cancedda, L., Pizzorusso, T., Viegi, A., Berardi, N., Maffei, L. (2010). Reducing intracortical inhibition in the adult visual cortex promotes ocular dominance plasticity. *J Neurosci, 30*(1), 361-371.
Has, A. T. C., Chebib, M. (2018). GABAA receptors: Various stoichiometrics of subunit arrangement in alpha1beta3 and alpha1beta3epsilon receptors. *Curr Pharm Des*.
Hasbargen, T., Ahmed, M. M., Miranpuri, G., Li, L., Kahle, K. T., Resnick, D., Sun, D. (2010). Role of NKCC1 and KCC2 in the development of chronic neuropathic pain following spinal cord injury. *Ann N Y Acad Sci, 1198*, 168-172.
He, Q., Arroyo, E. D., Smukowski, S. N., Xu, J., Piochon, C., Savas, J. N., Portera-Cailliau, C., Contractor, A. (2018). Critical period inhibition of NKCC1 rectifies synapse plasticity in the somatosensory cortex and restores adult tactile response maps in fragile X mice. *Mol Psychiatry*.
He, Q., Nomura, T., Xu, J., Contractor, A. (2014). The developmental switch in GABA polarity is delayed in fragile X mice. *J Neurosci, 34*(2), 446-450.
Heck, N., Kilb, W., Reiprich, P., Kubota, H., Furukawa, T., Fukuda, A., Luhmann, H. J. (2007). GABA-A receptors regulate neocortical neuronal migration in vitro and in vivo. *Cereb Cortex, 17*(1), 138-148.
Heinen, M., Hettich, M. M., Ryan, D. P., Schnell, S., Paesler, K., Ehninger, D. (2012). Adult-onset fluoxetine treatment does not improve behavioral impairments and may have adverse effects on the Ts65Dn mouse model of Down syndrome. *Neural Plast, 2012*, 467251.
Hensch, T. K. (2004). Critical period regulation. *Annu Rev Neurosci, 27*, 549-579.
Hensch, T. K., Fagiolini, M. (2005). Excitatory-inhibitory balance and critical period plasticity in developing visual cortex. *Prog Brain Res, 147*, 115-124.
Hensch, T. K., Quinlan, E. M. (2018). Critical periods in amblyopia. *Vis Neurosci, 35*, E014.
Hernandez-Gonzalez, S., Ballestin, R., Lopez-Hidalgo, R., Gilabert-Juan, J., Blasco-Ibanez, J. M., Crespo, C., Nacher, J., Varea, E. (2015). Altered distribution of hippocampal interneurons in the murine Down Syndrome model Ts65Dn. *Neurochem Res, 40*(1), 151-164.
Hernandez, S., Gilabert-Juan, J., Blasco-Ibanez, J. M., Crespo, C., Nacher, J., Varea, E. (2012). Altered expression of neuropeptides in the primary somatosensory cortex of the Down syndrome model Ts65Dn. *Neuropeptides, 46*(1), 29-37.
Hochman, D. W. (2012). The extracellular space and epileptic activity in the adult brain: explaining the antiepileptic effects of furosemide and bumetanide. *Epilepsia, 53 Suppl 1*, 18-25.
Hochman, D. W., Baraban, S. C., Owens, J. W., Schwartzkroin, P. A. (1995). Dissociation of synchronization and excitability in furosemide blockade of epileptiform activity. *Science, 270*(5233), 99-102.
Hochman, D. W., D'Ambrosio, R., Janigro, D., Schwartzkroin, P. A. (1999). Extracellular chloride and the maintenance of spontaneous epileptiform activity in rat hippocampal slices. *J Neurophysiol, 81*(1), 49-59.
Hochman, D. W., Schwartzkroin, P. A. (2000). Chloride-cotransport blockade desynchronizes neuronal discharge in the "epileptic" hippocampal slice. *J Neurophysiol, 83*(1), 406-417.
Horn, Z., Ringstedt, T., Blaesse, P., Kaila, K., Herlenius, E. (2010). Premature expression of KCC2 in embryonic mice perturbs neural development by an ion transport-independent mechanism. *Eur J Neurosci, 31*(12), 2142-2155.

Horta de Macedo, L. R., Zuardi, A. W., Machado-de-Sousa, J. P., Chagas, M. H., Hallak, J. E. (2014). Oxytocin does not improve performance of patients with schizophrenia and healthy volunteers in a facial emotion matching task. *Psychiatry Res, 220*(1-2), 125-128.
Howard, H. C., Mount, D. B., Rochefort, D., Byun, N., Dupre, N., Lu, J., Fan, X., Song, L., Riviere, J. B., Prevost, C., Horst, J., Simonati, A., Lemcke, B., Welch, R., England, R., Zhan, F. Q., Mercado, A., Siesser, W. B., George, A. L., Jr., McDonald, M. P., Bouchard, J. P., Mathieu, J., Delpire, E., Rouleau, G. A. (2002). The K-Cl cotransporter KCC3 is mutant in a severe peripheral neuropathy associated with agenesis of the corpus callosum. *Nat Genet, 32*(3), 384-392.
Hsu, Y. T., Chang, Y. G., Chang, C. P., Siew, J. J., Chen, H. M., Tsai, C. H., Chern, Y. (2017). Altered behavioral responses to gamma-aminobutyric acid pharmacological agents in a mouse model of Huntington's disease. *Mov Disord, 32*(11), 1600-1609.
Hu, J. J., Yang, X. L., Luo, W. D., Han, S., Yin, J., Liu, W. H., He, X. H., Peng, B. W. (2017). Bumetanide reduce the seizure susceptibility induced by pentylenetetrazol via inhibition of aberrant hippocampal neurogenesis in neonatal rats after hypoxia-ischemia. *Brain Res Bull, 130*, 188-199.
Huang, Z. J., Kirkwood, A., Pizzorusso, T., Porciatti, V., Morales, B., Bear, M. F., Maffei, L., Tonegawa, S. (1999). BDNF regulates the maturation of inhibition and the critical period of plasticity in mouse visual cortex. *Cell, 98*(6), 739-755.
Huberfeld, G., Blauwblomme, T., Miles, R. (2015). Hippocampus and epilepsy: Findings from human tissues. *Rev Neurol (Paris), 171*(3), 236-251.
Huberfeld, G., Wittner, L., Clemenceau, S., Baulac, M., Kaila, K., Miles, R., Rivera, C. (2007). Perturbed chloride homeostasis and GABAergic signaling in human temporal lobe epilepsy. *J Neurosci, 27*(37), 9866-9873.
Hubner, C. A., Stein, V., Hermans-Borgmeyer, I., Meyer, T., Ballanyi, K., Jentsch, T. J. (2001). Disruption of KCC2 reveals an essential role of K-Cl cotransport already in early synaptic inhibition. *Neuron, 30*(2), 515-524.
Hui, H., Rao, W., Zhang, L., Xie, Z., Peng, C., Su, N., Wang, K., Wang, L., Luo, P., Hao, Y. L., Zhang, S., Fei, Z. (2016). Inhibition of Na(+)-K(+)-2Cl(-) Cotransporter-1 attenuates traumatic brain injury-induced neuronal apoptosis via regulation of Erk signaling. *Neurochem Int, 94*, 23-31.
Hyde, T. M., Lipska, B. K., Ali, T., Mathew, S. V., Law, A. J., Metitiri, O. E., Straub, R. E., Ye, T., Colantuoni, C., Herman, M. M., Bigelow, L. B., Weinberger, D. R., Kleinman, J. E. (2011). Expression of GABA signaling molecules KCC2, NKCC1, and GAD1 in cortical development and schizophrenia. *J Neurosci, 31*(30), 11088-11095.
Inamura, N., Kimura, T., Tada, S., Kurahashi, T., Yanagida, M., Yanagawa, Y., Ikenaka, K., Murakami, F. (2012). Intrinsic and extrinsic mechanisms control the termination of cortical interneuron migration. *J Neurosci, 32*(17), 6032-6042.
Inoue, K., Furukawa, T., Kumada, T., Yamada, J., Wang, T., Inoue, R., Fukuda, A. (2012). Taurine inhibits K+-Cl- cotransporter KCC2 to regulate embryonic Cl- homeostasis via with-no-lysine (WNK) protein kinase signaling pathway. *J Biol Chem, 287*(25), 20839-20850.
Iwai, Y., Fagiolini, M., Obata, K., Hensch, T. K. (2003). Rapid critical period induction by tonic inhibition in visual cortex. *J Neurosci, 23*(17), 6695-6702.
Jaggi, A. S., Kaur, A., Bali, A., Singh, N. (2015). Expanding Spectrum of Sodium Potassium Chloride Co-transporters in the Pathophysiology of Diseases. *Curr Neuropharmacol, 13*(3), 369-388.
Jansen, L. A., Peugh, L. D., Roden, W. H., Ojemann, J. G. (2010). Impaired maturation of cortical GABA(A) receptor expression in pediatric epilepsy. *Epilepsia, 51*(8), 1456-1467.
Jarskog, L. F., Pedersen, C. A., Johnson, J. L., Hamer, R. M., Rau, S. W., Elliott, T., Penn, D. L. (2017). A 12-week randomized controlled trial of twice-daily intranasal oxytocin for social cognitive deficits in people with schizophrenia. *Schizophr Res, 185*, 88-95.
Jonsson, C. A., Catroppa, C., Godfrey, C., Smedler, A. C., Anderson, V. (2013). Cognitive recovery and development after traumatic brain injury in childhood: a person-oriented, longitudinal study. *J Neurotrauma, 30*(2), 76-83.
Kahle, K. T., Barnett, S. M., Sassower, K. C., Staley, K. J. (2009). Decreased seizure activity in a human neonate treated with bumetanide, an inhibitor of the Na(+)-K(+)-2Cl(-) cotransporter NKCC1. *J Child Neurol, 24*(5), 572-576.
Kahle, K. T., Deeb, T. Z., Puskarjov, M., Silayeva, L., Liang, B., Kaila, K., Moss, S. J. (2013). Modulation of neuronal activity by phosphorylation of the K-Cl cotransporter KCC2. *Trends Neurosci, 36*(12), 726-737.
Kahle, K. T., Khanna, A. R., Alper, S. L., Adragna, N. C., Lauf, P. K., Sun, D., Delpire, E. (2015). K-Cl cotransporters, cell volume homeostasis, and neurological disease. *Trends Mol Med, 21*(8), 513-523.
Kahle, K. T., Rinehart, J., Lifton, R. P. (2010). Phosphoregulation of the Na-K-2Cl and K-Cl cotransporters by the WNK kinases. *Biochim Biophys Acta, 1802*(12), 1150-1158.
Kahle, K. T., Simard, J. M., Staley, K. J., Nahed, B. V., Jones, P. S., Sun, D. (2009). Molecular mechanisms of ischemic cerebral edema: role of electroneutral ion transport. *Physiology (Bethesda), 24*, 257-265.
Kaila, K., Price, T. J., Payne, J. A., Puskarjov, M., Voipio, J. (2014). Cation-chloride cotransporters in neuronal development, plasticity and disease. *Nat Rev Neurosci, 15*(10), 637-654.
Kakigi, A., Nishimura, M., Takeda, T., Taguchi, D., Nishioka, R. (2009). Expression of aquaporin1, 3, and 4, NKCC1, and NKCC2 in the human endolymphatic sac. *Auris Nasus Larynx, 36*(2), 135-139.
Kanaka, C., Ohno, K., Okabe, A., Kuriyama, K., Itoh, T., Fukuda, A., Sato, K. (2001). The differential expression patterns of messenger RNAs encoding K-Cl cotransporters (KCC1,2) and Na-K-2Cl cotransporter (NKCC1) in the rat nervous system. *Neuroscience, 104*(4), 933-946.
Karlocai, M. R., Wittner, L., Toth, K., Magloczky, Z., Katarova, Z., Rasonyi, G., Eross, L., Czirjak, S., Halasz, P., Szabo, G., Payne, J. A., Kaila, K., Freund, T. F. (2016). Enhanced expression of potassium-chloride cotransporter KCC2 in human temporal lobe epilepsy. *Brain Struct Funct, 221*(7), 3601-3615.
Kaufmann, W. E., Kidd, S. A., Andrews, H. F., Budimirovic, D. B., Esler, A., Haas-Givler, B., Stackhouse, T., Riley, C., Peacock, G., Sherman, S. L., Brown, W. T., Berry-Kravis, E. (2017). Autism Spectrum Disorder in Fragile X Syndrome: Cooccurring Conditions and Current Treatment. *Pediatrics, 139*(Suppl 3), S194-S206.
Kaur, R., Mehan, S., Singh, S. (2018). Understanding multifactorial architecture of Parkinson's disease: pathophysiology to management. *Neurol Sci*.
Keenan, H. T., Hooper, S. R., Wetherington, C. E., Nocera, M., Runyan, D. K. (2007). Neurodevelopmental consequences of early traumatic brain injury in 3-year-old children. *Pediatrics, 119*(3), e616-623.

Kelley, M. R., Cardarelli, R. A., Smalley, J. L., Ollerhead, T. A., Andrew, P. M., Brandon, N. J., Deeb, T. Z., Moss, S. J. (2018). Locally Reducing KCC2 Activity in the Hippocampus is Sufficient to Induce Temporal Lobe Epilepsy. *EBioMedicine, 32*, 62-71.
Khalilov, I., Chazal, G., Chudotvorova, I., Pellegrino, C., Corby, S., Ferrand, N., Gubkina, O., Nardou, R., Tyzio, R., Yamamoto, S., Jentsch, T. J., Hubner, C. A., Gaiarsa, J. L., Ben-Ari, Y., Medina, I. (2011). Enhanced Synaptic Activity and Epileptiform Events in the Embryonic KCC2 Deficient Hippocampus. *Front Cell Neurosci, 5*, 23.
Khazipov, R., Esclapez, M., Caillard, O., Bernard, C., Khalilov, I., Tyzio, R., Hirsch, J., Dzhala, V., Berger, B., Ben-Ari, Y. (2001). Early development of neuronal activity in the primate hippocampus in utero. *J Neurosci, 21*(24), 9770-9781.
Khazipov, R., Luhmann, H. J. (2006). Early patterns of electrical activity in the developing cerebral cortex of humans and rodents. *Trends Neurosci, 29*(7), 414-418.
Khazipov, R., Tyzio, R., Ben-Ari, Y. (2008). Effects of oxytocin on GABA signalling in the foetal brain during delivery. *Prog Brain Res, 170*, 243-257.
Khirug, S., Ahmad, F., Puskarjov, M., Afzalov, R., Kaila, K., Blaesse, P. (2010). A single seizure episode leads to rapid functional activation of KCC2 in the neonatal rat hippocampus. *J Neurosci, 30*(36), 12028-12035.
Khwaja, O. S., Ho, E., Barnes, K. V., O'Leary, H. M., Pereira, L. M., Finkelstein, Y., Nelson, C. A., 3rd, Vogel-Farley, V., DeGregorio, G., Holm, I. A., Khatwa, U., Kapur, K., Alexander, M. E., Finnegan, D. M., Cantwell, N. G., Walco, A. C., Rappaport, L., Gregas, M., Fichorova, R. N., Shannon, M. W., Sur, M., Kaufmann, W. E. (2014). Safety, pharmacokinetics, and preliminary assessment of efficacy of mecasermin (recombinant human IGF-1) for the treatment of Rett syndrome. *Proc Natl Acad Sci U S A, 111*(12), 4596-4601.
Kilb, W., Kirischuk, S., Luhmann, H. J. (2013). Role of tonic GABAergic currents during pre- and early postnatal rodent development. *Front Neural Circuits, 7*, 139.
Kim, D. Y., Fenoglio, K. A., Simeone, T. A., Coons, S. W., Wu, J., Chang, Y., Kerrigan, J. F., Rho, J. M. (2008). GABAA receptor-mediated activation of L-type calcium channels induces neuronal excitation in surgically resected human hypothalamic hamartomas. *Epilepsia, 49*(5), 861-871.
Kim, J. Y., Liu, C. Y., Zhang, F., Duan, X., Wen, Z., Song, J., Feighery, E., Lu, B., Rujescu, D., St Clair, D., Christian, K., Callicott, J. H., Weinberger, D. R., Song, H., Ming, G. L. (2012). Interplay between DISC1 and GABA signaling regulates neurogenesis in mice and risk for schizophrenia. *Cell, 148*(5), 1051-1064.
Kleschevnikov, A. M., Belichenko, P. V., Faizi, M., Jacobs, L. F., Htun, K., Shamloo, M., Mobley, W. C. (2012). Deficits in cognition and synaptic plasticity in a mouse model of Down syndrome ameliorated by GABAB receptor antagonists. *J Neurosci, 32*(27), 9217-9227.
Kleschevnikov, A. M., Belichenko, P. V., Faizi, M., Jacobs, L. F., Htun, K., Shamloo, M., Mobley, W. C. (2012). Deficits in cognition and synaptic plasticity in a mouse model of Down syndrome ameliorated by GABAB receptor antagonists. *J Neurosci, 32*, 9217-9227.
Kleschevnikov, A. M., Belichenko, P. V., Gall, J., George, L., Nosheny, R., Maloney, M. T., Salehi, A., Mobley, W. C. (2012). Increased efficiency of the GABAA and GABAB receptor-mediated neurotransmission in the Ts65Dn mouse model of Down syndrome. *Neurobiol Dis, 45*(2), 683-691.
Kleschevnikov, A. M., Belichenko, P. V., Villar, A. J., Epstein, C. J., Malenka, R. C., Mobley, W. C. (2004). Hippocampal long-term potentiation suppressed by increased inhibition in the Ts65Dn mouse, a genetic model of Down syndrome. *J Neurosci, 24*(37), 8153-8160.
Ko, M. C., Lee, M. C., Tang, T. H., Amstislavskaya, T. G., Tikhonova, M. A., Yang, Y. L., Lu, K. T. (2018). Bumetanide blocks the acquisition of conditioned fear in adult rats. *Br J Pharmacol, 175*(10), 1580-1589.
Kobayashi, K., Emson, P. C., Mountjoy, C. Q., Thornton, S. N., Lawson, D. E., Mann, D. M. (1990). Cerebral cortical calbindin D28K and parvalbumin neurones in Down's syndrome. *Neurosci Lett, 113*(1), 17-22.
Koduvayur, S. P., Gussin, H. A., Parthasarathy, R., Hao, Z., Kay, B. K., Pepperberg, D. R. (2014). Generation of recombinant antibodies to rat GABAA receptor subunits by affinity selection on synthetic peptides. *PLoS One, 9*(2), e87964.
Konopacka, A., Qiu, J., Yao, S. T., Greenwood, M. P., Greenwood, M., Lancaster, T., Inoue, W., Mecawi, A. S., Vechiato, F. M., de Lima, J. B., Coletti, R., Hoe, S. Z., Martin, A., Lee, J., Joseph, M., Hindmarch, C., Paton, J., Antunes-Rodrigues, J., Bains, J., Murphy, D. (2015). Osmoregulation requires brain expression of the renal Na-K-2Cl cotransporter NKCC2. *J Neurosci, 35*(13), 5144-5155.
Korpi, E. R., Kuner, T., Seeburg, P. H., Luddens, H. (1995). Selective antagonist for the cerebellar granule cell-specific gamma-aminobutyric acid type A receptor. *Mol Pharmacol, 47*(2), 283-289.
Korpi, E. R., Luddens, H. (1997). Furosemide interactions with brain GABAA receptors. *Br J Pharmacol, 120*(5), 741-748.
Koyama, R., Tao, K., Sasaki, T., Ichikawa, J., Miyamoto, D., Muramatsu, R., Matsuki, N., Ikegaya, Y. (2012). GABAergic excitation after febrile seizures induces ectopic granule cells and adult epilepsy. *Nat Med, 18*(8), 1271-1278.
Kurt, M. A., Davies, D. C., Kidd, M., Dierssen, M., Florez, J. (2000). Synaptic deficit in the temporal cortex of partial trisomy 16 (Ts65Dn) mice. *Brain Res, 858*(1), 191-197.
Kurt, M. A., Kafa, M. I., Dierssen, M., Davies, D. C. (2004). Deficits of neuronal density in CA1 and synaptic density in the dentate gyrus, CA3 and CA1, in a mouse model of Down syndrome. *Brain Res, 1022*(1-2), 101-109.
Lam, T. I., Anderson, S. E., Glaser, N., O'Donnell, M. E. (2005). Bumetanide reduces cerebral edema formation in rats with diabetic ketoacidosis. *Diabetes, 54*(2), 510-516.
Larimore, J., Zlatic, S. A., Arnold, M., Singleton, K. S., Cross, R., Rudolph, H., Bruegge, M. V., Sweetman, A., Garza, C., Whisnant, E., Faundez, V. (2017). Dysbindin Deficiency Modifies the Expression of GABA Neuron and Ion Permeation Transcripts in the Developing Hippocampus. *Front Genet, 8*, 28.
Lee, M. R., Wehring, H. J., McMahon, R. P., Linthicum, J., Cascella, N., Liu, F., Bellack, A., Buchanan, R. W., Strauss, G. P., Contoreggi, C., Kelly, D. L. (2013). Effects of adjunctive intranasal oxytocin on olfactory identification and clinical symptoms in schizophrenia: results from a randomized double blind placebo controlled pilot study. *Schizophr Res, 145*(1-3), 110-115.
Leighton, A. H., Lohmann, C. (2016). The Wiring of Developing Sensory Circuits-From Patterned Spontaneous Activity to Synaptic Plasticity Mechanisms. *Front Neural Circuits, 10*, 71.

Leinekugel, X., Medina, I., Khalilov, I., Ben-Ari, Y., Khazipov, R. (1997). Ca2+ oscillations mediated by the synergistic excitatory actions of GABA(A) and NMDA receptors in the neonatal hippocampus. *Neuron, 18*(2), 243-255.
Leitch, E., Coaker, J., Young, C., Mehta, V., Sernagor, E. (2005). GABA type-A activity controls its own developmental polarity switch in the maturing retina. *J Neurosci, 25*(19), 4801-4805.
Lemonnier, E., Ben-Ari, Y. (2010). The diuretic bumetanide decreases autistic behaviour in five infants treated during 3 months with no side effects. *Acta Paediatr, 99*(12), 1885-1888.
Lemonnier, E., Degrez, C., Phelep, M., Tyzio, R., Josse, F., Grandgeorge, M., Hadjikhani, N., Ben-Ari, Y. (2012). A randomised controlled trial of bumetanide in the treatment of autism in children. *Transl Psychiatry, 2*, e202.
Lemonnier, E., Lazartigues, A., Ben-Ari, Y. (2016). Treating Schizophrenia With the Diuretic Bumetanide: A Case Report. *Clin Neuropharmacol, 39*(2), 115-117.
Lemonnier, E., Robin, G., Degrez, C., Tyzio, R., Grandgeorge, M., Ben-Ari, Y. (2013). Treating Fragile X syndrome with the diuretic bumetanide: a case report. *Acta Paediatr, 102*(6), e288-290.
Lemonnier, E., Villeneuve, N., Sonie, S., Serret, S., Rosier, A., Roue, M., Brosset, P., Viellard, M., Bernoux, D., Rondeau, S., Thummler, S., Ravel, D., Ben-Ari, Y. (2017). Effects of bumetanide on neurobehavioral function in children and adolescents with autism spectrum disorders. *Transl Psychiatry, 7*(3), e1056.
Leonzino, M., Busnelli, M., Antonucci, F., Verderio, C., Mazzanti, M., Chini, B. (2016). The Timing of the Excitatory-to-Inhibitory GABA Switch Is Regulated by the Oxytocin Receptor via KCC2. *Cell Rep, 15*(1), 96-103.
Lewis, D. A. (2012). Cortical circuit dysfunction and cognitive deficits in schizophrenia--implications for preemptive interventions. *Eur J Neurosci, 35*(12), 1871-1878.
Lewis, M. L., Kesler, M., Candy, S. A., Rho, J. M., Pittman, Q. J. (2018). Comorbid epilepsy in autism spectrum disorder: Implications of postnatal inflammation for brain excitability. *Epilepsia, 59*(7), 1316-1326.
Li, H., Khirug, S., Cai, C., Ludwig, A., Blaesse, P., Kolikova, J., Afzalov, R., Coleman, S. K., Lauri, S., Airaksinen, M. S., Keinanen, K., Khiroug, L., Saarma, M., Kaila, K., Rivera, C. (2007). KCC2 interacts with the dendritic cytoskeleton to promote spine development. *Neuron, 56*(6), 1019-1033.
Li, H., Tornberg, J., Kaila, K., Airaksinen, M. S., Rivera, C. (2002). Patterns of cation-chloride cotransporter expression during embryonic rodent CNS development. *Eur J Neurosci, 16*(12), 2358-2370.
Li, X., Zhou, J., Chen, Z., Chen, S., Zhu, F., Zhou, L. (2008). Long-term expressional changes of Na+ -K+ -Cl- co-transporter 1 (NKCC1) and K+ -Cl- co-transporter 2 (KCC2) in CA1 region of hippocampus following lithium-pilocarpine induced status epilepticus (PISE). *Brain Res, 1221*, 141-146.
Liang, B., Huang, J. H. (2017). Elevated NKCC1 transporter expression facilitates early post-traumatic brain injury seizures. *Neural Regen Res, 12*(3), 401-402.
Llano, O., Smirnov, S., Soni, S., Golubtsov, A., Guillemin, I., Hotulainen, P., Medina, I., Nothwang, H. G., Rivera, C., Ludwig, A. (2015). KCC2 regulates actin dynamics in dendritic spines via interaction with beta-PIX. *J Cell Biol, 209*(5), 671-686.
Lopez-Alvarez, V. M., Modol, L., Navarro, X., Cobianchi, S. (2015). Early increasing-intensity treadmill exercise reduces neuropathic pain by preventing nociceptor collateral sprouting and disruption of chloride cotransporters homeostasis after peripheral nerve injury. *Pain, 156*(9), 1812-1825.
Loscher, W., Puskarjov, M., Kaila, K. (2013). Cation-chloride cotransporters NKCC1 and KCC2 as potential targets for novel antiepileptic and antiepileptogenic treatments. *Neuropharmacology, 69*, 62-74.
Lott, I. T. (2012). Neurological phenotypes for Down syndrome across the life span. *Prog Brain Res, 197*, 101-121.
Lott, I. T., Dierssen, M. (2010). Cognitive deficits and associated neurological complications in individuals with Down's syndrome. *Lancet Neurol, 9*(6), 623-633.
Lozovaya, N., Eftekhari, S., Cloarec, R., Gouty-Colomer, L. A., Dufour, A., Riffault, B., Billon-Grand, M., Pons-Bennaceur, A., Oumar, N., Burnashev, N., Ben-Ari, Y., Hammond, C. (2018). GABAergic inhibition in dual-transmission cholinergic and GABAergic striatal interneurons is abolished in Parkinson disease. *Nat Commun, 9*(1), 1422.
Lu, K. T., Cheng, N. C., Wu, C. Y., Yang, Y. L. (2008). NKCC1-mediated traumatic brain injury-induced brain edema and neuron death via Raf/MEK/MAPK cascade. *Crit Care Med, 36*(3), 917-922.
Lu, K. T., Huang, T. C., Tsai, Y. H., Yang, Y. L. (2017). Transient receptor potential vanilloid type 4 channels mediate Na-K-Cl-co-transporter-induced brain edema after traumatic brain injury. *J Neurochem, 140*(5), 718-727.
Lu, K. T., Huang, T. C., Wang, J. Y., You, Y. S., Chou, J. L., Chan, M. W., Wo, P. Y., Amstislavskaya, T. G., Tikhonova, M. A., Yang, Y. L. (2015). NKCC1 mediates traumatic brain injury-induced hippocampal neurogenesis through CREB phosphorylation and HIF-1alpha expression. *Pflugers Arch, 467*(8), 1651-1661.
Lu, K. T., Wu, C. Y., Cheng, N. C., Wo, Y. Y., Yang, J. T., Yen, H. H., Yang, Y. L. (2006). Inhibition of the Na+ -K+ -2Cl- -cotransporter in choroid plexus attenuates traumatic brain injury-induced brain edema and neuronal damage. *Eur J Pharmacol, 548*(1-3), 99-105.
Lu, K. T., Wu, C. Y., Yen, H. H., Peng, J. H., Wang, C. L., Yang, Y. L. (2007). Bumetanide administration attenuated traumatic brain injury through IL-1 overexpression. *Neurol Res, 29*(4), 404-409.
Lykke, K., Tollner, K., Feit, P. W., Erker, T., MacAulay, N., Loscher, W. (2016). The search for NKCC1-selective drugs for the treatment of epilepsy: Structure-function relationship of bumetanide and various bumetanide derivatives in inhibiting the human cation-chloride cotransporter NKCC1A. *Epilepsy Behav, 59*, 42-49.
MacKenzie, G., Maguire, J. (2015). Chronic stress shifts the GABA reversal potential in the hippocampus and increases seizure susceptibility. *Epilepsy Res, 109*, 13-27.
MacKenzie, G., O'Toole, K. K., Moss, S. J., Maguire, J. (2016). Compromised GABAergic inhibition contributes to tumor-associated epilepsy. *Epilepsy Res, 126*, 185-196.
Magalhaes, A. C., Rivera, C. (2016). NKCC1-Deficiency Results in Abnormal Proliferation of Neural Progenitor Cells of the Lateral Ganglionic Eminence. *Front Cell Neurosci, 10*, 200.
Mak, K. K., Pichika, M. R. (2018). Artificial intelligence in drug development: present status and future prospects. *Drug Discov Today*.
Makinen, M. E., Yla-Outinen, L., Narkilahti, S. (2018). GABA and Gap Junctions in the Development of Synchronized Activity in Human Pluripotent Stem Cell-Derived Neural Networks. *Front Cell Neurosci, 12*, 56.

Marguet, S. L., Le-Schulte, V. T., Merseburg, A., Neu, A., Eichler, R., Jakovcevski, I., Ivanov, A., Hanganu-Opatz, I. L., Bernard, C., Morellini, F., Isbrandt, D. (2015). Treatment during a vulnerable developmental period rescues a genetic epilepsy. *Nat Med, 21*(12), 1436-1444.
Marrosu, F., Marrosu, G., Rachel, M. G., Biggio, G. (1987). Paradoxical reactions elicited by diazepam in children with classic autism. *Funct Neurol, 2*(3), 355-361.
Martinez-Cue, C., Baamonde, C., Lumbreras, M., Paz, J., Davisson, M. T., Schmidt, C., Dierssen, M., Florez, J. (2002). Differential effects of environmental enrichment on behavior and learning of male and female Ts65Dn mice, a model for Down syndrome. *Behav Brain Res, 134*(1-2), 185-200.
Martinez-Cue, C., Delatour, B., Potier, M. C. (2014). Treating enhanced GABAergic inhibition in Down syndrome: use of GABA alpha5-selective inverse agonists. *Neurosci Biobehav Rev, 46 Pt 2*, 218-227.
Martinez-Cue, C., Martinez, P., Rueda, N., Vidal, R., Garcia, S., Vidal, V., Corrales, A., Montero, J. A., Pazos, A., Florez, J., Gasser, R., Thomas, A. W., Honer, M., Knoflach, F., Trejo, J. L., Wettstein, J. G., Hernandez, M. C. (2013). Reducing GABAA alpha5 receptor-mediated inhibition rescues functional and neuromorphological deficits in a mouse model of down syndrome. *J Neurosci, 33*(9), 3953-3966.
Martinez-Cue, C., Rueda, N., Garcia, E., Davisson, M. T., Schmidt, C., Florez, J. (2005). Behavioral, cognitive and biochemical responses to different environmental conditions in male Ts65Dn mice, a model of Down syndrome. *Behav Brain Res, 163*(2), 174-185.
Maya Vetencourt, J. F., Sale, A., Viegi, A., Baroncelli, L., De Pasquale, R., O'Leary, O. F., Castren, E., Maffei, L. (2008). The antidepressant fluoxetine restores plasticity in the adult visual cortex. *Science, 320*(5874), 385-388.
Mazarati, A., Shin, D., Sankar, R. (2009). Bumetanide inhibits rapid kindling in neonatal rats. *Epilepsia, 50*(9), 2117-2122.
Medina, I., Friedel, P., Rivera, C., Kahle, K. T., Kourdougli, N., Uvarov, P., Pellegrino, C. (2014). Current view on the functional regulation of the neuronal K(+)-Cl(-) cotransporter KCC2. *Front Cell Neurosci, 8*, 27.
Mejia-Gervacio, S., Murray, K., Lledo, P. M. (2011). NKCC1 controls GABAergic signaling and neuroblast migration in the postnatal forebrain. *Neural Dev, 6*, 4.
Mendez, P., Pazienti, A., Szabo, G., Bacci, A. (2012). Direct alteration of a specific inhibitory circuit of the hippocampus by antidepressants. *J Neurosci, 32*(47), 16616-16628.
Merner, N. D., Chandler, M. R., Bourassa, C., Liang, B., Khanna, A. R., Dion, P., Rouleau, G. A., Kahle, K. T. (2015). Regulatory domain or CpG site variation in SLC12A5, encoding the chloride transporter KCC2, in human autism and schizophrenia. *Front Cell Neurosci, 9*, 386.
Merner, N. D., Mercado, A., Khanna, A. R., Hodgkinson, A., Bruat, V., Awadalla, P., Gamba, G., Rouleau, G. A., Kahle, K. T. (2016). Gain-of-function missense variant in SLC12A2, encoding the bumetanide-sensitive NKCC1 cotransporter, identified in human schizophrenia. *J Psychiatr Res, 77*, 22-26.
Mikawa, S., Wang, C., Shu, F., Wang, T., Fukuda, A., Sato, K. (2002). Developmental changes in KCC1, KCC2 and NKCC1 mRNAs in the rat cerebellum. *Brain Res Dev Brain Res, 136*(2), 93-100.
Minier, F., Sigel, E. (2004). Positioning of the alpha-subunit isoforms confers a functional signature to gamma-aminobutyric acid type A receptors. *Proc Natl Acad Sci U S A, 101*(20), 7769-7774.
Mitchell, K. J. (2011). The genetics of neurodevelopmental disease. *Curr Opin Neurobiol, 21*(1), 197-203.
Mitra, A., Blank, M., Madison, D. V. (2012). Developmentally altered inhibition in Ts65Dn, a mouse model of Down syndrome. *Brain Res, 1440*, 1-8.
Miyoshi, G., Fishell, G. (2011). GABAergic interneuron lineages selectively sort into specific cortical layers during early postnatal development. *Cereb Cortex, 21*(4), 845-852.
Modabbernia, A., Rezaei, F., Salehi, B., Jafarinia, M., Ashrafi, M., Tabrizi, M., Hosseini, S. M., Tajdini, M., Ghaleiha, A., Akhondzadeh, S. (2013). Intranasal oxytocin as an adjunct to risperidone in patients with schizophrenia : an 8-week, randomized, double-blind, placebo-controlled study. *CNS Drugs, 27*(1), 57-65.
Modol, L., Cobianchi, S., Navarro, X. (2014). Prevention of NKCC1 phosphorylation avoids downregulation of KCC2 in central sensory pathways and reduces neuropathic pain after peripheral nerve injury. *Pain, 155*(8), 1577-1590.
Modol, L., Santos, D., Cobianchi, S., Gonzalez-Perez, F., Lopez-Alvarez, V., Navarro, X. (2015). NKCC1 Activation Is Required for Myelinated Sensory Neurons Regeneration through JNK-Dependent Pathway. *J Neurosci, 35*(19), 7414-7427.
Mohler, H. (2012). Cognitive enhancement by pharmacological and behavioral interventions: the murine Down syndrome model. *Biochem Pharmacol, 84*(8), 994-999.
Mojabi, F. S., Fahimi, A., Moghadam, S., Moghadam, S., Windy McNerneny, M., Ponnusamy, R., Kleschevnikov, A., Mobley, W. C., Salehi, A. (2016). GABAergic hyperinnervation of dentate granule cells in the Ts65Dn mouse model of down syndrome: Exploring the role of App. *Hippocampus, 26*(12), 1641-1654.
Morales-Aza, B. M., Chillingworth, N. L., Payne, J. A., Donaldson, L. F. (2004). Inflammation alters cation chloride cotransporter expression in sensory neurons. *Neurobiol Dis, 17*(1), 62-69.
Morel, A., Peyroux, E., Leleu, A., Favre, E., Franck, N., Demily, C. (2018). Overview of Social Cognitive Dysfunctions in Rare Developmental Syndromes With Psychiatric Phenotype. *Front Pediatr, 6*, 102.
Moss, J., Richards, C., Nelson, L., Oliver, C. (2013). Prevalence of autism spectrum disorder symptomatology and related behavioural characteristics in individuals with Down syndrome. *Autism, 17*(4), 390-404.
Moss, J. F. (2017). Autism spectrum disorder and attention-deficit-hyperactivity disorder in Down syndrome. *Dev Med Child Neurol, 59*(3), 240.
Munoz, A., Mendez, P., DeFelipe, J., Alvarez-Leefmans, F. J. (2007). Cation-chloride cotransporters and GABA-ergic innervation in the human epileptic hippocampus. *Epilepsia, 48*(4), 663-673.
Nadel, L. (2003). Down's syndrome: a genetic disorder in biobehavioral perspective. *Genes Brain Behav, 2*(3), 156-166.
Nagao, H., Nakajima, K., Niisato, N., Hirota, R., Bando, H., Sakaguchi, H., Hisa, Y., Marunaka, Y. (2012). K(+)-Cl(-) cotransporter 1 (KCC1) negatively regulates NGF-induced neurite outgrowth in PC12 cells. *Cell Physiol Biochem, 30*(3), 538-551.
Nakajima, K., Miyazaki, H., Niisato, N., Marunaka, Y. (2007). Essential role of NKCC1 in NGF-induced neurite outgrowth. *Biochem Biophys Res Commun, 359*(3), 604-610.
Nakajima, K., Niisato, N., Marunaka, Y. (2011a). Genistein enhances the NGF-induced neurite outgrowth. *Biomed Res, 32*(5), 351-356.

Nakajima, K., Niisato, N., Marunaka, Y. (2011b). Quercetin stimulates NGF-induced neurite outgrowth in PC12 cells via activation of Na(+)/K(+)/2Cl(-) cotransporter. *Cell Physiol Biochem, 28*(1), 147-156.
Nakajima, K. I., Marunaka, Y. (2016). Intracellular chloride ion concentration in differentiating neuronal cell and its role in growing neurite. *Biochem Biophys Res Commun, 479*(2), 338-342.
Nakanishi, K., Yamada, J., Takayama, C., Oohira, A., Fukuda, A. (2007). NKCC1 activity modulates formation of functional inhibitory synapses in cultured neocortical neurons. *Synapse, 61*(3), 138-149.
Nardou, R., Ben-Ari, Y., Khalilov, I. (2009). Bumetanide, an NKCC1 antagonist, does not prevent formation of epileptogenic focus but blocks epileptic focus seizures in immature rat hippocampus. *J Neurophysiol, 101*(6), 2878-2888.
Noctor, S. C., Flint, A. C., Weissman, T. A., Dammerman, R. S., Kriegstein, A. R. (2001). Neurons derived from radial glial cells establish radial units in neocortex. *Nature, 409*(6821), 714-720.
Nomura, H., Sakai, A., Nagano, M., Umino, M., Suzuki, H. (2006). Expression changes of cation chloride cotransporters in the rat spinal cord following intraplantar formalin. *Neurosci Res, 56*(4), 435-440.
O'Donnell, M. E., Lam, T. I., Tran, L. Q., Foroutan, S., Anderson, S. E. (2006). Estradiol reduces activity of the blood-brain barrier Na-K-Cl cotransporter and decreases edema formation in permanent middle cerebral artery occlusion. *J Cereb Blood Flow Metab, 26*(10), 1234-1249.
O'Donnell, M. E., Tran, L., Lam, T. I., Liu, X. B., Anderson, S. E. (2004). Bumetanide inhibition of the blood-brain barrier Na-K-Cl cotransporter reduces edema formation in the rat middle cerebral artery occlusion model of stroke. *J Cereb Blood Flow Metab, 24*(9), 1046-1056.
Okabe, A., Ohno, K., Toyoda, H., Yokokura, M., Sato, K., Fukuda, A. (2002). Amygdala kindling induces upregulation of mRNA for NKCC1, a Na(+), K(+)-2Cl(-) cotransporter, in the rat piriform cortex. *Neurosci Res, 44*(2), 225-229.
Ostergaard, E. H., Magnussen, M. P., Nielsen, C. K., Eilertsen, E., Frey, H. H. (1972). Pharmacological properties of 3-n-butylamino-4-phenoxy-5-sulfamylbenzoic acid (Bumetanide), a new potent diuretic. *Arzneimittelforschung, 22*(1), 66-72.
Ota, M., Yoshida, S., Nakata, M., Yada, T., Kunugi, H. (2018). The effects of adjunctive intranasal oxytocin in patients with schizophrenia. *Postgrad Med, 130*(1), 122-128.
Pallud, J., Le Van Quyen, M., Bielle, F., Pellegrino, C., Varlet, P., Cresto, N., Baulac, M., Duyckaerts, C., Kourdougli, N., Chazal, G., Devaux, B., Rivera, C., Miles, R., Capelle, L., Huberfeld, G. (2014). Cortical GABAergic excitation contributes to epileptic activities around human glioma. *Sci Transl Med, 6*(244), 244ra289.
Palma, E., Amici, M., Sobrero, F., Spinelli, G., Di Angelantonio, S., Ragozzino, D., Mascia, A., Scoppetta, C., Esposito, V., Miledi, R., Eusebi, F. (2006). Anomalous levels of Cl- transporters in the hippocampal subiculum from temporal lobe epilepsy patients make GABA excitatory. *Proc Natl Acad Sci U S A, 103*(22), 8465-8468.
Park, E., Bell, J. D., Baker, A. J. (2008). Traumatic brain injury: can the consequences be stopped? *CMAJ, 178*(9), 1163-1170.
Parker, S. E., Mai, C. T., Canfield, M. A., Rickard, R., Wang, Y., Meyer, R. E., Anderson, P., Mason, C. A., Collins, J. S., Kirby, R. S., Correa, A., National Birth Defects Prevention, N. (2010). Updated National Birth Prevalence estimates for selected birth defects in the United States, 2004-2006. *Birth Defects Res A Clin Mol Teratol, 88*(12), 1008-1016.
Pearson, M. M., Lu, J., Mount, D. B., Delpire, E. (2001). Localization of the K(+)-Cl(-) cotransporter, KCC3, in the central and peripheral nervous systems: expression in the choroid plexus, large neurons and white matter tracts. *Neuroscience, 103*(2), 481-491.
Pedersen, C. A., Gibson, C. M., Rau, S. W., Salimi, K., Smedley, K. L., Casey, R. L., Leserman, J., Jarskog, L. F., Penn, D. L. (2011). Intranasal oxytocin reduces psychotic symptoms and improves Theory of Mind and social perception in schizophrenia. *Schizophr Res, 132*(1), 50-53.
Pennington, B. F., Moon, J., Edgin, J., Stedron, J., Nadel, L. (2003). The neuropsychology of Down syndrome: evidence for hippocampal dysfunction. *Child Dev, 74*(1), 75-93.
Percy, A. K. (2011). Rett syndrome: exploring the autism link. *Arch Neurol, 68*(8), 985-989.
Perez-Cremades, D., Hernandez, S., Blasco-Ibanez, J. M., Crespo, C., Nacher, J., Varea, E. (2010). Alteration of inhibitory circuits in the somatosensory cortex of Ts65Dn mice, a model for Down's syndrome. *J Neural Transm (Vienna), 117*(4), 445-455.
Pfeffer, C. K., Stein, V., Keating, D. J., Maier, H., Rinke, I., Rudhard, Y., Hentschke, M., Rune, G. M., Jentsch, T. J., Hubner, C. A. (2009). NKCC1-dependent GABAergic excitation drives synaptic network maturation during early hippocampal development. *J Neurosci, 29*(11), 3419-3430.
Pieraut, S., Laurent-Matha, V., Sar, C., Hubert, T., Mechaly, I., Hilaire, C., Mersel, M., Delpire, E., Valmier, J., Scamps, F. (2007). NKCC1 phosphorylation stimulates neurite growth of injured adult sensory neurons. *J Neurosci, 27*(25), 6751-6759.
Pieraut, S., Lucas, O., Sangari, S., Sar, C., Boudes, M., Bouffi, C., Noel, D., Scamps, F. (2011). An autocrine neuronal interleukin-6 loop mediates chloride accumulation and NKCC1 phosphorylation in axotomized sensory neurons. *J Neurosci, 31*(38), 13516-13526.
Pini, G., Congiu, L., Benincasa, A., DiMarco, P., Bigoni, S., Dyer, A. H., Mortimer, N., Della-Chiesa, A., O'Leary, S., McNamara, R., Mitchell, K. J., Gill, M., Tropea, D. (2016). Illness Severity, Social and Cognitive Ability, and EEG Analysis of Ten Patients with Rett Syndrome Treated with Mecasermin (Recombinant Human IGF-1). *Autism Res Treat, 2016*, 5073078.
Pizzarelli, R., Cherubini, E. (2011). Alterations of GABAergic signaling in autism spectrum disorders. *Neural Plast, 2011*, 297153.
Plotkin, M. D., Snyder, E. Y., Hebert, S. C., Delpire, E. (1997). Expression of the Na-K-2Cl cotransporter is developmentally regulated in postnatal rat brains: a possible mechanism underlying GABA's excitatory role in immature brain. *J Neurobiol, 33*(6), 781-795.
Potier, M. C., Braudeau, J., Dauphinot, L., Delatour, B. (2014). Reducing GABAergic inhibition restores cognitive functions in a mouse model of Down syndrome. *CNS Neurol Disord Drug Targets, 13*(1), 8-15.
Potkin, S. G., Turner, J. A., Guffanti, G., Lakatos, A., Fallon, J. H., Nguyen, D. D., Mathalon, D., Ford, J., Lauriello, J., Macciardi, F., Fbirn. (2009). A genome-wide association study of schizophrenia using brain activation as a quantitative phenotype. *Schizophr Bull, 35*(1), 96-108.
Pressler, R. M., Boylan, G. B., Marlow, N., Blennow, M., Chiron, C., Cross, J. H., de Vries, L. S., Hallberg, B., Hellstrom-Westas, L., Jullien, V., Livingstone, V., Mangum, B., Murphy, B., Murray, D., Pons, G., Rennie, J., Swarte, R., Toet, M. C., Vanhatalo, S., Zohar, S., consortium, N. E. s. t. w. M. O.-p. (2015). Bumetanide for the treatment of seizures in newborn babies with hypoxic ischaemic encephalopathy (NEMO): an open-label, dose finding, and feasibility phase 1/2 trial. *Lancet Neurol, 14*(5), 469-477.

Pueschel, S. M., Bernier, J. C., Pezzullo, J. C. (1991). Behavioural observations in children with Down's syndrome. *J Ment Defic Res, 35 (Pt 6)*, 502-511.
Puskarjov, M., Kahle, K. T., Ruusuvuori, E., Kaila, K. (2014). Pharmacotherapeutic targeting of cation-chloride cotransporters in neonatal seizures. *Epilepsia, 55*(6), 806-818.
Puskarjov, M., Seja, P., Heron, S. E., Williams, T. C., Ahmad, F., Iona, X., Oliver, K. L., Grinton, B. E., Vutskits, L., Scheffer, I. E., Petrou, S., Blaesse, P., Dibbens, L. M., Berkovic, S. F., Kaila, K. (2014). A variant of KCC2 from patients with febrile seizures impairs neuronal Cl- extrusion and dendritic spine formation. *EMBO Rep, 15*(6), 723-729.
Rahmanzadeh, R., Eftekhari, S., Shahbazi, A., Khodaei Ardakani, M. R., Rahmanzade, R., Mehrabi, S., Barati, M., Joghataei, M. T. (2017). Effect of bumetanide, a selective NKCC1 inhibitor, on hallucinations of schizophrenic patients; a double-blind randomized clinical trial. *Schizophr Res, 184*, 145-146.
Rahmanzadeh, R., Shahbazi, A., Ardakani, M. K., Mehrabi, S., Rahmanzade, R., Joghataei, M. T. (2017). Lack of the effect of bumetanide, a selective NKCC1 inhibitor, in patients with schizophrenia: A double-blind randomized trial. *Psychiatry Clin Neurosci, 71*(1), 72-73.
Ramsay, L. E., McInnes, G. T., Hettiarachchi, J., Shelton, J., Scott, P. (1978). Bumetanide and frusemide: a comparison of dose-response curves in healthy men. *Br J Clin Pharmacol, 5*(3), 243-247.
Reeves, R. H., Irving, N. G., Moran, T. H., Wohn, A., Kitt, C., Sisodia, S. S., Schmidt, C., Bronson, R. T., Davisson, M. T. (1995). A mouse model for Down syndrome exhibits learning and behaviour deficits. *Nat Genet, 11*(2), 177-184.
Reid, A. Y., Riazi, K., Campbell Teskey, G., Pittman, Q. J. (2013). Increased excitability and molecular changes in adult rats after a febrile seizure. *Epilepsia, 54*(4), e45-48.
Rissman, R. A., Mobley, W. C. (2011). Implications for treatment: GABAA receptors in aging, Down syndrome and Alzheimer's disease. *J Neurochem, 117*(4), 613-622.
Rivera, C., Li, H., Thomas-Crusells, J., Lahtinen, H., Viitanen, T., Nanobashvili, A., Kokaia, Z., Airaksinen, M. S., Voipio, J., Kaila, K., Saarma, M. (2002). BDNF-induced TrkB activation down-regulates the K+-Cl- cotransporter KCC2 and impairs neuronal Cl- extrusion. *J Cell Biol, 159*(5), 747-752.
Rivera, C., Voipio, J., Payne, J. A., Ruusuvuori, E., Lahtinen, H., Lamsa, K., Pirvola, U., Saarma, M., Kaila, K. (1999). The K+/Cl- co-transporter KCC2 renders GABA hyperpolarizing during neuronal maturation. *Nature, 397*(6716), 251-255.
Robel, S., Buckingham, S. C., Boni, J. L., Campbell, S. L., Danbolt, N. C., Riedemann, T., Sutor, B., Sontheimer, H. (2015). Reactive astrogliosis causes the development of spontaneous seizures. *J Neurosci, 35*(8), 3330-3345.
Robertson, J., Hatton, C., Emerson, E., Baines, S. (2015). Prevalence of epilepsy among people with intellectual disabilities: A systematic review. *Seizure, 29*, 46-62.
Romermann, K., Fedrowitz, M., Hampel, P., Kaczmarek, E., Tollner, K., Erker, T., Sweet, D. H., Loscher, W. (2017). Multiple blood-brain barrier transport mechanisms limit bumetanide accumulation, and therapeutic potential, in the mammalian brain. *Neuropharmacology, 117*, 182-194.
Ross, M. H., Galaburda, A. M., Kemper, T. L. (1984). Down's syndrome: is there a decreased population of neurons? *Neurology, 34*(7), 909-916.
Rueda, N., Florez, J., Martinez-Cue, C. (2008). Chronic pentylenetetrazole but not donepezil treatment rescues spatial cognition in Ts65Dn mice, a model for Down syndrome. *Neurosci Lett, 433*(1), 22-27.
Ruffolo, G., Cifelli, P., Roseti, C., Thom, M., van Vliet, E. A., Limatola, C., Aronica, E., Palma, E. (2018). A novel GABAergic dysfunction in human Dravet syndrome. *Epilepsia*.
Ruffolo, G., Iyer, A., Cifelli, P., Roseti, C., Muhlebner, A., van Scheppingen, J., Scholl, T., Hainfellner, J. A., Feucht, M., Krsek, P., Zamecnik, J., Jansen, F. E., Spliet, W. G., Limatola, C., Aronica, E., Palma, E. (2016). Functional aspects of early brain development are preserved in tuberous sclerosis complex (TSC) epileptogenic lesions. *Neurobiol Dis, 95*, 93-101.
Sago, H., Carlson, E. J., Smith, D. J., Rubin, E. M., Crnic, L. S., Huang, T. T., Epstein, C. J. (2000). Genetic dissection of region associated with behavioral abnormalities in mouse models for Down syndrome. *Pediatr Res, 48*(5), 606-613.
Sale, A., Maya Vetencourt, J. F., Medini, P., Cenni, M. C., Baroncelli, L., De Pasquale, R., Maffei, L. (2007). Environmental enrichment in adulthood promotes amblyopia recovery through a reduction of intracortical inhibition. *Nat Neurosci, 10*(6), 679-681.
Santos, L. E. C., Rodrigues, A. M., Lopes, M. R., Costa, V. D. C., Scorza, C. A., Scorza, F. A., Cavalheiro, E. A., Almeida, A. G. (2017). Long-term alcohol exposure elicits hippocampal nonsynaptic epileptiform activity changes associated with expression and functional changes in NKCC1, KCC2 co-transporters and Na(+)/K(+)-ATPase. *Neuroscience, 340*, 530-541.
Schiapparelli, P., Guerrero-Cazares, H., Magana-Maldonado, R., Hamilla, S. M., Ganaha, S., Goulin Lippi Fernandes, E., Huang, C. H., Aranda-Espinoza, H., Devreotes, P., Quinones-Hinojosa, A. (2017). NKCC1 Regulates Migration Ability of Glioblastoma Cells by Modulation of Actin Dynamics and Interacting with Cofilin. *EBioMedicine, 21*, 94-103.
Schiessl, I. M., Castrop, H. (2015). Regulation of NKCC2 splicing and phosphorylation. *Curr Opin Nephrol Hypertens, 24*(5), 457-462.
Schulte, J. T., Wierenga, C. J., Bruining, H. (2018). Chloride transporters and GABA polarity in developmental, neurological and psychiatric conditions. *Neurosci Biobehav Rev, 90*, 260-271.
Schwartzkroin, P. A., Baraban, S. C., Hochman, D. W. (1998). Osmolarity, ionic flux, and changes in brain excitability. *Epilepsy Res, 32*(1-2), 275-285.
Sedmak, G., Jovanov-Milosevic, N., Puskarjov, M., Ulamec, M., Kruslin, B., Kaila, K., Judas, M. (2016). Developmental Expression Patterns of KCC2 and Functionally Associated Molecules in the Human Brain. *Cereb Cortex, 26*(12), 4574-4589.
Sen, A., Martinian, L., Nikolic, M., Walker, M. C., Thom, M., Sisodiya, S. M. (2007). Increased NKCC1 expression in refractory human epilepsy. *Epilepsy Res, 74*(2-3), 220-227.
Shekarabi, M., Salin-Cantegrel, A., Laganiere, J., Gaudet, R., Dion, P., Rouleau, G. A. (2011). Cellular expression of the K+-Cl- cotransporter KCC3 in the central nervous system of mouse. *Brain Res, 1374*, 15-26.
Shimizu-Okabe, C., Okabe, A., Kilb, W., Sato, K., Luhmann, H. J., Fukuda, A. (2007). Changes in the expression of cation-Cl- cotransporters, NKCC1 and KCC2, during cortical malformation induced by neonatal freeze-lesion. *Neurosci Res, 59*(3), 288-295.

Shimizu-Okabe, C., Tanaka, M., Matsuda, K., Mihara, T., Okabe, A., Sato, K., Inoue, Y., Fujiwara, T., Yagi, K., Fukuda, A. (2011). KCC2 was downregulated in small neurons localized in epileptogenic human focal cortical dysplasia. *Epilepsy Res, 93*(2-3), 177-184.
Shimizu-Okabe, C., Yokokura, M., Okabe, A., Ikeda, M., Sato, K., Kilb, W., Luhmann, H. J., Fukuda, A. (2002). Layer-specific expression of Cl- transporters and differential [Cl-]i in newborn rat cortex. *Neuroreport, 13*(18), 2433-2437.
Shin, N. Y., Park, H. Y., Jung, W. H., Park, J. W., Yun, J. Y., Jang, J. H., Kim, S. N., Han, H. J., Kim, S. Y., Kang, D. H., Kwon, J. S. (2015). Effects of Oxytocin on Neural Response to Facial Expressions in Patients with Schizophrenia. *Neuropsychopharmacology, 40*(8), 1919-1927.
Siarey, R. J., Carlson, E. J., Epstein, C. J., Balbo, A., Rapoport, S. I., Galdzicki, Z. (1999). Increased synaptic depression in the Ts65Dn mouse, a model for mental retardation in Down syndrome. *Neuropharmacology, 38*(12), 1917-1920.
Siarey, R. J., Stoll, J., Rapoport, S. I., Galdzicki, Z. (1997). Altered long-term potentiation in the young and old Ts65Dn mouse, a model for Down Syndrome. *Neuropharmacology, 36*(11-12), 1549-1554.
Simard, J. M., Kahle, K. T., Gerzanich, V. (2010). Molecular mechanisms of microvascular failure in central nervous system injury--synergistic roles of NKCC1 and SUR1/TRPM4. *J Neurosurg, 113*(3), 622-629.
Simon, D. B., Karet, F. E., Hamdan, J. M., DiPietro, A., Sanjad, S. A., Lifton, R. P. (1996). Bartter's syndrome, hypokalaemic alkalosis with hypercalciuria, is caused by mutations in the Na-K-2Cl cotransporter NKCC2. *Nat Genet, 13*(2), 183-188.
Sivakumaran, S., Maguire, J. (2016). Bumetanide reduces seizure progression and the development of pharmacoresistant status epilepticus. *Epilepsia, 57*(2), 222-232.
Smigielska-Kuzia, J., Sobaniec, W., Kulak, W., Bockowski, L. (2009). Clinical and EEG features of epilepsy in children and adolescents in Down syndrome. *J Child Neurol, 24*(4), 416-420.
Sommeijer, J. P., Ahmadlou, M., Saiepour, M. H., Seignette, K., Min, R., Heimel, J. A., Levelt, C. N. (2017). Thalamic inhibition regulates critical-period plasticity in visual cortex and thalamus. *Nat Neurosci, 20*(12), 1715-1721.
Sontheimer, H. (2008). An unexpected role for ion channels in brain tumor metastasis. *Exp Biol Med (Maywood), 233*(7), 779-791.
Spitzer, N. C. (2006). Electrical activity in early neuronal development. *Nature, 444*(7120), 707-712.
Stafstrom, C. E., Patxot, O. F., Gilmore, H. E., Wisniewski, K. E. (1991). Seizures in children with Down syndrome: etiology, characteristics and outcome. *Dev Med Child Neurol, 33*(3), 191-200.
Stagni, F., Giacomini, A., Guidi, S., Ciani, E., Ragazzi, E., Filonzi, M., De Iasio, R., Rimondini, R., Bartesaghi, R. (2015). Long-term effects of neonatal treatment with fluoxetine on cognitive performance in Ts65Dn mice. *Neurobiol Dis, 74*, 204-218.
Stagni, F., Magistretti, J., Guidi, S., Ciani, E., Mangano, C., Calza, L., Bartesaghi, R. (2013). Pharmacotherapy with fluoxetine restores functional connectivity from the dentate gyrus to field CA3 in the Ts65Dn mouse model of down syndrome. *PLoS One, 8*(4), e61689.
Stefan, M. I., Le Novere, N. (2013). Cooperative binding. *PLoS Comput Biol, 9*(6), e1003106.
Steffensen, A. B., Oernbo, E. K., Stoica, A., Gerkau, N. J., Barbuskaite, D., Tritsaris, K., Rose, C. R., MacAulay, N. (2018). Cotransporter-mediated water transport underlying cerebrospinal fluid formation. *Nat Commun, 9*(1), 2167.
Stein, V., Hermans-Borgmeyer, I., Jentsch, T. J., Hubner, C. A. (2004). Expression of the KCl cotransporter KCC2 parallels neuronal maturation and the emergence of low intracellular chloride. *J Comp Neurol, 468*(1), 57-64.
Stewart, L. S., Persinger, M. A., Cortez, M. A., Snead, O. C., 3rd. (2007). Chronobiometry of behavioral activity in the Ts65Dn model of Down syndrome. *Behav Genet, 37*(2), 388-398.
Strittmatter, S. M. (2014). Overcoming Drug Development Bottlenecks With Repurposing: Old drugs learn new tricks. *Nat Med, 20*(6), 590-591.
Studer, A. (2012). A "Renaissance" in radical trifluoromethylation. *Angew Chem Int Ed Engl, 51*(36), 8950-8958.
Sun, L., Yu, Z., Wang, W., Liu, X. (2012). Both NKCC1 and anion exchangers contribute to Cl(-) accumulation in postnatal forebrain neuronal progenitors. *Eur J Neurosci, 35*(5), 661-672.
Takayama, C., Inoue, Y. (2010). Developmental localization of potassium chloride co-transporter 2 (KCC2), GABA and vesicular GABA transporter (VGAT) in the postnatal mouse somatosensory cortex. *Neurosci Res, 67*(2), 137-148.
Takesian, A. E., Hensch, T. K. (2013). Balancing plasticity/stability across brain development. *Prog Brain Res, 207*, 3-34.
Talos, D. M., Sun, H., Kosaras, B., Joseph, A., Folkerth, R. D., Poduri, A., Madsen, J. R., Black, P. M., Jensen, F. E. (2012). Altered inhibition in tuberous sclerosis and type IIb cortical dysplasia. *Ann Neurol, 71*(4), 539-551.
Tang, X., Kim, J., Zhou, L., Wengert, E., Zhang, L., Wu, Z., Carromeu, C., Muotri, A. R., Marchetto, M. C., Gage, F. H., Chen, G. (2016). KCC2 rescues functional deficits in human neurons derived from patients with Rett syndrome. *Proc Natl Acad Sci U S A, 113*(3), 751-756.
Tao, K., Ichikawa, J., Matsuki, N., Ikegaya, Y., Koyama, R. (2016). Experimental febrile seizures induce age-dependent structural plasticity and improve memory in mice. *Neuroscience, 318*, 34-44.
Tollner, K., Brandt, C., Erker, T., Loscher, W. (2015). Bumetanide is not capable of terminating status epilepticus but enhances phenobarbital efficacy in different rat models. *Eur J Pharmacol, 746*, 78-88.
Tollner, K., Brandt, C., Romermann, K., Loscher, W. (2015). The organic anion transport inhibitor probenecid increases brain concentrations of the NKCC1 inhibitor bumetanide. *Eur J Pharmacol, 746*, 167-173.
Tolonen, M., Palva, J. M., Andersson, S., Vanhatalo, S. (2007). Development of the spontaneous activity transients and ongoing cortical activity in human preterm babies. *Neuroscience, 145*(3), 997-1006.
Topfer, M., Tollner, K., Brandt, C., Twele, F., Broer, S., Loscher, W. (2014). Consequences of inhibition of bumetanide metabolism in rodents on brain penetration and effects of bumetanide in chronic models of epilepsy. *Eur J Neurosci, 39*(4), 673-687.
Tropea, D., Giacometti, E., Wilson, N. R., Beard, C., McCurry, C., Fu, D. D., Flannery, R., Jaenisch, R., Sur, M. (2009). Partial reversal of Rett Syndrome-like symptoms in MeCP2 mutant mice. *Proc Natl Acad Sci U S A, 106*(6), 2029-2034.
Tyzio, R., Cossart, R., Khalilov, I., Minlebaev, M., Hubner, C. A., Represa, A., Ben-Ari, Y., Khazipov, R. (2006). Maternal oxytocin triggers a transient inhibitory switch in GABA signaling in the fetal brain during delivery. *Science, 314*(5806), 1788-1792.
Tyzio, R., Nardou, R., Ferrari, D. C., Tsintsadze, T., Shahrokhi, A., Eftekhari, S., Khalilov, I., Tsintsadze, V., Brouchoud, C., Chazal, G., Lemonnier, E., Lozovaya, N., Burnashev, N., Ben-Ari, Y. (2014). Oxytocin-mediated GABA inhibition during delivery attenuates autism pathogenesis in rodent offspring. *Science, 343*(6171), 675-679.

Uyanik, G., Elcioglu, N., Penzien, J., Gross, C., Yilmaz, Y., Olmez, A., Demir, E., Wahl, D., Scheglmann, K., Winner, B., Bogdahn, U., Topaloglu, H., Hehr, U., Winkler, J. (2006). Novel truncating and missense mutations of the KCC3 gene associated with Andermann syndrome. *Neurology, 66*(7), 1044-1048.
Valencia-de Ita, S., Lawand, N. B., Lin, Q., Castaneda-Hernandez, G., Willis, W. D. (2006). Role of the Na+-K+-2Cl- cotransporter in the development of capsaicin-induced neurogenic inflammation. *J Neurophysiol, 95*(6), 3553-3561.
van Slegtenhorst, M., de Hoogt, R., Hermans, C., Nellist, M., Janssen, B., Verhoef, S., Lindhout, D., van den Ouweland, A., Halley, D., Young, J., Burley, M., Jeremiah, S., Woodward, K., Nahmias, J., Fox, M., Ekong, R., Osborne, J., Wolfe, J., Povey, S., Snell, R. G., Cheadle, J. P., Jones, A. C., Tachataki, M., Ravine, D., Sampson, J. R., Reeve, M. P., Richardson, P., Wilmer, F., Munro, C., Hawkins, T. L., Sepp, T., Ali, J. B., Ward, S., Green, A. J., Yates, J. R., Kwiatkowska, J., Henske, E. P., Short, M. P., Haines, J. H., Jozwiak, S., Kwiatkowski, D. J. (1997). Identification of the tuberous sclerosis gene TSC1 on chromosome 9q34. *Science, 277*(5327), 805-808.
Verkman, A. S., Sellers, M. C., Chao, A. C., Leung, T., Ketcham, R. (1989). Synthesis and characterization of improved chloride-sensitive fluorescent indicators for biological applications. *Anal Biochem, 178*(2), 355-361.
Versacci, P., Di Carlo, D., Digilio, M. C., Marino, B. (2018). Cardiovascular disease in Down syndrome. *Curr Opin Pediatr, 30*(5), 616-622.
Vicari, S., Pontillo, M., Armando, M. (2013). Neurodevelopmental and psychiatric issues in Down's syndrome: assessment and intervention. *Psychiatr Genet, 23*(3), 95-107.
Walcott, B. P., Kahle, K. T., Simard, J. M. (2012). Novel treatment targets for cerebral edema. *Neurotherapeutics, 9*(1), 65-72.
Wallace, B. K., Foroutan, S., O'Donnell, M. E. (2011). Ischemia-induced stimulation of Na-K-Cl cotransport in cerebral microvascular endothelial cells involves AMP kinase. *Am J Physiol Cell Physiol, 301*(2), C316-326.
Wallace, B. K., Jelks, K. A., O'Donnell, M. E. (2012). Ischemia-induced stimulation of cerebral microvascular endothelial cell Na-K-Cl cotransport involves p38 and JNK MAP kinases. *Am J Physiol Cell Physiol, 302*(3), C505-517.
Wang, C., Shimizu-Okabe, C., Watanabe, K., Okabe, A., Matsuzaki, H., Ogawa, T., Mori, N., Fukuda, A., Sato, K. (2002). Developmental changes in KCC1, KCC2, and NKCC1 mRNA expressions in the rat brain. *Brain Res Dev Brain Res, 139*(1), 59-66.
Wang, D. D., Kriegstein, A. R. (2008). GABA regulates excitatory synapse formation in the neocortex via NMDA receptor activation. *J Neurosci, 28*(21), 5547-5558.
Wang, D. D., Kriegstein, A. R. (2011). Blocking early GABA depolarization with bumetanide results in permanent alterations in cortical circuits and sensorimotor gating deficits. *Cereb Cortex, 21*(3), 574-587.
Wang, F., Wang, X., Shapiro, L. A., Cotrina, M. L., Liu, W., Wang, E. W., Gu, S., Wang, W., He, X., Nedergaard, M., Huang, J. H. (2017). NKCC1 up-regulation contributes to early post-traumatic seizures and increased post-traumatic seizure susceptibility. *Brain Struct Funct, 222*(3), 1543-1556.
Wang, S., Zhang, X. Q., Song, C. G., Xiao, T., Zhao, M., Zhu, G., Zhao, C. S. (2015). In vivo effects of bumetanide at brain concentrations incompatible with NKCC1 inhibition on newborn DGC structure and spontaneous EEG seizures following hypoxia-induced neonatal seizures. *Neuroscience, 286*, 203-215.
Ward, A., Heel, R. C. (1984). Bumetanide. A review of its pharmacodynamic and pharmacokinetic properties and therapeutic use. *Drugs, 28*(5), 426-464.
Watanabe, M., Fukuda, A. (2015). Development and regulation of chloride homeostasis in the central nervous system. *Front Cell Neurosci, 9*, 371.
Watts, S. D., Suchland, K. L., Amara, S. G., Ingram, S. L. (2012). A sensitive membrane-targeted biosensor for monitoring changes in intracellular chloride in neuronal processes. *PLoS One, 7*(4), e35373.
Wei, B., Kumada, T., Furukawa, T., Inoue, K., Watanabe, M., Sato, K., Fukuda, A. (2013). Pre- and post-synaptic switches of GABA actions associated with Cl- homeostatic changes are induced in the spinal nucleus of the trigeminal nerve in a rat model of trigeminal neuropathic pain. *Neuroscience, 228*, 334-348.
Westmark, C. J., Westmark, P. R., Malter, J. S. (2010). Alzheimer's disease and Down syndrome rodent models exhibit audiogenic seizures. *J Alzheimers Dis, 20*(4), 1009-1013.
Wong, R. O. (1999). Retinal waves and visual system development. *Annu Rev Neurosci, 22*, 29-47.
Woo, N. S., Lu, J., England, R., McClellan, R., Dufour, S., Mount, D. B., Deutch, A. Y., Lovinger, D. M., Delpire, E. (2002). Hyperexcitability and epilepsy associated with disruption of the mouse neuronal-specific K-Cl cotransporter gene. *Hippocampus, 12*(2), 258-268.
Woolley, J. D., Chuang, B., Fussell, C., Scherer, S., Biagianti, B., Fulford, D., Mathalon, D. H., Vinogradov, S. (2017). Intranasal oxytocin increases facial expressivity, but not ratings of trustworthiness, in patients with schizophrenia and healthy controls. *Psychol Med, 47*(7), 1311-1322.
Woolley, J. D., Chuang, B., Lam, O., Lai, W., O'Donovan, A., Rankin, K. P., Mathalon, D. H., Vinogradov, S. (2014). Oxytocin administration enhances controlled social cognition in patients with schizophrenia. *Psychoneuroendocrinology, 47*, 116-125.
Wu, H., Che, X., Tang, J., Ma, F., Pan, K., Zhao, M., Shao, A., Wu, Q., Zhang, J., Hong, Y. (2016). The K(+)-Cl(-) Cotransporter KCC2 and Chloride Homeostasis: Potential Therapeutic Target in Acute Central Nervous System Injury. *Mol Neurobiol, 53*(4), 2141-2151.
Wu, H., Shao, A., Zhao, M., Chen, S., Yu, J., Zhou, J., Liang, F., Shi, L., Dixon, B. J., Wang, Z., Ling, C., Hong, Y., Zhang, J. (2016). Melatonin attenuates neuronal apoptosis through up-regulation of K(+) -Cl(-) cotransporter KCC2 expression following traumatic brain injury in rats. *J Pineal Res, 61*(2), 241-250.
Xu, W., Mu, X., Wang, H., Song, C., Ma, W., Jolkkonen, J., Zhao, C. (2017). Chloride Co-transporter NKCC1 Inhibitor Bumetanide Enhances Neurogenesis and Behavioral Recovery in Rats After Experimental Stroke. *Mol Neurobiol, 54*(4), 2406-2414.
Yan, Y., Dempsey, R. J., Flemmer, A., Forbush, B., Sun, D. (2003). Inhibition of Na(+)-K(+)-Cl(-) cotransporter during focal cerebral ischemia decreases edema and neuronal damage. *Brain Res, 961*(1), 22-31.
Yan, Y., Dempsey, R. J., Sun, D. (2001). Na+-K+-Cl- cotransporter in rat focal cerebral ischemia. *J Cereb Blood Flow Metab, 21*(6), 711-721.

Yang, S. S., Huang, C. L., Chen, H. E., Tung, C. S., Shih, H. P., Liu, Y. P. (2015). Effects of SPAK knockout on sensorimotor gating, novelty exploration, and brain area-dependent expressions of NKCC1 and KCC2 in a mouse model of schizophrenia. *Prog Neuropsychopharmacol Biol Psychiatry, 61*, 30-36.
Young, S. Z., Taylor, M. M., Wu, S., Ikeda-Matsuo, Y., Kubera, C., Bordey, A. (2012). NKCC1 knockdown decreases neuron production through GABA(A)-regulated neural progenitor proliferation and delays dendrite development. *J Neurosci, 32*(39), 13630-13638.
Yuen, N., Anderson, S. E., Glaser, N., Tancredi, D. J., O'Donnell, M. E. (2008). Cerebral blood flow and cerebral edema in rats with diabetic ketoacidosis. *Diabetes, 57*(10), 2588-2594.
Yuen, N., Lam, T. I., Wallace, B. K., Klug, N. R., Anderson, S. E., O'Donnell, M. E. (2014). Ischemic factor-induced increases in cerebral microvascular endothelial cell Na/H exchange activity and abundance: evidence for involvement of ERK1/2 MAP kinase. *Am J Physiol Cell Physiol, 306*(10), C931-942.
Zeidler, S., de Boer, H., Hukema, R. K., Willemsen, R. (2017). Combination Therapy in Fragile X Syndrome; Possibilities and Pitfalls Illustrated by Targeting the mGluR5 and GABA Pathway Simultaneously. *Front Mol Neurosci, 10*, 368.
Zhang, H., Mu, L., Wang, D., Xia, D., Salmon, A., Liu, Q., Wong-Riley, M. T. T. (2018). Uncovering a critical period of synaptic imbalance during postnatal development of the rat visual cortex: role of brain-derived neurotrophic factor. *J Physiol*.
Zhang, J., Pu, H., Zhang, H., Wei, Z., Jiang, X., Xu, M., Zhang, L., Zhang, W., Liu, J., Meng, H., Stetler, R. A., Sun, D., Chen, J., Gao, Y., Chen, L. (2017). Inhibition of Na(+)-K(+)-2Cl(-) cotransporter attenuates blood-brain-barrier disruption in a mouse model of traumatic brain injury. *Neurochem Int, 111*, 23-31.
Zhang, J., Xu, C., Puentes, D. L., Seubert, C. N., Gravenstein, N., Martynyuk, A. E. (2016). Role of Steroids in Hyperexcitatory Adverse and Anesthetic Effects of Sevoflurane in Neonatal Rats. *Neuroendocrinology, 103*(5), 440-451.
Zhang, M., Cui, Z., Cui, H., Cao, Y., Zhong, C., Wang, Y. (2016). Astaxanthin alleviates cerebral edema by modulating NKCC1 and AQP4 expression after traumatic brain injury in mice. *BMC Neurosci, 17*(1), 60.
Zhang, M., Cui, Z., Cui, H., Wang, Y., Zhong, C. (2017). Astaxanthin protects astrocytes against trauma-induced apoptosis through inhibition of NKCC1 expression via the NF-kappaB signaling pathway. *BMC Neurosci, 18*(1), 42.
Zhang, W., Liu, L. Y., Xu, T. L. (2008). Reduced potassium-chloride co-transporter expression in spinal cord dorsal horn neurons contributes to inflammatory pain hypersensitivity in rats. *Neuroscience, 152*(2), 502-510.

Appendix I

In vivo methods for acute modulation of gene expression in the central nervous system.

Andrzej W. Cwetsch*, Bruno Pinto*, Annalisa Savardi*, Laura Cancedda.

***Equal contribution.**

Published in final edited form as:
Prog Neurobiol. 2018 September ; 168: 69–85. doi:10.1016/j.pneurobio.2018.04.008.

In vivo methods for acute modulation of gene expression in the central nervous system

Andrzej W. Cwetsch[#a,b], **Bruno Pinto**[#a,c], **Annalisa Savardi**[#a,b], and **Laura Cancedda**[a,d,*]

[a]Local Micro-environment and Brain Development Laboratory, Istituto Italiano di Tecnologia, via Morego, 30, 16163 Genova, Italy

[b]Università degli Studi di Genova, Via Balbi, 5, 16126 Genova, Italy

[c]Bio@SNS, Scuola Normale Superiore, Piazza dei Cavalieri 7, 56126, Pisa, Italy

[d]DulbeccoTelethon Institute, Italy

[#] These authors contributed equally to this work.

Abstract

Accurate and timely expression of specific genes guarantees the healthy development and function of the brain. Indeed, variations in the correct amount or timing of gene expression lead to improper development and/or pathological conditions. Almost forty years after the first successful gene transfection in *in vitro* cell cultures, it is currently possible to regulate gene expression in an area-specific manner at any step of central nervous system development and in adulthood in experimental animals *in vivo*, even overcoming the very poor accessibility of the brain. Here, we will review the diverse approaches for acute gene transfer *in vivo*, highlighting their advantages and disadvantages with respect to the efficiency and specificity of transfection as well as to brain accessibility. In particular, we will present well-established chemical, physical and virus-based approaches suitable for different animal models, pointing out their current and future possible applications in basic and translational research as well as in gene therapy.

Keywords

In vivo genetic manipulations; Nanoparticles; Polymers; Electroporation; Sonoporation; Viruses

1 Introduction

Proper development of the central nervous system (CNS) determines its function and consequent behaviors. Accordingly, numerous gene alterations during development lead to brain disorders characterized by a variety of abnormal behaviors, often depending on which brain area is mostly affected. On the other hand, gene alterations during adulthood may also lead to a variety of brain-related diseases and neurodegenerative disorders that vary in their symptoms, depending on the affected brain areas. This complexity highlights the need for

[*]Corresponding author. laura.cancedda@iit.it (L. Cancedda).

Europe PMC Funders Author Manuscripts

temporal and spatial regulation of specific genes for proper brain function. Accordingly, the development of reliable techniques for gene transfection *in vivo* has recently attracted the attention of an increasing number of researchers as a means to study and understand the roles of the diverse genes underlying the basic mechanisms of CNS development and function (basic research) and to study genes involved in CNS disorders to find new possible treatments (translational research). In particular, in recent years, basic research has benefited from new tools for gene editing (*e.g.*, CRISPR-Cas9 technology; Ahmad et al., 2018) and neuronal-activity modulation (optogenetics and chemogenetics; Dobrzanski and Kossut, 2017; Towne and Thompson, 2016), which both need to be coupled to a nucleic acid delivery system. For translational research, a fast-growing field of study focuses on the possibility of treating CNS disorders by manipulating gene expression (gene therapy) rather than by classical pharmacology, which has proven highly ineffective in the last 10 years (Gribkoff and Kaczmarek, 2017). Thus, regardless of the final application, the development of novel methods for modulating gene expression *in vivo* has acquired increasing importance in recent years. This modulation can be achieved either by the generation of genetically modified animals or by acute procedures for gene expression modulation. Here, we will only review the latter.

Generally, an acute modulation of gene expression requires a transfection or transduction process (*i.e.*, a procedure that introduces foreign nucleic acids, such as DNA/RNA, into a cell) to produce genetically modified cells or organisms by nonviral or viral methods, respectively. Indeed, many molecules, such as nucleic acids and certain drugs, are not able to diffuse through the lipophilic cell membrane due to their physicochemical properties (*e.g.*, hydrophilicity, charge) and/or size. Thus, the support of specific carriers or chemical/physical stimulation is often necessary to increase the efficiency of the transfection process.

Although highly efficient, acute introduction of DNA into mammalian cells *in vitro* was achieved a long time ago (Graham and van der Eb, 1973), for the last four decades, scientists have struggled to increase the efficiency of this process *in vivo* (Crystal, 2014). For example, circulating nucleic acids for transfection have a very short half-life *in vivo* because they are degraded by circulating nucleases in the blood. Moreover, targeting specific organs and cell types at discrete times is generally challenging *in vivo* and is particularly difficult in the case of the brain for a number of reasons. First, the brain is an isolated, inaccessible environment due to the presence of the skull and the blood-brain barrier (BBB), which separates circulating blood from the brain's extracellular fluid. Second, the brain contains several different areas that are each characterized by specific functions, rendering area-specific transfection crucial in this organ. Third, the CNS contains hundreds of billions of neuronal and glial cells characterized by high diversity (*e.g.*, even among neurons, there is a wide variety of diverse types with diverse functions). Finally, neurons are postmitotic cells that do not divide, requiring a cell cycle-independent introduction of genetic material.

Since almost ninety-five percent of the animals used in research are mice and rats (Badyal and Desai, 2014), we will focus this review on rodents. For a long time, the dominant approach for acute gene transfer *in vivo* in rodents was the design of different viral vectors with increasingly higher efficiency of transfection and tissue specificity (see viral methods below). Nevertheless, due to limitations related to the safety of viral gene transfer, many

physical strategies have also been adopted, such as electroporation and sonoporation (see physical methods below). However, physical methods require strong conditions (*e.g.*, strong electric field or ultrasound) for efficient transfection, and thus a range of synthetic carriers for nucleic acids suited for chemical transfection have also been created (see chemical methods below; Yin et al., 2014). In recent years, different methods have also been combined (*e.g.*, physical and chemical methods or viruses and physical methods) to try to overcome the shortcomings of one method *vs* the other while taking advantage of the positive features of both.

In this review, we describe the currently available methods for the delivery of nucleic acids to the CNS *in vivo*. First, we focus on chemical methods, which include a wide selection of nucleic acid carriers that allow crossing of the cell membrane. Second, we describe physical methods, which take advantage of physical forces to increase membrane permeability and possibly direct nucleic acids to the desired location. Third, we address viral-based techniques, which explore the intrinsic transfection ability of viruses. Interestingly, all of the described techniques are very different, but they each present some level of overlap, creating a great portfolio to choose from when designing diverse experiments with gene transfer *in vivo*. Here, we will note the advantages and disadvantages of each described method and will indicate their best-suited applications.

2 Chemical methods for transfection

Chemical methods of transfection are a set of techniques that rely on external carriers characterized by specific chemical properties that are essential for transfection of the exogenous nucleic acids of interest (Table 1). In particular, chemical carriers are prepared to favor the formation of complexes with the nucleic acids and internalization by endocytosis in the target cells. There, the genetic material is released into the cytoplasm through endosomal escape and subsequently enters the nucleus for transcription into messenger RNA (mRNA), followed by translation into functional proteins in the cytoplasm (Fig. 1). Chemical methods often have good gene-packaging capacity and low immunogenicity and toxicity, and they are relatively safe for the operator (Zhi et al., 2018). Nevertheless, most chemical methods have low efficiency, and they still rely on invasive methods of administration for *in vivo* applications (*e.g.*, intrathecal/intraventricular injections). Only recently, the rapid development of materials science and nanoscience has allowed the construction of more efficient chemical vectors for *in vivo* transfection; these vectors are useful for not only basic research but also the biomedical field (Glover et al., 2005; Lu and Jiang, 2017; Ramamoorth and Narvekar, 2015; Yin et al., 2014). Here, we will focus on three main groups of chemicals that are often used as vectors.

2.1 Lipids

The use of lipid carriers for transfection (*i.e.*, lipofection) for *in vitro* cell delivery has been widespread since the 1980s (Fraley et al., 1980; Lu et al., 1989). Cationic lipids – the most commonly used lipids – are synthetic lipids with a positively charged hydrophilic domain connected by a linker to a long lipophilic tail. During transfection, the negatively charged phosphate on the backbone of the nucleic acids interacts with the hydrophilic domain on the

lipid, creating a structure called *lipoplex* (2–200 nm in diameter; (Higuchi et al., 2006; Inoh et al., 2017; Ramamoorth and Narvekar, 2015; Ross and Hui et al., 1999)). Once the lipoplex reaches the cell membrane, it is internalized by endocytosis, and the genetic material is then released from the endosomes inside the cell (Nayerossadat et al., 2012; Fig. 1). Although the highly positive charge on the surface of the lipids protects the genetic material from cleavage by circulating endonucleases (Ramamoorth and Narvekar, 2015), lipid-based vectors still suffer from a short half-life *in vivo* because. This is due to the rapid degradation of lipid particles by the reticuloendothelial system, which is composed of phagocytic cells located in connective tissues (Nayerossadat et al., 2012; Petschauer et al., 2015; Song et al., 2014). To overcome this issue, the DNA and cationic lipid mixture is often supplemented with so-called helper lipids (the most common being polyethylene glycol (PEG) and 1,2-dioleoyl-phosphatidyl-ethanolamine (DOPE)). These are neutral lipids that increase the lipoplex's stability, thus increasing its serum half-life. Moreover, the addition of helper lipids also increases the fusion between the lipid particle and the cell membrane and facilitates the movement of genetic material between the endosomes and the cell nucleus (Hassani et al., 2005; Nayerossadat et al., 2012; Yin et al., 2014; Zhi et al., 2018). Finally, depending on the composition of the cationic lipid mixture and the concentration of the genetic material, lipoplexes may assume different tertiary structures that may favor transfection efficiency. This structural variation is mainly due to different charge distributions on their surface and different areas of interaction with the cell. For example, the hexagonal phases of a lipoplex can spontaneously release the DNA content when these lipoplexes are in contact with an anionic vesicle, whereas a multilamellar vesicular structure (where the genetic material is sandwiched between lipid multilayers) tends not to release its contents. Interestingly, the transition from multilamellar to hexagonal structures is favored by the addition of DOPE to the lipid-DNA mixtures (Dan, 2015; Ma et al., 2007). Due to all these practices that increase transfection efficiency, lipids have proven to be efficient *in vivo* for gene transfection by direct injection in the ventricle or brain of mice (Hassani et al., 2005; Roessler and Davidson et al., 1994). Moreover, lipids have been used as a gene-delivery method for the treatment of glioblastomas by intratumoral injection (Cikankowitz et al., 2017; Lagarce and Passirani, 2016; Pulkkanen and Yla-Herttuala, 2005).

Another structural arrangement that may occur among cationic lipids is a *nanoemulsion.* A lipid nanoemulsion (LNE) is a dispersion of nanoparticles of lipids (100–400 nm in diameter) in a liquid phase that is obtained *in vitro* by the addition of a surfactant agent to prevent the lipids from coalescing into a macroscopic phase. The main advantages of LNEs include easy processing, low costs and easy scale up to large-scale production (Liu and Yu et al., 2010; Ramamoorth and Narvekar, 2015). LNEs have been successfully used *in vitro,* showing a higher efficiency than liposomes (Liu and Yu et al., 2010). The usage of nanoemulsions *in vivo* is becoming more popular due to their low toxicity and high stability (Ramamoorth and Narvekar, 2015). For example, successful delivery of tumor necrosis factor alpha (TNF-α) small interfering RNA (siRNA) to treat lipopolysaccharide (LPS)-induced neuroinflammation has been achieved in rats (Kim et al., 2010). Of note, the small dimension of the nanoparticles has also allowed intranasal delivery, a convenient way of overcoming the impermeability of the BBB and preventing the action of blood-circulating nucleases that may digest the DNA of interest (Yadav et al., 2016).

Lastly, lipid carriers have also been recently used in the form of *solid lipid nanoparticles* (SLNs). SLNs are lipid nanospheres (70–230 nm in diameter) with an outer hydrophilic shell made of a phospholipid double layer and an inner core containing long-chained lipids, generating particles that are solid and stable at body temperature (Kaur et al., 2008). In the last decade, there has been increased interest in the use of these nanoparticles for gene delivery, mainly due to their stability and biocompatibility (Pathak et al., 2017). Interestingly, SLNs were used to deliver siRNAs against c-met in a murine model of glioblastoma *via* intravenous injection *in vivo*, and the treatment showed positive outcomes (Jin et al., 2011). This result highlights the fact that SLNs are very stable and may cross the BBB, making them a very desirable vector for *in vivo* gene transfection in the brain.

2.2 Nanoparticles

With the rapid development of nanotechnology in the last decade, the use of nanoparticles as a gene-delivery tool has quickly grown. The main advantage of this kind of carrier is its high stability, great protection against circulating nucleases and low risk of toxicity (Bharali et al., 2005). Here, we will focus on the most studied nanoparticles.

2.2.1 Silica and gold nanoparticles—*Silica* (an oxide of silicon) is a very malleable material that finds applications in all realms of science and engineering. Silica nanoparticles are spheres (30 nm in diameter) that can be relatively easily made and modified during synthesis. In particular, silica nanoparticles coated with organic amino acids can interact with nucleic acids and can protect the genetic material from endonucleases. *In vitro* studies have shown that upon phagocytosis, coated silica nanoparticles can then be internalized, subsequently releasing DNA (Kneuer et al., 2000a, b). Interestingly, silica nanoparticles have also been used to study the development of newly born neurons *in vivo* by transfecting an EFGFR1-coding plasmid in the subventricular zone of adult mice with no signs of cell degeneration or systemic or brain-specific toxicity (Bharali et al., 2005; Luo and Saltzman, 2006). However, a recent report showed signs of neuroinflammation in rats following intranasal administration of silica nanoparticles (Parveen et al., 2017). Further studies on the effect of these vectors in the brain are necessary.

Gold nanoparticles are also used as vectors for gene delivery, as gold has been extensively studied in a biological context due to its very low toxicity and its capability to bind a wide array of organic molecules. In particular, some *in vitro* studies have shown that gold nanoparticles coated with organic cationic molecules are able to bind nucleic acids and are endocytosed, providing efficient delivery of the genetic material (Bishop et al., 2015; Connor et al., 2005; Ekin et al., 2014; Jensen et al., 2013; Levy et al., 2010; Peng et al., 2016). In addition, gold nanoparticles also display strong and tunable optical properties that have been tested *in vitro* (Pissuwan et al., 2011; Wijaya and Hamad-Schifferli, 2008). Interestingly, gold nanoparticles can possibly cross the BBB, as tested in not only an *in vitro* model of the BBB (Bonoiu et al., 2009) but also *in vivo* (Jensen et al., 2013). In particular, successful transfection of a siRNA against the antiapoptotic gene Bcl2 L12 was achieved in glioma cells upon systemic injection of gold nanoparticles in mice. Notably, the siRNA showed little enzymatic degradation (Jensen et al., 2013). Recently, gold nanoparticles functionalized with PEG or other long organic molecules showed much higher BBB

permeability (Escudero-Francos et al., 2017; Takeuchi et al., 2018). Remarkably, gold nanoparticles were also used to downregulate α-synuclein in a murine model of Parkinson's disease following intraperitoneal injection and had positive outcomes on anatomical landmarks of Parkinson's (Hu et al., 2018).

2.2.2 Fullerenes—Fullerenes are carbon molecules of various shapes and dimensions: spherical fullerenes (SFs) are called Buckminster fullerenes, whereas cylindrical fullerenes with a hollow core are called carbon nanotubes (CNTs). The incredible properties of fullerenes, such as high thermal and electrical conductivity, great strength, and rigidity, put these molecules at the forefront of the fast-developing nanoengineering industry (Yang et al., 2006). Moreover, *SF*s can be functionalized with cationic charges and thus can stably condense double-stranded DNA into globules (< 100 nm in diameter), which are protective against intracellular and circulating nucleases. Nevertheless, the only known *in vivo* application to date of SFs is the successful delivery of the Insulin 2 gene directly to the liver in mice with no signs of systemic toxicity (Maeda-Mamiya et al., 2010). Finally, it has been reported that SFs are able to cross the BBB, although there are no reports of their use to deliver genes to the CNS (Quick et al., 2008).

Additionally, *CNTs* have been studied as a possible vector for gene delivery. Nevertheless, applying their use to the biomedical realm has proven difficult because CNTs are poorly soluble in water. One strategy to increase their water solubility is functionalization of their surface. Indeed, CNTs functionalized with peptides and conjugated to DNA or RNA are able to successfully penetrate the cell membrane, and the DNA-functionalized CNTs are able translocate to the nucleus in *in vitro* systems (Lacerda et al., 2008; Pantarotto et al., 2004; Singh et al., 2005). Nevertheless, the *in vivo* application of CNTs is still in its early stages (Lacerda et al., 2008; Zhang et al., 2014). Notably, Khuloud et al. transfected the brain cortex in a rat model of ischemia with CNTs functionalized with siRNA for Caspase 3. This treatment successfully decreased the apoptotic cells around the lesion, with amelioration of motor deficits in the operated rats (Al-Jamal et al., 2011; Costa et al., 2016). Thus, although the application of fullerenes in biology is still in its infancy, it is clear that these carbon nanomolecules offer a new, interesting perspective on the upcoming development of gene-delivery vectors (Montellano et al., 2011)

2.3 Polymers

Polymers are macromolecules composed of repeated units. Similar to lipoplexes, the polymers used for gene delivery have a positively charged surface that interacts with the negatively charged backbone of nucleic acids to form complexes called polyplexes. Among the polymer materials used for transfection, *polyethylenimine* (PEI) is one of the most effective vectors *in vitro* and *in vivo* (Pack et al., 2005). PEI is a synthetic, water-soluble polymer (0.8 −1000 kDa in molecular weight), and its structural complexity can vary from linear to highly branched (Ewe et al., 2016; Ramamoorth and Narvekar, 2015). PEIs are internalized through phagocytosis by cells and can avoid endosome digestion/degradation *via* a proton-sponge effect. Due to their highly positive charge (derived from the large number of partially protonated amino groups that they possess), PEIs can stop the natural acidification of the endosome, generating strong osmotic imbalances, ultimately causing

endosome rupture and release of the polymer and the conjugated genetic material into the cytoplasm. Moreover, the highly positive charge acts as a protective factor against the action of cytoplasmatic nucleases (Ewe et al., 2016). Interestingly, many studies showed promising prospects for the use of PEI *in vivo*. For example, in a classic study, PEI-based vectors were used to successfully and safely deliver luciferase DNA to the brain through intracortical and intrahippocampal injections with no animal morbidity (Abdallah et al., 1996). Since then, PEI-based vectors have been used to deliver genetic material to different CNS regions, such as the spinal cord (Shi et al., 2003; Shimamura et al., 2004), the cortex in a murine model of ischemia (Oh et al., 2017) and stem cells located in the subventricular zone (Lemkine et al., 2002). The delivery occurred by direct brain injection since PEI-based vectors were believed not to cross the BBB (Lungwitz et al., 2005). Recently, a PEI-based vector was used to successfully downregulate α-synuclein using a specific siRNA in a rat model of Parkinson's disease after one single intraventricular injection (Helmschrodt et al., 2017).

To overcome the potential low BBB permeability, PEI was linked to a peptide from the rabies virus (RVG), and this method was used to successfully deliver microRNA to the brain *in vivo* following tail injection (Hwang et al., 2011). Moreover, PEI functionalized with PEG was used to deliver a plasmid coding the gene CD200 in a mouse model of multiple sclerosis (CD200 shows decreased expression in this condition). Notably, the PEI-based carrier functionalized with PEG was able to cross the BBB (Nouri et al., 2017). Remarkably, the transfection of hypoglossal motor neurons was achieved by retrograde axonal transport, which followed the injection of PEI complexed with DNA into the tongue of an experimental rat (Wang et al., 2001).

Despite the abovementioned successes, further use of PEI for *in vivo* transfection has been hindered by the relatively high toxicity of this polymer and its low rate of uptake by living cells, leading to low transfection efficiency. Thus, in the past few years, attention has turned to less toxic polymers, such as *chitosans*. Chitosans are natural polymers made of randomly distributed β-(1-4)-linked D-glucosamine and N-acetyl-D-glucosamine and are considered very attractive vectors for gene delivery *in vivo*. Indeed, chitosans are nontoxic at all concentrations and can be efficiently functionalized (Duceppe and Tabrizian, 2010; Ramamoorth and Narvekar, 2015). For example, PEGylated chitosan polymers were used to deliver siRNA against Galectine-1 and EGFR, two genes known to increase the resistance of glioblastoma cells to treatment with temozolomide. The delivery, which was performed by intratumoral injection, resulted in an increased survival rate of the animals (Danhier et al., 2015). Although chitosan-based polymers cannot readily cross the BBB, this issue was overcome by extensively modifying the chitosan structure. In particular, chitosans were first trimethylated, generating a trimethylated chitosan (TMC), which increased the solubility and siRNA binding to the polymer. Subsequently, PEG was conjugated to TMC. Similar to the reports for lipid-based delivery methods, the addition of PEG increased the biocompatibility and serum stability of the construct. Notably, upon intravenous administration, the specific delivery of Cy5.5-siRNA (a fluorescent probe used to visualize RNA) to the brain *in vivo* was obtained by adding a fragment derived from a rabies virus glycoprotein to PEG-modified TMC (Gao et al., 2014). Remarkably, chitosan-based vectors were used to transfect HIV-infected astrocytes with siRNA against genes necessary for viral replication, successfully halting the HIV infection. In this study, the chitosan nanoparticles were

Europe PMC Funders Author Manuscripts

conjugated to antibodies that could bind to the transferrin receptor in the BBB strongly, increasing the permeability of the brain to the vectors (Gu et al., 2017).

Another class of polymers is *dendrimers*, highly branched synthetic polymers that have been growing in popularity in biomedical research. This interest is mainly due to their well-defined structure and high density of easily modifiable functional groups (Hu et al., 2016). Topologically, dendrimers are composed of a core, and the branching is organized around this core, forming a spherical structure that is usually positively charged with modifiable functional groups on the surface. Due to their high density of positive charges, dendrimers escape the endosome through the "proton sponge mechanism", similar to PEI-based polymers (Hu et al., 2016). Among the large array of dendrimers, the most commonly used and the best-characterized one is polyamidoamine (PAMAM; (Hu et al., 2016; Pack et al., 2005)). PAMAM has been extensively used *in vitro* due to its low cytotoxicity (Eichman et al., 2000). To increase gene transfer efficiency and biocompatibility, many functionalizations of PAMAM have been performed; these functionalizations include the substitution of positive charges with arginine groups (Choi et al., 2004), PEG (Luo and Saltzman, 2006; Wang et al., 2009), and pyridine/histidine (Hashemi et al., 2016) and the addition of hydrophobic chains, including lauroyl (Santos et al., 2010). Nevertheless, as a positively charged hydrophilic molecule, PAMAM cannot cross the BBB *in vivo*. To circumvent this problem, PAMAM was functionalized with PEG and SRL, a small, artificially generated peptide, and was able to cross the BBB. After internalization by phagocytosis and interaction with the low-density lipoprotein receptor-related protein (LRP) on the BBB, PAMAMs functionalized with SRL were able to efficiently transfect neurons *in vivo* with a plasmid DNA coding EGFP following their intravenous injection in the tail of mice (Zarebkohan et al., 2015). Similarly, different peptides that present high brain penetration, such as angiopep-2 (Ke et al., 2009), lactoferrin (Huang et al., 2008) and transferrin (Huang et al., 2007), were used to transfect brain cells *in vivo*. Thus, due to its possible functionalizations and increased BBB permeation, PAMAM potentially has great promise in applications as a gene-delivery vector *in vivo*.

3 Physical methods for transfection

Physical methods are a collection of nonviral techniques for cell transfection that rely on physical stimulation to deliver and direct genetic material inside the living cell (Table 2). Physical methods promote reversible alterations in the cell plasma membrane or endocytosis to allow the direct passage of the molecules of interest into the cell, either alone or with the support of chemical carriers, as described above (Fig. 2). Physical stimulations can, at least in part, overcome many of the side effects linked to biochemical or viral techniques. In particular, the lack of toxicity, the lack of limitations on the length of the coding sequence, and the low costs are among the main advantages. Physical methods have outstanding experimental value in basic brain research. On the other hand, their potential translational application in gene therapy is heavily hampered by the invasiveness of their procedures (*e.g.*, the application of strong electric fields and intraventricular injections) and their low efficiency when DNA delivery is performed systemically (*e.g.*, reduced brain accessibility through the BBB).

Europe PMC Funders Author Manuscripts

The first successful *in vitro* gene transfer supported by physical stimulation was performed in 1980 with transfers into mouse glioma cells by electroporation. The same approach was used for the first *in vivo* transfection in skin cells of mice (Titomirov et al., 1991). Over the years, other physical methods were proposed for *in vivo* gene transfer, including magnet-assisted transfection (Mah et al., 2002b; Scherer et al., 2002) and ultrasound application (Sheyn et al., 2008).

3.1 Electroporation

The electroporation technique was already used *in vitro* in the 1980s (Neumann et al., 1982; Potrykus et al., 1985; Potter, 1988) as an acute, quick, easy, highly efficient, low cost and mostly nontoxic procedure to transfect bacteria and most cell types and to create transgenic plants. Electroporation enables the transfection of large, highly charged molecules that cannot passively diffuse across the lipophilic cell membrane by creating temporary water-filled holes in the membrane (20–120 nm in diameter; (Chang and Reese et al., 1990)) through the application of a series of electric-field pulses. Moreover, application of the electric field also directs the charged molecules for transfection towards the anode side, thus driving them in the desired direction towards the area where the cells of interest are located. Conveniently, once the exposure to the electric pulse is completed, the cell membrane reorganizes by closing the temporary hydrophilic pores and returning to its physiological structure, which traps the exogenous material inside the cell. Recently, the electroporation technique has evolved into diverse applications *in vivo (in* and *ex ovo, in* and *ex utero*, as well as postnatal electroporation) with one of the main advantages being the fast onset of expression of the protein encoded by the transfected DNA. In general, all the *in vivo* electroporation methods for the CNS share the same concept: the DNA solution is injected into the lumen of the CNS ventricular system. Indeed, at the interface between the lumen of the ventricular system and the brain, there is a neuroepithelium where the neuronal progenitors of different brain areas are located. Thus, following exposure to an electric field applied by a multipolar electrode, negatively charged DNA is directed towards the positively charged electrode and incorporated in the specific populations of neuronal progenitor cells. Those progenitors will generate newly born neurons committed to different brain areas, where the neurons will start migrating upon birth, eventually allowing transfection of those discrete brain regions.

3.1.1 *In utero*, *exo utero* and postnatal electroporation—*In vivo* electroporation was applied as a gene transfer method in 1997 in chick embryos *in ovo* (Muramatsu et al., 1997). Just four years later, the first CNS transfections of mouse and rat embryos were performed using *in utero* and *exo utero* electroporation (Fukuchi-Shimogori and Grove et al., 2001; Saito and Nakatsuji, 2001; Tabata and Nakajima, 2001).

The *in utero* electroporation (IUE) technique is based on the direct injection of exogenous nucleic acids into the ventricular system of embryos through the uterine wall of a pregnant dam. Then, the electric field is applied to the neuronal progenitors by means of two extrauterine forceps-type electrodes placed on the sides on the embryo head. Since the injection of the nucleic acid solution occurs through the uterine walls with no major damage to the *uterus*, the pregnant dam is able to deliver the pups. This process allows both

embryonal and postnatal studies of the electroporated pups. High efficiency with the two standard forceps-type paddle electrodes has been achieved for the electroporation of pyramidal neurons in the rodent somatosensory cortex (Saito, 2006). Since then, IUE has become the gold standard for studies on cortical development *ex vivo*, both at the anatomical and functional levels (LoTurco et al., 2009; Tabata and Nakajima, 2008; Taniguchi et al., 2012). Over the years, researchers have achieved targeting of many other brain regions by simply changing the orientation of the forceps-type electrodes. Indeed, by tilting the bipolar electrode, it is possible to target the visual cortex (Cang et al., 2005; Mizuno et al., 2007; Saito and Nakatsuji, 2001), hippocampus (Conrad et al., 2010; Saito and Nakatsuji, 2001; Tomita et al., 2011), olfactory bulb (Imamura and Greer et al., 2013), ganglionic eminence (Borrell et al., 2005; Tanaka et al., 2006), thalamus (Haddad-Tovolli et al., 2013), hypothalamus (Haddad-Tovolli et al., 2013), midbrain, amygdala (Remedios et al., 2007; Soma et al., 2009) cerebellum (dal Maschio et al., 2012; Kita et al., 2013; Szczurkowska et al., 2016; Yamada et al., 2014), spinal cord (Saba et al., 2003) and brainstem (David et al., 2014), but with a highly variable degree of efficiency (dal Maschio et al., 2012; Szczurkowska et al., 2016). Recently, the addition of a third electrode to the standard electroporation configuration has enabled highly reliable bilateral transfection of the hippocampus; the prefrontal, motor and visual cortices; and the cerebellum in a single electroporation episode (dal Maschio et al., 2012; Szczurkowska et al., 2016, 2013). Notably, although transfection is confined to a specific brain region and although not all cells in that region are transfected, successful behavioral studies have been performed. For example, animals have been transfected *in utero* with DISC1 cDNA, leading to amphetamine hypersensitivity (Vomund et al., 2013), and DCX KO mice have been transfected with DCX cDNA, leading to rescued epileptic-seizure susceptibility (Manent et al., 2009). Moreover, IUE has also been used in studies on psychiatric disorders, such as schizophrenia, indicating the molecular pathways that lead to cognitive deficits (Kamiya, 2009; Taniguchi et al., 2012).

One of the possible variations of the IUE technique is *exo utero* electroporation (EUE). In this case, during surgery, embryos are removed from the *uterus*. After DNA injection and delivery of the electric field with the forceps-type electrodes, the embryos are placed back inside the abdominal cavity of the dam without stitching the uterine walls. Since EUE guarantees better accessibility to the embryos than IUE, difficult-to-reach structures, such as the rhombencephalon (Akamatsu et al., 1999), spinal cord and caudal hindbrain (Saba et al., 2003), can be transfected with higher precision. *Exo utero* electroporation is mostly used for studying prenatal stages, as development of the embryos out of the uterus does not allow vaginal delivery. However, for postnatal studies, it is possible to rescue the electroporated embryos right before birth (E18.5) by Cesarean section, followed by immediate fostering with a stranger mother. Nevertheless, this procedure carries the risk of the pup's rejection by the foster mother.

It is possible to use the same principle of IUE to transfect animal brains after birth, enabling the study of postnatal brain development. In early postnatal electroporation, DNA is delivered to the brain ventricle or to the subventricular zone using a stereotactic microinjector (Boutin et al., 2008; Chesler et al., 2008), and the animal's head is conveniently placed between the plates of the forceps-type electrodes. This process allows

transfection of the progenitors located in the lateral, septal, and dorsal walls of the lateral ventricle, resulting in the transfection of different types of olfactory bulb neurons (Boutin et al., 2008; Chesler et al., 2008; De Vry et al., 2010; Fernandez et al., 2011; Sonego et al., 2013).

Finally, in adult rodents (up to 3,5 months old), DNA can be injected into the ventricle or directly into the targeted brain area to achieve the selective transfection of specific brain regions without affecting neurodevelopment. In the case of adult electroporation, the electric pulses can be applied with the standard forceps electrode (Chesler et al., 2008; Kitamura et al., 2008), or - for more precise and region-specific electroporation - a needle-like electrode can be inserted directly in the targeted brain region after local application of the DNA solution (Tanaka et al., 2000; Zhao et al., 2005). Late postnatal electroporation has been used to target the dentate gyrus (DG; (De Vry et al., 2010)) and the CA1 region (Tanaka et al., 2000) of the hippocampus, the prefrontal cortex (Zhao et al., 2005), the barrel cortex (Kitamura et al., 2008), and the cerebellum (Kitamura et al., 2008).

3.2 Sonoporation

Sonoporation takes advantage of temporary pores created in the cell membrane by ultrasound (US) exposure. The uptake of the DNA carriers during exposure to US occurs by mechanical stress, which causes endocytosis and/or large membrane wounds that are later closed by endogenous vesicle-based repair mechanisms (Fig. 2; Escoffre et al., 2013). US pulses can be delivered on their own, but their delivery in combination with a local application of microbubbles increases the efficiency of transfection (Taniyama and Morishita, 2006). Indeed, microbubbles are gas-filled structures (1–8 μm in diameter) that can react to the ultrasound waves by sequential expansion and compression (Lentacker et al., 2014), causing their own local oscillation close to the cell membrane and increasing the permeability to exogenous material (*e.g.*, DNA). Moreover, the physicochemical composition of the microbubbles can increase their chances of binding or capturing DNA. In particular, the most commonly used microbubbles are proteins, lipids or polymers (see chemical methods above). So far, the most suitable solution for microbubbles comprises cationic lipids, which can easily bind negatively charged plasmid DNA and are easily disrupted by US.

Although sonoporation is a promising technique that is well established for *in vitro* gene transfer (Fischer et al., 2006), its *in vivo* application is hindered by the possible aversive reactions of live tissue to US exposure (*e.g.*, increased temperature and production of reactive oxygen species; Juffermans et al., 2006; Wu, 1998). In the embryonic or newborn mouse, brain ultrasound was nevertheless used to attempt transfection of plasmid DNA in combination with microbubbles, both by intraventricular injection and systemically. However, the transfection efficiency was relatively low, and 50% of the injected embryos suffered from hydrocephaly (Endoh et al., 2002). On the other hand, microbubble-enhanced ultrasound improved gene transfer to the sub-ventricular zone after intraventricular injection in adult mice *in vivo* (Tan et al., 2016).

Europe PMC Funders Author Manuscripts

3.3 Magnet-assisted transfection

Magnetism-based targeted delivery was first described almost forty years ago (Widder et al., 1978) as a means to use magnetic micro- and nanoparticles for drug delivery to the circulatory system *in vivo*. The technique takes advantage of a magnetic field to direct magnetic nanoparticles (MNPs) containing nucleic acids into the target cells. The MNPs used as carriers are mostly composed of an iron oxide (magnetic) core with an additional organic or inorganic coating (*e.g.*, arabic gum ((Zhang et al., 2009), liposomes (Linemann et al., 2013), polymers, peptides and ligands/receptors (Estelrich et al., 2015)). Coated MNPs have major advantages (Chatterjee et al., 2001; Estelrich et al., 2015). Moreover, due to their positively charged magnetic core, the binding of negatively charged molecules (*e.g.*, DNA) is a relatively fast and easy process. Upon activation of the magnetic field, MNPs are drawn towards the target cells, where they undergo endocytosis or pinocytosis, followed by nucleic-acid release, leaving the membrane composition of the target cell intact (Fig. 2).

In *in vitro* studies, magnetofection has been commonly used due to its simplicity and high efficiency (Scherer et al., 2002). The application of a magnetic field, together with MNPs, is also a promising approach for *in vivo* gene transfer due to its noninvasive nature, ability to direct DNA to the region of interest and lack of toxicity. Nevertheless, magnetofection in the CNS is still in its infancy. Indeed, in one report describing MNPs functionalized with PEI that were administered in the rat spinal cord after lumbar intrathecal injection (Song et al., 2010), the experiment was not fully successful due to the dispersion of MNPs in the cerebrospinal fluid after exposure to the magnetic field. On the other hand, highly efficient and long-term magnetofection of complexes of EYFP channelrhodopsin and MNPs for optogenetic applications in the rat visual cortex *in vivo* has also been reported upon direct brain injection (Soto-Sanchez et al., 2015).

4 Virus-mediated trasduction

Viruses are nanometric infective agents composed of a protein capsid that protects their genetic material and, in some cases, a lipid envelope derived from the host cell membrane that protects the capsid. Viruses can therefore be classified as *naked* or *enveloped* based on the absence or presence of this lipid structure, respectively. All viruses are dependent on the host cell to successfully replicate: they hijack the replication machinery of the host cell and guide it to replicate the viral genetic material. Indeed, during laboratory synthesis of viral particles for experimental applications, cells are first infected with the aim of synthetizing high numbers of new viral particles that are subsequently purified and used at a high concentration in future experiments (Farson et al., 2004). Depending on the type of virus used for the transfection during experimental applications, the genetic material can be integrated in the host DNA or can be temporarily expressed (Fig. 3, Table 3). All cells can be infected by specific viruses (Koonin et al., 2006), and it is the capsid itself or in some cases, the envelope protein sequence and shape that determines what kind of cell a virus will infect, a property called *tropism*. As the genetic material carried by a virus can be modified or substituted by a synthetic construct altogether, viruses have been widely utilized as a means to perform genetic manipulations in live cells. Interestingly, the capsid can also be

artificially modified, thus generating viruses with a desired tropism for specific cell types (Freire et al., 2015).

The use of viral vectors for gene delivery into living cells dates back to 1976 when, for the first time, a DNA segment of a bacteriophage lambda was transfected into mammalian cells using a Simian Virus 40 (SV40) vector (Goff and Berg, 1976). Since then, the use of viruses in biological and biomedical research grew exponentially, and today, viral vectors are the most powerful technique for gene delivery *in vitro* and *in vivo*. The main advantages of the use of viral vectors are their extremely high specificity towards a certain cellular type and the high efficiency of reliable transfection. On the other hand, once engineered, the viral particle has to be purified. Easy and fast purification protocols are currently available. However, the process may sometimes damage the genomic material (Kay et al., 2001). Moreover, the size of the construct is limited by the packing capacity of the capsid. Furthermore, viruses are administered *via* intrathecal or intraventricular injection, which is extremely invasive (Artegiani and Calegari et al., 2013; Kotterman et al., 2015a; Thomas et al., 2003). Finally, most viruses require several days before transduction of the genetic material, although the precise expression timing varies for each type of viruses (*e.g.*, herpes simplex peaks at 24 h following infection; adeno-associated viruses require approximately 3 weeks to peak, although the expression is already visible as soon as 24 h following administration; Penrod et al., 2015; Reimsnider et al., 2007). Unlike the other methods for gene delivery, some viral vectors can lead to viral genetic material becoming stably integrated into the host genome (*e.g.*, Herpes Simplex viruses), which makes viral vectors particularly suited for the transfection of dividing cells. On the other hand, integrated viruses may be dangerous because the integration may occur in undesirable zones of the genome, leading to harmful mutations, which hinders their usage in biomedical research (Thomas et al., 2003). Conversely, with some other viral vectors (*e.g.*, adenoviruses), the genetic material remains in the nucleus as a so-called episome. Thus, nonintegrative viruses are safer but are mostly suitable only for nondividing cells, as the nonintegrated plasmid becomes too diluted in rapidly dividing cells to give the desired level of transfection (Kotterman et al., 2015a; Thomas et al., 2003). Here, we will review the four main viral classes that have *in vivo* applications in basic and biomedical research.

4.1 Lentiviruses

Lentiviruses are enveloped viruses belonging to the class of retroviruses (viruses bearing RNA genetic material) with the unique characteristic of being able to infect nondividing cells in a long-term manner. Being in the class of viruses bearing RNA, these viruses rely on retrotranscription to integrate their genetic material in the host genome (Fig. 3). Retrotranscription involves transcribing RNA into DNA with the help of a reverse transcriptase enzyme, which is encoded by the virus genome. Although lentiviruses are efficient viral vectors used for gene delivery, they were originally derived from pathogenic agents (*i.e.*, human immunodeficiency virus, HIV). This hampers their use *in vivo*, due to the risks of eliciting strong immunogenic responses or even reconversion to the wild-type pathogenic form (Cockrell and Kafri, 2007; Mah et al., 2002a). One important step made towards the development of safe lentiviral vectors was the substitution of the envelope protein of pathogenic viruses with one derived from a different virus (most commonly,

vesicular stomatitis virus G glycoprotein, VSV-G), which cannot successfully multiply after infection of the host cell and presents a wider *tropism* (Artegiani and Calegari et al., 2013; Mah et al., 2002b). Nevertheless, lentiviruses have been successfully used for efficient gene delivery *in vivo* for a long time (Bonci et al., 2003; Li et al., 2016; Qiao et al., 2016). Indeed, an HIV-based VSV-G-pseudotyped virus was used for the first time *in vivo* in 1996 to stably transfect fully differentiated neurons and glial cells and deliver β-galactosidase to the hippocampus of adult rats for up to three months after inoculation, without any evident immunogenic reaction. The stability of the infection depended on integration of the viral genome into the host-cell genetic material (Naldini et al., 1996a, b). Other applications in the CNS followed, and lentiviral vectors injected intracranially were used to study the effect of ApoE isoforms on amyloid plaque deposition in a mouse model, allowing the determination of the isoform-specific effects of ApoE on the amyloid burden in the hippocampus (Dodart et al., 2005). Moreover, modifications of the envelope of lentiviruses allowed preferential targeting of discrete populations of cells in the CNS with high flexibility. For example, lentiviruses pseudotyped with a modified envelope displayed anti-GLAST (an astrocyte-specific protein) IgG on their surfaces and preferential astrocyte targeting *in vivo* (Fassler et al., 2013). Interestingly, due to their ability to infect fully differentiated cells, lentiviruses find widespread usage in the study and development of therapies for neurodegenerative diseases, such as Parkinson's (Azzouz et al., 2004; Bensadoun et al., 2000; Yin et al., 2017) Alzheimer's (Li et al., 2017; Parsi et al., 2015; Tan et al., 2018) and Huntington's disease (Cui et al., 2006; Schwab et al., 2017).

4.2 Adenoviruses

Adenoviruses (ADVs) are nonintegrating naked viruses that bear double-stranded DNA. ADVs can transfect dividing and nondividing cells with fairly high efficiency (Mah et al., 2002a). ADVs have been successfully used *in vitro* to target neocortical and glial cells in culture (Morelli et al., 1999; Smith-Arica et al., 2000; Southgate et al., 2008). Nevertheless, their usage *in vivo* has been challenging due to their high virulence (Thomas et al., 2003). To overcome this issue, ADVs have been extensively engineered during the last 35 years with the aim of generating nonimmunogenic vectors. The first generation of modified ADVs had their viral genome deleted, generating replication-defective ADVs; nonetheless, these ADVs still exhibited potent T-cell-related immunogenicity. These first-generation viruses showed potent toxicity to the CNS, causing the transfected cells to be phagocyted. Nevertheless, usage of these vectors still led to the successful treatment of glioma in mice (Germano et al., 2003; Immonen et al., 2004; Lentz et al., 2012). Due to their capacity to infect dividing cells, replication-defective ADVs were also used to transfect neuronal precursors in the adult mouse brain following intraventricular injections (Yoon et al., 1996). In a great leap forward, safe ADV vectors were made with the development of helper-dependent ADVs (HD-ADV; Thomas et al., 2003). The HD-ADVs lacked any viral genes; thus, another virus (the helper virus) was needed to carry the information for their replication during the laboratory preparation of viruses for infection. This development enabled the synthesis of viral vectors with the ability to carry long constructs (up to 30 kB) that almost completely lacked virulence. Nevertheless, it is virtually impossible to completely eliminate the helper virus during the laboratory purification procedure, although currently, the amount of contamination can be reduced to less than 0,1%. This is a promising achievement for future

studies and applications using HD-ADVs (Kay et al., 2001). Indeed, HD-ADV has been recently used to perform manipulations of the DNA in human pluripotent stem cells and induced pluripotent stem cells (iPS), opening up the prospect of gene manipulation of pluripotent stem cells for therapeutic applications (Mitani, 2014).

4.3 Adeno-associated viruses

Adeno-associated viruses (AAVs) are viruses strictly related to ADVs. Indeed, AAVs were first isolated in 1965 as a contaminant in the preparation of ADV (Atchison et al., 1965; Kay et al., 2001). AAVs have a single-stranded DNA (ssDNA) genome composed of two genes, one for their replication (rep) and one for their encapsulation (cap), even though AAVs cannot replicate on their own. Similar to ADVs, AAVs require a helper virus to multiply. The AAV genome remains in the nucleus of host cells as an episome, or at a lower frequency, the AAV genome stably integrates in the host genome. The natural replication deficiency of AAVs in the absence of an HV gives them a natural safety mechanism in *in vivo* applications (Kay et al., 2001; Mah et al., 2002b; Samulski and Muzyczka, 2014; Yan et al., 2005). Indeed, these viruses have never been associated with any pathology, and they are the most studied viral vectors for gene delivery *in vivo* (Mah et al., 2000). Their main drawback is their small packing capacity (not exceeding 5 kb), which can nevertheless be increased by clever molecular biology tricks (*e.g.*, dividing the expression plasmid into two vectors and reconstituting a fully functional expression cassette after concatemerization of episomes in the nucleus (Thomas et al., 2003)). So far, AAVs are the method of choice for the study of *in vivo* brain physiology, since the transfection can be stable for strikingly long times. Moreover, different serotypes of AAVs can have different tropisms for discrete cell populations (Burger et al., 2004; Lentz et al., 2012). For example, an AAV infection was stably expressed up to six months in the rat brain (Klein et al., 1999) and up to 6 years in the bone marrow of nonhuman primates (Rivera et al., 2005). Moreover, due to their neurotropism and their ability to be transported along the axon, AAV9 and AAVrh10 may be used for the development of therapeutic approaches for local interventions of axonally connected structures (Choudhury et al., 2016b). Finally, different AAV serotypes can transfect different cell types (*e.g.*, astrocytes and oligodendrocytes) in the brain *in vivo* (Foust et al., 2009; Lawlor et al., 2009). This transfection was achieved by shuffling random pieces of the *cap* gene together to generate a large variety of different *cap* proteins and later screening for specific tropism for different cell types. Indeed, gene shuffling of the heparin-binding domain (HBD) in individual hybrid capsids of various AAV serotypes (AAV-type 2/type 8/type 9 chimera) helped in the creation of the AAV-DJ-derived viral peptide library for cell-specific tropism *in vivo* in mice (Grimm et al., 2008). The effect of the HBD on viral tropism was demonstrated by transduction to diverse tissues, including the brain (Grimm et al., 2008). Notably, cap-gene shuffling was also used to develop chimeric AAVs with the remarkable ability to pass through the seizure-compromised BBB in rats after kainic acid-induced seizures (Gray et al., 2010). In addition to capsid shuffling, packaged plasmids with specific promoters can also be used to achieve the goal of cell specificity (see the discussion section for further information about promoters). Interestingly, other AAV serotypes -when administered intravenously - were unexpectedly shown to cross even an intact BBB in young and adult animals (Bourdenx et al., 2014; Duque et al., 2009; Foust and Kaspar et al., 2009;

Europe PMC Funders Author Manuscripts

Foust et al., 2009). All these findings further fuel the interest in basic and biomedical research on AAVs.

4.4 Herpes simplex viruses

The herpes simplex viruses (HSVs) are enveloped viruses bearing double-stranded DNA genetic material. Their genome is relatively large, having a length of approximately 152 kb and containing more than 80 genes. Because many of the genes are not essential for viral replication, HSVs can carry at least 30 kb of nonviral DNA suitable for experimental purposes (Kay et al., 2001). The main advantages of HSVs are their high tropism for the CNS (for an unknown reason, especially sensory neurons; Menendez and Carr, 2017) and the fact that after infection, the HSV genome mostly remains in a latent form as a stable circular episome in the nucleus of fully differentiated cells for a very long time without eliciting any immunogenic response (Lentz et al., 2012). On the other hand, their strikingly complex envelope makes the development of cell-specific HSVs very challenging, although pseudotyping of HSV with the VSV-G protein can reduce off-target transfection *in vitro* (Andersen et al., 1982). Moreover, HSVs may still cause a massive activation of the immune system by starting replication in the host cell. This activation remains one of the main concerns for the use of HSV for gene delivery *in vivo*. One way to avoid self-replication is to delete some of the viral genetic material, generating nonself-replicating viral particles, which nevertheless need to be coupled to helper viruses for their replication during preparation (Kay et al., 2001; Spaete and Frenkel, 1982). With this process, cytotoxicity was strongly reduced, and neurons in culture were stably transfected for more than three weeks (Krisky et al., 1998). Although HSVs have been widely studied *in vivo* to treat glioblastoma in rodents (Nakashima et al., 2018; Ning and Wakimoto, 2014; Wollmann et al., 2005), their application to the transduction of neurons is still limited. Nevertheless, HSVs have been already used to transfect the striatum (for up to 7 months) in a rat model of Parkinson's disease with genes necessary for the functioning of dopaminergic neurons, providing significant recovery of the phenotype (Sun et al., 2003).

5 Discussion

5.1 Challenges of *in vivo* gene delivery to the brain

The study of the CNS through acute genetic manipulations *in vivo* to understand brain function in health and disease has always been a challenging issue for scientists. First, there are technical issues related to the inaccessibility of the brain due to the presence of the skull and the BBB. Additionally, the great complexity of brain circuits (*i.e.*, the variety of neuronal and nonneuronal cell types) and network functionality (*i.e.*, the long- and short-range connectivity among different brain regions) renders it difficult to establish causal relationships between genetic manipulations and cellular/behavioral outcomes in basic research. Finally, the invasiveness of surgical procedures and viral vector safety constitute additional challenges for translational applications. The various methods for *in vivo* gene manipulations highlighted above present positives and negatives in regard to applications for basic research or translational purposes in the difficult to access brain, which we will discuss below.

Europe PMC Funders Author Manuscripts

5.1.1 CNS penetration—The first difficulty in achieving acute gene manipulations in the brain *in vivo* is the need to bypass the skull or the BBB. To this end, tremendous efforts have been made to improve brain-delivery methods or maximize vector permeability. One of the first and simplest ideas developed in the past was the injection of DNA directly into the brain area of interest. The first studies in this regard were performed in the late 1980s and early 1990s (Breakefield and Geller, 1987), when different groups performed genetic manipulations by viral injection directly into the rodent retina and brain (Davidson et al., 1993; Palella et al., 1989; Price et al., 1987). Furthermore, lipofectin-supported DNA transfection, which overcomes the electrostatic repulsion of DNA by the cell membrane, was also successfully performed by direct injection into the mouse brain (Ono et al., 1990). Subsequently, chemical polymers such as PEI were used to directly inject genetic material into the cortex, hippocampus (Abdallah et al., 1996), spinal cord (Shi et al., 2003), and SVZ (Lemkine et al., 2002) of rodents. Moreover, lipid vectors were also effectively injected in the ventricles of early postnatal mice (Hassani et al., 2005; Roessler and Davidson et al., 1994) for basic research or in rodent glioblastoma to investigate possible therapeutic approaches (Cikankowitz et al., 2017; Lagarce and Passirani, 2016; Pulkkanen and Yla-Herttuala, 2005). Currently, physical methods, such as IUE and EUE, are particularly suitable for studies of neurodevelopment, as DNA can be directly injected into the large ventricles of developing embryos and a strong electric field can be easily applied to the head of the embryos. Indeed, embryos have no bony skull, which guarantees high transfection efficiency (Saito, 2006; Szczurkowska et al., 2016). Moreover, the quick expression of transfected genetic material upon electroporation also contributes to the successful application of this technique for neurodevelopmental studies. On the other hand, for viral vectors, the main strategy used for their delivery in the brain remains the direct intraparenchymal infusion of viral particles. Indeed, ventricle injection requires a large quantity of viral material at high concentrations, which may be difficult to obtain, as well as costly. Thus, viral injection is more suitable for local transfection in the postnatal and adult brain. Moreover, unlike electroporation, which becomes difficult when the electric field needs to be delivered through the bony skull of an adult animal, small amounts of viral vectors can be delivered by direct stereotaxic injection in a specific brain region of adult animals, following a minor craniotomy. Thus, viral vectors are the technique of choice for the study of brain functionality at later postnatal ages, which is also compatible with the fact that these vectors may require days before driving efficient expression of the genetic material that they carry.

Since direct injection in the brain - especially when considered for translational applications - is still an invasive technique due to the procedure itself and the risks of possible side effects related to the surgical intervention, new strategies have been developed to bypass the BBB in recent years. In particular, lipids and polymers supplemented with helper lipids or functionalized with peptides to increase their BBB permeation were successfully used with intravenous injection. For example, dendrimers, PEI and nanoparticles have been functionalized with PEG and other organic molecules to enable them to cross the BBB (Zarebkohan et al., 2015). In addition, viral capsids have been engineered to be more BBB permeable (Choudhury et al., 2016a, c; Deverman et al., 2016; Zhang et al., 2011). Moreover, a portion of the produced AAV particles remain associated with cell membranes

(exosome-AAVs). Compared with AAVs, exosome-AAVs have a longer half-life in the blood and increased BBB permeability (Hudry et al., 2016; Maguire et al., 2012). Alternatively, nanoparticles have been conjugated to genetic material, and their small dimensions allow direct intranasal delivery; thus, this method guarantees direct brain access because it does not require BBB crossing (Yadav et al., 2016).

5.1.2 Transfection specificity in the brain—Another open issue to address when studying brain function and possibly conceiving new treatments for brain disorders is the complexity of brain networks: the ability to transfect a precise cell population among many others has always been a challenge. The possibility of directing the electric field and thus the DNA in a specific direction allowed the easy transfection of discrete populations of neuronal progenitors of specific brain areas by IUE and EUE (dal Maschio et al., 2012; Saito, 2006; Saito and Nakatsuji, 2001; Szczurkowska et al., 2016). Nevertheless, while this method is very useful for *in vivo* developmental studies, it is less suitable for studies performed in adult animals, where chemical methods or viruses are the method of choice. With these chemical or viral methods, the selection of an appropriate cell-specific promoter upstream of the gene of interest enables the transfection of discrete cell types (Murlidharan et al., 2014; Ojala et al., 2015). For this purpose, several neuron- and glial-specific promoters have been identified and tested for their ability to enable cell-specific transduction (Hashimoto et al., 1996; Miura et al., 1990; Morelli et al., 1999; Oellig and Seliger, 1990; Quinn, 1996). Nevertheless, the cell-specific promoters tend to be too large to be packaged into viral vectors, and the resulting gene expression is weaker than that driven by constitutive viral promoters (*e.g.*, CMV; Hioki et al., 2007; Shevtsova et al., 2005). Thus, novel, smaller hybrid promoters that are able to efficiently induce a strong, specific gene expression pattern have been generated (Gray et al., 2011; Hioki et al., 2007; Kugler, 2016).

5.1.3 Combinations of the diverse *in vivo* transfection methods—To try and further overcome the difficulties related to modulation of gene expression *in vivo* in the CNS in terms of brain accessibility, transfection efficiency and/or space and time specificity, coupling of the different delivery techniques has offered unquestionable advantages. For example, BBB opening by focused US was combined with systemic administration of DNA bound to nanoparticles, resulting in a noninvasive strategy for achieving safe, highly localized, robust, and sustained transgene expression in the CNS (Mead et al., 2016). Moreover, a combination of US with the intravenous administration of naked microbubbles - together with naked plasmid DNA (Shimamura et al., 2004), AAVs (Hsu et al., 2013; Wang et al., 2017), liposomal-plasmid DNA (Lin et al., 2015), liposome-shRNA-NGR complexes (Zhao et al., 2018), polyethylene glycol-modified lipid-based bubbles (Negishi et al., 2015), or folate-conjugated gene-carrying microbubbles (Fan et al., 2016) - can induce reversible openings in the BBB and can increase the transfection efficiency in rodents. Furthermore, a more efficient, brain area-specific infection was achieved by coupling adenoviral vectors with magnet-assisted transfection in the brain of rodent embryos *in utero* (Hashimoto and Hisano, 2011; Sapet et al., 2012).

5.1.4 Combinations of *in vivo* transfection methods with newly emerging techniques—The coupling of molecular biology tools, including newly emerging

techniques, with techniques for gene delivery *in vivo* also has tremendous potential. For example, to achieve a transfection that is better confined in time and space, IUE was coupled to the Cre/loxP system in the study of retinal development (Matsuda and Cepko et al., 2007), and AAV transfection was coupled to the tetracycline-controlled transcriptional activation system (tet-on/off) in the study of the structure of the neural circuits in the mouse neostriatum and primary somatosensory cortex (Sohn et al., 2017). Moreover, both viral vectors and/or IUE were successfully used to introduce optogenetic proteins, chemogenetic receptors or voltage sensors into specific cell-types, cortex layers or brain areas, allowing the study of neural circuits *in vivo* (Ghitani et al., 2015). Furthermore, CRISPR-Cas9 technology, which allows genome editing, regulation and visualization (Gilbert et al., 2013; Mali et al., 2013; Qi et al., 2013), was recently coupled to IUE to study the role of specific genes in brain development *in vivo* by knockout (Chen et al., 2015; Cheng et al., 2016; Kalebic et al., 2016; Rannals et al., 2016a, b; Shinmyo et al., 2016; Straub et al., 2014; Wang, 2018) or knock-in (Tsunekawa et al., 2016). CRISPR-Cas9 technology coupled to IUE also enabled the study of the subcellular localization of specific proteins by inserting a sequence for a fluorescent protein into their encoding gene (Mikuni et al., 2016). Moreover, CRISPR-Cas9, despite its large size, can be packaged in viral vectors for *in vivo* delivery, thus enabling robust transfection in the adult mouse brain (Chen and Goncalves, 2016; Chew et al., 2016; Ortinski et al., 2017; Schmidt and Grimm, 2015). Interestingly, to increase Cas9 editing efficiency and decrease the risks of off-target effects, different groups tested the delivery of a protein Cas9-guide RNA (gRNA) complex by nucleofection (Kim et al., 2014; Lin et al., 2014), cationic lipids (Zuris et al., 2015), lipid nanoparticles (Wang et al., 2016; Yu et al., 2016) and cell-penetrating peptides (Ramakrishna et al., 2014) in mammalian cells *in vitro*, thus opening the possibility of a new delivery strategy to be applied *in vivo*. Indeed, the protein Cas9/gRNA complex was recently coupled to IUE to study the effect of the Tbr2 knockout in mouse neocortical progenitors (Kalebic et al., 2016) and was injected in the hippocampus, dorsal striatum, primary somatosensory cortex and primary visual cortex of adult mice with a positive outcome (Staahl et al., 2017).

5.2 Specific challenges for translational research and possible therapeutic applications

Gene therapy is defined as the transfer of genetic materials to specific target cells of a patient with the final goal of preventing or rescuing a particular disease state (Mali, 2013). The main strategies for gene therapy utilized so far entail the introduction of a replacement allele into cells to compensate for the loss of function of a gene, the silencing of a dominant mutant pathological allele and the introduction of trophic factors or compensatory proteins (Choudhury et al., 2016c). The first gene delivery in the human brain was performed by stereotactic injection of retrovirus- and ADV-containing nuclear-targeted β-galactosidase cDNA in 10 patients with malignant glioma (Puumalainen et al., 1998). For the first time, this study evaluated the feasibility and safety of virus-mediated gene transfer in human glioma *in vivo*, and it showed a positive outcome (Puumalainen et al., 1998). Since then, due to the therapeutic benefits and the safety found in subsequent clinical trials, gene therapy has become a possible option for clinical intervention in some otherwise terminal or severely disabling conditions (Naldini, 2015). Indeed, in recent years, a large effort has been put into continuously improving gene-delivery methods, and currently, more than 2000 approved

Europe PMC Funders Author Manuscripts

gene-therapy clinical trials have been conducted or are ongoing worldwide (http://www.abedia.com/wiley/).

However, the vast majority of the gene-therapy clinical trials so far have addressed cancer (64,5%), with neurological diseases representing only 1.8% of the studies (http://www.abedia.com/wiley/). On the one hand, this scarcity may be because the neuropathological mechanisms underlying several neurological disorders are still poorly understood. In this respect, *in vivo* methods for gene delivery that have been discovered by emerging basic research may also hold great potential in the long run for increasing our understanding of brain pathology. On the other hand, the low number of gene-therapy clinical trials for brain disorders may be due to the low availability of safe and efficient delivery vectors that can cross the BBB or can be directly injected in the brain without major complications. Nevertheless, the increasing prevalence of some neurodevelopmental disorders (*e.g.*, autism spectrum disorders; Neggers, 2014) and of neurodegenerative disease (due to the increase in the average age of the population; Johnson, 2015), in combination with the identification of clearly causative mutations and the paucity of standard pharmacological treatments for these brain disorders, highlights the need to search for alternative therapeutic approaches, including gene therapy. Currently, AAV vectors have become the vehicle of choice for *in vivo* gene transfer in most of the clinical trials targeting the brain. Nevertheless, although some AAVs that are being currently tested in animal models can effectively cross the BBB (Choudhury et al., 2016b, c; Deverman et al., 2016; Zhang et al., 2011), so far, the AAVs used in clinical trials are less permeable. Therefore, these AAVs are commonly injected directly into the brain parenchyma, nevertheless enabling long-term, relatively safe expression (Choudhury et al., 2016c). For example, an ongoing phase I/II study is testing intraputaminal brain infusion of an AAV encoding human aromatic L-amino acid decarboxylase as a possible treatment in subjects with Parkinson's disease (http://www.abedia.com/wiley/). Interestingly, AAVs were recently engineered to be able to efficiently transduce neural stem cells (Choudhury et al., 2016b; Kotterman et al., 2015b). To avoid the risk of the surgery-related side effects of classic parenchymal injection for virus delivery, a less invasive method, such as administration into the cerebrospinal fluid *via* intracerebroventricular (ICV) or intrathecal (IT) injection, has also been proposed (Choudhury et al., 2016c). Nevertheless, these methods of application seem to be less effective in bypassing the BBB and less safe due to the activation of immunogenic responses (Choudhury et al., 2016c).

Despite the rapidly increasing usage of viruses for *in vivo* genetic manipulations, they still present drawbacks (*e.g.*, the possibility of mutagenesis following viral integration in the host genome with the risk of tumorigenesis, toxicity and immunogenicity, as well as the limited genomic capacity). Thus, considerable interest has been recently concentrated on the development of nonviral vectors (*e.g.*, lipids, nanoparticles and polymers) for translational purposes. Interestingly, some clinical trials based on the use of lipofection to treat glioblastoma are ongoing (http://www.abedia.com/wiley/), and the use of US combined with microbubbles to deliver nanoparticles carrying the tumor-suppressive miRNA-34a was recently evaluated in mice as a new possible treatment (Vega et al., 2016). Moreover, the C2-9r peptide delivering a siRNA against α-synuclein (Javed et al., 2016) and the US-mediated delivery of the GDNF plasmid (Fan et al., 2016) or of nanomicrobubbles

Europe PMC Funders Author Manuscripts

containing the factor Nrf2 (Long et al., 2017) were recently tested in rodents as a novel approach to treat Parkinson's disease.

Finally, development of the CRISPR-Cas9 tool has opened new avenues and possibilities for translational research and gene therapy. Recently, some groups have started to investigate the potential of CRISPR-Cas9 technology to recover mutations and correct monogenic disorders in both cultured and *in vivo* stem cells (Maeder and Gersbach, 2016; Prakash et al., 2016). Moreover, CRISPR-Cas9 technology has also been used to manipulate the cancer genome or epigenome for therapeutic purposes *in vivo*. These changes include loss- or gain-of-function mutations in oncogenes, tumor suppressor genes, and modulators of cellular transformation or drug response (Sanchez-Rivera and Jacks, 2015). Nevertheless, the application of CRISPR-Cas9 technology as a therapeutic approach for brain disorders has been slowed down, in part, by difficulties in delivery due to its large dimensions (Walters et al., 2015). Interestingly, recent promising results have been obtained in a Huntington mouse model by reducing the mutant Huntingtin (mHTT) gene expression through the injection of Cas9 and mHTT-gRNA packaged in an AAV vector in the striatum (Yang et al., 2017).

5.3 Concluding remarks

Starting from the first attempts to deliver DNA to the difficult-to-reach brain, much progress has been obtained in terms of the efficiency of transfection, target specificity and safety in the CNS. This issue is of great importance since the basic mechanisms of brain functions are far from being resolved and since most brain disorders are still lacking a cure. In this respect, the currently available variety of delivery methods, which can be chosen to meet different experimental needs, and the continuous effort to find new and/or more efficient and safer ways to perform gene delivery *in vivo* will possibly aid basic research on animal models and translational attempts. The coupling of different delivery systems, such as chemical, physical and viral methods, together with new technological revolutions, such as optogenetics, chemogenetics and CRISPR-Cas9 technology, will further advance the field to further broaden our understanding of the brain and address several neurological disorders with new possible treatment options.

Acknowledgments

This work was funded by the European Research Council (ERC) under the European Union's Horizon 2020 research and innovation program (725563 to LC) and by the Telethon Foundation (GGP13187 and No TCP15021).

Abbreviations

AAV	adeno-associated viruses
ADV	adenoviruses
ApoE	apolypoprotein E
BBB	blood brain barrier
cap	encapsulation
Cas9	CRISPR associated protein 9

Europe PMC Funders Author Manuscripts

cDNA	coding DNA
CMV	cytomegalovirus
CNS	central nervous system
CNT	carbon nanotubes
CRISPR	clustered regularly interspaced short palindromic repeats
DCX	doublecortin
DNA	deoxyribonucleic acid
DOPE	1,2-dioleoyl-phosphatidyl-ethanolamine
EGFP	enhanced green fluorescent protein
EUE	exo utero electroporation
EYFP	enhanced yellow fluorescent protein
gRNA	guide RNA
HBD	heparin-binding domain
HD-ADV	helper-dependent ADVs
HIV	human immunodeficiency virus
HSV	herpes simplex viruses
HV	helper virus
ICV	intracerebroventricular
iPS	induced pluripotent stem-cells
IT	intrathecal
IUE	*in utero* electroporation
LNE	lipid nanoemulsion
LPS	lipopolysaccharide
LRP	lipoprotein receptor-related protein
mHTT	mutant huntingtin
miRNA	micro-RNA
MNP	magnetic nanoparticles
mRNA	messenger RNA
PAMAM	polyamidoamine

Europe PMC Funders Author Manuscripts

PEG	polyethylene Glycol
PEI	polyethylenimine
rep	replication
RNA	ribonucleic acid
RVG	rabies virus glycoprotein
SF	spherical fullerenes
shRNA	short hairpin RNA
siRNA	small-interfering RNA
SLN	solid lipid nanoparticles
ssDNA	single-stranded DNA
SV40	simian virus 40
SVZ	subventricular zone
TMC	trimethylated chitosan
TNF-α	tumor necrosis factor alpha
US	ultrasound
VSV-G	vesicular stomatitis virus glycoprotein

References

Abdallah B, Hassan A, Benoist C, Goula D, Behr JP, Demeneix BA. A powerful nonviral vector for in vivo gene transfer into the adult mammalian brain: polyethylenimine. Hum Gene Ther. 1996; 7:1947–1954. [PubMed: 8930654]

Ahmad HI, Ahmad MJ, Asif AR, Adnan M, Iqbal MK, Mehmood K, Muhammad SA, Bhuiyan AA, Elokil A, Du X, et al. A review of CRISPR-based genome editing: survival, evolution and challenges. Curr Issues Mol Biol. 2018; 28:47–68. [PubMed: 29428910]

Akamatsu W, Okano HJ, Osumi N, Inoue T, Nakamura S, Sakakibara S, Miura M, Matsuo N, Darnell RB, Okano H. Mammalian ELAV-like neuronal RNA-binding proteins HuB and HuC promote neuronal development in both the central and the peripheral nervous systems. Proc Natl Acad Sci U S A. 1999; 96:9885–9890. [PubMed: 10449789]

Al-Jamal KT, Gherardini L, Bardi G, Nunes A, Guo C, Bussy C, Herrero MA, Bianco A, Prato M, Kostarelos K, et al. Functional motor recovery from brain ischemic insult by carbon nanotube-mediated siRNA silencing. Proc Natl Acad Sci U S A. 2011; 108:10952–10957. [PubMed: 21690348]

Andersen HB, Benveniste D, Bitsch-Larsen L, Carl P, Crawford M, Djernes M, Eriksen J, Grell AM, Henriksen H, Jansen E, et al. Long-term treatment with epidural opiates. A multicenter account of 125 patients. Ugeskr Laeger. 1982; 144:2633–2637. [PubMed: 6758261]

Artegiani B, Calegari F. Lentiviruses allow widespread and conditional manipulation of gene expression in the developing mouse brain. Development. 2013; 140:2818–2822. [PubMed: 23757413]

Atchison RW, Casto BC, Hammon WM. Adenovirus-associated defective virus particles. Science. 1965; 149:754–756. [PubMed: 14325163]

Azzouz M, Ralph S, Wong LF, Day D, Askham Z, Barber RD, Mitrophanous KA, Kingsman SM, Mazarakis ND. Neuroprotection in a rat Parkinson model by GDNF gene therapy using EIAV vector. Neuroreport. 2004; 15:985–990. [PubMed: 15076720]

Badyal DK, Desai C. Animal use in pharmacology education and research: the changing scenario. Indian J Pharmacol. 2014; 46:257–265. [PubMed: 24987170]

Bensadoun JC, Deglon N, Tseng JL, Ridet JL, Zurn AD, Aebischer P. Lentiviral vectors as a gene delivery system in the mouse midbrain: cellular and behavioral improvements in a 6-OHDA model of Parkinson's disease using GDNF. Exp Neurol. 2000; 164:15–24. [PubMed: 10877911]

Bharali DJ, Klejbor I, Stachowiak EK, Dutta P, Roy I, Kaur N, Bergey EJ, Prasad PN, Stachowiak MK. Organically modified silica nanoparticles: a nonviral vector for in vivo gene delivery and expression in the brain. Proc Natl Acad Sci U S A. 2005; 102:11539–11544. [PubMed: 16051701]

Bishop CJ, Tzeng SY, Green JJ. Degradable polymer-coated gold nanoparticles for co-delivery of DNA and siRNA. Acta Biomater. 2015; 11:393–403. [PubMed: 25246314]

Bonci D, Cittadini A, Latronico MV, Borello U, Aycock JK, Drusco A, Innocenzi A, Follenzi A, Lavitrano M, Monti MG, et al. Advanced' generation lentiviruses as efficient vectors for cardiomyocyte gene transduction in vitro and in vivo. Gene Ther. 2003; 10:630–636. [PubMed: 12692591]

Bonoiu AC, Mahajan SD, Ding H, Roy I, Yong KT, Kumar R, Hu R, Bergey EJ, Schwartz SA, Prasad PN. Nanotechnology approach for drug addiction therapy: gene silencing using delivery of gold nanorod-siRNA nanoplex in dopaminergic neurons. Proc Natl Acad Sci U S A. 2009; 106:5546–5550. [PubMed: 19307583]

Borrell V, Yoshimura Y, Callaway EM. Targeted gene delivery to telencephalic inhibitory neurons by directional in utero electroporation. J Neurosci Methods. 2005; 143:151–158. [PubMed: 15814147]

Bourdenx M, Dutheil N, Bezard E, Dehay B. Systemic gene delivery to the central nervous system using Adeno-associated virus. Front Mol Neurosci. 2014; 7:50. [PubMed: 24917785]

Boutin C, Diestel S, Desoeuvre A, Tiveron MC, Cremer H. Efficient in vivo electroporation of the postnatal rodent forebrain. PLoS One. 2008; 3:e1883. [PubMed: 18382666]

Breakefield XO, Geller AI. Gene transfer into the nervous system. Mol Neurobiol. 1987; 1:339–371. [PubMed: 3077063]

Burger C, Gorbatyuk OS, Velardo MJ, Peden CS, Williams P, Zolotukhin S, Reier PJ, Mandel RJ, Muzyczka N. Recombinant AAV viral vectors pseudotyped with viral capsids from serotypes 1, 2, and 5 display differential efficiency and cell tropism after delivery to different regions of the central nervous system. Mol Ther. 2004; 10:302–317. [PubMed: 15294177]

Cang J, Kaneko M, Yamada J, Woods G, Stryker MP, Feldheim DA. Ephrinas guide the formation of functional maps in the visual cortex. Neuron. 2005; 48:577–589. [PubMed: 16301175]

Chang DC, Reese TS. Changes in membrane structure induced by electroporation as revealed by rapid-freezing electron microscopy. Biophys J. 1990; 58:1–12. [PubMed: 2383626]

Chatterjee J, Haik Y, Chen CJ. Modification and characterization of polystyrene-based magnetic microspheres and comparison with albumin-based magnetic microspheres. J Magn Magn Mater. 2001; 225:21–29.

Chen F, Rosiene J, Che A, Becker A, LoTurco J. Tracking and transforming neocortical progenitors by CRISPR/Cas9 gene targeting and piggyBac transposase lineage labeling. Development. 2015; 142:3601–3611. [PubMed: 26400094]

Chen X, Goncalves MA. Engineered viruses as genome editing devices. Mol Ther. 2016; 24:447–457. [PubMed: 26336974]

Cheng M, Jin X, Mu L, Wang F, Li W, Zhong X, Liu X, Shen W, Liu Y, Zhou Y. Combination of the clustered regularly interspaced short palindromic repeats (CRISPR)-associated 9 technique with the piggybac transposon system for mouse in utero electroporation to study cortical development. J Neurosci Res. 2016; 94:814–824. [PubMed: 27317429]

Chesler AT, Le Pichon CE, Brann JH, Araneda RC, Zou DJ, Firestein S. Selective gene expression by postnatal electroporation during olfactory interneuron neurogenesis. PLoS One. 2008; 3:e1517. [PubMed: 18231603]

Chew WL, Tabebordbar M, Cheng JK, Mali P, Wu EY, Ng AH, Zhu K, Wagers AJ, Church GM. A multifunctional AAV-CRISPR-Cas9 and its host response. Nat Methods. 2016; 13:868–874. [PubMed: 27595405]

Choi JS, Nam K, Park JY, Kim JB, Lee JK, Park JS. Enhanced transfection efficiency of PAMAM dendrimer by surface modification with L-arginine. J Control Release. 2004; 99:445–456. [PubMed: 15451602]

Choudhury SR, Fitzpatrick Z, Harris AF, Maitland SA, Ferreira JS, Zhang Y, Ma S, Sharma RB, Gray-Edwards HL, Johnson JA, et al. In vivo selection yields AAV-B1 capsid for central nervous system and muscle Gene therapy. Mol Ther. 2016a; 24:1247–1257. [PubMed: 27117222]

Choudhury SR, Harris AF, Cabral DJ, Keeler AM, Sapp E, Ferreira JS, Gray-Edwards HL, Johnson JA, Johnson AK, Su Q, et al. Widespread central nervous system gene transfer and silencing after systemic delivery of novel AAV-AS vector. Mol Ther. 2016b; 24:726–735. [PubMed: 26708003]

Choudhury SR, Hudry E, Maguire CA, Sena-Esteves M, Breakefield XO, Grandi P. Viral vectors for therapy of neurologic diseases. Neuropharmacology. 2016c; 120:63–80. [PubMed: 26905292]

Cikankowitz A, Clavreul A, Tetaud C, Lemaire L, Rousseau A, Lepareur N, Dabli D, Bouchet F, Garcion E, Menei P, et al. Characterization of the distribution, retention, and efficacy of internal radiation of 188Re-lipid nanocapsules in an immunocompromised human glioblastoma model. J Neuro Oncol. 2017; 131:49–58.

Cockrell AS, Kafri T. Gene delivery by lentivirus vectors. Mol Biotechnol. 2007; 36:184–204. [PubMed: 17873406]

Connor EE, Mwamuka J, Gole A, Murphy CJ, Wyatt MD. Gold nanoparticles are taken up by human cells but do not cause acute cytotoxicity. Small. 2005; 1:325–327. [PubMed: 17193451]

Conrad S, Stimpfle F, Montazeri S, Oldekamp J, Seid K, Alvarez-Bolado G, Skutella T. RGMb controls aggregation and migration of Neogenin-positive cells in vitro and in vivo. Mol Cell Neurosci. 2010; 43:222–231. [PubMed: 19944164]

Costa PM, Bourgognon M, Wang JT, Al-Jamal KT. Functionalised carbon nanotubes: from intracellular uptake and cell-related toxicity to systemic brain delivery. J Control Release. 2016; 241:200–219. [PubMed: 27693751]

Crystal RG. Adenovirus: the first effective in vivo gene delivery vector. Hum Gene Ther. 2014; 25:3–11. [PubMed: 24444179]

Cui L, Jeong H, Borovecki F, Parkhurst CN, Tanese N, Krainc D. Transcriptional repression of PGC-1alpha by mutant huntingtin leads to mitochondrial dysfunction and neurodegeneration. Cell. 2006; 127:59–69. [PubMed: 17018277]

dal Maschio M, Ghezzi D, Bony G, Alabastri A, Deidda G, Brondi M, Sato SS, Zaccaria RP, Di Fabrizio E, Ratto GM, et al. High-performance and site-directed in utero electroporation by a triple-electrode probe. Nat Commun. 2012; 3:960. [PubMed: 22805567]

Dan N. Lipid-nucleic acid supramolecular complexes: lipoplex structure and the kinetics of formation. AIMS Biophys. 2015; 2:163–183.

Danhier F, Messaoudi K, Lemaire L, Benoit JP, Lagarce F. Combined anti-Galectin-1 and anti-EGFR siRNA-loaded chitosan-lipid nanocapsules decrease temozolomide resistance in glioblastoma: in vivo evaluation. Int J Pharm. 2015; 481:154–161. [PubMed: 25644286]

David LS, Aitoubah J, Lesperance LS, Wang LY. Gene delivery in mouse auditory brainstem and hindbrain using in utero electroporation. Mol Brain. 2014; 7:51. [PubMed: 25063346]

Davidson BL, Allen ED, Kozarsky KF, Wilson JM, Roessler BJ. A model system for in vivo gene transfer into the central nervous system using an adenoviral vector. Nat Genet. 1993; 3:219–223. [PubMed: 8387378]

De Vry J, Martinez-Martinez P, Losen M, Temel Y, Steckler T, Steinbusch HW, De Baets MH, Prickaerts J. In vivo electroporation of the central nervous system: a non-viral approach for targeted gene delivery. Prog Neurobiol. 2010; 92:227–244. [PubMed: 20937354]

Deverman BE, Pravdo PL, Simpson BP, Kumar SR, Chan KY, Banerjee A, Wu WL, Yang B, Huber N, Pasca SP, et al. Cre-dependent selection yields AAV variants for widespread gene transfer to the adult brain. Nat Biotechnol. 2016; 34:204–209. [PubMed: 26829320]

Dobrzanski G, Kossut M. Application of the DREADD technique in biomedical brain research. Pharmacol Rep. 2017; 69:213–221. [PubMed: 28092807]

Dodart JC, Marr RA, Koistinaho M, Gregersen BM, Malkani S, Verma IM, Paul SM. Gene delivery of human apolipoprotein E alters brain Abeta burden in a mouse model of Alzheimer's disease. Proc Natl Acad Sci U S A. 2005; 102:1211–1216. [PubMed: 15657137]

Duceppe N, Tabrizian M. Advances in using chitosan-based nanoparticles for in vitro and in vivo drug and gene delivery. Expert Opin Drug Deliv. 2010; 7:1191–1207. [PubMed: 20836623]

Duque S, Joussemet B, Riviere C, Marais T, Dubreil L, Douar AM, Fyfe J, Moullier P, Colle MA, Barkats M. Intravenous administration of self-complementary AAV9 enables transgene delivery to adult motor neurons. Mol Ther. 2009; 17:1187–1196. [PubMed: 19367261]

Eichman JD, Bielinska AU, Kukowska-Latallo JF, Baker JR Jr. The use of PAMAM dendrimers in the efficient transfer of genetic material into cells. Pharm Sci Technol Today. 2000; 3:232–245. [PubMed: 10884679]

Ekin A, Karatas OF, Culha M, Ozen M. Designing a gold nanoparticle-based nanocarrier for microRNA transfection into the prostate and breast cancer cells. J Gene Med. 2014; 16:331–335. [PubMed: 25331590]

Endoh M, Koibuchi N, Sato M, Morishita R, Kanzaki T, Murata Y, Kaneda Y. Fetal gene transfer by intrauterine injection with microbubble-enhanced ultrasound. Mol Ther. 2002; 5:501–508. [PubMed: 11991740]

Escoffre JM, Zeghimi A, Novell A, Bouakaz A. In-vivo gene delivery by sonoporation: recent progress and prospects. Curr Gene Ther. 2013; 13:2–14. [PubMed: 23157546]

Escudero-Francos MA, Cepas V, Gonzalez-Menedez P, Badia-Laino R, Diaz-Garcia ME, Sainz RM, Mayo JC, Hevia D. Cellular uptake and tissue biodistribution of functionalized gold nanoparticles and nanoclusters. J Biomed Nanotechnol. 2017; 13:167–179. [PubMed: 29377647]

Estelrich J, Escribano E, Queralt J, Busquets MA. Iron oxide nanoparticles for magnetically-guided and magnetically-responsive drug delivery. Int J Mol Sci. 2015; 16:8070–8101. [PubMed: 25867479]

Ewe A, Przybylski S, Burkhardt J, Janke A, Appelhans D, Aigner A. A novel tyrosine-modified low molecular weight polyethylenimine (P10Y) for efficient siRNA delivery in vitro and in vivo. J Control Release. 2016; 230:13–25. [PubMed: 27061141]

Fan CH, Chang EL, Ting CY, Lin YC, Liao EC, Huang CY, Chang YC, Chan HL, Wei KC, Yeh CK. Folate-conjugated gene-carrying microbubbles with focused ultrasound for concurrent blood-brain barrier opening and local gene delivery. Biomaterials. 2016; 106:46–57. [PubMed: 27544926]

Farson D, Harding TC, Tao L, Liu J, Powell S, Vimal V, Yendluri S, Koprivnikar K, Ho K, Twitty C, et al. Development and characterization of a cell line for large-scale, serum-free production of recombinant adeno-associated viral vectors. J Gene Med. 2004; 6:1369–1381. [PubMed: 15538729]

Fassler M, Weissberg I, Levy N, Diaz-Griffero F, Monsonego A, Friedman A, Taube R. Preferential lentiviral targeting of astrocytes in the central nervous system. PLoS One. 2013; 8:e76092. [PubMed: 24098426]

Fernandez ME, Croce S, Boutin C, Cremer H, Raineteau O. Targeted electroporation of defined lateral ventricular walls: a novel and rapid method to study fate specification during postnatal forebrain neurogenesis. Neural Dev. 2011; 6:13. [PubMed: 21466691]

Fischer AJ, Stanke JJ, Omar G, Askwith CC, Burry RW. Ultrasound-mediated gene transfer into neuronal cells. J Biotechnol. 2006; 122:393–411. [PubMed: 16309774]

Foust KD, Kaspar BK. Over the barrier and through the blood: to CNS delivery we go. Cell Cycle. 2009; 8:4017–4018. [PubMed: 19949299]

Foust KD, Nurre E, Montgomery CL, Hernandez A, Chan CM, Kaspar BK. Intravascular AAV9 preferentially targets neonatal neurons and adult astrocytes. Nat Biotechnol. 2009; 27:59–65. [PubMed: 19098898]

Fraley R, Subramani S, Berg P, Papahadjopoulos D. Introduction of liposome-encapsulated SV40 DNA into cells. J Biol Chem. 1980; 255:10431–10435. [PubMed: 6253474]

Freire JM, Santos NC, Veiga AS, Da Poian AT, Castanho MA. Rethinking the capsid proteins of enveloped viruses: multifunctionality from genome packaging to genome transfection. FEBS J. 2015; 282:2267–2278. [PubMed: 25808179]

Fukuchi-Shimogori T, Grove EA. Neocortex patterning by the secreted signaling molecule FGF8. Science. 2001; 294:1071–1074. [PubMed: 11567107]

Gao Y, Wang ZY, Zhang J, Zhang Y, Huo H, Wang T, Jiang T, Wang S. RVG-peptide-linked trimethylated chitosan for delivery of siRNA to the brain. Biomacromolecules. 2014; 15:1010–1018. [PubMed: 24547943]

Germano IM, Fable J, Humayun Gultekin SEA. Adenovirus/herpes simplex-thymidine kinase/ganciclovir complex: preliminary results of a Phase I trial in patients with recurrent malignant gliomas. J Neuro Oncol. 2003; 65(279)

Ghitani N, Bayguinov PO, Ma Y, Jackson MB. Single-trial imaging of spikes and synaptic potentials in single neurons in brain slices with genetically encoded hybrid voltage sensor. J Neurophysiol. 2015; 113:1249–1259. [PubMed: 25411462]

Gilbert LA, Larson MH, Morsut L, Liu Z, Brar GA, Torres SE, Stern-Ginossar N, Brandman O, Whitehead EH, Doudna JA, et al. CRISPR-mediated modular RNA-guided regulation of transcription in eukaryotes. Cell. 2013; 154:442–451. [PubMed: 23849981]

Glover DJ, Lipps HJ, Jans DA. Towards safe, non-viral therapeutic gene expression in humans. Nat Rev Genet. 2005; 6:299–310. [PubMed: 15761468]

Goff SP, Berg P. Construction of hybrid viruses containing SV40 and lambda phage DNA segments and their propagation in cultured monkey cells. Cell. 1976; 9:695–705. [PubMed: 189942]

Graham FL, van der Eb AJ. Transformation of rat cells by DNA of human adenovirus 5. Virology. 1973; 54:536–539. [PubMed: 4737663]

Gray SJ, Blake BL, Criswell HE, Nicolson SC, Samulski RJ, McCown TJ, Li W. Directed evolution of a novel adeno-associated virus (AAV) vector that crosses the seizure-compromised blood-brain barrier (BBB). Mol Ther. 2010; 18:570–578. [PubMed: 20040913]

Gray SJ, Foti SB, Schwartz JW, Bachaboina L, Taylor-Blake B, Coleman J, Ehlers MD, Zylka MJ, McCown TJ, Samulski RJ. Optimizing promoters for recombinant adeno-associated virus-mediated gene expression in the peripheral and central nervous system using self-complementary vectors. Hum Gene Ther. 2011; 22:1143–1153. [PubMed: 21476867]

Gribkoff VK, Kaczmarek LK. The need for new approaches in CNS drug discovery: why drugs have failed, and what can be done to improve outcomes. Neuropharmacology. 2017; 120:11–19. [PubMed: 26979921]

Grimm D, Lee JS, Wang L, Desai T, Akache B, Storm TA, Kay MA. In vitro and in vivo gene therapy vector evolution via multispecies interbreeding and retargeting of adeno-associated viruses. J Virol. 2008; 82:5887–5911. [PubMed: 18400866]

Gu J, Al-Bayati K, Ho EA. Development of antibody-modified chitosan nanoparticles for the targeted delivery of siRNA across the blood-brain barrier as a strategy for inhibiting HIV replication in astrocytes. Drug Deliv Transl Res. 2017; 7:497–506. [PubMed: 28315051]

Haddad-Tovolli R, Szabo NE, Zhou X, Alvarez-Bolado G. Genetic manipulation of the mouse developing hypothalamus through in utero electroporation. J Vis Exp. 2013; 24(77)

Hashemi M, Tabatabai SM, Parhiz H, Milanizadeh S, Amel Farzad S, Abnous K, Ramezani M. Gene delivery efficiency and cytotoxicity of heterocyclic amine-modified PAMAM and PPI dendrimers. Mater Sci Eng C Mater Biol Appl. 2016; 61:791–800. [PubMed: 26838910]

Hashimoto M, Aruga J, Hosoya Y, Kanegae Y, Saito I, Mikoshiba K. A neural cell-type-specific expression system using recombinant adenovirus vectors. Hum Gene Ther. 1996; 7:149–158. [PubMed: 8788166]

Hashimoto M, Hisano Y. Directional gene-transfer into the brain by an adenoviral vector tagged with magnetic nanoparticles. J Neurosci Methods. 2011; 194:316–320. [PubMed: 21074563]

Hassani Z, Lemkine GF, Erbacher P, Palmier K, Alfama G, Giovannangeli C, Behr JP, Demeneix BA. Lipid-mediated siRNA delivery down-regulates exogenous gene expression in the mouse brain at picomolar levels. J Gene Med. 2005; 7:198–207. [PubMed: 15515135]

Helmschrodt C, Hobel S, Schoniger S, Bauer A, Bonicelli J, Gringmuth M, Fietz SA, Aigner A, Richter A, Richter F. Polyethylenimine nanoparticle-mediated siRNA delivery to reduce alpha-synuclein expression in a model of Parkinson's disease. Mol Ther Nucleic Acids. 2017; 9:57–68. [PubMed: 29246324]

Higuchi Y, Kawakami S, Fumoto S, Yamashita F, Hashida M. Effect of the particle size of galactosylated lipoplex on hepatocyte-selective gene transfection after intraportal administration. Biol Pharm Bull. 2006; 29:1521–1523. [PubMed: 16819204]

Hioki H, Kameda H, Nakamura H, Okunomiya T, Ohira K, Nakamura K, Kuroda M, Furuta T, Kaneko T. Efficient gene transduction of neurons by lentivirus with enhanced neuron-specific promoters. Gene Ther. 2007; 14:872–882. [PubMed: 17361216]

Hsu PH, Wei KC, Huang CY, Wen CJ, Yen TC, Liu CL, Lin YT, Chen JC, Shen CR, Liu HL. Noninvasive and targeted gene delivery into the brain using microbubble-facilitated focused ultrasound. PLoS One. 2013; 8:e57682. [PubMed: 23460893]

Hu J, Hu K, Cheng Y. Tailoring the dendrimer core for efficient gene delivery. Acta Biomater. 2016; 35:1–11. [PubMed: 26923528]

Hu K, Chen X, Chen W, Zhang L, Li J, Ye J, Zhang Y, Zhang L, Li CH, Yin L, et al. Neuroprotective effect of gold nanoparticles composites in Parkinson's disease model. Nanomed : Nanotechnol, Biol, Med. 2018; 14:1123–1136.

Huang R, Ke W, Liu Y, Jiang C, Pei Y. The use of lactoferrin as a ligand for targeting the polyamidoamine-based gene delivery system to the brain. Biomaterials. 2008; 29:238–246. [PubMed: 17935779]

Huang RQ, Qu YH, Ke WL, Zhu JH, Pei YY, Jiang C. Efficient gene delivery targeted to the brain using a transferrin-conjugated polyethyleneglycol-modified polyamidoamine dendrimer. FASEB J. 2007; 21:1117–1125. [PubMed: 17218540]

Hudry E, Martin C, Gandhi S, Gyorgy B, Scheffer DI, Mu D, Merkel SF, Mingozzi F, Fitzpatrick Z, Dimant H, et al. Exosome-associated AAV vector as a robust and convenient neuroscience tool. Gene Ther. 2016; 23:819. [PubMed: 27808124]

Hwang DW, Son S, Jang J, Youn H, Lee S, Lee D, Lee YS, Jeong JM, Kim WJ, Lee DS. A brain-targeted rabies virus glycoprotein-disulfide linked PEI nanocarrier for delivery of neurogenic microRNA. Biomaterials. 2011; 32:4968–4975. [PubMed: 21489620]

Imamura F, Greer CA. Pax6 regulates Tbr1 and Tbr2 expressions in olfactory bulb mitral cells. Mol Cell Neurosci. 2013; 54:58–70. [PubMed: 23353076]

Immonen A, Vapalahti M, Tyynela K, Hurskainen H, Sandmair A, Vanninen R, Langford G, Murray N, Yla-Herttuala S. AdvHSV-tk gene therapy with intravenous ganciclovir improves survival in human malignant glioma: a randomised, controlled study. Mol Ther. 2004; 10:967–972. [PubMed: 15509514]

Inoh Y, Nagai M, Matsushita K, Nakanishi M, Furuno T. Gene transfection efficiency into dendritic cells is influenced by the size of cationic liposomes/DNA complexes. Eur J Pharm Sci. 2017; 102:230–236. [PubMed: 28323115]

Javed H, Menon SA, Al-Mansoori KM, Al-Wandi A, Majbour NK, Ardah MT, Varghese S, Vaikath NN, Haque ME, Azzouz M, et al. Development of nonviral vectors targeting the brain as a therapeutic approach for Parkinson's disease and other brain disorders. Mol Ther. 2016; 24:746–758. [PubMed: 26700614]

Jensen SA, Day ES, Ko CH, Hurley LA, Luciano JP, Kouri FM, Merkel TJ, Luthi AJ, Patel PC, Cutler JI, et al. Spherical nucleic acid nanoparticle conjugates as an RNAi-based therapy for glioblastoma. Sci Transl Med. 2013; 5:209ra.

Jin J, Bae KH, Yang H, Lee SJ, Kim H, Kim Y, Joo KM, Seo SW, Park TG, Nam DH. In vivo specific delivery of c-Met siRNA to glioblastoma using cationic solid lipid nanoparticles. Bioconjug Chem. 2011; 22:2568–2572. [PubMed: 22070554]

Johnson IP. Age-related neurodegenerative disease research needs aging models. Front Aging Neurosci. 2015; 7:168. [PubMed: 26388766]

Juffermans LJ, Dijkmans PA, Musters RJ, Visser CA, Kamp O. Transient permeabilization of cell membranes by ultrasound-exposed microbubbles is related to formation of hydrogen peroxide. Am J Physiol Heart Circ Physiol. 2006; 291:H1595–H1601. [PubMed: 16632548]

Kalebic N, Taverna E, Tavano S, Wong FK, Suchold D, Winkler S, Huttner WB, Sarov M. CRISPR/Cas9-induced disruption of gene expression in mouse embryonic brain and single neural stem cells in vivo. EMBO Rep. 2016; 17:338–348. [PubMed: 26758805]

Kamiya A. Animal models for schizophrenia via in utero gene transfer: understanding roles for genetic susceptibility factors in brain development. Prog Brain Res. 2009; 179:9–15. [PubMed: 20302813]

Kaur IP, Bhandari R, Bhandari S, Kakkar V. Potential of solid lipid nanoparticles in brain targeting. J Control Release. 2008; 127:97–109. [PubMed: 18313785]

Kay MA, Glorioso JC, Naldini L. Viral vectors for gene therapy: the art of turning infectious agents into vehicles of therapeutics. Nat Med. 2001; 7:33–40. [PubMed: 11135613]

Ke W, Shao K, Huang R, Han L, Liu Y, Li J, Kuang Y, Ye L, Lou J, Jiang C. Gene delivery targeted to the brain using an Angiopep-conjugated polyethyleneglycol-modified polyamidoamine dendrimer. Biomaterials. 2009; 30:6976–6985. [PubMed: 19765819]

Kim S, Kim D, Cho SW, Kim J, Kim JS. Highly efficient RNA-guided genome editing in human cells via delivery of purified Cas9 ribonucleoproteins. Genome Res. 2014; 24:1012–1019. [PubMed: 24696461]

Kim SS, Ye C, Kumar P, Chiu I, Subramanya S, Wu H, Shankar P, Manjunath N. Targeted delivery of siRNA to macrophages for anti-inflammatory treatment. Mol Ther. 2010; 18:993–1001. [PubMed: 20216529]

Kita Y, Kawakami K, Takahashi Y, Murakami F. Development of cerebellar neurons and glias revealed by in utero electroporation: Golgi-like labeling of cerebellar neurons and glias. PLoS One. 2013; 8:e70091. [PubMed: 23894597]

Kitamura K, Judkewitz B, Kano M, Denk W, Hausser M. Targeted patch-clamp recordings and single-cell electroporation of unlabeled neurons in vivo. Nat Methods. 2008; 5:61–67. [PubMed: 18157136]

Klein RL, Muir D, King MA, Peel AL, Zolotukhin S, Moller JC, Kruttgen A, Heymach JV Jr, Muzyczka N, Meyer EM. Long-term actions of vector-derived nerve growth factor or brain-derived neurotrophic factor on choline acetyltransferase and Trk receptor levels in the adult rat basal forebrain. Neuroscience. 1999; 90:815–821. [PubMed: 10218782]

Kneuer C, Sameti M, Bakowsky U, Schiestel T, Schirra H, Schmidt H, Lehr CM. A nonviral DNA delivery system based on surface modified silica-nanoparticles can efficiently transfect cells in vitro. Bioconjug Chem. 2000a; 11:926–932. [PubMed: 11087343]

Kneuer C, Sameti M, Haltner EG, Schiestel T, Schirra H, Schmidt H, Lehr CM. Silica nanoparticles modified with aminosilanes as carriers for plasmid DNA. Int J Pharm. 2000b; 196:257–261. [PubMed: 10699731]

Koonin EV, Senkevich TG, Dolja VV. The ancient virus world and evolution of cells. Biol Direct. 2006; 1:29. [PubMed: 16984643]

Kotterman MA, Chalberg TW, Schaffer DV. Viral vectors for gene therapy: translational and clinical outlook. Annu Rev Biomed Eng. 2015a; 17:63–89. [PubMed: 26643018]

Kotterman MA, Vazin T, Schaffer DV. Enhanced selective gene delivery to neural stem cells in vivo by an adeno-associated viral variant. Development. 2015b; 142:1885–1892. [PubMed: 25968319]

Krisky DM, Wolfe D, Goins WF, Marconi PC, Ramakrishnan R, Mata M, Rouse RJ, Fink DJ, Glorioso JC. Deletion of multiple immediate-early genes from herpes simplex virus reduces cytotoxicity and permits long-term gene expression in neurons. Gene Ther. 1998; 5:1593–1603. [PubMed: 10023438]

Kugler S. Tissue-specific promoters in the CNS. Methods Mol Biol. 2016; 1382:81–91. [PubMed: 26611580]

Lacerda L, Ali-Boucetta H, Herrero MA, Pastorin G, Bianco A, Prato M, Kostarelos K. Tissue histology and physiology following intravenous administration of different types of functionalized multiwalled carbon nanotubes. Nanomedicine (Lond.). 2008; 3:149–161. [PubMed: 18373422]

Lagarce F, Passirani C. Nucleic-acid delivery using lipid nanocapsules. Curr Pharm Biotechnol. 2016; 17:723–727. [PubMed: 27033510]

Lawlor PA, Bland RJ, Mouravlev A, Young D, During MJ. Efficient gene delivery and selective transduction of glial cells in the mammalian brain by AAV serotypes isolated from nonhuman primates. Mol Ther. 2009; 17:1692–1702. [PubMed: 19638961]

Lemkine GF, Mantero S, Migne C, Raji A, Goula D, Normandie P, Levi G, Demeneix BA. Preferential transfection of adult mouse neural stem cells and their immediate progeny in vivo with polyethylenimine. Mol Cell Neurosci. 2002; 19:165–174. [PubMed: 11860270]

Lentacker I, De Cock I, Deckers R, De Smedt SC, Moonen CT. Understanding ultrasound induced sonoporation: definitions and underlying mechanisms. Adv Drug Deliv Rev. 2014; 72:49–64. [PubMed: 24270006]

Lentz TB, Gray SJ, Samulski RJ. Viral vectors for gene delivery to the central nervous system. Neurobiol Dis. 2012; 48:179–188. [PubMed: 22001604]

Levy R, Shaheen U, Cesbron Y, See V. Gold nanoparticles delivery in mammalian live cells: a critical review. Nano Rev. 2010; 1

Li HL, Gee P, Ishida K, Hotta A. Efficient genomic correction methods in human iPS cells using CRISPR-Cas9 system. Methods. 2016; 101:27–35. [PubMed: 26525194]

Li M, Yuan Y, Hu B, Wu L. Study on lentivirus-mediated ABCA7 improves neurocognitive function and related mechanisms in the C57BL/6 mouse model of Alzheimer's disease. J Mol Neurosci. 2017; 61:489–497. [PubMed: 28124230]

Lin CY, Hsieh HY, Pitt WG, Huang CY, Tseng IC, Yeh CK, Wei KC, Liu HL. Focused ultrasound-induced blood-brain barrier opening for non-viral, non-invasive, and targeted gene delivery. J Control Release. 2015; 212:1–9. [PubMed: 26071631]

Lin S, Staahl BT, Alla RK, Doudna JA. Enhanced homology-directed human genome engineering by controlled timing of CRISPR/Cas9 delivery. eLife. 2014; 3:e04766. [PubMed: 25497837]

Linemann T, Thomsen LB, Jardin KG, Laursen JC, Jensen JB, Lichota J, Moos T. Development of a novel lipophilic, magnetic nanoparticle for in vivo drug delivery. Pharmaceutics. 2013; 5:246–260. [PubMed: 24300449]

Liu CH, Yu SY. Cationic nanoemulsions as non-viral vectors for plasmid DNA delivery. Colloids Surf B Biointerfaces. 2010; 79:509–515. [PubMed: 20541375]

Long L, Cai X, Guo R, Wang P, Wu L, Yin T, Liao S, Lu Z. Treatment of Parkinson's disease in rats by Nrf2 transfection using MRI-guided focused ultrasound delivery of nanomicrobubbles. Biochem Biophys Res Commun. 2017; 482:75–80. [PubMed: 27810365]

LoTurco J, Manent JB, Sidiqi F. New and improved tools for in utero electroporation studies of developing cerebral cortex. Cereb Cortex. 2009; 19(Suppl 1):i120–125. [PubMed: 19395528]

Lu L, Zeitlin PL, Guggino WB, Craig RW. Gene transfer by lipofection in rabbit and human secretory epithelial cells. Pflugers Arch. 1989; 415:198–203. [PubMed: 2594476]

Lu Y, Jiang C. Brain-targeted polymers for gene delivery in the treatment of brain diseases. Top Curr Chem (Cham). 2017; 375:48. [PubMed: 28397188]

Lungwitz U, Breunig M, Blunk T, Gopferich A. Polyethylenimine-based non-viral gene delivery systems. Eur J Pharm Biopharm. 2005; 60:247–266. [PubMed: 15939236]

Luo D, Saltzman WM. Nonviral gene delivery: thinking of silica. Gene Ther. 2006; 13:585–586. [PubMed: 17526071]

Ma B, Zhang S, Jiang H, Zhao B, Lv H. Lipoplex morphologies and their influences on transfection efficiency in gene delivery. J Control Release. 2007; 123:184–194. [PubMed: 17913276]

Maeda-Mamiya R, Noiri E, Isobe H, Nakanishi W, Okamoto K, Doi K, Sugaya T, Izumi T, Homma T, Nakamura E. In vivo gene delivery by cationic tetraamino fullerene. Proc Natl Acad Sci U S A. 2010; 107:5339–5344. [PubMed: 20194788]

Maeder ML, Gersbach CA. Genome-editing technologies for gene and cell therapy. Mol Ther. 2016; 24:430–446. [PubMed: 26755333]

Maguire CA, Balaj L, Sivaraman S, Crommentuijn MH, Ericsson M, Mincheva-Nilsson L, Baranov V, Gianni D, Tannous BA, Sena-Esteves M, et al. Microvesicle-associated AAV vector as a novel gene delivery system. Mol Ther. 2012; 20:960–971. [PubMed: 22314290]

Mah C, Byrne BJ, Flotte TR. Virus-based gene delivery systems. Clin Pharmacokinet. 2002a; 41:901–911. [PubMed: 12222993]

Mah C, Fraites TJ Jr, Zolotukhin I, Song S, Flotte TR, Dobson J, Batich C, Byrne BJ. Improved method of recombinant AAV2 delivery for systemic targeted gene therapy. Mol Ther. 2002b; 6:106–112. [PubMed: 12095310]

Europe PMC Funders Author Manuscripts

Mah CS, Zolotukhin I, Fraites T, Dobson J, Batich C. Microsphere-mediated delivery of recombinant AAV vectors in vitro and in vivo. Mol Ther. 2000; 1:S239.

Mali P, Esvelt KM, Church GM. Cas9 as a versatile tool for engineering biology. Nat Methods. 2013; 10:957–963. [PubMed: 24076990]

Mali S. Delivery systems for gene therapy. Indian J Hum Genet. 2013; 19:3–8. [PubMed: 23901186]

Manent JB, Wang Y, Chang Y, Paramasivam M, LoTurco JJ. Dcx re-expression reduces subcortical band heterotopia and seizure threshold in an animal model of neuronal migration disorder. Nat Med. 2009; 15:84–90. [PubMed: 19098909]

Matsuda T, Cepko CL. Controlled expression of transgenes introduced by in vivo electroporation. Proc Natl Acad Sci U S A. 2007; 104:1027–1032. [PubMed: 17209010]

Mead BP, Mastorakos P, Suk JS, Klibanov AL, Hanes J, Price RJ. Targeted gene transfer to the brain via the delivery of brain-penetrating DNA nanoparticles with focused ultrasound. J Control Release. 2016; 223:109–117. [PubMed: 26732553]

Menendez CM, Carr DJ. Defining nervous system susceptibility during acute and latent herpes simplex virus-1 infection. J Neuroimmunol. 2017; 308:43–49. [PubMed: 28302316]

Mikuni T, Nishiyama J, Sun Y, Kamasawa N, Yasuda R. High-Throughput, High-Resolution Mapping of Protein Localization in Mammalian Brain by In Vivo Genome Editing. Cell. 2016; 165:1803–1817. [PubMed: 27180908]

Mitani K. Gene targeting in human-induced pluripotent stem cells with adenoviral vectors. Methods Mol Biol. 2014; 1114:163–167. [PubMed: 24557902]

Miura M, Tamura T, Mikoshiba K. Cell-specific expression of the mouse glial fibrillary acidic protein gene: identification of the cis- and trans-acting promoter elements for astrocyte-specific expression. J Neurochem. 1990; 55:1180–1188. [PubMed: 2398353]

Mizuno H, Hirano T, Tagawa Y. Evidence for activity-dependent cortical wiring: formation of interhemispheric connections in neonatal mouse visual cortex requires projection neuron activity. J Neurosci. 2007; 27:6760–6770. [PubMed: 17581963]

Montellano A, Da Ros T, Bianco A, Prato M. Fullerene C(6)(0) as a multi-functional system for drug and gene delivery. Nanoscale. 2011; 3:4035–4041. [PubMed: 21897967]

Morelli AE, Larregina AT, Smith-Arica J, Dewey RA, Southgate TD, Ambar B, Fontana A, Castro MG, Lowenstein PR. Neuronal and glial cell type-specific promoters within adenovirus recombinants restrict the expression of the apoptosis-inducing molecule Fas ligand to predetermined brain cell types, and abolish peripheral liver toxicity. J Gen Virol. 1999; 80(Pt. 3): 571–583. [PubMed: 10091995]

Muramatsu T, Mizutani Y, Ohmori Y, Okumura J. Comparison of three non-viral transfection methods for foreign gene expression in early chicken embryos in ovo. Biochem Biophys Res Commun. 1997; 230:376–380. [PubMed: 9016787]

Murlidharan G, Samulski RJ, Asokan A. Biology of adeno-associated viral vectors in the central nervous system. Front Mol Neurosci. 2014; 7:76. [PubMed: 25285067]

Nakashima H, Nguyen T, Kasai K, Passaro C, Ito H, Goins WF, Shaikh I, Erdelyi R, Nishihara R, Nakano I, et al. Toxicity and efficacy of a novel GADD34-expressing oncolytic HSV-1 for the treatment of experimental glioblastoma. Clin Cancer Res. 2018 Mar 6.

Naldini L. Gene therapy returns to centre stage. Nature. 2015; 526:351–360. [PubMed: 26469046]

Naldini L, Blomer U, Gage FH, Trono D, Verma IM. Efficient transfer, integration, and sustained long-term expression of the transgene in adult rat brains injected with a lentiviral vector. Proc Natl Acad Sci U S A. 1996a; 93:11382–11388. [PubMed: 8876144]

Naldini L, Blomer U, Gallay P, Ory D, Mulligan R, Gage FH, Verma IM, Trono D. In vivo gene delivery and stable transduction of nondividing cells by a lentiviral vector. Science. 1996b; 272:263–267. [PubMed: 8602510]

Nayerossadat N, Maedeh T, Ali PA. Viral and nonviral delivery systems for gene delivery. Adv Biomed Res. 2012; 1:27. [PubMed: 23210086]

Neggers YH. Increasing prevalence, changes in diagnostic criteria, and nutritional risk factors for autism spectrum disorders. ISRN Nutr. 2014; 2014:514026. [PubMed: 24967269]

Negishi Y, Yamane M, Kurihara N, Endo-Takahashi Y, Sashida S, Takagi N, Suzuki R, Maruyama K. Enhancement of Blood-Brain Barrier Permeability and Delivery of Antisense Oligonucleotides or

Plasmid DNA to the Brain by the Combination of Bubble Liposomes and High-Intensity Focused Ultrasound. Pharmaceutics. 2015; 7:344–362. [PubMed: 26402694]

Neumann E, Schaefer-Ridder M, Wang Y, Hofschneider PH. Gene transfer into mouse lyoma cells by electroporation in high electric fields. EMBO J. 1982; 1:841–845. [PubMed: 6329708]

Ning J, Wakimoto H. Oncolytic herpes simplex virus-based strategies: toward a breakthrough in glioblastoma therapy. Front Microbiol. 2014; 5:303. [PubMed: 24999342]

Nouri F, Sadeghpour H, Heidari R, Dehshahri A. Preparation, characterization, and transfection efficiency of low molecular weight polyethylenimine-based nanoparticles for delivery of the plasmid encoding CD200 gene. Int J Nanomed. 2017; 12:5557–5569.

Oellig C, Seliger B. Gene transfer into brain tumor cell lines: reporter gene expression using various cellular and viral promoters. J Neurosci Res. 1990; 26:390–396. [PubMed: 2398515]

Oh J, Lee MS, Jeong JH, Lee M. Deoxycholic Acid-Conjugated Polyethylenimine for Delivery of Heme Oxygenase-1 Gene in Rat Ischemic Stroke Model. J Pharm Sci. 2017; 106:3524–3532. [PubMed: 28780392]

Ojala DS, Amara DP, Schaffer DV. Adeno-associated virus vectors and neurological gene therapy. Neuroscientist. 2015; 21:84–98. [PubMed: 24557878]

Ono T, Fujino Y, Tsuchiya T, Tsuda M. Plasmid DNAs directly injected into mouse brain with lipofectin can be incorporated and expressed by brain cells. Neurosci Lett. 1990; 117:259–263. [PubMed: 1710037]

Ortinski PI, O'Donovan B, Dong X, Kantor B. Integrase-Deficient Lentiviral Vector as an All-in-One Platform for Highly Efficient CRISPR/Cas9-Mediated Gene Editing. Mol Ther Methods Clin Dev. 2017; 5:153–164. [PubMed: 28497073]

Pack DW, Hoffman AS, Pun S, Stayton PS. Design and development of polymers for gene delivery. Nat Rev Drug Discov. 2005; 4:581–593. [PubMed: 16052241]

Palella TD, Hidaka Y, Silverman LJ, Levine M, Glorioso J, Kelley WN. Expression of human HPRT mRNA in brains of mice infected with a recombinant herpes simplex virus-1 vector. Gene. 1989; 80:137–144. [PubMed: 2551779]

Pantarotto D, Singh R, McCarthy D, Erhardt M, Briand JP, Prato M, Kostarelos K, Bianco A. Functionalized carbon nanotubes for plasmid DNA gene delivery. Angew Chem Int Ed Engl. 2004; 43:5242–5246. [PubMed: 15455428]

Parsi S, Pandamooz S, Heidari S, Naji M, Morfini G, Ahmadiani A, Dargahi L. A novel rat model of Alzheimer's disease based on lentiviral-mediated expression of mutant APP. Neuroscience. 2015; 284:99–106. [PubMed: 25270904]

Parveen A, Rizvi SH, Sushma, Mahdi F, Ahmad I, Singh PP, Mahdi AA. Intranasal exposure to silica nanoparticles induces alterations in pro-inflammatory environment of rat brain. Toxicol Ind Health. 2017; 33:119–132. [PubMed: 26431867]

Pathak K, Shankar R, Joshi M. An Update of Patents, Preclinical and Clinical Outcomes of Lipid Nanoparticulate Systems. Curr Pharm Des. 2017 Nov 21.

Peng LH, Huang YF, Zhang CZ, Niu J, Chen Y, Chu Y, Jiang ZH, Gao JQ, Mao ZW. Integration of antimicrobial peptides with gold nanoparticles as unique non-viral vectors for gene delivery to mesenchymal stem cells with antibacterial activity. Biomaterials. 2016; 103:137–149. [PubMed: 27376562]

Penrod RD, Wells AM, Carlezon WA Jr, Cowan CW. Use of Adeno-Associated and Herpes Simplex Viral Vectors for In Vivo Neuronal Expression in Mice. Curr Protoc Neurosci. 2015; 73(4):31–37.

Petschauer JS, Madden AJ, Kirschbrown WP, Song G, Zamboni WC. The effects of nanoparticle drug loading on the pharmacokinetics of anticancer agents. Nanomedicine (Lond.). 2015; 10:447–463. [PubMed: 25707978]

Pissuwan D, Niidome T, Cortie MB. The forthcoming applications of gold nanoparticles in drug and gene delivery systems. J Control Release. 2011; 149:65–71. [PubMed: 20004222]

Potrykus I, Paszkowski J, Saul MW, Petruska J, Shillito RD. Molecular and general genetics of a hybrid foreign gene introduced into tobacco by direct gene transfer. Mol Gen Gen. 1985; 199:169–177.

Potter H. Electroporation in biology: methods, applications, and instrumentation. Anal Biochem. 1988; 174:361–373. [PubMed: 3071177]

Prakash V, Moore M, Yanez-Munoz RJ. Current Progress in Therapeutic Gene Editing for Monogenic Diseases. Mol Ther. 2016; 24:465–474. [PubMed: 26765770]

Price J, Turner D, Cepko C. Lineage analysis in the vertebrate nervous system by retrovirus-mediated gene transfer. Proc Natl Acad Sci U S A. 1987; 84:156–160. [PubMed: 3099292]

Pulkkanen KJ, Yla-Herttuala S. Gene therapy for malignant glioma: current clinical status. Mol Ther. 2005; 12:585–598. [PubMed: 16095972]

Puumalainen AM, Vapalahti M, Agrawal RS, Kossila M, Laukkanen J, Lehtolainen P, Viita H, Paljarvi L, Vanninen R, Yla-Herttuala S. Beta-galactosidase gene transfer to human malignant glioma in vivo using replication-deficient retroviruses and adenoviruses. Hum Gene Ther. 1998; 9:1769–1774. [PubMed: 9721087]

Qi LS, Larson MH, Gilbert LA, Doudna JA, Weissman JS, Arkin AP, Lim WA. Repurposing CRISPR as an RNA-guided platform for sequence-specific control of gene expression. Cell. 2013; 152:1173–1183. [PubMed: 23452860]

Qiao WL, Hu HY, Shi BW, Zang LJ, Jin W, Lin Q. Lentivirus-mediated knockdown of TSP50 suppresses the growth of non-small cell lung cancer cells via G0/G1 phase arrest. Oncol Rep. 2016; 35:3409–3418. [PubMed: 27109614]

Quick KL, Ali SS, Arch R, Xiong C, Wozniak D, Dugan LL. A carboxyfullerene SOD mimetic improves cognition and extends the lifespan of mice. Neurobiol Aging. 2008; 29:117–128. [PubMed: 17079053]

Quinn JP. Neuronal-specific gene expression–the interaction of both positive and negative transcriptional regulators. Prog Neurobiol. 1996; 50:363–379. [PubMed: 9004350]

Ramakrishna S, Kwaku Dad AB, Beloor J, Gopalappa R, Lee SK, Kim H. Gene disruption by cell-penetrating peptide-mediated delivery of Cas9 protein and guide RNA. Genome Res. 2014; 24:1020–1027. [PubMed: 24696462]

Ramamoorth M, Narvekar A. Non viral vectors in gene therapy- an overview. J Clin Diagn Res. 2015; 9:GE01–GE06.

Rannals MD, Hamersky GR, Page SC, Campbell MN, Briley A, Gallo RA, Phan BN, Hyde TM, Kleinman JE, Shin JH, et al. Psychiatric Risk Gene Transcription Factor 4 Regulates Intrinsic Excitability of Prefrontal Neurons via Repression of SCN10a and KCNQ1. Neuron. 2016a; 90:43–55. [PubMed: 26971948]

Rannals MD, Page SC, Campbell MN, Gallo RA, Mayfield B, Maher BJ. Neurodevelopmental models of transcription factor 4 deficiency converge on a common ion channel as a potential therapeutic target for Pitt Hopkins syndrome. Rare Dis. 2016b; 4:e1220468. [PubMed: 28032012]

Reimsnider S, Manfredsson FP, Muzyczka N, Mandel RJ. Time course of transgene expression after intrastriatal pseudotyped rAAV2/1, rAAV2/2, rAAV2/5, and rAAV2/8 transduction in the rat. Mol Ther. 2007; 15:1504–1511. [PubMed: 17565350]

Remedios R, Huilgol D, Saha B, Hari P, Bhatnagar L, Kowalczyk T, Hevner RF, Suda Y, Aizawa S, Ohshima T, et al. A stream of cells migrating from the caudal telencephalon reveals a link between the amygdala and neocortex. Nat Neurosci. 2007; 10:1141–1150. [PubMed: 17694053]

Rivera VM, Gao GP, Grant RL, Schnell MA, Zoltick PW, Rozamus LW, Clackson T, Wilson JM. Long-term pharmacologically regulated expression of erythropoietin in primates following AAV-mediated gene transfer. Blood. 2005; 105:1424–1430. [PubMed: 15507527]

Roessler BJ, Davidson BL. Direct plasmid mediated transfection of adult murine brain cells in vivo using cationic liposomes. Neurosci Lett. 1994; 167:5–10. [PubMed: 8177529]

Ross PC, Hui SW. Lipoplex size is a major determinant of in vitro lipofection efficiency. Gene Ther. 1999; 6:651–659. [PubMed: 10476225]

Saba R, Nakatsuji N, Saito T. Mammalian BarH1 confers commissural neuron identity on dorsal cells in the spinal cord. J Neurosci. 2003; 23:1987–1991. [PubMed: 12657654]

Saito T. In vivo electroporation in the embryonic mouse central nervous system. Nat Protoc. 2006; 1:1552–1558. [PubMed: 17406448]

Saito T, Nakatsuji N. Efficient gene transfer into the embryonic mouse brain using in vivo electroporation. Dev Biol. 2001; 240:237–246. [PubMed: 11784059]

Samulski RJ, Muzyczka N. AAV-Mediated Gene Therapy for Research and Therapeutic Purposes. Annu Rev Virol. 2014; 1:427–451. [PubMed: 26958729]

Sanchez-Rivera FJ, Jacks T. Applications of the CRISPR-Cas9 system in cancer biology. Nat Rev Cancer. 2015; 15:387–395. [PubMed: 26040603]

Santos JL, Oliveira H, Pandita D, Rodrigues J, Pego AP, Granja PL, Tomas H. Functionalization of poly(amidoamine) dendrimers with hydrophobic chains for improved gene delivery in mesenchymal stem cells. J Control Release. 2010; 144:55–64. [PubMed: 20138937]

Sapet C, Pellegrino C, Laurent N, Sicard F, Zelphati O. Magnetic nanoparticles enhance adenovirus transduction in vitro and in vivo. Pharm Res. 2012; 29:1203–1218. [PubMed: 22146803]

Scherer F, Anton M, Schillinger U, Henke J, Bergemann C, Kruger A, Gansbacher B, Plank C. Magnetofection: enhancing and targeting gene delivery by magnetic force in vitro and in vivo. Gene Ther. 2002; 9:102–109. [PubMed: 11857068]

Schmidt F, Grimm D. CRISPR genome engineering and viral gene delivery: a case of mutual attraction. Biotechnol J. 2015; 10:258–272. [PubMed: 25663455]

Schwab LC, Richetin K, Barker RA, Deglon N. Formation of hippocampal mHTT aggregates leads to impaired spatial memory, hippocampal activation and adult neurogenesis. Neurobiol Dis. 2017; 102:105–112. [PubMed: 28286179]

Shevtsova Z, Malik JM, Michel U, Bahr M, Kugler S. Promoters and serotypes: targeting of adeno-associated virus vectors for gene transfer in the rat central nervous system in vitro and in vivo. Exp Physiol. 2005; 90:53–59. [PubMed: 15542619]

Sheyn D, Kimelman-Bleich N, Pelled G, Zilberman Y, Gazit D, Gazit Z. Ultrasound-based nonviral gene delivery induces bone formation in vivo. Gene Ther. 2008; 15:257–266. [PubMed: 18033309]

Shi L, Tang GP, Gao SJ, Ma YX, Liu BH, Li Y, Zeng JM, Ng YK, Leong KW, Wang S. Repeated intrathecal administration of plasmid DNA complexed with polyethylene glycol-grafted polyethylenimine led to prolonged transgene expression in the spinal cord. Gene Ther. 2003; 10:1179–1188. [PubMed: 12833127]

Shimamura M, Sato N, Taniyama Y, Yamamoto S, Endoh M, Kurinami H, Aoki M, Ogihara T, Kaneda Y, Morishita R. Development of efficient plasmid DNA transfer into adult rat central nervous system using microbubble-enhanced ultrasound. Gene Ther. 2004; 11:1532–1539. [PubMed: 15269716]

Shinmyo Y, Tanaka S, Tsunoda S, Hosomichi K, Tajima A, Kawasaki H. CRISPR/Cas9-mediated gene knockout in the mouse brain using in utero electroporation. Sci Rep. 2016; 6:20611. [PubMed: 26857612]

Singh R, Pantarotto D, McCarthy D, Chaloin O, Hoebeke J, Partidos CD, Briand JP, Prato M, Bianco A, Kostarelos K. Binding and condensation of plasmid DNA onto functionalized carbon nanotubes: toward the construction of nanotube-based gene delivery vectors. J Am Chem Soc. 2005; 127:4388–4396. [PubMed: 15783221]

Smith-Arica JR, Morelli AE, Larregina AT, Smith J, Lowenstein PR, Castro MG. Cell-type-specific and regulatable transgenesis in the adult brain: adenovirus-encoded combined transcriptional targeting and inducible transgene expression. Mol Ther. 2000; 2:579–587. [PubMed: 11124058]

Sohn J, Takahashi M, Okamoto S, Ishida Y, Furuta T, Hioki H. A Single Vector Platform for High-Level Gene Transduction of Central Neurons: Adeno-Associated Virus Vector Equipped with the Tet-Off System. PLoS One. 2017; 12:e0169611. [PubMed: 28060929]

Soma M, Aizawa H, Ito Y, Maekawa M, Osumi N, Nakahira E, Okamoto H, Tanaka K, Yuasa S. Development of the mouse amygdala as revealed by enhanced green fluorescent protein gene transfer by means of in utero electroporation. J Comp Neurol. 2009; 513:113–128. [PubMed: 19107806]

Sonego M, Zhou Y, Oudin MJ, Doherty P, Lalli G. In vivo postnatal electroporation and time-lapse imaging of neuroblast migration in mouse acute brain slices. J Vis Exp. 2013; (81)

Song G, Petschauer JS, Madden AJ, Zamboni WC. Nanoparticles and the mononuclear phagocyte system: pharmacokinetics and applications for inflammatory diseases. Curr Rheumatol Rev. 2014; 10:22–34. [PubMed: 25229496]

Song HP, Yang JY, Lo SL, Wang Y, Fan WM, Tang XS, Xue JM, Wang S. Gene transfer using self-assembled ternary complexes of cationic magnetic nanoparticles, plasmid DNA and cell-penetrating Tat peptide. Biomaterials. 2010; 31:769–778. [PubMed: 19819012]

Soto-Sanchez C, Martinez-Navarrete G, Humphreys L, Puras G, Zarate J, Pedraz JL, Fernandez E. Enduring high-efficiency in vivo transfection of neurons with non-viral magnetoparticles in the rat visual cortex for optogenetic applications. Nanomed : Nanotechnol, Biol, Med. 2015; 11:835–843.

Southgate T, Kroeger KM, Liu C, Lowenstein PR, Castro MG. Gene transfer into neural cells in vitro using adenoviral vectors. Curr Protoc Neurosci. 2008 (Unit 4), 23 Chapter 4.

Spaete RR, Frenkel N. The herpes simplex virus amplicon: a new eucaryotic defective-virus cloning-amplifying vector. Cell. 1982; 30:295–304. [PubMed: 6290080]

Staahl BT, Benekareddy M, Coulon-Bainier C, Banfal AA, Floor SN, Sabo JK, Urnes C, Munares GA, Ghosh A, Doudna JA. Efficient genome editing in the mouse brain by local delivery of engineered Cas9 ribonucleoprotein complexes. Nat Biotechnol. 2017; 35:431–434. [PubMed: 28191903]

Straub C, Granger AJ, Saulnier JL, Sabatini BL. CRISPR/Cas9-mediated gene knock-down in post-mitotic neurons. PLoS One. 2014; 9:e105584. [PubMed: 25140704]

Sun M, Zhang GR, Kong L, Holmes C, Wang X, Zhang W, Goldstein DS, Geller AI. Correction of a rat model of Parkinson's disease by coexpression of tyrosine hydroxylase and aromatic amino acid decarboxylase from a helper virus-free herpes simplex virus type 1 vector. Hum Gene Ther. 2003; 14:415–424. [PubMed: 12691607]

Szczurkowska J, Cwetsch AW, dal Maschio M, Ghezzi D, Ratto GM, Cancedda L. Targeted in vivo genetic manipulation of the mouse or rat brain by in utero electroporation with a triple-electrode probe. Nat Protoc. 2016; 11:399–412. [PubMed: 26844428]

Szczurkowska J, dal Maschio M, Cwetsch AW, Ghezzi D, Bony G, Alabastri A, Zaccaria RP, di Fabrizio E, Ratto GM, Cancedda L. Increased performance in genetic manipulation by modeling the dielectric properties of the rodent brain. Conf Proc IEEE Eng Med Biol Soc. 2013; 2013:1615–1618. [PubMed: 24110012]

Tabata H, Nakajima K. Efficient in utero gene transfer system to the developing mouse brain using electroporation: visualization of neuronal migration in the developing cortex. Neuroscience. 2001; 103:865–872. [PubMed: 11301197]

Tabata H, Nakajima K. Labeling embryonic mouse central nervous system cells by in utero electroporation. Dev Growth Differ. 2008; 50:507–511. [PubMed: 18482404]

Takeuchi I, Onaka H, Makino K. Biodistribution of colloidal gold nanoparticles after intravenous injection: Effects of PEGylation at the same particle size. Biomed Mater Eng. 2018; 29:205–215. [PubMed: 29457594]

Tan JK, Pham B, Zong Y, Perez C, Maris DO, Hemphill A, Miao CH, Matula TJ, Mourad PD, Wei H, et al. Microbubbles and ultrasound increase intraventricular polyplex gene transfer to the brain. J Control Release. 2016; 231:86–93. [PubMed: 26860281]

Tan VTY, Mockett BG, Ohline SM, Parfitt KD, Wicky HE, Peppercorn K, Schoderboeck L, Yahaya MFB, Tate WP, Hughes SM, et al. Lentivirus-mediated expression of human secreted amyloid precursor protein-alpha prevents development of memory and plasticity deficits in a mouse model of Alzheimer's disease. Mol Brain. 2018; 11:7. [PubMed: 29426354]

Tanaka DH, Maekawa K, Yanagawa Y, Obata K, Murakami F. Multidirectional and multizonal tangential migration of GABAergic interneurons in the developing cerebral cortex. Development. 2006; 133:2167–2176. [PubMed: 16672340]

Tanaka S, Uehara T, Nomura Y. Up-regulation of protein-disulfide isomerase in response to hypoxia/brain ischemia and its protective effect against apoptotic cell death. J Biol Chem. 2000; 275:10388–10393. [PubMed: 10744727]

Taniguchi Y, Young-Pearse T, Sawa A, Kamiya A. In utero electroporation as a tool for genetic manipulation in vivo to study psychiatric disorders: from genes to circuits and behaviors. Neuroscientist. 2012; 18:169–179. [PubMed: 21551077]

Taniyama Y, Morishita R. [Development of plasmid DNA-based gene transfer]. Yakugaku Zasshi. 2006; 126:1039–1045. [PubMed: 17077610]

Thomas CE, Ehrhardt A, Kay MA. Progress and problems with the use of viral vectors for gene therapy. Nat Rev Genet. 2003; 4:346–358. [PubMed: 12728277]

Titomirov AV, Sukharev S, Kistanova E. In vivo electroporation and stable transformation of skin cells of newborn mice by plasmid DNA. Biochim Biophys Acta. 1991; 1088:131–134. [PubMed: 1703441]

Tomita K, Kubo K, Ishii K, Nakajima K. Disrupted-in-Schizophrenia-1 (Disc1) is necessary for migration of the pyramidal neurons during mouse hippocampal development. Hum Mol Genet. 2011; 20:2834–2845. [PubMed: 21540240]

Towne C, Thompson KR. Overview on Research and Clinical Applications of Optogenetics. Curr Protoc Pharmacol. 2016; 75(11):1911–1921.

Tsunekawa Y, Terhune RK, Fujita I, Shitamukai A, Suetsugu T, Matsuzaki F. Developing a de novo targeted knock-in method based on in utero electroporation into the mammalian brain. Development. 2016; 143:3216–3222. [PubMed: 27578183]

Vega RA, Zhang Y, Curley C, Price RL, Abounader R. 370 Magnetic Resonance-Guided Focused Ultrasound Delivery of Polymeric Brain-Penetrating Nanoparticle MicroRNA Conjugates in Glioblastoma. Neurosurgery. 2016; 63(Suppl. 1):210.

Vomund S, Sapir T, Reiner O, Silva MA, Korth C. Generation of topically transgenic rats by in utero electroporation and in vivo bioluminescence screening. J Vis Exp. 2013:e50146. [PubMed: 24084570]

Walters BJ, Azam AB, Gillon CJ, Josselyn SA, Zovkic IB. Advanced In vivo Use of CRISPR/Cas9 and Anti-sense DNA Inhibition for Gene Manipulation in the Brain. Front Genet. 2015; 6:362. [PubMed: 26793235]

Wang K. Manipulating Potassium Channel Expression and Function in Hippocampal Neurons by In Utero Electroporation. Methods Mol Biol. 2018; 1684:1–5. [PubMed: 29058179]

Wang M, Zuris JA, Meng F, Rees H, Sun S, Deng P, Han Y, Gao X, Pouli D, Wu Q, et al. Efficient delivery of genome-editing proteins using bioreducible lipid nanoparticles. Proc Natl Acad Sci U S A. 2016; 113:2868–2873. [PubMed: 26929348]

Wang S, Karakatsani ME, Fung C, Sun T, Acosta C, Konofagou E. Direct brain infusion can be enhanced with focused ultrasound and microbubbles. J Cereb Blood Flow Metab. 2017; 37:706–714. [PubMed: 26969468]

Wang S, Ma N, Gao SJ, Yu H, Leong KW. Transgene expression in the brain stem effected by intramuscular injection of polyethylenimine/DNA complexes. Mol Ther. 2001; 3:658–664. [PubMed: 11356070]

Wang W, Xiong W, Wan J, Sun X, Xu H, Yang X. The decrease of PAMAM dendrimer-induced cytotoxicity by PEGylation via attenuation of oxidative stress. Nanotechnology. 2009; 20:105103. [PubMed: 19417510]

Widder KJ, Senyei AE, Scarpelli GD. Magnetic microspheres: a model system of site specific drug delivery in vivo. Proc Soc Exp Biol Med. 1978; 158:141–146. [PubMed: 674215]

Wijaya A, Hamad-Schifferli K. Ligand customization and DNA functionalization of gold nanorods via round-trip phase transfer ligand exchange. Langmuir. 2008; 24:9966–9969. [PubMed: 18717601]

Wollmann G, Tattersall P, van den Pol AN. Targeting human glioblastoma cells: comparison of nine viruses with oncolytic potential. J Virol. 2005; 79:6005–6022. [PubMed: 15857987]

Wu J. Temperature rise generated by ultrasound in the presence of contrast agent. Ultrasound Med Biol. 1998; 24:267–274. [PubMed: 9550185]

Yadav S, Gandham SK, Panicucci R, Amiji MM. Intranasal brain delivery of cationic nanoemulsion-encapsulated TNFalpha siRNA in prevention of experimental neuroinflammation. Nanomed : Nanotechnol, Biol, Med. 2016; 12:987–1002.

Yamada M, Seto Y, Taya S, Owa T, Inoue YU, Inoue T, Kawaguchi Y, Nabeshima Y, Hoshino M. Specification of spatial identities of cerebellar neuron progenitors by ptf1a and atoh1 for proper production of GABAergic and glutamatergic neurons. J Neurosci. 2014; 34:4786–4800. [PubMed: 24695699]

Yan Z, Zak R, Zhang Y, Engelhardt JF. Inverted terminal repeat sequences are important for intermolecular recombination and circularization of adeno-associated virus genomes. J Virol. 2005; 79:364–379. [PubMed: 15596830]

Yang R, Yang X, Zhang Z, Zhang Y, Wang S, Cai Z, Jia Y, Ma Y, Zheng C, Lu Y, et al. Single-walled carbon nanotubes-mediated in vivo and in vitro delivery of siRNA into antigen-presenting cells. Gene Ther. 2006; 13:1714–1723. [PubMed: 16838032]

Yang S, Chang R, Yang H, Zhao T, Hong Y, Kong HE, Sun X, Qin Z, Jin P, Li S, et al. CRISPR/Cas9-mediated gene editing ameliorates neurotoxicity in mouse model of Huntington's disease. J Clin Invest. 2017; 127:2719–2724. [PubMed: 28628038]

Yin H, Kanasty RL, Eltoukhy AA, Vegas AJ, Dorkin JR, Anderson DG. Non-viral vectors for gene-based therapy. Nat Rev Genet. 2014; 15:541–555. [PubMed: 25022906]

Yin WL, Yin WG, Huang BS, Wu LX. Neuroprotective effects of lentivirus-mediated cystathionine-beta-synthase overexpression against 6-OHDA-induced parkinson's disease rats. Neurosci Lett. 2017; 657:45–52. [PubMed: 28764908]

Yoon SO, Lois C, Alvirez M, Alvarez-Buylla A, Falck-Pedersen E, Chao MV. Adenovirus-mediated gene delivery into neuronal precursors of the adult mouse brain. Proc Natl Acad Sci U S A. 1996; 93:11974–11979. [PubMed: 8876247]

Yu X, Liang X, Xie H, Kumar S, Ravinder N, Potter J, de Mollerat du Jeu X, Chesnut JD. Improved delivery of Cas9 protein/gRNA complexes using lipofectamine CRISPRMAX. Biotechnol Lett. 2016; 38:919–929. [PubMed: 26892225]

Zarebkohan A, Najafi F, Moghimi HR, Hemmati M, Deevband MR, Kazemi B. Synthesis and characterization of a PAMAM dendrimer nanocarrier functionalized by SRL peptide for targeted gene delivery to the brain. Eur J Pharm Sci. 2015; 78:19–30. [PubMed: 26118442]

Zhang H, Yang B, Mu X, Ahmed SS, Su Q, He R, Wang H, Mueller C, Sena-Esteves M, Brown R, et al. Several rAAV vectors efficiently cross the blood-brain barrier and transduce neurons and astrocytes in the neonatal mouse central nervous system. Mol Ther. 2011; 19:1440–1448. [PubMed: 21610699]

Zhang L, Yu F, Cole AJ, Chertok B, David AE, Wang J, Yang VC. Gum arabic-coated magnetic nanoparticles for potential application in simultaneous magnetic targeting and tumor imaging. AAPS J. 2009; 11:693–699. [PubMed: 19842043]

Zhang Y, Petibone D, Xu Y, Mahmood M, Karmakar A, Casciano D, Ali S, Biris AS. Toxicity and efficacy of carbon nanotubes and graphene: the utility of carbon-based nanoparticles in nanomedicine. Drug Metab Rev. 2014; 46:232–246. [PubMed: 24506522]

Zhao G, Huang Q, Wang F, Zhang X, Hu J, Tan Y, Huang N, Wang Z, Wang Z, Cheng Y. Targeted shRNA-loaded liposome complex combined with focused ultrasound for blood brain barrier disruption and suppressing glioma growth. Cancer Lett. 2018; 418:147–158. [PubMed: 29339208]

Zhao MG, Toyoda H, Lee YS, Wu LJ, Ko SW, Zhang XH, Jia Y, Shum F, Xu H, Li BM, et al. Roles of NMDA NR2B subtype receptor in prefrontal long-term potentiation and contextual fear memory. Neuron. 2005; 47:859–872. [PubMed: 16157280]

Zhi D, Bai Y, Yang J, Cui S, Zhao Y, Chen H, Zhang S. A review on cationic lipids with different linkers for gene delivery. Adv Colloid Interface Sci. 2018; 253:117–140. [PubMed: 29454463]

Zuris JA, Thompson DB, Shu Y, Guilinger JP, Bessen JL, Hu JH, Maeder ML, Joung JK, Chen ZY, Liu DR. Cationic lipid-mediated delivery of proteins enables efficient protein-based genome editing in vitro and in vivo. Nat Biotechnol. 2015; 33:73–80. [PubMed: 25357182]

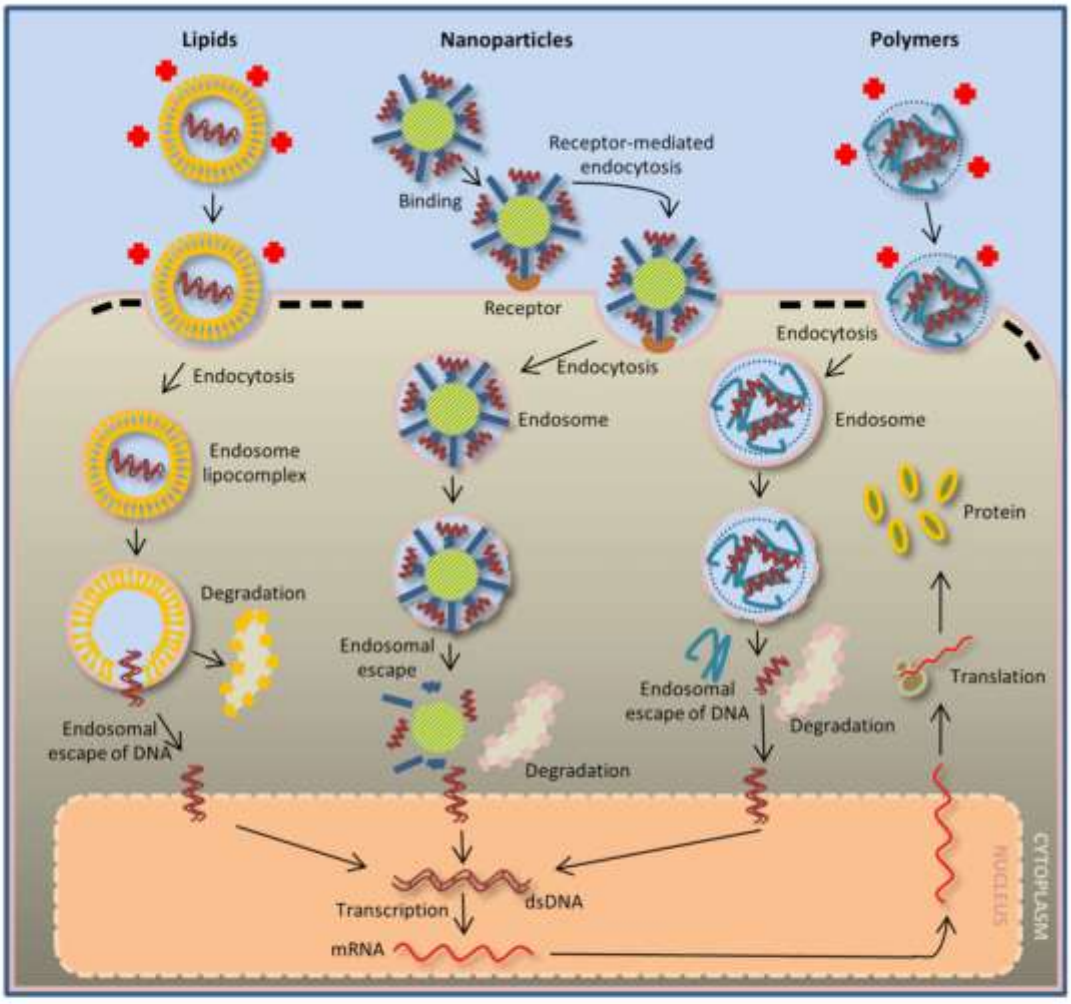

Fig. 1. Chemical methods of gene delivery.

Lipid-mediated gene transfer (left) occurs by the interaction between the positively charged surface of the carriers and the negatively charged cell membrane. This interaction promotes endocytosis, creating an endosome lipocomplex. The complex is then degraded in the cell cytoplasm, and the released DNA is transported to the nucleus. *Nanoparticle*-mediated gene transfer (middle) occurs by the nanoparticles binding to receptors on the cell surface, followed by endocytosis. During endosome degradation in the cell cytoplasm, the DNA attached to the core of the nanoparticles is released and transported to the nucleus. Similar to lipid-mediated gene transfer, *polymer*-mediated gene transfer (right) occurs *via* charge differences between the carriers and the cell membrane, which promotes binding and endocytosis. During endosome degradation, the DNA is released from the polymer structure

and is transported to the nucleus. After DNA transcription, the mRNA exits the nucleus, and it is translated into a protein in the cytoplasm.

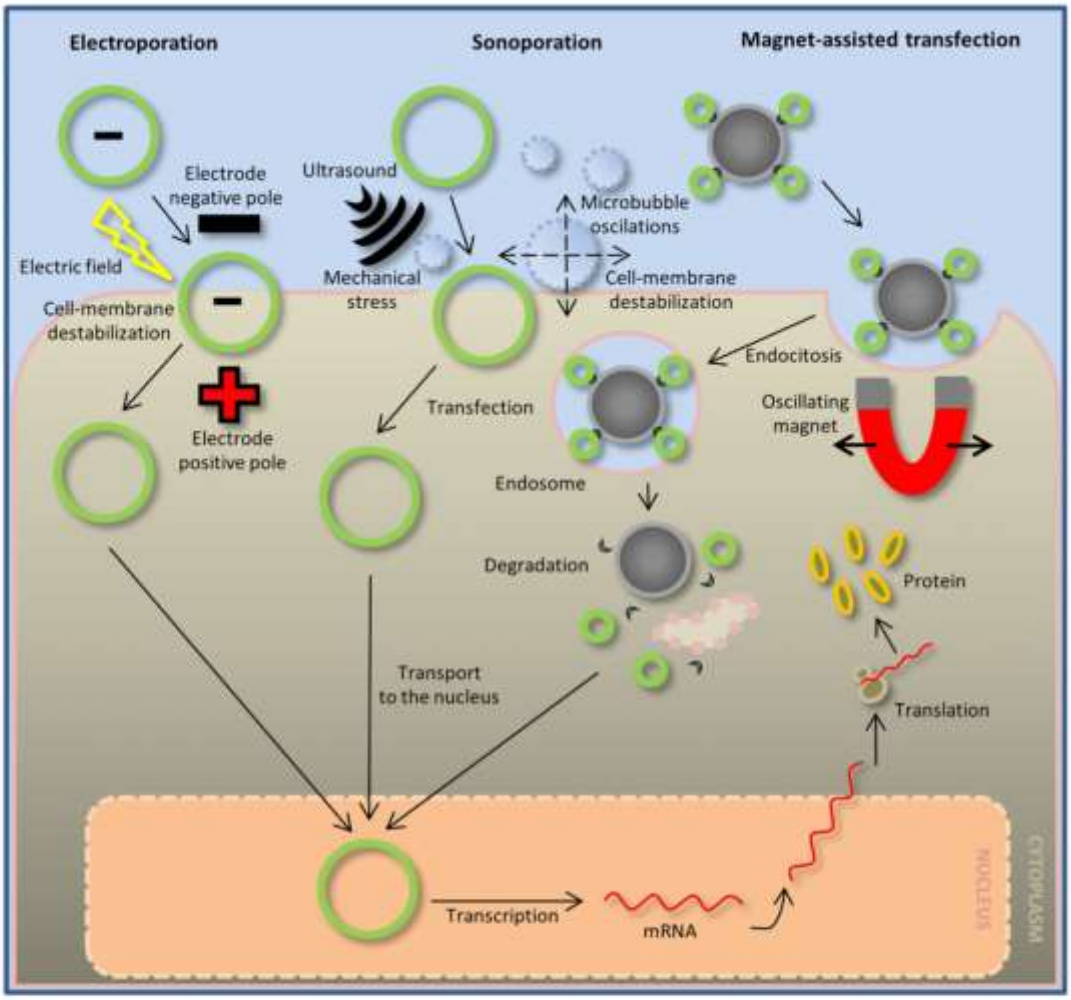

Fig. 2. Physical methods of gene delivery.

Electroporation-mediated gene transfer (left) enables the directional guidance of plasmids carrying the negatively charged DNA of interest towards the positive pole of the electrode. At the same time, electroporation causes destabilization of the structure of the cell membrane, creating temporary pores in its surface and allowing the plasmid to enter the cell. The plasmid is then transported to the nucleus. *Sonoporation*-mediated gene transfer (middle) occurs by ultrasound application, which promotes destabilization of the cell membrane in the presence of oscillating microbubbles. During this process, the plasmid contained in the microbubble mixture enters the cell and is then transported to the nucleus. *Magnet*-assisted transfection (right) is mediated by magnetic field oscillations that guide and promote endocytosis of the magnetic carriers with attached DNA. In the cytoplasm of the

cell, the endosome undergoes degradation and the released DNA enters the cell nucleus. After DNA transcription, the mRNA exits the nucleus, and it is translated into a protein in the cytoplasm.

Europe PMC Funders Author Manuscripts

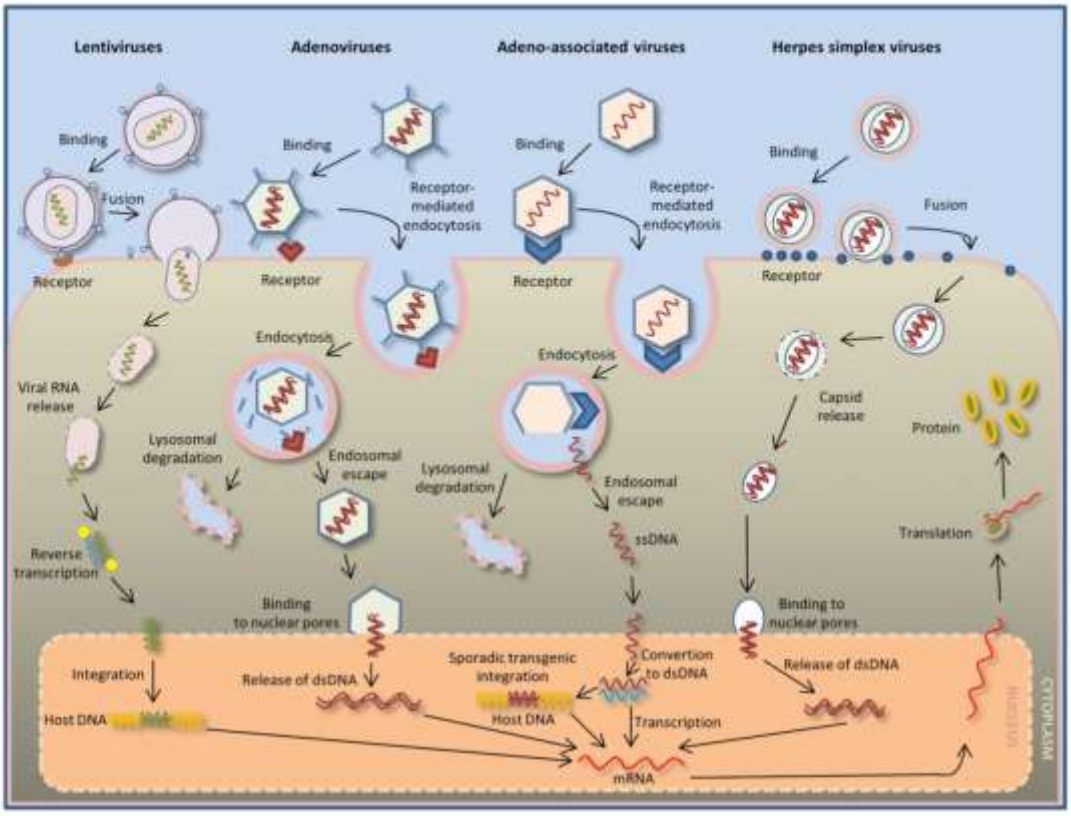

Fig. 3. Virus-mediated transduction.

A *lentivirus* (left) can carry RNA inside its capsid. Contact with cell-specific receptors induces the fusion of the capsid with the cell membrane, followed by RNA release. In the cell cytoplasm, the released RNA undergoes reverse transcription, and upon transport to the nucleus, the RNA is integrated with the host DNA. *Adenovirus* infection (middle left) is mediated by specific receptor binding on the cell membrane, followed by endocytosis. Endosome degradation then results in the release of the virus capsid and lysosomal degradation of the endosome. The released virus capsid binds to the nuclear pore of the infected-cell nucleus, allowing the introduction of the double-stranded DNA inside the nucleus. *Adeno-associated virus* infection (middle right) is mediated by receptor binding on the host-cell surface and endocytosis. Endosome degradation results in the release of single-stranded DNA. The single-stranded DNA enters the nucleus and undergoes a conversion to double-stranded DNA, which can be either integrated in the host DNA (and later transcribed) or can remain in the host cell nucleus as nonintegrated viral DNA. *Herpes simplex virus*-mediated gene delivery (right) is the result of receptor binding and fusion of the virus with the cell membrane of the host cell. Inside the cell, the released capsid binds to the nuclear pore and introduces double-stranded DNA into the nucleus to be transcribed. The

viral DNA in the host cell nucleus is transcribed into mRNA. The transcribed viral mRNA exits the nucleus, and it is translated into a protein in the cytoplasm of the host cell.

Europe PMC Funders Author Manuscripts

Table 1

Chemical methods for transfection.

Group	Type/Helper	Toxicity	*In vivo* delivery method	Efficiency/Stability	BBB accessibility	Most Prominent Applications (references)
Lipids	Liposomes	→*	N/A	↓	N/A	Nayerossadat et al., 2012
	Cationic lipid mix/PEG	↓	Intraventricular injection	→	N/A	Hassani et al., 2005; Nayerossadat et al., 2012; Yin et al., 2014;Zhi et al., 2018
	Cationic lipid mix/DOPE	↓	Intraventricular injection, Intratumoral (glioblastoma) injection	↑	N/A	Roessler and Davidson et al., 1994; Hassani et al., 2005; Pulkkanen and Yla-Herttuala, 2005; Lagarce and Passirani, 2016;Cikankowitz et al., 2017
	Lipid Nanoemulsions	↓	Intranasal	↑	N/A	Ramamoorth and Narvekar, 2015; Yadav et al., 2016
	Solid lipid nanoparticles	↓	Intravenous injection	↑	Possibly	Jin et al., 2011; Pathak et al., 2017
Nanoparticles	Silica	↓	Subventricular injection, Intracortical injection	↑	N/A	Bharali et al., 2005; Luo and Saltzman, 2006
	Gold nanoparticles	↓	Systemic injection	→	+	Jensen et al., 2013; Escudero-Francos et al., 2017; Takeuchi et al., 2018; Hu et al., 2018
	Carbon Nanotubes	↓	Intraventricular injection	↑	N/A	Al-Jamal et al., 2011; Costa et al., 2016
Polymers	Polyethylenimine	↑	Intracortical injection	↓	(+ with PEG)	Abdallah et al., 1996; Lungwitz et al., 2005; Nouri et al., 2017
	Polyethylenimine/RVG	↑	Tail injection	↓	+	Hwang et al., 2011
	Chitosans/PEG	↓	Intratumoral (glioblastoma) injection	↑	–	Duceppe and Tabrizian, 2010; Danhier et al., 2015; Ramamoorth and Narvekar, 2015
	Chitosans Trimethylated/PEG + RVG	↓	Intravenous injection	↑	+	Gao et al., 2014
	Polyamidoamine (with various functionalizations)	↓	Tail injection, Systemic injection, Intravenous administration	↑	+	Huang et al., 2007;Huang et al., 2008;Ke et al., 2009;Zarebkohan et al., 2015

↓high / →medium / ↓low / +yes / -no / N/A-information not available.

Europe PMC Funders Author Manuscripts

Table 2

Physical methods for transfection.

Group	Type/Helper	Toxicity	*In vivo* delivery method	Efficiency/Stability	BBB accessibility	Most Prominent Applications (references)
Electroporation	*In utero*	↓	Intraventricular injection	↑	N/A	Saito, 2006;Dal Maschio et al., 2012;Szczurkowska et al., 2016
	Exo utero	↓	Intraventricular injection	↑	N/A	Akamatsu et al., 1999; Saba et al., 2003
	Postnatal	↓	Intraventricular injection, Stereotaxic micro injection	↑	N/A	Boutin et al., 2008; Chesler et al., 2008;Kitamura et al., 2008
Sonoporation	Microbubbles	→	Systemic injection, Intraventricular injection	↓	–	Endoh et al., 2002;Tan et al., 2016
Magnet-assisted transfection	Magnetic nanoparticles/PEI	↓	Lumbar intrathecal injection, Stereotaxic injection	→	–	Song et al., 2010;Soto-Sanchez et al., 2015

↑high / →medium / ↓low / +yes / -no / N/A-information not available.

Table 3

Virus-mediated transduction.

Group	Type / Helper	Toxicity	*In vivo* delivery method	Efficiency /Stability	BBB accessibility	Most Prominent Applications (references)
Lentivirus	HIV / VSV-G	↓	Stereotaxic micro injection	↑	N/A	Naldini et al., 1996a; Mah et al., 2002b;Artegiani and Calegari et al., 2013
Adenovirus	Replication-defective ADV	↑	Stereotaxic micro injection, Intraventricular injection	↑	N/A	Yoon et al., 1996;Germano et al., 2003
Adeno-associated virus	AAV	↓	Stereotaxic micro injection	↑	N/A	Mah et al., 2000; Kay et al., 2001;Mah et al., 2002a
	AAV-DJ	↓	Stereotaxic micro injection, Intravenous injection	↑	+	Grimm et al., 2008; Duque et al., 2009; Foust et al., 2009Gray et al., 2010; Bourdenx et al., 2014
Herpes simplex virus	HSV / helper virus	→	Stereotaxic micro injection	↑	N/A	Spaete and Frenkel, 1982; Krisky et al., 1998; Sun et al., 2003

↑high / →medium / ↓low / +yes / -no / N/A-information not available.

Appendix II

APache Is an AP2-Interacting Protein Involved in Synaptic Vesicle Trafficking and Neuronal Development.

Piccini A, Castroflorio E, Valente P, Guarnieri FC, Aprile D, Michetti C, Bramini M, Giansante G, Pinto B, Savardi A, Cesca F, Bachi A, Cattaneo A, Wren JD, Fassio A, Valtorta F, Benfenati F, Giovedì S.

Article

Cell Reports

APache Is an AP2-Interacting Protein Involved in Synaptic Vesicle Trafficking and Neuronal Development

Graphical Abstract

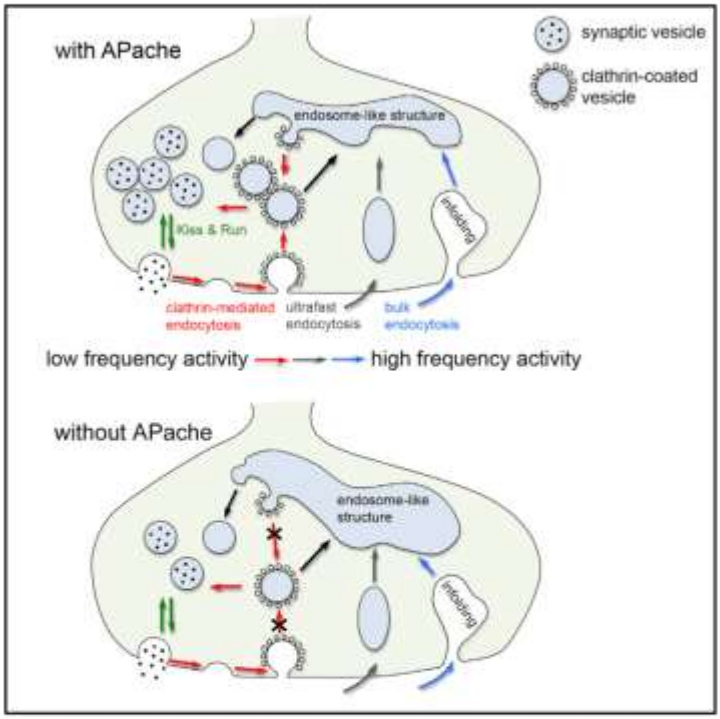

Authors

Alessandra Piccini, Enrico Castroflorio, Pierluigi Valente, ..., Flavia Valtorta, Fabio Benfenati, Silvia Giovedì

Correspondence

fabio.benfenati@iit.it (F.B.),
silvia.giovedi@unige.it (S.G.)

In Brief

Piccini et al. uncovered the AP2-interacting protein APache that acts in the clathrin-mediated endocytic machinery and synaptic vesicle trafficking. They found that silencing APache impairs neuronal development and neurotransmitter release during repetitive stimulation by markedly reducing vesicle recycling.

Highlights

- APache is a presynaptic AP2 interactor on clathrin-coated vesicles
- APache silencing affects the early neuronal development *in vitro* and *in vivo*
- APache-silenced synapses exhibit a marked endocytic phenotype
- APache silencing impairs clathrin-mediated endocytosis and synaptic function

Piccini et al., 2017, Cell Reports *21*, 3596–3611
December 19, 2017
https://doi.org/10.1016/j.celrep.2017.11.073

CellPress

OPEN ACCESS
CellPress

Cell Reports
Article

APache Is an AP2-Interacting Protein Involved in Synaptic Vesicle Trafficking and Neuronal Development

Alessandra Piccini,[1] Enrico Castroflorio,[2] Pierluigi Valente,[1] Fabrizia C. Guarnieri,[3] Davide Aprile,[1] Caterina Michetti,[2] Mattia Bramini,[2] Giorgia Giansante,[1] Bruno Pinto,[4,5] Annalisa Savardi,[1,4] Fabrizia Cesca,[2] Angela Bachi,[6] Angela Cattaneo,[6] Jonathan D. Wren,[7] Anna Fassio,[1,2] Flavia Valtorta,[3] Fabio Benfenati,[1,2,8,*] and Silvia Giovedì[1,8,9,*]

[1]Department of Experimental Medicine, University of Genova, 16132 Genova, Italy
[2]Center for Synaptic Neuroscience and Technology, Istituto Italiano di Tecnologia, 16132 Genova, Italy
[3]San Raffaele Scientific Institute and Vita Salute University, 20132 Milano, Italy
[4]Local Micro-environment and Brain Development Laboratory, Istituto Italiano di Tecnologia, 16163 Genova, Italy
[5]Bio@SNS, Scuola Normale Superiore, 56126 Pisa, Italy
[6]IFOM, FIRC Institute of Molecular Oncology, 20132 Milano, Italy
[7]Department of Arthritis and Clinical Immunology, Oklahoma Medical Research Foundation, Oklahoma City, OK 73104-5005, USA
[8]These authors contributed equally
[9]Lead Contact
*Correspondence: fabio.benfenati@iit.it (F.B.), silvia.giovedi@unige.it (S.G.)
https://doi.org/10.1016/j.celrep.2017.11.073

SUMMARY

Synaptic transmission is critically dependent on synaptic vesicle (SV) recycling. Although the precise mechanisms of SV retrieval are still debated, it is widely accepted that a fundamental role is played by clathrin-mediated endocytosis, a form of endocytosis that capitalizes on the clathrin/adaptor protein complex 2 (AP2) coat and several accessory factors. Here, we show that the previously uncharacterized protein KIAA1107, predicted by bioinformatics analysis to be involved in the SV cycle, is an AP2-interacting clathrin-endocytosis protein (APache). We found that APache is highly enriched in the CNS and is associated with clathrin-coated vesicles via interaction with AP2. APache-silenced neurons exhibit a severe impairment of maturation at early developmental stages, reduced SV density, enlarged endosome-like structures, and defects in synaptic transmission, consistent with an impaired clathrin/AP2-mediated SV recycling. Our data implicate APache as an actor in the complex regulation of SV trafficking, neuronal development, and synaptic plasticity.

INTRODUCTION

High-frequency and sustained neurotransmitter release is dependent on the correct reformation of exocytosed synaptic vesicles (SVs) by efficient endocytosis. During physiological activity, clathrin-mediated endocytosis (CME) represents the best-characterized pathway for recycling of fully fused SVs (Heuser and Reese, 1973; Granseth et al., 2006; Dittman and Ryan, 2009; Saheki and De Camilli, 2012), although the precise mechanisms of SV membrane retrieval and functional SV reconstitution remain highly controversial (Soykan et al., 2016; Cousin, 2017).

At the plasma membrane, the most abundant adaptor coordinating coat recruitment and cargo selection into endocytic pits is the heterotetrameric adaptor protein complex 2 (AP2), comprised of two large α and β2 subunits, a medium-size μ2 subunit, and a small δ2 subunit. Among the numerous accessory proteins believed to control the internalization pathway (Slepnev and De Camilli, 2000), clathrin and AP2 constitute the two main protein interaction hubs, around which an extensive and highly dynamic endocytic network is organized to achieve clathrin-coated vesicle (CCV) formation (Schmid and McMahon, 2007). However, other alternate clathrin-associated sorting proteins (CLASP) have recently been identified for the internalization of selected cargo membrane proteins (Traub and Bonifacino, 2013). Thus, synapses have evolved distinct mechanisms to maintain membrane homeostasis and the dominant mode for SV recycling may depend on the type of neuron and its activity pattern (Valtorta et al., 2001; Kononenko and Haucke, 2015; Park et al., 2016). Despite intense research, much remains to be learned about the exact molecular components of the endocytic pathways.

Here, we characterize the highly conserved AP2-interacting clathrin-endocytosis protein APache (NP_001007575.2) and investigate its physiological role in neuronal development and synaptic function. APache is a neuron-specific protein, expressed in axonal processes and presynaptic terminals, that specifically interacts with AP2 on CCVs. Our data indicate that APache plays a role in neuronal development and is required to maintain normal SV recycling in mature neurons. APache can thus be considered an important actor of the clathrin-mediated endocytic machinery at the synapse that is required for normal synaptic transmission.

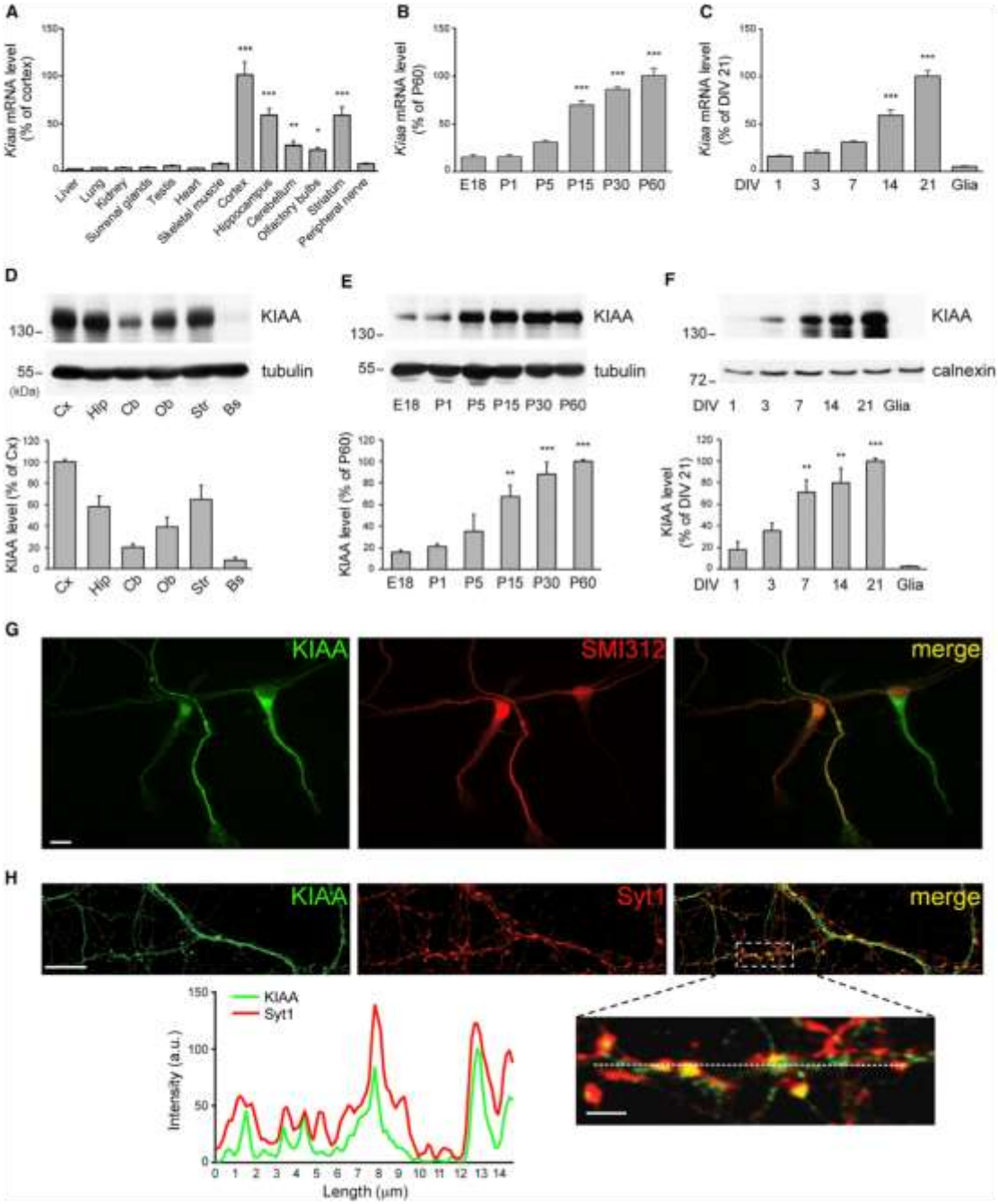

Figure 1. Expression and Localization of Endogenous KIAA1107 in Neurons

(A) Real-time PCR analysis of *Kiaa1107* mRNA levels in various mouse tissues. Means ± SEM of n = 3 animals; one-way ANOVA/Bonferroni's multiple comparison test; *p < 0.05; **p < 0.01; ***p < 0.001 versus liver.

(legend continued on next page)

RESULTS

Identification of KIAA1107 by GAMMA

Global Microarray Meta-Analysis (GAMMA) is a program previously developed to identify highly correlated transcripts within microarray experiments, which can then be used to infer function, phenotype, genetic network, and disease relevance for uncharacterized genes (Wren, 2009). GAMMA was used to search for uncharacterized genes associated with SV recycling, and KIAA1107 was the highest scoring gene without prior publications. The predicted phenotypes associated with KIAA1107 disruption, predicted disease relevance, and predicted cellular/anatomical structures of relevance to KIAA1107 activity are shown in Figure S1.

KIAA1107 is evolutionarily conserved from zebrafish to human. The murine *Kiaa1107* gene (official symbol: A830010M20Rik) is located on chromosome 5 (forward strand). According to the Ensembl database, the gene gives rise to five differentially spliced transcripts, four of which are predicted to be protein coding. Conversely, the NCBI database includes only two splicing variants (NCBI Refseq NM_001007574.2 and NM_001168557.1, corresponding to ENSMUST00000112671.8 and ENSMUST00000060553.7, respectively, in the Ensembl database). Among these two, one transcript codes for a protein of 1,088 amino acids (aas) and is considered the main isoform, whereas the other codes for a smaller protein of 443 aas. We cloned the major isoform, with an expected molecular mass of 117 kDa, and will refer to it as KIAA1107 throughout. No significant similarity with other proteins could be identified with a BLAST search of the murine KIAA1107 against the *Mus musculus* RefSeq protein database. No conserved protein domains were predicted using bioinformatics tools, such as SMART and InterProScan, but one coiled-coil region was predicted at aa position 820–841 with COILS2 (probability 62.9% with window 21; MTIDK matrix; no weights). Hence, the sequence of KIAA1107 does not reveal any particular information about its possible function or localization, but the GAMMA predictions on its involvement in synaptic function were really strong and persuaded us to investigate it further.

To characterize KIAA1107, we first generated a polyclonal antibody directed against a conserved region comprising aas 732–894 of the mouse ortholog (Figure S2A). The affinity-purified antibody recognized both overexpressed and endogenous KIAA1107 as a band of ~140 kDa in immunoblotting assays (Figures S2B and S2C). Its specificity was further proved by preadsorbing the primary antibody with a molar excess of the recombinant immunizing peptide (Figure S2D).

To silence KIAA1107 expression, we designed 3 short hairpin RNAs (shRNAs) based on the coding sequence (shRNA#1) and the 3′ UTR (shRNA#2 and #3) of the mouse *Kiaa1107* transcript, inserted them into a bicistronic lentiviral vector expressing the fluorescent reporter mCherry, and validated their specificity and efficacy by immunoblotting (Figures S2B and S2C). shRNA#2 was chosen for the subsequent studies, being the most active in knocking down the endogenous KIAA1107 expression. The specificity of the KIAA1107 antibody was subsequently demonstrated by immunocytochemistry of silenced neurons (Figure S2E).

KIAA1107 Is a Neuron-Specific and Developmentally Regulated Protein

We evaluated *Kiaa1107* mRNA and protein levels in various tissues and brain areas of adult mice and determined its developmental expression profile in the intact mouse cortex and primary neuronal cultures (Figures 1A–1F). KIAA1107 was primarily expressed in brain, with the highest mRNA and protein levels in the cerebral cortex, hippocampus, and striatum (Figures 1A and 1D). It was already present in the mouse brain at prenatal and early postnatal stages (embryonic day 18 [E18]–postnatal day 5 [P5]), and its expression increased during postnatal development to reach a plateau at 1 month of age (Figures 1B and 1E). A similar pattern was reproduced in primary cortical neurons, where *Kiaa1107* mRNA and protein levels were discernible at early stages of development (1–3 days in vitro [DIV]) and were greatly enhanced between 7 and 21 DIV (Figures 1C and 1F). Consistent with the strictly neuron-specific expression of the protein, KIAA1107 was not detected in primary astroglial cultures.

To examine the localization of KIAA1107 in neurons during development, 5 and 17 DIV primary cortical neurons were analyzed by immunocytochemistry. In early stages of *in vitro* development, KIAA1107 was expressed in the cell body and growing processes, including the axon, as shown by the colocalization with the pan-axonal neurofilament marker SMI312

(B) Real-time PCR analysis of *Kiaa1107* mRNA expression in the cerebral cortex of developing mice (from embryonic day 18 [E18] to postnatal day 60 [P60]). Means ± SEM of n = 3 animals/developmental stage; one-way ANOVA/Bonferroni's multiple comparison test; ***p < 0.001 versus E18.
(C) Real-time PCR analysis of *Kiaa1107* mRNA expression in primary cultures of cortical neurons at various stages of development (from 1 to 21 DIV). Means ± SEM of n = 3 independent cultures/developmental stage; one-way ANOVA/Bonferroni's multiple comparison test; ***p < 0.001 versus DIV 1.
(D) Regional expression of KIAA1107 in the adult mouse brain. Representative immunoblot (top) and relative densitometric quantification normalized on βIII tubulin levels (bottom) are shown. Means ± SEM of n = 4 animals. Bs, brain stem; Cb, cerebellum; Cx, cortex; Hip, hippocampus; Ob, olfactory bulb; Str, striatum.
(E) Temporal expression profile of KIAA1107 in the developing mouse cerebral cortex (from E18 to P60). Representative immunoblot of KIAA1107 levels (top) and relative densitometric quantification normalized on βIII tubulin (bottom) are shown. Means ± SEM of n = 3 animals/developmental stage; one-way ANOVA/Bonferroni's multiple comparison test; **p < 0.01; ***p < 0.001 versus E18.
(F) Temporal expression profile of KIAA1107 in primary cortical neurons at various stages of development (from 1 to 21 DIV). Representative immunoblot of KIAA1107 levels (top) and relative densitometric quantification normalized on calnexin (bottom) are shown. Means ± SEM of n = 3 independent neuronal cultures/developmental stage; one-way ANOVA/Bonferroni's multiple comparison test; **p < 0.01; ***p < 0.001 versus DIV 1.
(G and H) Localization of KIAA1107 in cultured neurons during development. Representative images of cortical neurons fixed and double stained for KIAA1107 (green) and SMI312 (red) at 5 DIV (G) or for KIAA1107 (green) and synaptotagmin-1 (Syt1) (red) at 17 DIV (H) are shown. The scale bars represent 10 μm. In the bottom panel, linear intensity profiles of KIAA1107 (green) and Syt1 (red) fluorescence (measured along the dashed lines as indicated in the merge field) illustrate the presynaptic localization of KIAA1107 in mature neurons. The scale bar represents 2 μm.
See also Figures S1 and S2.

(Figure 1G). In mature neurons, the antibody also revealed a punctate nerve terminal pattern that partially colocalized with the presynaptic marker synaptotagmin-1 (Figure 1H). These data indicate that KIAA1107 is a developmentally regulated, widely expressed neuron-specific protein, mainly present at axonal and presynaptic terminal levels.

KIAA1107 Is an AP2 Interactor

In order to identify KIAA1107 protein-interacting partners, we employed a mass spectrometry (MS) approach using FLAG-KIAA1107, purified from SH-SY5Y human neuroblastoma or COS-7 cells, as a bait to pull-down KIAA1107 interactors from SH-SY5Y cell or subcellular fractions of mouse brain extracts (Figure 2A). The bands of interest were excised from the Coomassie-blue-stained gels, analyzed by liquid chromatography (LC)-MS/MS, and the MS/MS spectra were assigned to peptides with a >95% confidence level. In two independent preparations, a total of 163 proteins were reproducibly identified as specific KIAA1107-binding partners (MSdataSHSY5Y_XTandem.sf3 and MSdataCOS7_XTandem.sf3 in Data S1), seven of which resulted to be in common between the human and murine cellular models (Figure 2B). These included AP2 (α1 and β subunits) and AP3 (β2 and δ1 subunits) found in CCVs that traffic cargoes from the plasma membrane and between the endosomal and lysosomal systems, respectively (Robinson, 2004); Numb-like protein (NUMBL) involved in neural development and clathrin-dependent endocytosis (Sestan et al., 1999; Nishimura et al., 2003; Santolini et al., 2000); Bcl-2-associated transcription factor that interacts with antiapoptotic members of the Bcl-2 family (Kasof et al., 1999); V-type proton ATPase catalytic subunit A, a component of vacuolar ATPase (van Hille et al., 1993); and dynactin subunit1 (DCTN1) involved in organelle transport (Schroer, 2004).

We first focused our attention on AP2, the main adaptor protein responsible for CME (Conner and Schmid, 2003) and proceeded to co-immunoprecipitation assays to validate the potential interaction with KIAA1107. After verifying by MS analysis that the ~140-kDa protein band immunoprecipitated from mouse brain extract with the KIAA1107 polyclonal antibody was indeed the endogenous 1,088-aa KIAA1107 isoform, we found that both AP2 α and β subunits were specifically co-immunoprecipitated with endogenous KIAA1107 from mouse brain extracts (Figure 2C), whereas no interaction of KIAA1107 with clathrin was observed under the same conditions in which the AP2/clathrin binding was evident (Figure 2D). Interestingly, KIAA1107 was also co-immunoprecipitated from mouse brain extracts with anti-AP2α antibodies (Figure 2D), demonstrating the reciprocity of the interaction between KIAA1107 and AP2.

To restrict the part of the protein that interacts with AP2, we performed additional pull-down assays in mouse brain extracts using FLAG-KIAA1107 full-length, N- and C-terminal fragments. Interestingly, AP2α and AP2β were affinity purified only by the N-terminal fragment, whereas no interactions were observed with the C-terminal fragment (Figures S3A and S3B). In addition, the possibility of a nonspecific immunoprecipitation of AP2 was excluded by performing analogous co-immunoprecipitation assays in mouse liver extracts, a tissue that expresses AP2, but not KIAA1107 (Figure S3C).

We then combined the KIAA1107 binding proteins detected in our study with the results of another large proteomic study (Hein et al., 2015) that also identified KIAA1107 as a potential NUMBL interactor. Thus, we searched for additional shared interactions and overlaps with genes that GAMMA predicted to be relevant to KIAA1107 to infer a potential genetic neighborhood for KIAA1107 (Figure 2E). Such a predictive study revealed connections between KIAA1107 and clusters of genes playing key roles in exocytosis (SNAP25, syntaxin, syntaxin-binding protein, VAMP, NSF, and synaptotagmin-1), endocytosis (dynamin1, AP2, AP3, and Eps15), and neuronal development (Notch1, NUMB, and NUMBL).

KIAA1107 Is Expressed at Nerve Terminals and Associates with CCVs

As AP2 is one of the major coat proteins of CCVs, it was important to determine whether KIAA1107 is associated with CCVs. We isolated a CCV-enriched fraction from cultured rat neurons, successively stripped it and analyzed by immunoblotting the various fractions. The CCV preparation was highly enriched in the coat proteins clathrin and AP2, which were efficiently stripped from the purified vesicles, and in the integral vesicle membrane proteins synaptotagmin-1 and synaptophysin, which were not stripped (Figure 3A). In contrast, an accessory protein of CME, such as dynamin, was neither enriched on CCVs nor stripped, indicating that it does not function as classical clathrin adaptor (Slepnev and De Camilli, 2000). KIAA1107 was significantly enriched in the CCV fraction, although to a lesser extent than clathrin, and could be stripped by treatment with Tris buffer (Figure 3A). These data show that KIAA1107 is a protein associated with the coat component and not with the vesicle fraction.

In subcellular fractions prepared from rat forebrain, KIAA1107 immunoreactivity was mostly associated with the S2 fraction, consistent with the widespread localization of the protein in neurons (Figure 3B). However, it co-enriched with AP2 in the nerve-terminal-derived fractions LS1 and LP2, containing SVs and endosomal membranes, and its distribution roughly paralleled that of AP2 in other fractions (Figure 3B). Consistent with the biochemical data, a close colocalization of endogenous KIAA1107 with the essential components of the endocytic machinery AP2 and dynamin1 was observed in primary cortical neurons (17 DIV; Figure 3C). Notably, dynamin1 was identified as an indirect KIAA1107 interactor in a recent proteomics study (Gorini et al., 2010). These data suggest that KIAA1107 is closely associated with intracellular vesicular structures and binds specifically to AP2 on CCVs.

KIAA1107 Silencing Affects the Early Neuronal Development

CME controls cell surface expression of receptors, including those for axon guidance cues (Tojima et al., 2010), and AP2 plays a key role in directed cell migration (Raman et al., 2014). To interrogate the role of KIAA1107 in neuronal development, we acutely downregulated KIAA1107 expression in primary cortical neurons by RNAi with KIAA1107 shRNA#2

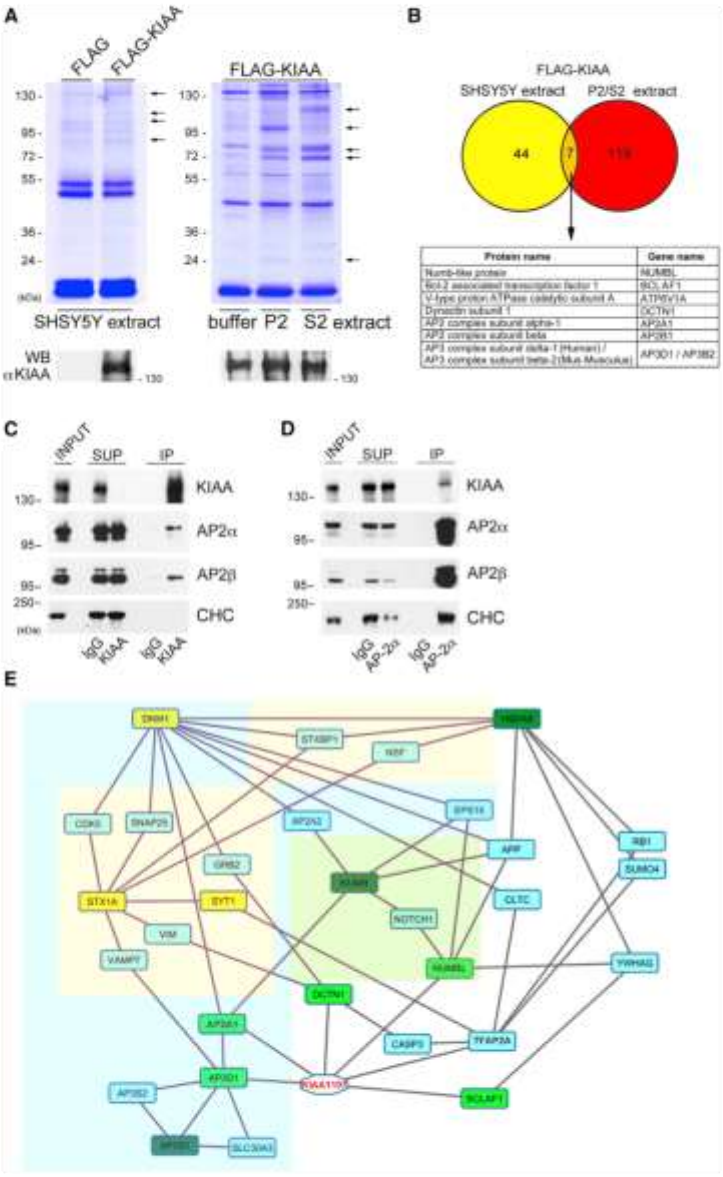

Figure 2. Identification of AP2 as a Specific KIAA1107 Interactor

(A and B) MS analysis of KIAA1107 interactors.

(A, top) Coomassie blue stained SDS-PAGE gels for proteins affinity purified by pull-down with overexpressed FLAG-KIAA1107 or FLAG-control in extracts of either SH-SY5Y cells (left panel) or subcellular fractions of mouse brain (cytosolic/microsomal S2 fraction or synaptosomal P2 fraction; right panel) are shown. Selected gel bands (arrows) were excised from the gels and analyzed by LC-MS/MS. (Bottom) KIAA1107 expression and specific precipitation in the samples was confirmed by western blotting (WB). The procedure was repeated twice with independent preparations.

(B) Venn diagram of the number of proteins identified by LC-MS/MS analysis exclusively in FLAG-KIAA1107 samples. The result showed 7 proteins (orange area) shared by both experimental models (protein and gene names are listed in the table) within 44 (yellow area) and 119 (red area) specific proteins for SH-SY5Y cells and mouse brain, respectively.

(C and D) Co-immunoprecipitation of KIAA1107 and AP2. Mouse brain extracts were subjected to immunoprecipitation (IP) with anti-KIAA1107 polyclonal antibodies (C), anti-AP2α monoclonal antibodies (D), or control immunoglobulin Gs (IgGs). Equal aliquots (2% of total) of the starting material (INPUT) and the supernatants (SUP) together with the IP samples were subjected to immunoblotting with the indicated antibodies (CHC [clathrin heavy chain]). The same membranes were stripped and re-probed for AP2α and β. The IPs were performed three times with similar results.

(E) Putative KIAA1107 genetic neighborhood based upon protein-protein interactions (PPIs). Our data (light green) were combined with PPIs found in a large proteomics study by Hein et al. (2015; dark green). Then, we searched for their shared PPIs (blue), as documented in Entrez Gene, and looked for overlap with GAMMA-predicted genes that fit into this network (yellow) to infer a potential genetic neighborhood for KIAA1107. Exocytic (yellow area), endocytic (blue area), and developmental (green area) clusters of genes are highlighted.

See also Figure S3 and Data S1.

(Figure S4). Cell morphology analysis revealed that silenced neurons displayed a significant impairment in neuronal development in terms of neurite number and length at early stages *in vitro* (3 and 5 DIV) compared to cells treated with control shRNA (shRNActr) (Figures 4A–4C). Interestingly, silenced neurons also showed a reduced expression level of AP2 (Figure S4), potentially due to partial degradation of the protein in the absence of complex formation with KIAA1107. The defective neurite outgrowth was completely rescued by the expression of EGFP-KIAA1107, a construct intrinsically resistant to shRNA#2 (Figures 4A–4C), indicating that the developmental impairment was specifically due to the downregulation of endogenous KIAA1107 and not to shRNA-mediated off-target effects. Moreover, KIAA1107 overexpression per se did not affect neuronal maturation, as length and number of processes did not differ between control and EGFP-KIAA1107-overexpressing neurons at both 3 and 5 DIV.

To further investigate the role of KIAA1107 in neocortical development *in vivo*, we downregulated its expression by in

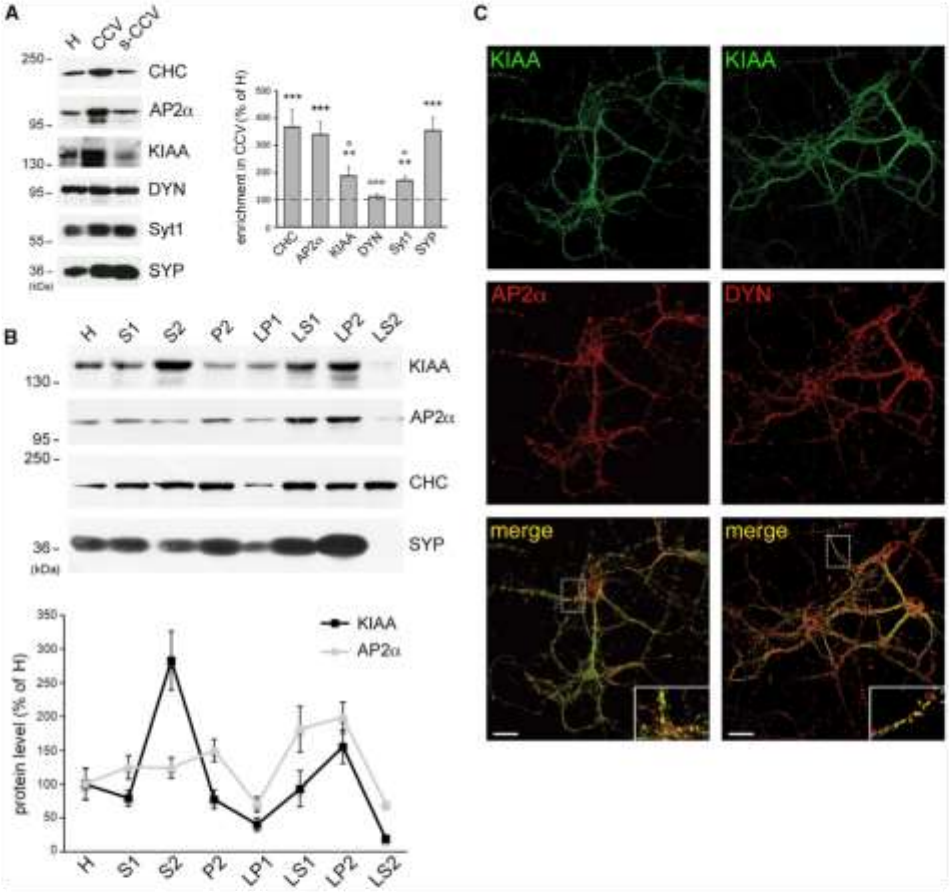

Figure 3. KIAA1107 Is a CCV-Associated Protein

(A) KIAA1107 is enriched in CCVs. (Left) The distribution of KIAA1107 immunoreactivity is compared with that of components of clathrin coats (CHC and AP2α), SVs (Syt1 and synaptophysin [SYP]), and CCV accessory proteins (dynamin1 [DYN]). Representative immunoblots are shown. Equal amounts of protein were loaded. H, total homogenate; s-CCV, stripped-CCV. (Right) Densitometric quantification of protein levels in the CCV-enriched fraction expressed as mean (±SEM) percentages of H is shown (n = 3 independent experiments); $^{**}p < 0.01$, $^{***}p < 0.001$ versus H, unpaired Student's t test; $^{\circ}p < 0.05$, $^{\circ\circ\circ}p < 0.001$ versus CHC, one-way ANOVA/Bonferroni's multiple comparison test.

(B) KIAA1107 co-fractionates with AP2. (Top) Subcellular fractions of rat forebrain were analyzed by immunoblotting using KIAA1107, AP2α, and CHC antibodies. The distribution of the specific SV marker SYP in the same fractions is shown for comparison. LP1, crude synaptic plasma membranes; LP2, crude SVs; LS1, SV-enriched supernatant fraction; LS2, synaptosol; P2, crude synaptosomes; S1, post-nuclear supernatant; S2, cytosolic and microsomal fraction. (Bottom) Densitometric quantification of KIAA1107 and AP2α immunoreactivities in the various subcellular fractions is shown. Data are expressed in percent of the relative H value (means ± SEM of n = 4 independent experiments).

(C) KIAA1107 colocalizes with the endocytic network. Representative confocal images of mature cortical neurons (17 DIV) double stained for KIAA1107 (green) and AP2α (red, left panels) or dynamin1 (DYN) (red, right panels) showing a largely overlapping staining of the proteins (magnified in the insets) are shown. The scale bars represent 10 μm (4.2 μm in the insets). Pearson's correlation coefficient is 0.846 ± 0.041 and 0.796 ± 0.039 for KIAA1107/AP2α and KIAA1107/DYN, respectively (n = 25 images obtained from n = 2 independent experiments were used for each protein).

utero electroporation (IUE) at E15.5 and analyzed the development of newly generated cortical pyramidal neurons (PNs) derived from shRNA#2-positive progenitors at P7. Whereas the knockdown (KD) of KIAA1107 did not affect radial migration of neural progenitors to layer II/III of the somatosensory cortex (Figures 4D and 4E), it significantly impaired maturation of PNs that exhibited an aberrant morphology with a significant reduction of total number and length of neurites (Figures 4F and 4G).

These data suggest a crucial role of KIAA1107 in the early stages of *in vitro* and *in vivo* neuronal development, when active SV exo/endocytotic activity at the growth cone is essential for

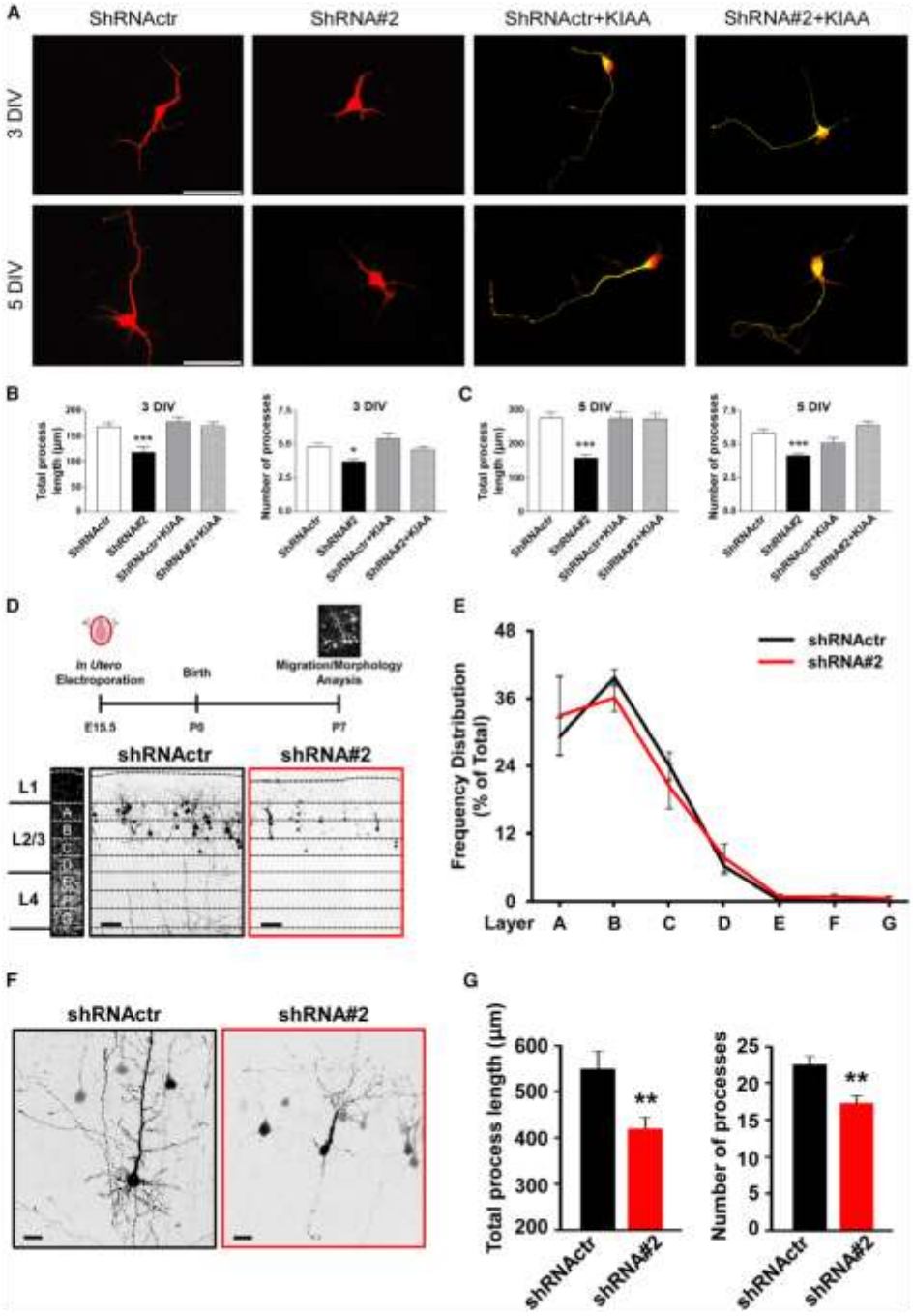

(legend on next page)

process outgrowth (Matteoli et al., 1992; Sabo and McAllister, 2003).

KIAA1107 Markedly Alters the Synaptic Ultrastructure

In view of the potential implication of KIAA1107 in SV endocytosis at mature synapses, we examined the presynaptic ultrastructure of KIAA1107-KD neurons by performing conventional transmission electron microscopy (TEM). Mouse cortical neurons were transduced with a lentiviral vector driving the expression of shRNA#2 or shRNActr at 12 DIV. After 5 days, KIAA1107 became undetectable (Figure S5A), whereas no difference in viability was observed between uninfected (ctr) and infected cells (Figure S5B). Notably, KIAA1107-KD synapses were characterized by a markedly reduced density of total SVs (~50% reduction; Figures 5A and 5B), whereas synaptic area, active zone (AZ) length, density of docked SVs, and distribution of SVs with respect to the AZ were comparable to control synapses (Figure 5C). These data were corroborated by a reduced expression level of synaptophysin and AP2 in KIAA1107-KD neurons compared to control (~40% reduction; Figure S5A). Moreover, the density of CCVs was dramatically reduced in silenced synapses (Figure 5B). Finally, KIAA1107-KD synapses displayed enlarged endosome-like structures (~50% increase in size) but with a preserved endosome density (Figure 5B), as confirmed by the increased immunoreactivity of the endosomal marker Rab5 at KIAA1107-KD synapses (Figures S6A and S6B).

To analyze in greater detail the morphology of synaptic terminals, we performed serial sectioning followed by 3D reconstruction of control and KIAA1107-KD synapses (Figure 5D). The morphometric analysis confirmed the severe reduction in the number of SVs and the parallel depletion of CCVs in silenced synapses compared to control (Figure 5E) and revealed that the enlarged endosome-like structures were fully separated from the plasma membrane (Figure 5D). Notably, the ultrastructural effects of KIAA1107 KD were reversible; the silencing phenotype was completely rescued by coinfection of the neurons with EGFP-KIAA1107 (Figures 5D and 5E) resistant to shRNA#2 silencing (Figure S5C). These results show that KIAA1107-silenced synapses, in spite of a normal gross morphology, display severe ultrastructural defects that are consistent with an important role of KIAA1107 in the regulation of SV recycling and in the maintenance of SV pools.

Clathrin/AP2-Mediated Endocytosis Is Impaired in KIAA1107-Silenced Synapses

Mutations in the genes that encode AP2 and other adaptor-like proteins, which are intrinsic components of the clathrin coat and are implicated in the early steps of SV recovery, lead to ultrastructural phenotypes that are similar to that induced by KIAA1107 silencing (González-Gaitán and Jäckle, 1997; Fergestad et al., 1999; Zhang et al., 1998).

To uncover whether SV recycling is impaired in KIAA1107-KD synapses, we imaged shRNActr- and shRNA#2-infected neurons by electron microscopy upon action potential (AP) firing in the presence of soluble horseradish peroxidase (HRP) to visualize the formation of endocytic intermediates.

We first analyzed synapses under conditions of low-frequency stimulation, when compensatory during-stimulus membrane retrieval largely (but not exclusively) occurs through CME (Granseth et al., 2006; Dittman and Ryan, 2009; Kononenko et al., 2014). Samples were fixed under basal conditions, immediately at the end of the field stimulation (200 APs at 5 Hz) or after 2- and 20-min wash in the absence of HRP. At the end of the stimulus, a significantly decreased density of HRP-positive (HRP^+) SVs, HRP^+ CCVs, and HRP^+ endosome-like structures, all representative of active cycling during stimulation, was observed in KIAA1107-KD terminals compared to control (Figures 6A and 6B). Moreover, the percentage of synapses displaying HRP^+ CCVs at the end of the stimulus versus total synapses was decreased by about 75% in silenced neurons compared to control (40.9% ± 2.7% and 10.3% ± 6.9% for shRNActr and shRNA#-2-infected neurons, respectively). After 2-min wash in the absence of HRP, a significant impairment in the formation of HRP^+ SVs was still evident in KIAA1107-KD terminals, whereas the formation of HRP^+ endosomal vacuoles recovered to control levels. Finally, after 20-min wash in the absence of HRP, SVs and endosomal structures lost their HRP content in both experimental groups, indicating an active and complete recovery. These results indicate that, in KIAA1107-KD synapses, the recovery of SVs, budding either directly from the plasma membrane or from endosome-like structures, was delayed during mild stimulation. The formation of HRP^+ endosomal structures derived from either homotypic fusion of CME-derived vesicles or fusion of such vesicles with early endosomes (Heuser and Reese, 1973; Rizzoli et al., 2006; Hoopmann et al., 2010) was

Figure 4. KIAA1107-Silenced Cortical Neurons Display an Impaired Maturation at Early Stages of *In Vitro* and *In Vivo* Development

(A) Representative merged images of 3 and 5 DIV cortical neurons nucleofected before plating with either ShRNActr or ShRNA#2 (red) and Sh-resistant EGFP-KIAA1107 (green). The scale bars represent 50 μm.

(B and C) Quantification of total process length and number of processes at 3 (B) and 5 (C) DIV using ImageJ. Data are means ± SEM (n = 101 and 83 for ShRNActr neurons; n = 98 and 105 for ShRNA#2 neurons; n = 74 and 89 for ShRNActr+KIAA1107 neurons; n = 66 and 61 for ShRNA#2+KIAA1107 neurons; at 3 and 5 DIV, respectively, from n = 3 independent experiments). *p < 0.05; ***p < 0.001 versus ShRNActr neurons; one-way ANOVA/Bonferroni's multiple comparison test.

(D–G) KIAA1107-silencing *in vivo* does not impair radial migration but causes impairment in pyramidal neurons' morphology.

(D, top) Cartoon depicting the experimental design of the *in vivo* experiments is shown. (Bottom) Representative images of GFP fluorescence in neurons transfected with either ShRNActr (black) or ShRNA#2 (red) in the somatosensory cortex are shown. The slices were counterstained with DAPI to allow the visualization of cortical layers 2/3/4 (L2/3 and L4), here divided in 8 sub-layers (named from A to G, left). The scale bars represent 50 μm.

(E) Quantification of the percentage of total transfected cells in each layer is shown. Data are means ± SEM (n = 8 animals per condition, 1 slice per animal).

(F) Representative high-magnification images of GFP fluorescence in neurons transfected with either ShRNActr (black) or ShRNA#2 (red) in layer II/III of the somatosensory cortex are shown. The scale bars represent 15 μm.

(G) Quantification of total process length (left) and number (right) using ImageJ is shown. Data are means ± SEM (n = 21 cells from 8 different animals for ShRNActr; n = 23 cells from 8 different animals for ShRNA#2); **p < 0.01; unpaired Student's t test.

See also Figure S4.

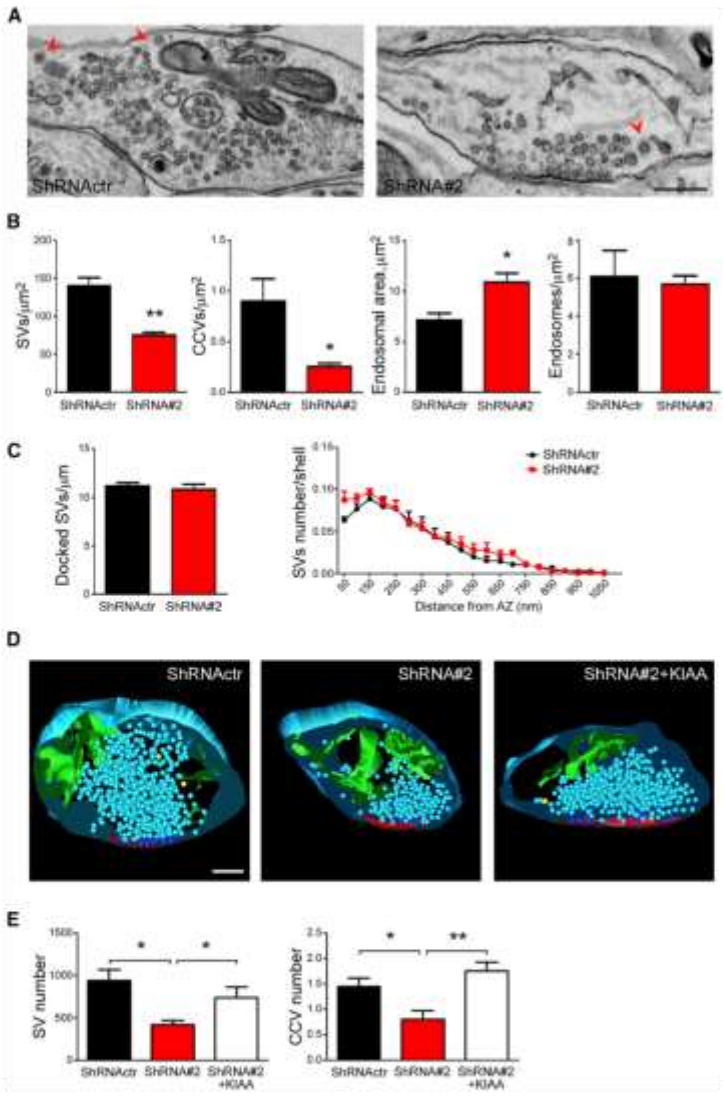

Figure 5. Reduced SV Density and Increased Size of Endosome-like Structures at KIAA1107-Silenced Cortical Synapses

(A) Representative TEM images of nerve terminals from cultured cortical neurons transduced with either ShRNActr or ShRNA#2 at 12 DIV and processed at 17 DIV. Note the reduced SV density in the KIAA1107-KD synapse compared to control (CCVs, red arrowheads). The scale bar represents 200 nm.

(B) Morphometric analysis from serial ultrathin sections obtained from ShRNActr- (black bars) and ShRNA#2- (red bars) treated synapses revealed (from left to right) a reduction in the density of total SVs and CCVs and an increase in the area of endosome-like structures in KIAA1107-KD synapses compared to control. $^{*}p < 0.05$; $^{**}p < 0.01$; unpaired Student's t test.

(C) No changes were observed in the density of AZ-docked SVs and in the spatial distribution of SVs in the nerve terminals of KIAA1107-KD neurons compared to control. The density of SVs located within successive 50-nm shells from the AZ was normalized for the total SV content of each terminals and is given as a function of the distance from the AZ. Nerve terminal areas (0.716 ± 0.059 μm^2 and 0.800 ± 0.024 μm^2 for ShRNActr and ShRNA#2-infected neurons, respectively) and AZ lengths (0.350 ± 0.016 µm and 0.335 ± 0.007 µm for ShRNActr and ShRNA#2-infected neurons, respectively) were similar in the two experimental groups. Data are means ± SEM (n = 157 and n = 160 synapses for ShRNActr and ShRNA#2-infected neurons, respectively, from n = 4 independent preparations).

(D) Representative 3D reconstructions of synaptic terminals from 60-nm-thick serial sections obtained from cortical neurons confirmed the severe reduction in SV (light blue spheres) and CCV (yellow spheres) number in ShRNA#2-treated neurons, which was completely rescued in ShRNA#2+KIAA1107-treated neurons. Endosomal structures (green), not connected with the plasma membrane, are also visible. The AZ and AZ-docked SVs are shown in red and blue, respectively. The scale bar represents 200 nm.

(E) Morphometric analysis of the number of SVs and CCVs in 3D-reconstructed synapses from neurons transduced with ShRNActr (black bars), ShRNA#2 (red bars), or ShRNA#2+KIAA1107 (white bars). Docked SVs (19.3 ± 2.38, 14.57 ± 2.37, and 20.37 ± 4.15 for ShRNActr, ShRNA#2, and ShRNA#2+KIAA1107-infected neurons, respectively) were similar in the three experimental groups. Data are means ± SEM (n = 10 synapses per genotype from n = 3 independent preparations). $^{*}p < 0.05$; $^{**}p < 0.01$; one-way ANOVA/Bonferroni's multiple comparison test.

See also Figures S5 and S6.

also delayed in silenced terminals compared to controls. The increased endosomal size observed in silenced synapses both under basal conditions (Figures 5B, S6A, and S6B) and after stimulation (Figure S6C) is compatible with a longer retention of SVs at endosomal level, strongly suggesting an impaired clathrin-mediated SV reformation from endosomal structures.

When neurons were stimulated at higher frequency (200 APs at 40 Hz), i.e., a frequency known to trigger fast membrane retrieval via endocytic intermediates upstream of clathrin-coat assembly (Clayton et al., 2008; Cheung et al., 2010; Kononenko et al., 2014; Watanabe et al., 2013, 2014), a decreased density of HRP^{+} SVs was observed only at the end of the stimulus in KIAA1107-KD terminals compared to control (Figure 6C), evidence of a moderate impairment of SV reformation at this intense activity level. HRP^{+} CCVs were nearly absent in both genotypes, consistent with the idea that CME is largely dispensable for

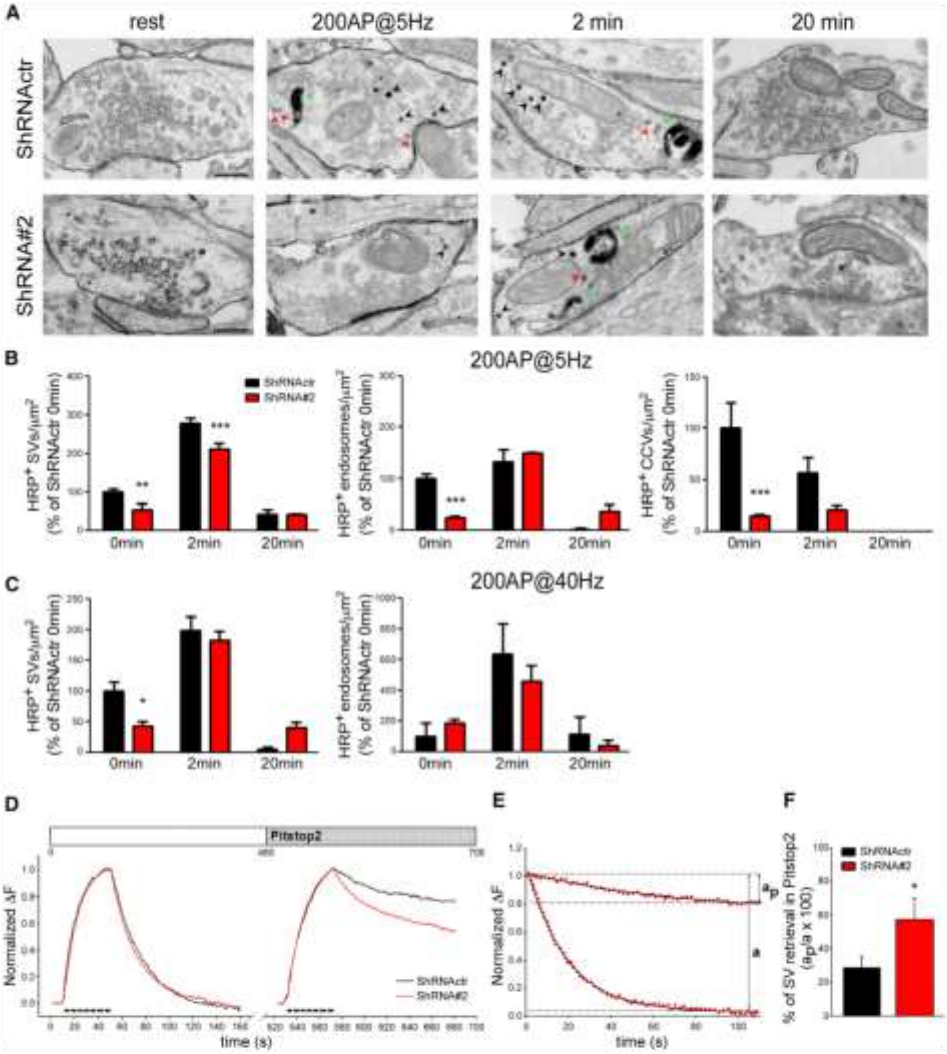

Figure 6. KIAA1107 Knockdown Impairs Clathrin-Mediated Endocytosis in Cortical Synapses

(A) Representative TEM images of presynaptic terminals from control (ShRNActr) and KIAA1107-KD (ShRNA#2) neurons infected at 12 DIV and stimulated at 17 DIV with 200 APs at 5 Hz in the presence of soluble HRP. Synaptic ultrastructure was evaluated by fixing neurons under basal conditions (rest), immediately after the stimulus (0 min), and after 2 or 20 min of recovery in the absence of HRP (HRP$^+$ SVs, black arrowheads; HRP$^+$ CCVs, red arrowheads; HRP$^+$ endosomes, green arrowheads). The scale bars represent 200 nm.

(B and C) Morphometric analysis of HRP-labeled structures after the train stimulation at 5 (B) and 40 (C) Hz (200 APs). The density of HRP-positive (HRP$^+$) SVs, HRP$^+$ endosome-like structures, and HRP$^+$ CCVs in control (black bars) and KIAA1107-KD (red bars) neurons are reported as mean (±SEM) percentages of the respective values observed in the control (ShRNActr) group at 0 min (5 Hz: ShRNActr HRP$^+$SVs, 3.15 ± 0.25; ShRNActr HRP$^+$CCVs, 0.90 ± 0.23; ShRNActr HRP$^+$endosomes, 1.11 ± 0.17; 40 Hz: ShRNActr HRP$^+$SVs, 1.54 ± 0.23; ShRNActr HRP$^+$endosomes, 0.1 ± 0.07). n = 150 and n = 120 images per genotype for the 5- and 40-Hz protocols, respectively, from n = 4 independent preparations. *p < 0.05; **p < 0.01; ***p < 0.001 across genotype, two-way ANOVA/Bonferroni's multiple comparison test.

(D) Ensemble average normalized traces of SypHy fluorescence plotted for control (black trace, n = 8) and KIAA1107-KD (red trace, n = 5) neurons sequentially stimulated with 200 APs at 5 Hz (dotted line) in the absence or presence of 30 µM Pitstop-2.

(E) Representative control data points (red dots) and relative fitting (black traces) by a single exponential function ($y = y_0 + a^{-bx}$). The *a* values in the absence (a) or presence (a_p) of Pitstop-2 are shown.

(legend continued on next page)

plasma membrane retrieval at this stimulation frequency (Kononenko et al., 2014; Park et al., 2016). In addition, the density of HRP$^+$ endosomal vacuoles was not altered in silenced synapses (Figure 6C), although their size was increased also at this stimulation frequency (Figure S6D).

We then used Synaptophysin-pHluorin (SypHy) (Tagliatti et al., 2016), co-expressed in hippocampal neurons transduced with either shRNActr or shRNA#2, to further assay membrane recycling following low-frequency stimulation (200 APs at 5 Hz). Surprisingly, no differences in the fluorescence increase, indicative of the rate of release, as well as in the fluorescence decay, representative of post-stimulus endocytosis, were observed in KIAA1107-KD synapses compared to control synapses (Figure 6D). The inability of the SypHy assay to detect an endocytic phenotype in silenced terminals could in principle be due either to a compensatory SV membrane retrieval contributed by clathrin-independent endocytosis (CIE) or, alternatively, to a major involvement of KIAA1107 in SV budding from endosomes rather than from the presynaptic membrane. To sort this out, we challenged neurons with the clathrin inhibitor Pitstop-2 (von Kleist et al., 2011; Figure 6D). The inhibitory effect of Pitstop-2 on endocytosis was severe in both control and KIAA1107-KD synapses, despite the presence of a modest compensation mediated by CIE in the latter (Figures 6D–6F). This suggests that KIAA1107 silencing does not primarily impair SV membrane retrieval or vesicle reacidification but rather SV reformation from endosomes.

In summary, these functional data provide strong evidence that KIAA1107 plays an important role both in CME at the plasma membrane and in the reformation of SVs by clathrin coats budding from endosomes. The kinetics of SV reformation, especially under conditions of low-frequency activity when CME is the predominant pathway for SV recycling, is affected by KIAA1107 silencing. Based on these data, we named the KIAA1107 protein APache, for AP2-interacting clathrin-endocytosis protein.

APache-Silenced Autaptic Neurons Exhibit Impaired Presynaptic Function

To determine whether APache plays a role in synaptic transmission, we performed whole-cell patch-clamp recordings in autaptic hippocampal neurons silenced for APache at 6 DIV and analyzed 5 or 6 days after infection. We preliminarily analyzed the effects of APache silencing on the autapse density and found that the density of synaptic contacts was preserved in APache-KD autaptic neurons (Figure S7A).

Then, we proceeded to the analysis of synaptic transmission. Neurons were stimulated with paired stimuli (50-ms interpulse interval) to evaluate evoked excitatory postsynaptic current (eEPSC) amplitude and paired-pulse facilitation, a presynaptic form of short-term plasticity and an indirect measure of the release probability (Pr) (Fioravante and Regehr, 2011). APache-KD neurons displayed a significant reduction of eEPSC amplitude in response to single stimuli but no changes in paired-pulse facilitation (Figures 7A and 7B). To investigate which of the quantal parameters of release was responsible for the decreased synaptic strength in APache-KD synapses, the cumulative eEPSC amplitude analysis was performed by subjecting neurons to high-frequency trains (2 s at 40 Hz) that induce a complete depletion of the readily releasable pool of SVs (RRP) (Figures 7C–7E). Under this condition, the depression during the steady-state phase is limited by the constant recycling of SVs so that an equilibrium is reached between released and recycled SVs (Schneggenburger et al., 1999). The analysis showed that the RRP size was significantly decreased in APache-KD neurons, to the same extent of the reduction in eEPSC amplitude, whereas Pr was not affected (Figure 7F). This suggests that the impairment in evoked release in APache-KD neurons is likely to involve the constant replenishment of the RRP by the recycling SV pool. Despite the change in RRP, the dynamics of facilitation and depression during the 2-s train at 40 Hz were not significantly affected in silenced neurons compared to control (Figure 7D). Because the various endocytic mechanisms are known to be recruited in a frequency-dependent manner, autaptic neurons were challenged with short 2-s trains at frequencies ranging from 5 to 20 Hz and with a long 30-s train at 10 Hz to analyze the expression of facilitation/depression over time (Figures 7G, 7H, S7B, and S7C). APache-silenced neurons exhibited a more pronounced depression that was tightly dependent on the stimulus frequency. Synaptic depression was faster, more intense, and prolonged in APache-KD synapses during 5-Hz stimulation (Figures 7G and 7H) and progressively attenuated with the increase in stimulation frequency (Figure S7B). The strong increase in synaptic depression at 5 Hz, consistent with the RRP depletion and inactivation of release sites (Fioravante and Regehr, 2011), is likely due, similarly to other endocytic mutants (Milosevic et al., 2011), to the impaired clathrin-mediated recycling of SVs. APache silencing was also associated with an accelerated kinetics of depression evoked by long trains (30 s at 10 Hz; Figure S7C). In addition, post-tetanic potentiation (PTP), a form of short-term plasticity evoked after a short high-frequency stimulation and contributed by increases in both Pr and RRP (Valente et al., 2012), was also impaired in APache-KD neurons (~35% reduction; Figure S7D), consistent with the SV depletion observed upon APache silencing.

DISCUSSION

In the present study, using the bioinformatics GAMMA program to search for uncharacterized genes associated with SVs and presynaptic physiology, we identified KIAA1107 with the highest score. The mouse KIAA1107 main isoform is a protein of 1,088 aas lacking both structural data and known function. Our results demonstrate that KIAA1107 is an AP2 interactor that plays a role in early neuronal development and in CME at mature

(F) The a_0/a ratio, representing the percentage of retrieved SVs in the presence of Pitstop-2 versus the retrieved SVs in its absence, is plotted for control (black bar, n = 8) and KIAA1107-KD (red bar, n = 5) synapses. Data are means ± SEM from the indicated number of coverslips from n = 3 independent preparations. *$p < 0.05$; unpaired Student's t test.
See also Figure S6.

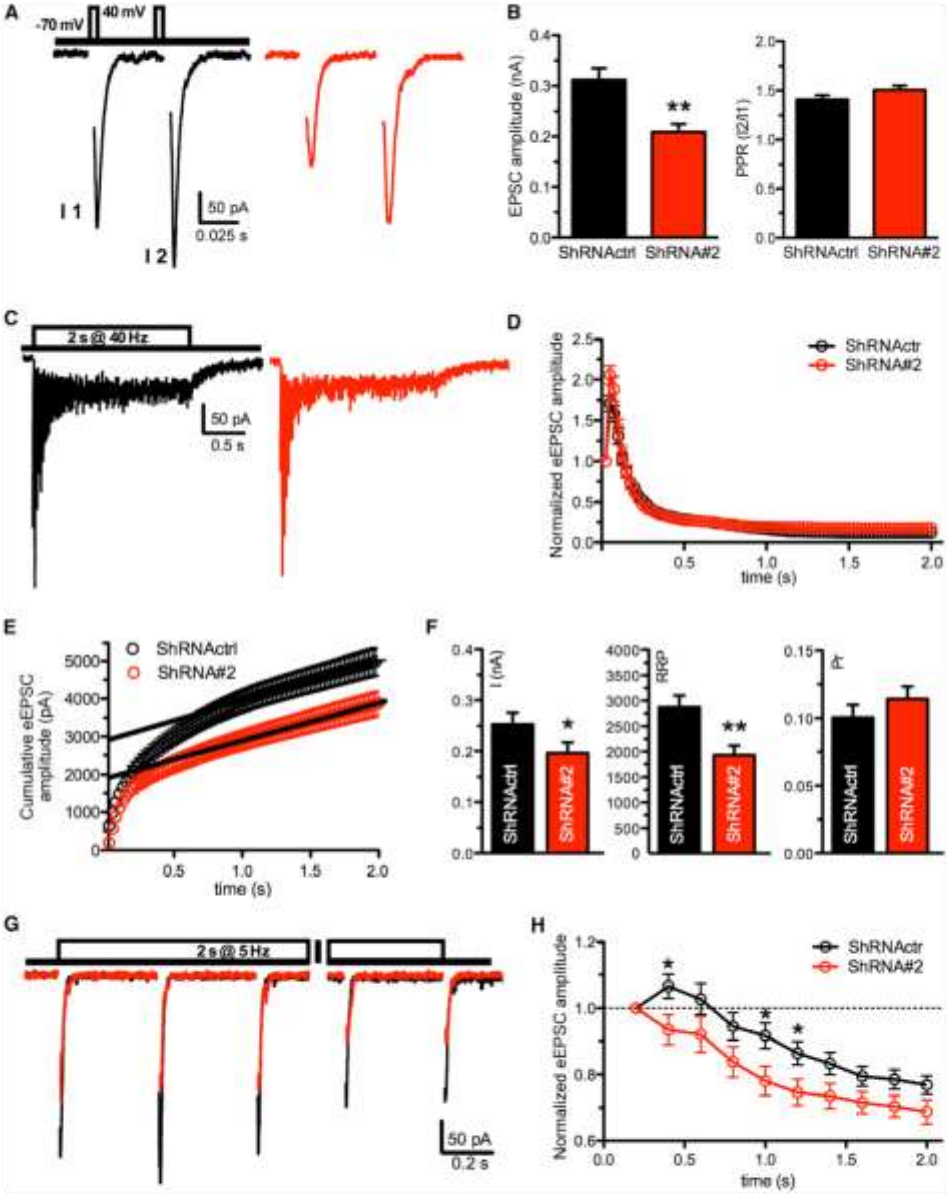

Figure 7. KIAA1107 Silencing Decreases Evoked Excitatory Synaptic Transmission and Enhances Synaptic Depression in Autaptic Hippocampal Neurons

(A) Representative eEPSCs recorded in autaptic neurons transduced with either ShRNActr (black traces, n = 67) or ShRNA#2 (red traces, n = 63). eEPSCs were elicited by clamping the cell at −70 mV and stimulating it with two voltage steps to + 40 mV lasting 0.5 ms at an inter-stimulus interval of 50 ms (inset).

(B) eEPSC amplitude evoked by the first pulse (I1, left) and paired-pulse ratio (PPR) (I2/I1, right) recorded under the same conditions of (A).

(C) Representative recordings of eEPSC evoked by a 2-s tetanic stimulation at 40 Hz in autaptic neurons transduced with ShRNActr (black) or ShRNA#2 (red).

(D) Normalized values of eEPSC amplitude showing the time course of synaptic facilitation and depression in autaptic neurons stimulated as in (C).

(E) Cumulative mean amplitude profiles for eEPSCs during the tetanic stimulation shown in (C) in neurons infected with ShRNActr (black trace, n = 40) or ShRNA#2 (red trace, n = 37). Data points in the 1- to 2-s range were fitted by linear regression and backextrapolated to time 0 (solid lines) to estimate the RRP.

(legend continued on next page)

synapses. We named the protein APache and consider it a molecular component of the clathrin/AP2-dependent endocytic machinery that regulates the fate of endocytosed SVs.

CME has a range of different functions that also include sampling the cell environment for growth and guidance cues and bringing nutrients into cells in developing neurons. An active SV exo/endocytosis in the growth cone has been demonstrated in cultured neurons (Matteoli et al., 1992; Sabo and McAllister, 2003). The present data suggest that, in developing neurons, APache may function in vesicle trafficking events. APache is expressed since the early stages of neuronal development and is present in axonal processes and growth cones, where it promotes neuronal maturation and process outgrowth both *in vitro* and *in vivo*. Moreover, the expression level of AP2 is reduced in developing silenced neurons. It is tempting to speculate that the developmental role of APache is obtained through the clathrin-mediated trafficking pathways that control axon and dendrite outgrowth in developing neurons that are characterized by abundant CCVs (Roos and Kelly, 1999). Intriguingly, AP180 and CALM, two clathrin assembly proteins involved in CME, also play critical roles in controlling the outgrowth of axons and dendrites in embryonic hippocampal neurons (Bushlin et al., 2008), and their silencing elicits morphological phenotypes reminiscent of those of APache-depleted cortical neurons.

Other potential interactors detected in the MS scans can contribute to the effects of APache in neuronal development. NUMBL, an endocytic adaptor binding to the AP2 complex and Eps15 and implicated in CME and neurite outgrowth (Santolini et al., 2000; Sestan et al., 1999; Nishimura et al., 2003) was identified as an APache interactor in our study as well as in a recent proteomic study (Hein et al., 2015). Dynactin, a direct AP2-binding partner that regulates bidirectional transport of vesicles in mammalian neurons, microtubule advance during growth cone remodeling (Kwinter et al., 2009; Grabham et al., 2007), and trafficking of BDNF-TrkB signaling endosomes (Kononenko et al., 2017; Zhou et al., 2012) was also identified as an APache interactor. Thus, in addition to its role in endocytosis at the plasma membrane, APache may also play a role in the internal vesicular/endosomal transport.

Several lines of evidence suggest a potential role for APache in CME at mature synapses. APache is most abundant in brain and, in mature synapses, is concentrated at presynaptic terminals, where it colocalizes with synaptotagmin-1, AP2, and dynamin-1. We have identified AP2 as an APache interactor with the following evidence: (1) APache co-immunoprecipitates with AP2α and β subunits from brain extracts, suggesting that it may participate in the complex network of interactions regulating CME and SV recycling; (2) APache is enriched in CCVs to levels comparable to the coat proteins AP2 and clathrin and at a much larger extent than CME accessory proteins, such as dynamin, synaptojanin, amphiphysin, or endophilin; and (3) APache can be stripped from purified CCVs by treatment with Tris buffer, a well-established procedure to remove coat components from SVs. Synapses that lack APache display the typical features of endocytic mutants. The ultrastructural changes include a severe depletion of SVs and CCVs and the presence of enlarged endosome-like structures. The morpho-functional phenotype of APache silencing consists in a global impairment of SV recycling and synaptic strength that peaks under conditions of low-frequency activity.

Mature synapses use multiple activity-dependent SV recycling mechanisms that operate in parallel and influence neurotransmitter release and synaptic plasticity: "kiss and run"; CME; and clathrin-independent mechanisms (i.e., ultrafast or bulk endocytosis). Whereas the retrieval of the majority of fully fused SVs during mild electrical activity occurs through CME, with vesicles reforming directly from the plasma membrane or from endosomal structures (Hoopmann et al., 2010; Uytterhoeven et al., 2011), during intense high-frequency activity, SV membranes are mostly retrieved through CIE.

The experimental evidence indicates that APache is required to maintain normal SV recycling and RRP refilling at the synapse under conditions of mild stimulation by acting in the clathrin/AP2-mediated regeneration of SVs both from the cell surface and from internalized endosomal structures. The latter mechanism seems to be the predominant one, given the lack of effect of APache silencing on SV reacidification in the SypHy assay. Consistent with this, enlarged endosomal vacuoles accumulate at silenced synapses and may contribute to the depression of neurotransmitter release. On the other hand, APache is dispensable for plasma membrane retrieval at high frequencies, although it may be required for the clathrin-mediated SV reformation from endosomal vacuoles generated by CIE. This model is consistent with prior data demonstrating that silencing or conditional knockout of either AP2 (Kim and Ryan, 2009; Kononenko et al., 2014) or AP2-associated endocytic adaptor proteins (Fergestad et al., 1999; Kononenko et al., 2013) significantly slows down, but does not abolish, SV endocytosis and validates the view that alternative molecules or different mechanisms that normally operate in conjunction with AP2 are required to ensure efficient SV and cargo retrieval over a wide range of stimulation frequencies.

Although further structure function studies will be needed to unravel the precise molecular mechanisms that mediate the described APache functions, the identification of an additional molecular component of the complex endocytic pathway is a

(F) Quantal analysis of release in neurons infected with ShRNActr (black bars) or ShRNA#2 (red bars). From left to right, amplitude of the first eEPSC, RRP size, and probability of release (Pr) are shown.
(G) Representative recordings of eEPSC evoked by a 2-s tetanic stimulation at 5 Hz in autaptic neurons transduced with either ShRNActr (black, n = 31) or ShRNA#2 (red, n = 21).
(H) Normalized values of eEPSC amplitude showing the time course of synaptic facilitation and depression in autaptic neurons stimulated as in (G). In all graphed currents, stimulation artifacts were blanked for clarity. Data are means ± SEM from the indicated numbers of cells recorded at least from n = 3 independent cell culture preparations. *$p < 0.05$; **$p < 0.01$; unpaired Student's t test or Mann-Whitney U test.
See also Figure S7.

step forward for getting insights into fundamental aspects of SV recycling in the healthy and diseased brain.

EXPERIMENTAL PROCEDURES

C57BL/6J mice and Sprague-Dawley rats of either sex were from Charles River Laboratories (Calco, Italy). All experiments, conducted at various stages of development (from E18 to adult mice), were carried out in accordance with the guidelines established by the European Communities Council (directive 2010/63/EU of March 4, 2014) and were approved by the Italian Ministry of Health. The standard procedures for western blotting, CCV purification, pull-down and co-immunoprecipitation assays, immunocytochemistry, real-time PCR, and cultures of low-density and autaptic neurons are reported in detail in the Supplemental Experimental Procedures.

GAMMA

GAMMA relies on identifying gene-gene expression correlations using thousands of publicly available microarray datasets available from the GEO repository. Additional data are reported in the Supplemental Experimental Procedures.

KIAA1107 Antibodies and Constructs

A polyclonal KIAA1107-specific antibody was raised in the rabbit against a conserved region comprising aas 732–894 of mouse KIAA1107. cDNA of *Kiaa1107* was amplified from total mRNA extracted from mouse brain and inserted into the p3XFLAG-CMV-14 or p277.pCCLsin.cPPT.hPGK.eGFP.WPRE vector. shRNAs#1–3 and control shRNA were inserted into the pLKO.1-CMV-mCherry lentiviral vector and used to knockdown the endogenous KIAA1107 in neurons. For detailed description of antibodies, constructs, and neuronal and cellular transfection, see the Supplemental Experimental Procedures.

MS Analysis

Sample preparation, LC-MS/MS analysis, database searching, and criteria for protein identification were conducted as reported in details in the Supplemental Experimental Procedures.

IUE

Standard IUE was performed as previously described (Szczurkowska et al., 2016). The images were acquired using a confocal laser-scanning microscope (TCS SP5; Leica Microsystem) or an epifluorescence microscope equipped with Neurolucida (MicroBrightField) software. For detailed procedures and reagents, see the Supplemental Experimental Procedures.

TEM

Low-density cultures of cortical neurons were infected at 12 DIV with either control shRNA or KIAA1107 shRNA and processed for TEM. For detailed procedures, see the Supplemental Experimental Procedures.

Live Imaging and Patch-Clamp Experiments

Optical recordings with Syphy fluorescent probe were performed at 17 DIV (5 days postinfection). Whole-cell patch-clamp recordings were made from autaptic neurons grown on microislands infected at 6 DIV with either control shRNA or KIAA1107 shRNA. For detailed procedures, see the Supplemental Experimental Procedures.

Statistical Analysis

Data with normal distribution were analyzed by one- or two-way ANOVA followed by the Bonferroni's multiple comparison test or the unpaired Student's t test. Non-normally distributed data were analyzed by the Mann-Whitney's U test. Statistical analysis was carried out using Prism (GraphPad Software, La Jolla, CA, USA) and OriginPro-8 (OriginLab, Northampton, MA, USA) software. Significance level was preset to $p < 0.05$. Data were expressed as means ± SEM for number of samples/cells (n) as detailed in the figure legends.

SUPPLEMENTAL INFORMATION

Supplemental Information includes seven figures and one data file and can be found with this article online at https://doi.org/10.1016/j.celrep.2017.11.073.

ACKNOWLEDGMENTS

We thank Dr. Silvia Casagrande (University of Genova, Italy) for assistance in the preparation of primary cultures, Dr. Elena Monzani (San Raffaele Scientific Institute, Milan, Italy) for preparation of lentiviral constructs, and Prof. Luigi Naldini (TIGET, San Raffaele Scientific Institute, Milan, Italy) for the kind supply of the lentiviral vector. This study was supported by research grants from the Italian Ministry of University and Research (FIRB 2010 "Futuro in Ricerca" to S.G.), CARIPLO Foundation (2013 0879 to F.V. and F.B.), and Compagnia di San Paolo (2015.0546 to F.B.). The support of Telethon-Italy (GGP13033 to F.B.) is also acknowledged and NIH grant number 5P20GM103636 (to J.D.W.).

AUTHOR CONTRIBUTIONS

A.P. participated in the design of the experiments and performed research. E.C. performed and analyzed the ultrastructural experiments. F.C.G. and F.C. ran the developmental studies and provided experimental tools. P.V. and G.G. performed the electrophysiological experiments and analyzed the data. D.A. performed the live imaging experiments. M.B. participated in image acquisition. C.M., B.P., and A.S. performed IUE, slice histology, and image acquisition and analysis. A.B. and A.C. performed the MS analysis. A.F. supervised the live imaging experiments. J.D.W. performed the bioinformatic analysis. F.V. contributed to the research design. S.G. performed research, analyzed data, and made the figures. S.G. and F.B. designed and supervised the research and wrote the paper. All authors revised the manuscript.

DECLARATION OF INTERESTS

The authors declare no competing interests.

Received: April 24, 2017
Revised: October 23, 2017
Accepted: November 20, 2017
Published: December 19, 2017

REFERENCES

Bushlin, I., Petralia, R.S., Wu, F., Harel, A., Mughal, M.R., Mattson, M.P., and Yao, P.J. (2008). Clathrin assembly protein AP180 and CALM differentially control axogenesis and dendrite outgrowth in embryonic hippocampal neurons. J. Neurosci. *28*, 10257–10271.

Cheung, G., Jupp, O.J., and Cousin, M.A. (2010). Activity-dependent bulk endocytosis and clathrin-dependent endocytosis replenish specific synaptic vesicle pools in central nerve terminals. J. Neurosci. *30*, 8151–8161.

Clayton, E.L., Evans, G.J., and Cousin, M.A. (2008). Bulk synaptic vesicle endocytosis is rapidly triggered during strong stimulation. J. Neurosci. *28*, 6627–6632.

Conner, S.D., and Schmid, S.L. (2003). Regulated portals of entry into the cell. Nature *422*, 37–44.

Cousin, M.A. (2017). Integration of synaptic vesicle cargo retrieval with endocytosis at central nerve terminals. Front. Cell. Neurosci. *11*, 234.

Dittman, J., and Ryan, T.A. (2009). Molecular circuitry of endocytosis at nerve terminals. Annu. Rev. Cell Dev. Biol. *25*, 133–160.

Fergestad, T., Davis, W.S., and Broadie, K. (1999). The stoned proteins regulate synaptic vesicle recycling in the presynaptic terminal. J. Neurosci. *19*, 5847–5860.

Fioravante, D., and Regehr, W.G. (2011). Short-term forms of presynaptic plasticity. Curr. Opin. Neurobiol. *21*, 269–274.

González-Gaitán, M., and Jäckle, H. (1997). Role of Drosophila alpha-adaptin in presynaptic vesicle recycling. Cell *88*, 767–776.

Gorini, G., Ponomareva, O., Shores, K.S., Person, M.D., Harris, R.A., and Mayfield, R.D. (2010). Dynamin-1 co-associates with native mouse brain BKCa channels: proteomics analysis of synaptic protein complexes. FEBS Lett. *584*, 845–851.

Grabham, P.W., Seale, G.E., Bennecib, M., Goldberg, D.J., and Vallee, R.B. (2007). Cytoplasmic dynein and LIS1 are required for microtubule advance during growth cone remodeling and fast axonal outgrowth. J. Neurosci. *27*, 5823–5834.

Granseth, B., Odermatt, B., Royle, S.J., and Lagnado, L. (2006). Clathrin-mediated endocytosis is the dominant mechanism of vesicle retrieval at hippocampal synapses. Neuron *51*, 773–786.

Hein, M.Y., Hubner, N.C., Poser, I., Cox, J., Nagaraj, N., Toyoda, Y., Gak, I.A., Weisswange, I., Mansfeld, J., Buchholz, F., et al. (2015). A human interactome in three quantitative dimensions organized by stoichiometries and abundances. Cell *163*, 712–723.

Heuser, J.E., and Reese, T.S. (1973). Evidence for recycling of synaptic vesicle membrane during transmitter release at the frog neuromuscular junction. J. Cell Biol. *57*, 315–344.

Hoopmann, P., Punge, A., Barysch, S.V., Westphal, V., Bückers, J., Opazo, F., Bethani, I., Lauterbach, M.A., Hell, S.W., and Rizzoli, S.O. (2010). Endosomal sorting of readily releasable synaptic vesicles. Proc. Natl. Acad. Sci. USA *107*, 19055–19060.

Kasof, G.M., Goyal, L., and White, E. (1999). Btf, a novel death-promoting transcriptional repressor that interacts with Bcl-2-related proteins. Mol. Cell. Biol. *19*, 4390–4404.

Kim, S.H., and Ryan, T.A. (2009). Synaptic vesicle recycling at CNS snapses without AP-2. J. Neurosci. *29*, 3865–3874.

Kononenko, N.L., and Haucke, V. (2015). Molecular mechanisms of presynaptic membrane retrieval and synaptic vesicle reformation. Neuron *85*, 484–496.

Kononenko, N.L., Diril, M.K., Puchkov, D., Kintscher, M., Koo, S.J., Pfuhl, G., Winter, Y., Wienisch, M., Klingauf, J., Breustedt, J., et al. (2013). Compromised fidelity of endocytic synaptic vesicle protein sorting in the absence of stonin 2. Proc. Natl. Acad. Sci. USA *110*, E526–E535.

Kononenko, N.L., Puchkov, D., Classen, G.A., Walter, A.M., Pechstein, A., Sawade, L., Kaempf, N., Trimbuch, T., Lorenz, D., Rosenmund, C., et al. (2014). Clathrin/AP-2 mediate synaptic vesicle reformation from endosome-like vacuoles but are not essential for membrane retrieval at central synapses. Neuron *82*, 981–988.

Kononenko, N.L., Claßen, G.A., Kuijpers, M., Puchkov, D., Maritzen, T., Tempes, A., Malik, A.R., Skalecka, A., Bera, S., Jaworski, J., and Haucke, V. (2017). Retrograde transport of TrkB-containing autophagosomes via the adaptor AP-2 mediates neuronal complexity and prevents neurodegeneration. Nat. Commun. *8*, 14819.

Kwinter, D.M., Lo, K., Mafi, P., and Silverman, M.A. (2009). Dynactin regulates bidirectional transport of dense-core vesicles in the axon and dendrites of cultured hippocampal neurons. Neuroscience *162*, 1001–1010.

Matteoli, M., Takei, K., Perin, M.S., Südhof, T.C., and De Camilli, P. (1992). Exo-endocytotic recycling of synaptic vesicles in developing processes of cultured hippocampal neurons. J. Cell Biol. *117*, 849–861.

Milosevic, I., Giovedi, S., Lou, X., Raimondi, A., Collesi, C., Shen, H., Paradise, S., O'Toole, E., Ferguson, S., Cremona, O., and De Camilli, P. (2011). Recruitment of endophilin to clathrin-coated pit necks is required for efficient vesicle uncoating after fission. Neuron *72*, 587–601.

Nishimura, T., Fukata, Y., Kato, K., Yamaguchi, T., Matsuura, Y., Kamiguchi, H., and Kaibuchi, K. (2003). CRMP-2 regulates polarized Numb-mediated endocytosis for axon growth. Nat. Cell Biol. *5*, 819–826.

Park, J., Cho, O.Y., Kim, J.A., and Chang, S. (2016). Endosome-mediated endocytic mechanism replenishes the majority of synaptic vesicles at mature CNS synapses in an activity-dependent manner. Sci. Rep. *6*, 31807.

Raman, D., Sai, J., Hawkins, O., and Richmond, A. (2014). Adaptor protein2 (AP2) orchestrates CXCR2-mediated cell migration. Traffic *15*, 451–469.

Rizzoli, S.O., Bethani, I., Zwilling, D., Wenzel, D., Siddiqui, T.J., Brandhorst, D., and Jahn, R. (2006). Evidence for early endosome-like fusion of recently endocytosed synaptic vesicles. Traffic *7*, 1163–1176.

Robinson, M.S. (2004). Adaptable adaptors for coated vesicles. Trends Cell Biol. *14*, 167–174.

Roos, J., and Kelly, R.B. (1999). The endocytic machinery in nerve terminals surrounds sites of exocytosis. Curr. Biol. *9*, 1411–1414.

Sabo, S.L., and McAllister, A.K. (2003). Mobility and cycling of synaptic protein-containing vesicles in axonal growth cone filopodia. Nat. Neurosci. *6*, 1264–1269.

Saheki, Y., and De Camilli, P. (2012). Synaptic vesicle endocytosis. Cold Spring Harb. Perspect. Biol. *4*, a005645.

Santolini, E., Puri, C., Salcini, A.E., Gagliani, M.C., Pelicci, P.G., Tacchetti, C., and Di Fiore, P.P. (2000). Numb is an endocytic protein. J. Cell Biol. *151*, 1345–1352.

Schmid, E.M., and McMahon, H.T. (2007). Integrating molecular and network biology to decode endocytosis. Nature *448*, 883–888.

Schneggenburger, R., Meyer, A.C., and Neher, E. (1999). Released fraction and total size of a pool of immediately available transmitter quanta at a calyx synapse. Neuron *23*, 399–409.

Schroer, T.A. (2004). Dynactin. Annu. Rev. Cell Dev. Biol. *20*, 759–779.

Sestan, N., Artavanis-Tsakonas, S., and Rakic, P. (1999). Contact-dependent inhibition of cortical neurite growth mediated by notch signaling. Science *286*, 741–746.

Slepnev, V.I., and De Camilli, P. (2000). Accessory factors in clathrin-dependent synaptic vesicle endocytosis. Nat. Rev. Neurosci. *1*, 161–172.

Soykan, T., Maritzen, T., and Haucke, V. (2016). Modes and mechanisms of synaptic vesicle recycling. Curr. Opin. Neurobiol. *39*, 17–23.

Szczurkowska, J., Cwetsch, A.W., dal Maschio, M., Ghezzi, D., Ratto, G.M., and Cancedda, L. (2016). Targeted in vivo genetic manipulation of the mouse or rat brain by in utero electroporation with a triple-electrode probe. Nat. Protoc. *11*, 399–412.

Tagliatti, E., Fadda, M., Falace, A., Benfenati, F., and Fassio, A. (2016). Arf6 regulates the cycling and the readily releasable pool of synaptic vesicles at hippocampal synapse. eLife *5*, e10116.

Tojima, T., Itofusa, R., and Kamiguchi, H. (2010). Asymmetric clathrin-mediated endocytosis drives repulsive growth cone guidance. Neuron *66*, 370–377.

Traub, L.M., and Bonifacino, J.S. (2013). Cargo recognition in clathrin-mediated endocytosis. Cold Spring Harb. Perspect. Biol. *5*, a016790.

Uytterhoeven, V., Kuenen, S., Kasprowicz, J., Miskiewicz, K., and Verstreken, P. (2011). Loss of skywalker reveals synaptic endosomes as sorting stations for synaptic vesicle proteins. Cell *145*, 117–132.

Valente, P., Casagrande, S., Nieus, T., Verstegen, A.M., Valtorta, F., Benfenati, F., and Baldelli, P. (2012). Site-specific synapsin I phosphorylation participates in the expression of post-tetanic potentiation and its enhancement by BDNF. J. Neurosci. *32*, 5868–5879.

Valtorta, F., Meldolesi, J., and Fesce, R. (2001). Synaptic vesicles: is kissing a matter of competence? Trends Cell Biol. *11*, 324–328.

van Hille, B., Richener, H., Evans, D.B., Green, J.R., and Bilbe, G. (1993). Identification of two subunit A isoforms of the vacuolar H(+)-ATPase in human osteoclastoma. J. Biol. Chem. *268*, 7075–7080.

von Kleist, L., Stahlschmidt, W., Bulut, H., Gromova, K., Puchkov, D., Robertson, M.J., MacGregor, K.A., Tomilin, N., Pechstein, A., Chau, N., et al. (2011). Role of the clathrin terminal domain in regulating coated pit dynamics revealed by small molecule inhibition. Cell *146*, 471–484.

Watanabe, S., Rost, B.R., Camacho-Pérez, M., Davis, M.W., Söhl-Kielczynski, B., Rosenmund, C., and Jorgensen, E.M. (2013). Ultrafast endocytosis at mouse hippocampal synapses. Nature *504*, 242–247.

Watanabe, S., Trimbuch, T., Camacho-Pérez, M., Rost, B.R., Brokowski, B., Söhl-Kielczynski, B., Felies, A., Davis, M.W., Rosenmund, C., and Jorgensen, E.M. (2014). Clathrin regenerates synaptic vesicles from endosomes. Nature *515*, 228–233.

Wren, J.D. (2009). A global meta-analysis of microarray expression data to predict unknown gene functions and estimate the literature-data divide. Bioinformatics *25*, 1694–1701.

Zhang, B., Koh, Y.H., Beckstead, R.B., Budnik, V., Ganetzky, B., and Bellen, H.J. (1998). Synaptic vesicle size and number are regulated by a clathrin adaptor protein required for endocytosis. Neuron *21*, 1465–1475.

Zhou, B., Cai, Q., Xie, Y., and Sheng, Z.-H. (2012). Snapin recruits dynein to BDNF-TrkB signaling endosomes for retrograde axonal transport and is essential for dendrite growth of cortical neurons. Cell Rep. *2*, 42–51.